ISSN Print 0970 - 3268
ISSN Online 2582 - 2020

The Journal of the Indian Association of Sedimentologists

The Indian Association of Sedimentologists

Volume 38 No. 2 July - Dec., 2021

Sand dunes at Hunder, Nubra valley, UT of Ladakh

**** Photograph showing cold desert sand dunes at village Hunder in the Nubra – Shyok Valley, UT of Ladakh where double hump camels of Chinese origin still exists. This is an international tourist destination where these camels are used as safaris. Nubra valley is in the north of Leh town and the road to the valley passes through 18,380ft high Khardungla pass (Khardongla), hence known to be one of the highest motorable roads of the world. Nubra was earlier known as Ladorma, which means "valley of flowers"*

ISSN Print 0970 – 3268
ISSN online 2582 - 2020

The journal of the Indian Association of Sedimentologists

The Journal of the Indian Association of Sedimentologists (IAS) is both an international open access online journal and print journal and is leader in its field and publishes ground-breaking research from across the spectrum of sedimentology, sedimentary geology, sedimentary geochemistry, experimental and theoretical sediment transport, mass movement fluxes, modern and ancient sedimentary environments, sequence-, cyclo-, chrono-and chemostratigraphy, sediment-biological interaction, palaeosols, diagenesis, stable isotope geochemistry, environmental sedimentology, neotectonics, geohazards, stratigraphy, palynology, sedimentary mineral resources and hydrocarbons, and allied branches of sedimentary -stratigraphic research. It also publishes review articles, editorials, conference reports, tributes, announcements, advertisements, etc. It is currently distributed to universities and research laboratories in India and abroad. Access to the complete electronic journal archive. Subscribers also have the option to buy the printed journal at subsidized cost.

Indian Association of Sedimentologists

TABLE OF CONTENTS

JOURNAL INDIAN ASSOCIATION OF SEDIMENTOLOGISTS ISSN NO 2582 – 2020
Vol. 38, Issue 2, 2021, pp. 1-2
DOI: https://doi.org/10.51710/jias.v38i2.214

Indus Water Treaty in the Backdrop of Climate Change and its Consequences

Climate change is the main driving force that shall affect global distribution of water in future. It has already effected water variation in some regions in the world including the Himalayan countries which face rapid decline in water reserves. This climate change-driven water variation is likely to affect transboundary water sharing treaties and agreements, and may force the water sharing nations either to conflict or cooperation policies. Great river systems emanating from huge glaciers in the Himalaya; the Brahmaputra, the Indus, the Sutlej, the Salween and the Mekong pass through 11 countries and nourish about 2 billion peoples in South Asia. Alone, the Indus River system feeds about half a billion people in North India and Pakistan. After the partition in 1948, India virtually imposed "Harmon Doctrine" propounded by the US and stopped waters of the Indus basin flowing into Pakistan. It was at the intervention of the World Bank who successfully mediated the Indus water Treaty (IWT) between the two countries in 1960. Pakistan had to be content with 80% waters of the three western rivers; the Indus, the Jehlum and the Chenab in accordance with the IWT. However, Pakistan faces upstream water control challenges and downstream distribution challenges. This long time but strained agreement over sharing water of the Indus River and its tributaries, flowing from Indian territories (Jammu, Kashmir and Ladakh) into Pakistan, has survived three wars and disputes for about six decades now. However, Pakistan feels that she is facing challenges brought about by climate change which were not anticipated at the time of negotiations for the IWT.

The dispute over Kashmir between India and Pakistan for more than seven decades is also linked with water security. Field Marshal Ayub Khan, the then President of Pakistan, was candid in stating Pakistan's compulsions to capture Jammu and Kashmir to have physical control over the upper reaches of Indus basin for their maximum utilisation of water. Pakistan has been blaming India of violating the IWT by constructing dams over the rivers flowing into Pakistan from Kashmir. Construction of run of the river projects on western rivers by India has resulted in displacement of local populations, threat to downstream habitation and has adverse effect on water flows of lower riparian Pakistan. Water security, especially in South Asia, "has become a regional security threat particularly due to rapidly melting glaciers in the Himalaya. For Pakistan, the Indus waters are a lifeline: it serves as the primary source of freshwater for the country and supports 90 percent of its agricultural industry. The International Monetary Fund in a 2018 report ranked Pakistan third among the water stressed countries. India came close to terminate the IWT after Pakistani militants allegedly attacked on Indian army personnel in Kashmir in September 2016. If they were actually to terminate the IWT, it would have strained relations between the two countries and resulted in military conflict. During the 2019 elections, India vowed to tap on the western rivers to starve lower riparian Pakistan by increasing storage capacity of dams for hydropower, flood control and diversion of waters for agriculture as the 'new national policy'.

As of now, instability in the Indo-Pak region and lack of regional integration and cooperation is a matter of great concern. The threat of war is largely looming in the region on account of Kashmir dispute, control on water resources including Siachen Glacier and, intra- and interstate water politics. Pakistan is worried about tapping of the western rivers by India as she had already used this weapon in 1948 which forced Pakistan to go for IWT. Unfortunately, thought process on these issues in New Delhi and Western powers is lacking particularly towards the unintended consequences of this strategy. In addition, the growing imbalance in India-Pakistan conventional defence capabilities has forced Pakistan to rely increasingly on the nuclear option to maintain credible deterrence. The unresolved disputes between India and Pakistan, especially Kashmir, and terrorist incidents and a threat of nuclear conflict are the greatest threat to international peace and security. National interests could be at stake for both the nations, if another war broke out, by design or accident between them. Nesbit, whose 2018 book 'This is the Way the World Ends' which has reference to the India-Pakistan water dispute, is of the opinion, "Water dispute between them has the potential to become the most deadly climate change-attributed conflict in the world".

In spite of all this, the current strained relations between the two nations do not seem to change in near future but it is unlikely to result in military confrontation, either conventional or nuclear. However, it can result in new external alliances leading to further polarisation in Asia, and compromises on the internal choices of each country. China is a naturally poised decisive player in this gamut of international game plan. Even though, China is completely independent dent in its water requirements, but it has a problem of its unequal distribution. Almost 81% of its water is in South China with only 19% in North China. When required, it will ruthlessly tap into resources which provide water to India, Kazakhstan, Laos and Cambodia. It has direct control over water availability to lower riparian countries. The right to use the water of a trans-border river involves a combination of 'de facto and de jure control' – control in fact and control in law. China has a strong hand by both the measures. The Helsinki Rules adopted in 1966, set forth the basic principle that countries are allowed to use the water which flows within their borders. Also rules were codified in the UN Convention on the Law of the Non-Navigational uses of International Water courses, which was adopted by the UN General Assembly in 1997 but has yet to go into force. China is neither a party nor a signatory to this treaty. The two countries (China and India) have faced four post-independence border conflicts—the 1962 Sino-Indian War, the 1967 Chola Incident, the 1987 Sino-Indian Skirmish, 2017 Doklam, 2020 Galwan Valley border conflict and asylum to Dalai Lama in India — which have left a legacy of mistrust between them.

China's policy on river waters is based on the Doctrine of Absolute Territorial Integrity (Harmon Doctrine). India itself is dependent on 34% water resources from China and, Bangladesh depends on India and China together accounting for 91% of its water requirements. Kashmir's 'location' and occupational relevance to Pakistan and China, has always been significant and has now become a driver in its own right as China is building the "China-Pakistan Economic Corridor (CPEC)" through the disputed territory of Jammu and Kashmir to reach West Asia and Africa. Also China-India has a long pending unsettled border dispute in Kashmir and Arunachal Pradesh. The issue of river waters compounds the situation, since Kashmir is either the source or conduit of the rivers emanating in China for both India and Pakistan. China being the upper riparian has hand on tap and can cut-off Indian access to water run-off from the glaciers in the Himalaya under its control. China has a time tested alliance with Pakistan since its birth and has always stood by them through thick and thin; this factor will restrict India from cutting off Pakistan's access to the Indus waters. China is watching the India-Pakistan water dispute quite closely and will act at an appropriate time conducive to them. So India may not aggressively venture to cut access to Pakistan on western rivers, as she knows, the same thing could happen to her. In the existing scenario of border disputes, emerging water sharing disputes, impact of climate change, pressure of growing population and attendant problems, etc., South Asian Region shall continue to be a potential flash point for threat to international peace and security.

So it is time to make efforts for peace and regional cooperation rather than talk about nuclear spree. Water treaties and nuclear technologies could be used as deterrence from wars. The problems arising from water security need to be addressed in the form of trans-boundary and sub-regional cooperation. China and India have already institutional arrangements for cooperation on data-sharing to address climate change and related problems in the Himalayan and Tibetan regions. Keeping in view, the unprecedented heavy precipitation during the recent years causing devastating floods in South Asia, it is necessary to extend these arrangements to other countries in the region particularly to those sharing the trans-border waters. The speculation about China's plans to build dams at the Eastern Syntaxial Bend on the Yarlung Tsangpo River and India's River-Linking project are matters of concern, as they can reduce river flows in low season. Since the Himalayan region is prone to high seismicity, an earthquake of great magnitude, as predicted for this region, can damage dams and flood an entire region, causing devastation. Unfortunately, change of political camps has changed the mind of international institutions which follow America more than the Law of Natural Justice. The biggest challenge facing the South Asian region is the ecological crisis, with degradation of the environment and melting of the glaciers in the Himalaya. Its impact shall determine the region's future. Continuous dialogue on these issues among the South Asian leaders could change the chemistry of the relations among them. The attitude in climate change negotiations needs to be changed from "to extract the most from the other side while giving the least". Unless this mindset is changed, we can't make much headway in mitigation of the environmental issues which are bound to affect trans-border water treaties and agreements, and international security.

Professor G. M. Bhat
University of Jammu
bhatgm@jugaa.com

JOURNAL INDIAN ASSOCIATION OF SEDIMENTOLOGISTS ISSN NO 2582 – 2020
Vol. 38, Issue 2, 2021, pp. 3-14
DOI: https://doi.org/10.51710/jias.v38i2.113

Lithofacies Analysis of the Tista River Deposits, Rangpur, Bangladesh

Sudip Saha, Mrinal Kanti Roy and A.H.M. Selim Reza

Department of Geology and Mining, University of Rajshahi, Rajshahi-6205, Bangladesh
E-mail: sudips_geologist@yahoo.com

Abstract

Eight (8) distinct lithofacies within the fluviatile reach of the Tista River have been recognized by the detailed study of the sediments as exposed along the river bank and river bars. Genetically, the matrix-supported conglomerate (Gms), massive sand (Sm), Trough cross stratified sand (St), planar cross stratified sand (Sp), ripple laminated sand (Sr) comprise the channel deposits whereas, the ripple laminated sand (Sr), parallel laminated sand (Sh), clay with silt (Fl) and massive Clay (Fm) represent overbank fine deposits. The channel deposits were laid down under relatively high energy conditions compared to the sediments of overbank fines. The stratigraphic succession is indicative of fining upward sequence. The dominance of coarser-grained sediments at the base of the lithostratigraphic unit, especially the matrix supported conglomerate (Gms) suggests that the deposition took place in the proximal part of the Tista Fan, which might be of glacial origin. Massive clay (Fm) is the final stage of vertical aggradations in the overbanks, possibly in the floodplains, flood basins, and back swamps when the velocity of the transporting medium was virtually lean that promotes the deposition of clay materials from suspension. The growth of cracks in the sedimentary succession is resulting from the compaction of the sediments and/or instant change in the paleoslope direction. The unimodal distribution of paleocurrent data with high mode value indicates mainly unidirectional sediment transport. The study of the lithofacies manifests that the deposits are produced by the braided river and debris flows. The modification of the depositional pattern from debris flow to overbank fines discloses the change of climatic condition in the Quaternary period.

Keywords: Lithofacies, Tista, channel deposits, overbank fine or bar top deposits and suspension.

INTRODUCTION

Facies analysis has been an important procedure among sedimentologists for decades. The main basis used for defining facies follow those of Miall (1978, 1996), that have been accepted by many authors. These criteria predominantly concern grain sizes, and sedimentary structure, the geometry of sedimentary bodies, and the presence or absence of identifiable plant or animal remain. Facies moreover occur in predictable patterns in terms of lateral and vertical distribution and can also be linked to sedimentary processes and depositional environments.

The concept of facies has been ever used since geologists, engineers and miners recognized that features found in particular rock units were helpful in correlations and predicting the occurrence of coal, oil or mineral ores.

Facies analysis is significantly applied to the old sedimentary succession for the reconstruction of the depositional environment, paleoclimate. Roy et al. 2004 established three different depositional environments for the Tertiary Dupi Tila formation of Lalmai Hills, Comilla by the detailed examinations of lithofacies. The lithofacies analysis of Gondwana sequences suggests their origin from the sedimentation of fluvio-glacial braided stream to backswamp environments in Bangladesh (Islam and Islam 2006). The lithofacies examinations of modern sediments lay out the 3D view of the stratigraphic succession that is subsequently applicable for the characterization of old sedimentary basins. The Recent fluviatile deposits of the Padma river show the variations in lithofacies compositions while the deposition ranged from channels to backswamps in different seasons of the year (Roy *et al.* 2002).

The present research work is executed with the sedimentology of the transboundary Tista river and is adjoining areas, that is located in the parts Nilphamari, Lalmonirhat, Rangpur, Kurigram and Gaibandha districts of Rangpur division, Bangladesh. The Tista is a fast flowing river and fed by the rainfall, glacial melt and groundwater flow. It emanated from the Himalayan Mountain Ranges and runs through India and Bangladesh (Chakraborty and Ghosh 2010). The landslides are a common incident in the mountainous part of the basin whereas the basin is inundated with seasonal flood events in it lower course in the plain lands (Pal *et al*,. 2016).

The petrographic of analysis of Tista fan sandstone reveals the dominance quartz, feldspar and mica (Akter *et al.* 2003). Chakraborty and Ghosh 2010 worked on the geomorphology and sedimentology of the Tista megafan in Darjeeling Himalaya and concluded the advancement of the paleochannels southwestward after analyzing the paleocurrents data. Chakraborty *et al.* 2018 studied the subsurface lithofacies and they identified seven different lithofacies of fluvial origin in West Bengal, India. Saha *et. al.* 2017 worked on the textural aspects of the deposits as exposed along the banks and bars and reported the dominance of coarse particles especially sand laden with pebbles over the finer sized sediments. The application of illite crystallization index implies that the physical weathering is the prominent process for the production of these sediments (Saha *et al.*2020). The slope and geomorphic characteristics of the Tista river is influenced by the presence of the Tista fault along the course of the Tista river (Sarker et al. 2009). Khan and Islam 2015, deciphers the anthropogenic impacts on the morphology of the Tista river in Northern Bangladesh like the construction of bridges and barrage, bank stabilization, human settlements, intensive agriculture and sand mining. It was reported that the grain size becomes finer vertically upwards and along the downward course of the Tista river.

The wide and rapid spectral variations in sedimentary structures and textures in the Quaternary deposits on the banks of the mighty river Teesta at the Himalayan foothills in Bangladesh bear a snapshot of an extremely unstable depositional regime. The sedimentation entropy involved is further manifested in biogenic responses that include human settlements as well. Recent additions of bridges, barrages, dams, sand mining, cultivation and channel diversions cause modifications of the primary attributes of the deposits. To understand the complex Quaternary sedimentation mileu a holistic lithofacies analysis is attempted in this paper. Lateral and vertical facies transitions are worked out across diastems present in high frequency. Sedimentation continuum is thus studied in piecemeal and then integrated in an evolutionary history which is long awaited.

Study area

The Tista is the fourth main river in terms of discharge in Bangladesh (Khan and Islam, 2015). It is a right tributary of the Brahmaputra (Wiejaczka *et al.*, 2014) (Figure 1a). It originates in the Pauhunri massif

Figure 1a: Location map showing the Study area (modified after Saha et al. 2019

(7127m amsl). The Tista River flows through the Tista lineament. The lineament was presumably mapped by remote sensing (Nandy *et al.*, 1993; Mukul *et al.*, 2014). Tista is the principal river of Rangpur district. The area is drained by numerous other rivers like Brahmaputra, Jamuneshwari, Ghaghat, Karatoya, Chikali, Buri Tista etc. The Tista is a braided river in its lower part in Bangladesh. The sedimentation pattern of the river is also influenced by the construction of the barrages in the upper course of the river.

The Tista megafan is a huge triangular sediment body characterized by a radiating drainage pattern (Chakraborty and Ghosh, 2010). The apex of the megafan coincides with the point of emergence of the Tista River from the mountain belt. The Tista River sediments are characterized by the dominance of the sand particles that are mixed with cobbles and pebbles (Saha et al. 2017). The percentage of sand decreases to the downstream direction at expense of an increasing fraction of mud.

Table 1 Stratigraphic succession of the Rangpur Saddle, Bangladesh *(*Modified after Hossain, 1999 and UNDP, 1982*)*

Age	**Group/Formation**	**Lithology**	**Thickness**
Recent to Sub-Recent	Alluvium	Sand, silt and clay	53m.
Late Pleistocene-Holocene	Tista Gravel	Gravels with sand and silt	89 to 97m
Pleistocene	Barind Clay	Clay, sandy clay, yellow-brown sticky	15m
Middle Pliocene to Late Miocene	Dupi Tila Formation	Sandstone with subordinate pebble bed, grit bed and shale	171m.
Early Miocene	Surma Group undifferentiated (?)	Fine to medium grain sandstone, sandy and silty shale, siltstone, and shale.	125m.
Middle Eocene	Tura Sandstone (?) Formation	Gray and white sandstone with subordinate greenish gray shale and coal.	128m.
Late Permian	Gondwana sediments	Feldspathic sandstone, shale, coal beds	475m.
Precambrian	Basement complex	Gneiss, schist, granodiorite, quartz diorite	

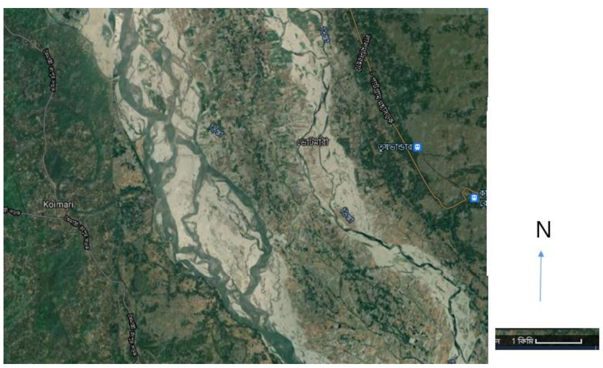

Figure 1b: Satellite image showing the growth of medial bars, Tista river basin, Bangladesh

Table 1 shows the stratigraphic succession of the Rangpur Saddle. The study area composed of Alluvial deposits that contains gravel, sand, silt and clay of Recent age. The aquifers of the Tista Fan, both active fan and inactive, that lie in Rangpur and Dinajpur districts are composed of coarser sediments have the highest transmissivity in Bangladesh that vary from 1000-7000 square meters/day (UNDP 1982; Hussain and Abdullah 2001). The present day Tista river is flowing through the upper part of the megafan. Figure 1b shows the development of the medial bars, which helps to identify the braided nature of the Tista river in Bangladesh.

Methods

The Sedimentary deposits are exposed along the vertical channel banks and medial sand bars throughout the Tista river from west to east. The field work was carried out from February to June in the year of 2014. The lithologies of various stations were examined by the aid of pocket lenses and also tested with the concentric hydrochloric acid to identify the carbonate rocks (Roy *et al.*2012). The attitudes and thickness of the sediments were quantified using clinometer and a measuring tape. The identification of the sedimentary structures was done as described by Collinson and Thompson (1982) and Reineck and Singh (1980). All the field data were recorded in a note book and the lithologs were drawn in situ. Large grains of platy minerals like muscovite was identified with the naked eye. The average thickness of the investigated sections was calculated as 1.34 m. The exposed sediments assigned to number of distinct facies. Facies identifications and interpretations were based on detailed examination of colour, texture, composition, sedimentary structures and bedding characteristics (Miall, 1984; Reading, 1986; Roy *et al.,* 2001). Photographs were taken in the field using digital camera. The stratigraphic lithologs were drawn using a

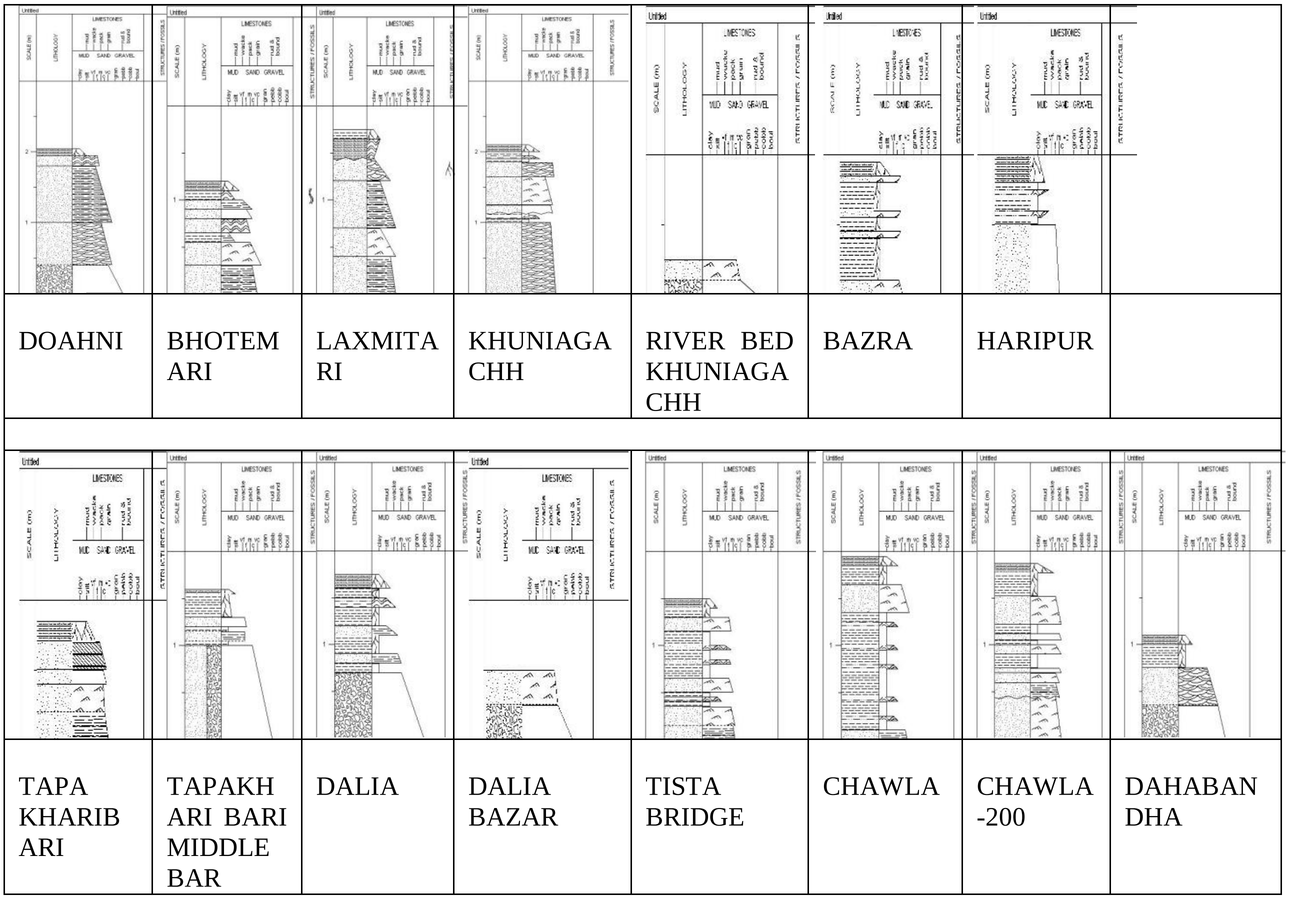

gure 2: Sedimentological lithologs of the Tista River Basin, Rangpur, Bangladesh

computer software, Sedlog 3.0, Rockworks-17 in the laboratory. The rose diagram was prepared for the interpretation of paleocurrent direction with necessary computer software.

RESULTS

The studied sections show the findings of the detailed stratigraphic and sedimentological analyses of the deposits observed in the sections as exposed along the both banks of the Tista River and its medial bars. An inspection of the sedimentological logs reveals a total of eight facies, which are explained in order of their occurrence from base to top.

The fluvial facies of the Tista River are characterized by normal graded bedding sandstone and conglomerates that fine and thin upward and mudstone. It contains channel and overbank subfacies and occurs in. The channel subfacies include distributary channels, bed form lag deposits, and point bars and the overbank subfacies include natural levees, crevasse splays, and floodplain deposits.

DESCRIPTION OF DIFFERENT LITHOFACIES

Eight different lithofacies were identified in the studied lithosuccession and they are namely Matrix supported conglomerate (Gms), Massive sand (Sm), Trough cross stratified sand (St), Planar cross stratified sand (Sp), Ripple laminated sand (Sr), Parallel laminated sand (Sh), Clay with silt (Fl) and Massive Clay (Fm). These are observed along the river bank and bars within the study area. These are described in order of grain size i.e. coarse grain facies are followed by fine grained facies.

Matrix supported conglomerate facies, Gms

Matrix supported conglomerate facies is a well-developed lithofacies that occurs at the base of the lithocolumn within the area of investigation. The thickness of this facies varies from 10 to 100 cm. The facies is exposed in Doahni, Khuniagachh Bar, Tapa Kharibari Middle Bar, Dalia, Dalia Bazar, and Dahabandha sections. The maximum thickness is recorded in Tapa Kharibari Middle Bar section

Table 2: Lithofacies Scheme of Tista River sediments, Rangpur, Bangladesh

Facies Code	Lithofacies	Sedimentary structure	Thickness	Interpretation
Gms	Matrix supported conglomerate	None	10-100 cm	Debris flow deposit
Sm	Massive sand	Massive	5-50 cm	Rapid deposition from fluidized flow
St	Trough cross stratified sand	Grouped trough cross bedding	20-60 cm	Dunes (lower flow regime)
Sp	Planar cross stratified sand	Grouped planar cross bedded	20 cm	Two-dimensional bed form, sandwaves, linguid and transverse bars.
Sr	Ripple laminated sand	Ripple marks or ripple laminations	5-45cm	Ripple, current generated
Sh	Parallel laminated sand	Horizontal or flat bedding	10-80 cm	Lower flow regime plane bed
Fl	Clay with silt	Ripple laminated	5-50 cm	Over bank/waning flood deposit
Fm	Clay	Massive	5-30 cm	Non channelized swamp deposit

which is 100cm. This gravelliferous deposit is devoid of any sedimentary structures and composed of cobbles, pebbles and granules. The coarser deposits are found in the upstream part of the Tista River within the study area

Figure 3: Massive sandstone, Trough cross stratified sand facies (St) as exposed in the Tista River Basin, Sundarganj, Bangladesh.

Interpretation

Matrix supported conglomerate may be the product of debris flow deposits which are promoted by a steep slope, lack of vegetation. Short period of abundant water supply given by heavy rainfall and/or melting, and it is a source providing debris with a sandy matrix (Bull, 1977; Starkel *et al.*, 2015). This flow may be confined to high lobed braided channels but commonly spread out at lobate sheets on the lower reaches of the proximal part of the river forming levees and having characteristics of debris flow deposits (Miall, 1978; Blair and McPherson, 1994). Lack of organized fabric is a common aspect of debris-flow deposits (Rust and Koster, 1984). Because of its high viscosity, the debris flow deposits do not travel a longer distance. Hence these deposits are normally observed in the proximal fan. Short-term fluctuation of precipitation in fan area undoubtedly produces debris flow in a humid area (Curry, 1966; Blair and McPherson, 1994).

Massive sand facies, Sm

The massive sand facies consists of fine to very coarse-grained, feldspar bearing sands. The thickness of the facies varies from 5 cm to 50cm, and the maximum thickness is found at the lithocolumn of Haripur (Figure2 and 3). The colour of this is pale to brownish. The sand grains are angular to subrounded and poorly to moderately sorted. Scattered pebbles ranging from 1cm to 2cm in diameter are present at some locations. This facies is unconsolidated and does not exhibit ant sedimentary structure or any fossil.

Interpretation

Massive sandy beds of Sm might be formed in response to depositional processes (McCabe, 1977; Jones and Rust, 1983; Udo and Mode, 2013) or by post-depositional deformation (Allen, 1986). In the present interpretation, deformation is considered irrelevant in the absence of its indicators in any bed associated with Massive sand, Sm. Accordingly, this facies is interpreted as resulting from transport and deposition by short-lived mass flows. This lithofacies has been interpreted as reflecting deposition in a sand-dominated braided fluvial environment (Morton *et al.,* 2011).

Trough cross stratified sand facies, St

Trough cross stratified sand facies (St) constitutes 11% of the total lithosuccession. The thickness of this lithofacies ranges from 20 to 60 cm and the highest thickness was recorded at the lithocolumns of Doahni and Laxmitary. The base of trough cross stratified sand facies is gradational to sharp. The grain size varies from medium to very coarse sand, and sand is dark grayish white in colour. St comprises mainly well to moderately sorted, subrounded to rounded grains of quartz with black and white mica.

Interpretation

Most commonly this facies may have been deposited as migrating sinuous crested dunes or lunate bars on the top of a gravel facies, in association with planar cross bedded sand body (Sp) facies, or in local depressions of mega ripples showing evidence of scour –fill episodes (Miall, 1978; Walker and Cant, 1984). Trough cross stratified sand facies (St) along with the upward as well as down slope of the litho-columns within the present Tista Basin area is interpreted as response to shallowing of water over the gravelliferous bars and active gravelliferous braided channels with a decrease of stream competence, accompanied by or in response to migration of active tract of channels over the fan (Wasson, 1977; Reineck and Singh, 1980).

Planar cross stratified sand facies, Sp

Planar cross stratified sand facies (Sp) is exposed at the lithosuccession of Tapa Kharibari of Nilphamari district and the thickness of the bed is 20 cm. The planar cross stratified sand overlies on massive sand (Sm) with a sharp base. The grain size varies from fine sand to very coarse sand.

Interpretation

The deposition of small scale planar cross-bedded (Sp) facies has been attributed to current migration of linear ripple whereas large scale planar cross-bedding is produced both by linear (two-dimensional) mega ripple and sand waves or migration of three-dimensional medium subaqueous dunes (Ashley, 1990). Sets of planar cross-bedded sand (Sp) facies associated with other finer facies may also represent chute bars in the lower mid to distal part of the alluvial fan (McGowen and Garner, 1970). Low angle planar cross-bedded sand is common in the fining upward litho-column of water-laid deposits (Bull, 1972; Reineck and Singh, 1980).

Ripple laminated sand facies, Sr

Ripple laminated sand facies (Sr) is composed of quartz, muscovite, and biotite minerals. The colour of this facies grayish white, and the thickness varies from 5cm to 45 cm. It is exposed at Doahni, Bhotemari, Laxmitari, Khuniagachch, Bazra, Tapa Kharibari, Dalia Bazar, Tista Bridge, Chawla and Chawla-200 sections and the maximum thickness was recorded at Chawla-200. The grain size ranges from very fine sand to coarse sand.

Interpretation

Ripple laminated sand is developed due to migration of small-scale 2D and 3D ripples during minimum flow strength in relatively shallow water condition (Jopling and Walker, 1968). The ripples may indicate partial abandonment of channels (Gardis and McCade, 1981). These may be deposited partly filled channels in dying stages within unconfined channels or by sheet floods in the alluvial fan (Reineck and Singh, 1980). These ripples may locally present in the sandy layers within the upper part of the stacked channel deposits of lower part and inactive lobes of proximal fan (McGowen and Groat, 1971; Roy *et al.*, 2004a).

Parallel laminated sand facies, Sh

Parallel laminated sand facies (Sh) is constituted gray to yellowish brown parallel, horizontal or flat bedding very fine to very coarse-grained sand. It overlies massive sand, trough cross stratified sand and ripple laminated sand. Sometimes this facies overlies the massive clay facies. The thickness of parallel laminated sand varies from 10 cm to 80cm.

Interpretation

Parallel laminated sand (Sh) facies are product of upper part of lower flow regime when the flow velocity is sluggish (Middleton and Southward, 1978). The coarser nature, unsorted character and faint laminations/horizontal laminations of the sediments are suggestive of flood deposits in the overbank of the Tista River.

Clay with silt facies (Fl)

Clay with silt facies (Fl) comprises silt and clay. Clay constitutes 70-75 percent by volume of this facies. Clay is gray to brownish gray in colour. Silt with certain amount of very fine sand comprises rest of the facies Fl. Silt is gray to grayish white in colour. The thickness of the facies Fl varies from 5 to 50 cm. Silt in the lower part of the facies is parallel laminated, while that in upper part shows current ripple laminations. This facies overlies sharply ripple laminated sand (Sr), parallel laminated sand (Sh), trough cross stratified sand (St) and occasionally over massive clay (Fm).

Interpretation

These deposits are virtually suspension products in slow moving shallow water (Roy *et al.*, 2001). Parallel laminations indicate settling from suspension from slow moving or stagnant water (Roy *et al.*, 2004a). The sediments of Clay with silt facies (Fl) are over bank fine or waning flood deposits. From the field observations, it may be concluded that the coarser sediments (silt and very fine sand) of this facies might have been deposited during the rainy season when the river stage is highest and inundate the floodplains.

Massive clay facies (Fm)

Massive clay facies (Fm) is the dominant facies in the upper part of the litho-column. The material of this facies is generally clay and the colour of the clay varies from bluish gray to grayish white. The clay is sticky when wet. The facies is characterized by mottling nature and ped development. The presence of rootlets is a common feature of the facies, Fm. The facies sharply overlies matrix supported conglomerate, Gms (at Tapa Kharibari Middle Bar, Dalia), massive sand, Sm (at Tapa Kharibari Middle Bar, Chawla-200), trough cross stratified sand facies, St (at Khuniagachh, Dahabandha), parallel laminated sand, Sp (at Tapa Kharibari), ripple laminated sand, Sr (at Doahni, Bazra, Tista Bazar, Chawla, Chawla-200), parallel laminated sand, Sh (at Tapa Kharibari

Middle Bar, Dalia, Chawla) and clay with silt, Fl (at Bhotemari, Laxmitari, Khuniagachh, Haripur,

Figure 4: Massive clay facies (Fm) as exposed in the Tista River Basin, Bojra, Ulipur, Bangladesh.

Dalia, Tista Bazar). The thickness ranges from 5 to 30 cm and the maximum thickness were found at Bojra (Figure 4), Tapa Kharibari Middle Bar and Chawla sections.

Interpretation

The deposits of Massive clay facies, Fm represent well drained swampy environment (Roy *et al.*, 2004b). Massive clay (Fm) is the final stage of vertical aggradations in the overbanks possibly in the floodplains, flood basins and back swamps when the velocity of the transporting medium was virtually lean that promotes the deposition of clay materials from suspension.

Facies model

The vertical relationship of different facies can be shown by the construction of facies model. The facies model is a useful tool for better understanding of the stratigraphy of an area. It is the most common figure that provides the genetic explanation of the past geologic processes that that played the vital role for the formation of the facies present in the litho-columns of the Tista River basin (Figure 5). A facies model is a general summery of the sedimentary environments represent by the rock record (Walker 1984).

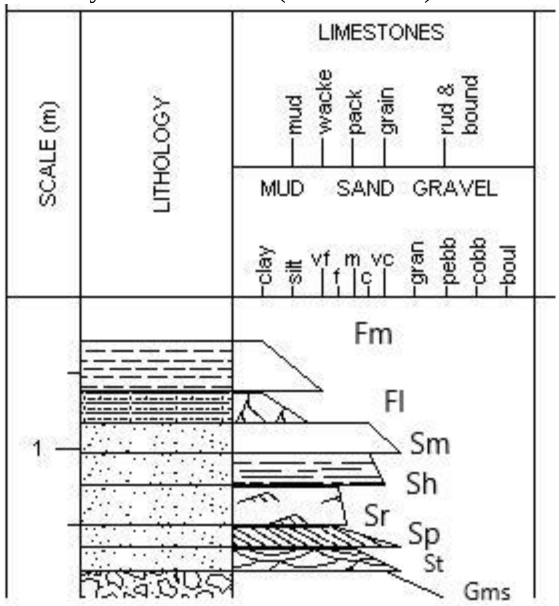

Figure 5: Facies model of the Tista River deposits

The basal facies Matrix supported conglomerate (Gms) is the Oldest facies which is formed under high energy conditions. Trough cross stratified sands (St) is the products of the migration of 3D sub-aqueous dunes in the deeper part of the channel in relatively high energy conditions. Planar cross stratified sand (Sp) has been attributed to current migration of linear ripples. Ripple laminated sand (Sr) is formed due to migration of small-scale 2D and 3D ripples during minimum flow strength in relatively shallow water condition (Jopling and Walker, 1968). Parallel laminated sand (Sh) facies is a product of low energy conditions. Massive sand (Sm) are resulting from transport and deposition by short-lived mass flows. Faintly laminated clays (Fl) are the product when the velocity of the running water is comparatively low in shallow water condition in the overbank. Massive clay (Fm) is a product of flood basins and back swamps when the velocity of the transporting medium is lowest and suspension took place.

Facies association

There are two types of facies association in the sediments of the Tista River under investigation. These are as follows—A) Channel deposits and B) Overbank fines, including flood deposits. The channel deposits consist of Matrix supported conglomerate (Gms), Massive sand (Sm), Trough cross stratified sand (St), Planar cross stratified sand (Sp), Ripple laminated sand (Sr), whereas, the overbank fines, including flood deposits comprise of Ripple laminated sand (Sr), Parallel laminated sand (Sh), Clay with silt (Fl) and Massive Clay (Fm).

A) Channel deposits

The channel deposits are laid down under high energy in the channel. The Matrix supported conglomerate (Gms) deposited under high energy condition having sufficient paleoslopes to carry the sediments. These sediments represent high energy graveliferous river at piedmont alluvial plain or proximal part of alluvial fan.

The Massive sand (Sm) sediments are tractive current deposits under high energy condition and the deposition took place rapidly that did not allow to develop and sedimentary structure. Trough cross stratified sands (St) is the products of the migration of 3D sub-aqueous dunes in the deeper part of the channel in relatively high energy conditions.

Planar cross stratified sands (Sp) are deposits of the migration of 2D sand waves in relatively shallower part of the channel.

Current ripple cross laminated sand (Sr) has been deposited by the migration of small scale 2D and 3D ripples in shallower part of the channel. The channel deposits represent lateral accretion (point bar), downstream accretion (mid channel bar) and channel fill deposits.

B) Overbank fines

The overbank fine sediments are constituted by the facies of Ripple laminated sand (Sr), Parallel laminated sand (Sh), Clay with silt (Fl) and Massive Clay (Fm). occurring in the uppermost part of the lithosuccessions. These deposits represent vertical accretions.

Ripple laminated sand (Sr) represents the shallow deposits of top part of the channel and the deposits of flood on the overbanks. These deposits are represented by 2D ripples; with sufficient supply of sediments the ripples sometimes climb to form climbing cross ripples.

Parallel laminated sand (Sh) is somewhat coarse in grain size and parallel laminated. These deposits are product of upper part of lower flow regime when the flow velocity is sluggish (Middleton and Southward, 1978). The coarser nature, unsorted character and faint laminations/horizontal laminations of the sediments are suggestive of flood deposits in the overbank of the Tista River. Faintly laminated clays (Fl) are the product when the velocity of the running water is comparatively low in shallow water condition in the overbank.

Massive clay (Fm) is the final stage of vertical aggradations in the overbanks possibly in the floodplains, flood basins and back swamps when the velocity of the transporting medium was virtually lean that promotes the deposition of clay materials from suspension. These are suspension fall outs of the river and flood in the overbanks. The presence of root/rootlets (in form of small rootlets, decomposed ped marks and coalifed rootlets) are suggestive of short time gap when small scale plants, shrubs and/or grass would grow.

The rose diagram is showing the paleocurrent directions of the investigated area (Figure 7). The calculated vector mean magnitudes are suggestive of northeasterly and southeasterly paleocurrent. The unimodal distribution with high mode value indicates mainly unidirectional sediment transport (Bhattacharyya and Das 2018). The cracks in the sedimentary succession results due to either the compaction of the sediments or the abrupt change in the paleoslope of the depositional basin (Figure 7).

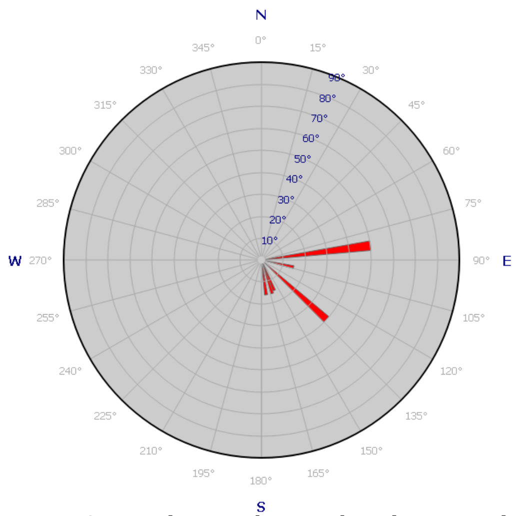

Figure 6: Rose diagram showing the paleocurrent direction

Figure 7: Cracks developed in sedimentary succession at the mouth of the Tista river, Haripur, Sundarganj

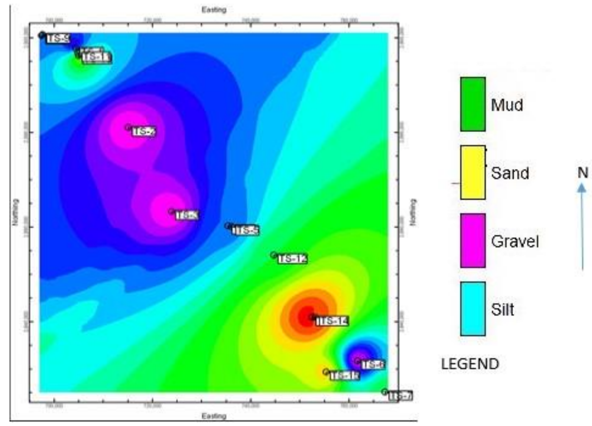

a

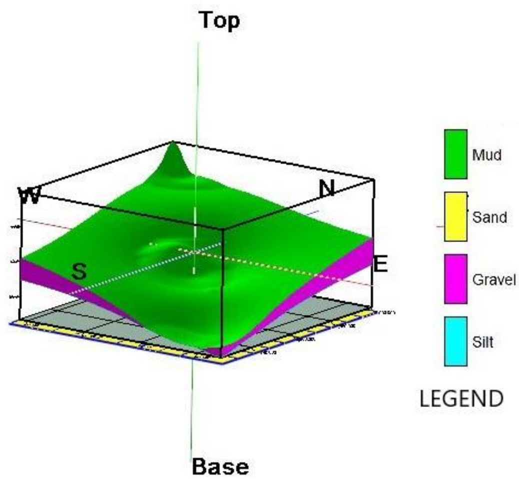

b

Figure 8: a) The distribution spatial of different rocks, b) Sedimentary model of the formation of the Tista river deposits in the Tista Fan, Bangladesh

Figure 8a shows that the coarser gravelliferous deposits are exposed in the upstream directions whereas the finer sediments comprise the areas of downstream. The basal coarser Gms deposits of the sedimentary sequence are poorly sorted and represent debris flow deposit (Meetei et al. 2007). The matrix-supported conglomerate facies belongs to the Tista Gravel formation of Late Pleistocene-Holocene. The three-dimensional inspection of the sedimentary basin reveals that the channel fill deposits are transformed by the overbank fines which is indicative of climatic change in the investigated area during the Quaternary (Figure 8b).

The lithofacies analysis distinguishes their deposition from braided channels and debris flows.

CONCLUSION

Eight different lithofacies were identified in the studied sedimentary succession and they are namely Matrix supported conglomerate (Gms), Massive sand (Sm), Trough cross stratified sand (St), Planar cross stratified sand (Sp), Ripple laminated sand (Sr), Parallel laminated sand (Sh), Clay with silt (Fl) and Massive Clay (Fm). The field observations show that the finer clay sediments are also mixed with sand particles. The colour mottling and colour banding are resulted the mixing of light coloured minerals with dark coloured heavy minerals. Both muscovite and biotite are found in the study area. The channel deposits are laid down under high energy in the channel. The overbank fine sediments are constituted by the facies of Ripple laminated sand (Sr), Parallel laminated sand (Sh), Clay with silt (Fl), and Massive Clay (Fm). occurring in the uppermost part of the sedimentary succession. The presence of root/rootlets (in form of small rootlets, decomposed ped marks and coalifed rootlets) are suggestive of short time gap when small scale plants, shrubs and/or grass would grow. The finer sediments were deposited from the suspension in floodplains or back swamps. The sediments are deposited by the braided river and debris flows. The change in the depositional pattern from debris flow to overbank fines signifies the alteration of climatic condition in the Quaternary period.

Acknowledgement

The authors are pleased to express sincere thanks to Professor Dr. Golam Shabbir Sattar, Ex-Chairman, Professor Dr. Khondaker Emamul Haque, Ex-Chairman and Professor Dr. Md. Sultan-ul-Islam, Chairman Department of Geology and Mining, University of Rajshahi, Bangladesh for arranging the research work. The authors are also thankful to Mr. Md. Azizul Alam for his kind preparation of the map of the study area.

Funding: No funding.

Conflict of interest: The authors do not have any conflict of interest.

References

Allen, J. R. L. (1986) Earthquake magnitude frequency, epicenter distance and soft sediment deformation in Sedimentary basins, Sedimentary Geology, 46, pp. 67-75.

Ashley, G.M. (1990) Classification of large scale subaqueous bedforms: a new look at an old problem, Journal of Sedimentary Petrology, 60(1), pp. 160-172.

Blair, T. C., and McPherson, G. (1994) Alluvial Fan and their Natural Distinction from Rivers based on Morphology, Hydraulic Processes, and Facies Assemblages, Journal of Sedimentary Research,64A (3), pp. 450-489.

Bull, W. B. (1972) Recognition of Alluvial Fan Deposits in the Stratigraphic Record, Society of Economic Paleontology and Mineralogy, Special Publication No. 16, pp. 63-83.

Bull, W. B. (1977) The Alluvial Fan Environments, Progress in Physical Geography, 1, pp. 222-270.

Chakraborty, T., and Ghosh, P. (2010) The geomorphology and Sedimentology of the Tista megafan, Darjeeling Himalaya: Implications for megafan building processes, Geomorphology, 115, pp. 252-266.

Curry, R. R. (1966) Observation of Alpine Mudflows in the Tenmile Range, Central Colorado, Geological Society of America Bulletin, 77, p. 771-776.

Garbis, G. A., and McCabe, P. J. (1981) Continental Coal-bearing Sediments of the Part flood Formation (Carboniferous), Cape Linzee, Nova Scotia, Canada, Society of Economic Paleonlogists and Mineralogists, Special Publications 31.

Hossain I., 1999, Lithofacies and petrographic study of the Gondwana Group in the boreholes GDH-40 and GDH-43, Barapukuria Basin, Dinajpur, Bangladesh. An unpublished M.Sc thesis, Dept. of Geology and Mining, University of Rajshahi.

Hussain MM and Abdullah SKM (2001) Geological Setting of The Areas of Arsenic Aquifers, Ground Water Task Force, Interim Report No.1, Local Government Division, Minitry of Local Government, Rural Development and Cooperatives, Bangladesh, pp. A 1-A 45. http://fineprint.com.

Jones, B. G., and Rust, B. R. (1983) Massive Sandstone Facies in the Hawkesbury Sandstone, a Triassic fluvial deposit near Sydney, Australia, Journal of Sedimentary Petrology, 53, pp. 1249-1259.

Jopling, A. V., and Walker, R. G. (1968) Morphology and Origin of Ripple-drift Cross-lamination, with Examples from the Pleistocene of Massachusetts, Journal of Sedimentary Petrology, 38, pp.971-984.

Khan, M. S. S., and Islam, A. R. M. T. (2015) Anthropogenic Impact on Morphology of Teesta River in Northern Bangladesh: An Exploratory Study, Journal of

Geosciences and Geomatics, 3(3), pp.50-55. doi:10.12691/jgg-3-3-1.

Krumbein, W. C., and Sloss, L. L. (1963) Stratigraphy and Sedimentation, San Francisco and London: W. H. Freeman and Co., 2nd Ed, p. 660.

McCabe, P. J. (1977) Deep Distribution Channels and Giant Bedforms in the Upper Carboniferous of the Central Pennines, Northern England, Sedimentology, 24, pp. 271-290.

McGowen, J. H., and Garner, L. E. (1970) Physiographic Features and Stratification Types of Coarse-grained Pointbars: Modern and Ancient Examples, Sedimentology, 14, pp. 77-111.

McGowen, J. H., and Groat, C. G. (1971) Van Horn Sandtone, West Texas: An Alluvial Fan Model for Mineral Exploration, Bureau of Economic Geology, Austin, TX, Report of Investigation No. 72, p.57.

Meetei L. I., Pattanayaka S. K., Bhaskara A., Pandita, M. K. and Tandonb S. K. (2007) Climatic imprints in Quaternary valley fill deposits of the middle Teesta valley, Sikkim Himalaya, Quaternary International 159, pp. 32–46.

Miall, A. D. (1978) Fluvial Sedimentology: a historical review, Can. Soc. Petrol. Geol. Mem., 5, pp. 1-47.

Miall, A. D. (1984) Principles of Sedimentary Basin Analysis, Springer-Verlag, New York.

Miall, A. D. (1996) The Geology of Fluvial Deposits, Sedimentary facies, Basin Analysis, and Petroleum Geology, Springer-Verlag, Germany.

Middleton, G. V. (1973) Johannes Walther's Law of Correlation of Facies, Bulletin Geological Society of America, 84, pp. 979-988.

Middleton, V., and Southward, S. (1978) Mechanics of Sediment Movment, Society of Economic Paleontology, Mineralogists Short Course, 3, p. 246.

Morton, A. C., Meinhold, G., Howard, J. P., Phillips, R. J., Strogen, D., Abutarruma, Y., Elgadry, M., Thusu, B., and Whitham, A. G. (2011) A Heavy Mineral Study of Sandstones from the eastern Murzuq Basin, Libya: Constraints on Provenance and Stratigraphic Correlations, Journal of African Earth Sciences, 61, pp. 308-330.

Mukul, M., Jade, S., Ansari, K., and Matin, A. (2014) Seismotectonic implications of strike-slip earthquakes in the Darjeeling-Sikkim Himalaya, Current Science, 106 (2), pp. 198-210.

Nandy, D. et al. (1993) Bihar-Nepal Earthquake, 20 August, 1988, Geological Survey of India, 31, p. 104.

Reading, H.G. (1986) Sedimentary Environments and Facies, Blackwell Scientific Publications, Oxford London, 2nd Ed.

Reineck, H. E., and Singh, I. B. (1980) Depositional Sedimentary Environments, Sprniger-Verlag, Berlin, p. 549.

Roy, M. K., Ahmed, S. S., and Saha, S. (2001) Sedimentology of a River-Dominated Estuary, South-Eastern Bangladesh, Proceedings of the International Seminar on Quaternary Development and Coastal Hydrodynamics of the Ganges Delta in Bangladesh, Geological Survey of Bangladesh, pp. 127-149.

Roy, M. K., Jahan, C. S., and Saha, S. (2004b) Holocene Sequence Stratigraphy in a Part of the Meghna Estuary and Ganges Delta, South Central Bangladesh, Institute of Landscape, Ecology and Ekistics, Department of Geography, University of Calcutta, India, 27, pp. 87-94.

Roy, M. K., Karmakar, B. C, Saha, S., and Chaudhuri (2004a) Facies and Depositional Environment of the Dupitila Formation, Dupitila Hill Range, Jaintiapur, Sylhet, Bangladesh, Journal of Geological Society of India, 63(2), pp. 139-157.

Rust, B. R., and Koster, E. H. (1984) Coarse Alluvial Deposits, In: Walker, R. G. (ed.) Facies Models, 2nd Ed., Geosciences Canada, Geological Association of Canada, Reprint Series 1, pp. 53-69.

Saha S., Reza, A.H.M.S. and Roy M.K., 2019 Hydrochemical evaluation of the groundwater quality of the Tista floodplain, Rangpur, Bangladesh: Applied Water Science, 9,198. https://doi.org/10/1007/s13201-01-1085-7

Saha S., Roy M.K. and Reza, A.H.M.S., 2017 Textural Characteristics of the Sediments of the Tista River, Rangpur, Bangladesh: Journal of Life and Earth Sciences 12, pp. 73-79, 2017, JLES, RU.

Starkel, L., Ploskonka, D., and Adamiec, G. (2015) Reconstruction of Late Quaternary Neotectonic Movements and Fluvial Activity in Sikkimese-Bhutanese Himalayan Piedmont, Studia Geomorphologica Carpatho-Balcanica, XLIX, pp. 71-82.

Teichert, C. (1958) Concept of Facies, Bulletin American Association of Petroleum Geologists, 42, pp. 2718-2744.

Udo, I. G., and Mode, A. W. (2013) Sedimentary Facies Analysis of Conglomerate Deposits in Northeastern Part of Akwa Ibom State, Niger Delta Basin, Nigeria, The International Journal of Engineering and Science, 2 (11), pp. 79-90.

UNDP (United Nations Development Programme) (1982) Groundwater survey: The hydrogeological conditions of Bangladesh. UNDP Technical Report DP/UN/BGD-74-009/1.

Walker, R. G. (1984) Facies Models, Geoscience, Canada, 2nd edition.

Walker, R. G. and Cant, D.J., (1984) Sandy fluvial systems, 71-89. In: Walker,R.G.(Ed.) Facies models: Geoscience Canada Reprint Series 1, Geological Association of Canada.

Wasson, R. J. (1977) Last Glacial Alluvial Fan Sedimentation in the Lower Derwent Valley, Tasmania, Sedimentology, 24(6), p. 781-799.

Wiejaczka, L., Bucala, A., and Sarkar, S. (2014) Human role in shaping the hydromorphology of the Himalayan rivers: study of the Tista River in Darjeeling Himalaya, Current Science, 106 (5), pp. 717-724.

Received: 19th April, 2020
Revised Accepted 26th July, 2021

JOURNAL INDIAN ASSOCIATION OF SEDIMENTOLOGISTS ISSN NO 2582 – 2020
Vol. 38, Issue 2, 2021, pp. 15-24
DOI: **https://doi.org/10.51710/jias.v38i2.115**

A Mass Balance Approach in Sediment Budgeting of Large Alluvial Rivers with special emphasis on the Brahmaputra in Assam

Lalit Saikia[1]and Chandan Mahanta[2]
*[1]Department of Earth Science, University of Science and Technology, Meghalaya, India; Email: lalitsaikia@yahoo.com, Email: lalitsaikia2008@gmail.com
[2]Department of Civil Engineering, Indian Institute of Technology Guwahati, India;
Email: mahantaiit@gmail.com

Abstract:

Morphology of an alluvial river channel is the consequence of erosion, sediment transport and sedimentation in a river. Sediment budget accounts for the sources, sinks and redistribution pathways of sediments, solutes and nutrients in a unit region over unit time. Human activities are the most important factors that affect the variation in the pattern of river sediment load. This paper discusses sediment budget of a few large rivers by review of literature and estimation of sediment budget of Brahmaputra River in Assam using mass balance approach. An attempt has also been made to discuss human and climatic impact on sediment load of major rivers of the world. Total sediment load in the Brahmaputra River at downstream location (India-Bangladesh border) was estimated to be 814×106 t/year. Considering 10% of sediment load of the Brahmaputra as bed load, suspended sediment load at downstream was estimated to be 733×106 t/year. Tributaries, bank erosion and scouring of river bed were found to contribute 52%, 27% and 21% respectively to sediment load of Brahmaputra at downstream locations. In spite of limitations of the dependable data, future complexity due to climate change impact and hydropower dam initiative in upstream of the River, the study is a simplified approach in sediment budgeting of the Brahmaputra.

Key words: Sediment budget, Brahmaputra, Assam.

INTRODUCTION

Sediment is naturally occurring substance, originally derived from underlying bedrocks, which is broken down by weathering and erosion and is subsequently transported by the action of fluids such as wind, water or ice and/ or by the force of gravity acting on the particle itself. Although the term is often used to indicate soil-based mineral matter, decomposing organic substances and inorganic biogenic materials are also considered as sediment (Wetzel, 2001). Mineral sediments come from erosion and weathering, while organic sediment is typically detritus and decomposing material such as algae (EPA, 2014). Coarse materials are transported as bed load along the bed of a river through rolling, sliding or saltation. Finer materials are carried aloft, suspended above the channel bed by turbulent eddies, and is transported downstream as suspended load and wash load by the process of advection and turbulent diffusion. There is a balance, described as a qualitative equation by Lane (1959), between the supply of bed load at the upstream end of a channel reach and the stream power available to transport it. If both the variables are balanced, neither erosion nor deposition will predominate. Increase of volume of the sediment load in relation to the available stream power leads to aggradations with net deposition along the reach. When the stream power exceeds, degradation predominates. Sediments accumulate on flood-plain surfaces by various processes of accretion, i.e., vertical, lateral and braid bar accretion (Nanson and Croke, 1992).

The concept of 'Sediment budget' was coined in Norway (Rapp, 1960) and in the USA in the 1970-80's to account the sources, sinks and redistribution pathways of sediments, solutes and nutrients in a unit region over unit time (Slaymaker, 2003). Construction of detailed sediment budgets (Walling and Collins, 2008) relies on the mean values of the sediment load calculated at the catchment outlet. This paper discusses sediment budget of a few large rivers of the world namely the Amazon, the Mississippi, the Nile, the Yangtze and the Yellow, followed by estimation of sediment budget of Brahmaputra River in Assam, using mass balance approach.

Material and Methods

The study on sediment budget of a few large riversnamely the Amazon, the Mississippi, the Nile, the Yangtze and the Yellow River is based on review of literature. Estimation of sediment budget for the Brahmaputra River in Assam, India is attempted using a mass-balance approach from secondary data.

There are a few limitations in collecting secondary data related to Brahmaputra River:

I. Non-availability of enough hydrological data for Brahmaputra and its tributaries, particularly in Assam plains.
II. Most of the available data is discrete, i.e., confined to particular site or location and not continuous. Several organisations/

departments such as Brahmaputra Board, Water Resources Department, Assam PWD, Central Water and Power Commission, Joint River Commission, etc. are dealing with different hydrological aspects of Brahmaputra; with the result that data remained dispersed in different offices and is difficult to locate and access.

Construction of a sediment budget for the Brahmaputra in Assam is attempted using a broad mass balance approach:

Total sediment in a channel at a downstream cross section = Sediment contribution from main stream and tributaries + sediment contribution from river bank erosion + sediment contribution from scouring – sediment deposition on river bed– sediment deposition on river bank – sediment deposition on floodplains

Sediment data were collected from different sources as follows:

1. Sediment load of tributaries of the Brahmaputra were considered from work of Pahuja and Goswami (2006).
2. 60% sediments from the tributaries were considered to contribute to sediments of Brahmaputra (after Goodbred and Kuehl, 1998; Goodbred and Kuehl, 1999; Liu et al., 2009)
3. Sediment input from bank erosion and sediment sink due to deposition on river banks were calculated from erosion and deposition data for the period 1973 – 2014 (Saikia et al., 2019).
4. Annual inputs from scouring and sediment deposition on river bed were calculated from aggradation and degradation data of the Brahmaputra for the period 1957 – 1989.

Similar mass - balance equation with different data sources was used in the Yangtze River for quantitative estimation of the contribution of the river mouth reach to the sediment load before and after impoundment of the Three Gorges Dam (Wang et al., 2015).

RESULTS AND DISCUSSIONS

Sediment Budget of the Amazon River

The Amazon River accounts for almost one-fifth of global freshwater discharge (Callède et al 2010) and supplies 40% sediment flux of the Atlanttic ocean (Milliman and Farnsworth 2011). Amount of sediment transported by the Amazon River to ocean was estimated to be about 1200×10^6 tons. Erosion in the Andes mountains is the main source of sediments. Almost half of the Amazon River transport (488×10^6 t/y) is attributable to one tributary, the Rio Madeira (Martinelli et al., 1989).

The fluvial transport and storage of sediments within channel–floodplain systems can act as an important sinks of sediments. In Amazon River, the floodplains act as a temporary storage system of dissolved and particulate elements as well as an exporting system of these elements into the main stream during floods (Maurice-Bourgoin et al., 2007). Dunne et al. (1998) estimated the magnitude of sediment exchange between the channel and the flood plain through the Brazilian sector of Amazon River valley based on sediment sampling and flow records. Deposition on the sand bars and floodplain exceeded bank erosion by 500 Mt y^{-1} over a 10–16year period. Another 300–400 Mt y^{-1} were deposited in a downstream delta plain. Maurice-Bourgoin et al. (2007) documented the role of an Amazon floodplain for sediment storage from studies on network of gauging, meteorological and sediment monitoring stations and satellite data. The area under discussion is, located on the right bank of Amazon River, 900 km upstream of the mouth, contains more than 30 interconnected lakes linked to the mainstream by permanent and temporary channels. With an open-water area varying between 600 km^2 and 2500 km^2, it represents ~13% of the total flooded area of Amazon River. Sediment accumulation occurred during the five months of the flood rise, from December to April. The mean average sediment storage calculated varies between 41% and 53% of the annual flux of sediments entering the floodplain through the main channels.

Martinez et al. (2009) attempted to quantify Amazon River sediment budget from suspended sediment discharge monitoring network and remote sensing data. Suspended sediment discharge was found to increase by about 20% during 12 years from 1995. An increase in sediment discharge may be attributed to stronger erosion processes caused either by a global change (rainfall), or regional changes (land cover change resulting from deforestation for example) or both.

Sediment Budget of the Mississippi River

The Mississippi River can be divided into three sections: the Upper Mississippi River, the Middle Mississippi River and the Lower Mississippi River. The lower Mississippi River transports approximately 150 million tons of sediment annually (Thorne et al., 2008). Historically, the quantity and caliber of sediment derived from catchment erosion have been affected by changes in land-use and River management. Knox (2006) used ^{14}C and ^{137}Cs isotopic dating methods to estimate sedimentation rate and and morphologic change for a reach of the upper Mississippi River. The shift from pre-agriculture, natural land cover to landscape dominance by agricultural land use of the last 175–200 years typically increased rates and magnitudes of floodplain sedimentation in the Upper Mississippi Valley. Large floods have frequently provided major increments of sedimentation on floodplains of tributaries and the main valley upper Mississippi River. Recently, modification of River flow by flood control structures and a reduction of sediment supply by upstream dams and artificial levees have greatly reduced sediment supplied to deltaic wetlands.

Sediment Budget of the Nile River

The Nile is the longest river in the world stretching more than 6800 km across north-eastern Africa (Fielding et al., 2018) to its delta in Egypt on the Mediterranean Sea. The Nile has three main tributaries: the White Nile, the Blue Nile and the Atbara. Sediment supplied to the Nile trunk in Egypt is dominated by contributions from the Blue Nile (50–61%) and Atbara (30–42%) (Padoan et al., 2011). Major portion of White Nile sediment load is trapped in swamps in South Sudan and do not reach the main Nile trunk, thus accounting for less than 3% of the sediment reaching the modern delta. ElMonshid et al (1997) estimated the sediment load of the Blue Nile at the entrance of the river to Sudan to be 140 million tons per year (Ahmed, 2008). Detritus supplied to the Nile trunk is derived from the volcanic Ethiopian highlands, Precambrian basement rocks and Phanerozoic sedimentary cover that blankets much of the region, together with a contribution from Aeolian sources (Fielding et al., 2017). However little is known about the changing influences of tectonics and climate through time (Paul et al., 2014; Woodward et al., 2015).

Sediment Budget of the Yangtze River

The Yangtze is the largest River in China and ranks the third in the world (He et al., 2012). In the Yangtze River, the amount of sediment discharged to the East China sea accounts for 68% of the total sediment supplied into the trunk River in the middle and lower reaches. The remaining 32% is deposited in the River channel and linked lakes. Dai and Lu (2010) examined the sediment process in two large flood years, i.e., 1954 and 1998 based on the re-evaluated sediment supply from the tributaries and the data from selected gauge stations on the main channel. Total supplied sediments of 58% and 52% were deposited in the river channel and floodplain in 1954 and 1998 respectively. The floodplains and channels in the middle and lower reaches of Yangtze River played an important role in regulating sediment discharge during extreme flood events.

Sediment Budget of the Yellow River

The Yellow River was once the world's largest sediment carrying River and peaked at about 1.6 Gt /yr in the middle of the twentieth century. Butthe river is one exception where erosion and sediment delivery have successfully been reduced (Wang et al., 2016). For control of soil erosion and ecosystems restoration in an effective way, the Chinese government has adopted various measures and policies like construction of silt dams (Zhao et al., 2016; Jin et al., 2012), reservoirs (Huang et al., 2019), terraces (Liu et al., 2018) and policy of returning farmland to forests (Deng 2014; Zhou et al., 2009). These measures have altered sediment supply in natural watersheds and the geomorphology of rivers, thereby affecting the soil erosion and drastically reducing sediment load in the Yellow River (Yu et al., 2013). Nearly 90% of the sediment load was originated and transported from the Loess Plateau in the middle reach (Wang et al., 2007). The current input of sediment from the Loess Plateau is less than one quarter of what it was before 1980 (Wang et al., 2016) and the sediment export to the ocean is now only 10.7% of the 1950s' level (Yu et al., 2013).

Sediment Budget of the Brahmaputra River in Assam, India

Originated as the Yarlung Tsangpo from Angsi glacier near Manasarovar lake in the Kailash range in southern Tibet, the Brahmaputra a transboundary river flowing to the Bay of Bengal through China (Tibet), India and Bangladesh. The Brahmaputra basin in India is shared by Arunachal Pradesh (41.9%), Assam (36.3%), Nagaland (5.5%), Meghalaya (6.1%), Sikkim (3.7%) and West Bengal (6.5%) (Ojha and Singh, 2004). The Brahmaputra is an extremely dynamic, predominantly braided river. The river is unique due to peculiar drainage pattern through diverse environments, high sediment load, critical flood and bank erosion problem. Sediment yield of Brahmaputra (852.4 t/km2 /y) is the highest in the world (Latrubesse, 2008). Causes of high sediment load in the river are young lithology, seismicity, unconsolidated sedimentary rocks of the Himalayas, steep slope of the river and tributaries, heavy rainfall in monsoon months (June -- September), deforestation and faulty land use practice like jhum cultivation and forest fire.

Wasson (2003) attempted construction of an approximate sediment budget for the Ganga-Brahmaputra catchment based on published data and Nd/Sr tracer results. Subramanian and Ramanathan (1996) reported highly variable sediment load of Brahmaputra River ranging from 402 to 710 million t/y^{-1}. Islam et al. (1999) estimated suspended load flux ranging from 402 to 1157 million t/y^{-1} for the Brahmaputra to the Bay of Bengal. In this paper, sediment budgeting is studied from a mass balance approach.

Sediment input from tributaries of the Brahmaputra River in Assam

The major Rivers and tributaries within the state of Assam with high sediment load are shown in Figure 1.

Volume of sediments to the Brahmaputra River from tributaries in a year (from Pahuja and Goswami, 2007) = 51,316 ha m = 513.2×10^6 m^3.

Considering sediment density 1.36 g/cm^3 from Agarwal and Singh (2007), mass of suspended sediments collectively contributed by tributaries in a year was found to be 698×10^6 t.

Floodplains are important sites for sediment storage in fluvial systems (Phillips, 1992; Steiger et al., 2001; Noe and Hupp, 2009). Approximately one third of the annual sediment load of the Ganges-Brahmaputra is deposited in the river flood-plains (Goodbred and Kuehl, 1998; Goodbred and Kuehl, 1999). Liu et al. (2009) mentioned that 30-50% River-derived sediments of the Tibetan Rivers like Yellow, Yangtze, Brahmaputra, Ganges, Indus, Mekong and Irrawaddy are trapped in the river's low reaches and contribute to extensive floodplain and delta plain development.

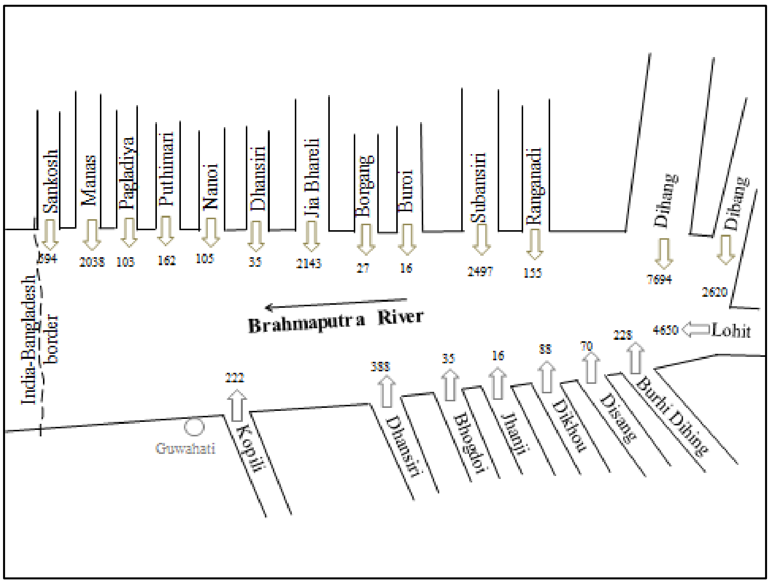

Figure 1. Rivers/ tributaries within Assam with high sediment load
**(The numbers indicate annual average suspended sediment load in ha m)*river deposits in the Tista Fan, Bangladesh

Sediment deposited on river bed and floodplain =279×10^6 t (i.e., 40% of 698×10^6 t, considering trapping of 40% of riverine sediments)
Net sediment contribution from all rivers/ tributaries to total sediment at downstream location = 419×10^6 t (60% of total sediments).

Sediment contribution from scouring of river bed

Development and movement of scour have significant influence on the total sediment transports in the Brahmaputra; they may equate up to 25% of total sediment transports in Brahmaputra (FAP24, 1996).

Scour during 1957 – 1989 = 5649.6 × 10^6 m^3
Scour in a year = 5649.6×10^6 m^3/32 =177×10^6 m^3
Mass of sediment from scouring = 241×10^6 t

Sediment deposition on river bed

Deposition in bed during 1957–1989 = 1625×10^6 m^3
Volume of deposition in a year = 1625×106 m^3/32 = 51×106 m3
Mass of deposited sediment in a year = 69×10^6 t

Sediment contribution from river bank erosion

From Saikia (2017), bank erosion in the Brahmaputra in 41 years (1973 – 2014) = 1557 km^2
Thus, bank erosion in a year = 1557 km^2/41 = 38 km^2 = 38×10^6 m^2. Average difference of yearly observed highest and the lowest water levels of Brahmaputra for the period 1914 – 1990 was 4.7 m. Assuming depth of bank erosion as 4.7 m, volume of bank erosion in a year = 179×10^6 m^3
Mass of eroded materials = 243×10^6 t

Sediment deposition in banks

From Saikia (2017), total deposition in Brahmaputra (Between Dibrugarh and Dhubri in Assam) during 1973–2014 = 204 km^2
Bank deposition in a year = 204 km^2/41 = 4.97 km^2 = 4.97×10^6 m^2
Garzanti et al. (2010) suggested that dominant bedform in Brahmaputra are sand dunes with heights ≤6 m and wavelengths (λ) ≤330 m. Considering sandbars as spherical domes of height 6 m and radius of base 82.5 m (half of λ/2), average height of deposition is 3 m.

Volume of deposition = 15×10^6 m^3
Mass of deposited sediments = 20×10^6 t

Now, Total sediment in a channel at a downstream cross section = Sediment contribution from main stream and tributaries + sediment contribution from River bank erosion + sediment contribution from scouring – sediment deposition on River bed–sediment deposition on River banks & floodplains
= 419×10^6 t + 243×10^6 t + 241×10^6 t – 69×10^6 t – 20×10^6 t= 814×10^6 t

Lane and Borland (1951) postulated that suspended load of a river carries 90% of the sediment, while bed load transport accounts for approximately 10% of sediment. Thus, 90% of the total suspended sediment load at a catchment outlet may be explained by the total amount of sediments coming from upstream nested catchments (Gay et al., 2014). Considering 10% of sediment load of Brahmaputra as bed load, suspended sediment load at downstream is 733×10^6 t (90% of 814×10^6 t).

Table 1. Sediment load of Brahmaputra from different studies

Suspended sediment load (10^6 t y^{-1})	Reference	Gauging stations/ sampling locations	Period of measurement
617	Coleman, 1969	Bahadurabad, Bangladesh	1958 – 1962
541	BWDB, 1972	Bahadurabad, Bangladesh	1967 – 1969
1157	Milliman and Meade, 1983	Bahadurabad, Bangladesh	1966 – 1967
402	Goswami, 1985	Pandu, Assam	1955 – 1979
650	Hossain, 1992	Bahadurabad, Bangladesh	1982 – 1988
721	Islam, 1999	Bahadurabad, Bangladesh	1989 – 1994
595-672	Darby et al., 2015	Bahadurabad, Bangladesh	1981 – 1995
733	Present study	Secondary data compiled from multiple sources	Different period for different data

Based on these estimates, a schematic sediment budget for Brahmaputra in Assam can be arrived at Fig. 2.

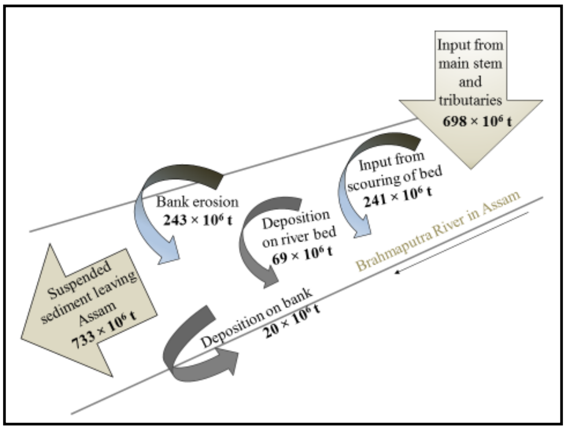

Figure 2. A schematic diagram to show sediment budget for Brahmaputra River in Assam

Sediment deposition on river bed/ banks and contribution to sediment load from different sources are shown in Figure 3. Tributaries including the main stem are the major contributor of sediment in Brahmaputra. More than half of total sediment of Brahmaputra at downstream (i.e., 52%) comes from the main stem and the tributaries (Figure 4). Calculated mass of eroded materials from bank erosion in a year was 243×10^6 t. Amount of yearly deposition on River bank and floodplains was 20×10^6 t. 223×10^6 t sediments (27%) were contributed to annual sediment load of the River from bank erosion.

Major contribution (52%) of sediment loads

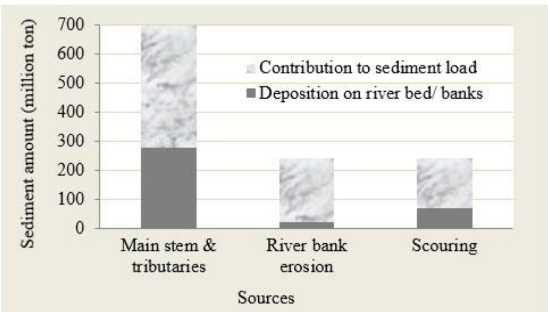

Figure 3. Deposition of sediment and contribution to sediment load to the Brahmaputra from different sources

from bank erosion is common in most of the rivers (Bull, 1997; Church and Slaymaker, 1989; Lawler et al., 1999). But sediment load of Brahmaputra can't be compared with that of other Tibetan rivers like Yellow and Yangtze in case of sediment input from bank erosion. In Yellow River, bank-to-channel sediment transfer process was found to cause the overall increase in channel deposition with little influences on the down-stream suspended sediment load and transport (Ta et al., 2013). A remote sensing investigation on a 1479 km-long reach of Yangtze River for the period of 1970 – 1998 indicated that volume of bank failure (267×106 m3) and volume of

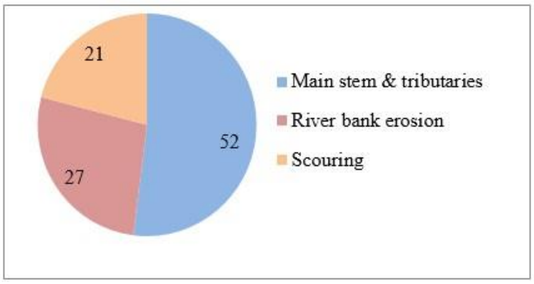

Figure 4. Percent contribution to sediment load of the Brahmaputra from different sources

bed deposition (291×106 m3) was almost same (Xu et al., 2001). But, in case of Brahmaputra, volume of bank erosion in a year (243×106 m3) was more than ten times of volume of deposition (20×106 m3).

Modified Sediment Load due to Human Interventions

Human activities are the most important factors that affect the variation in the pattern of river sediment load (Syvitski et al., 2005; Walling, 2006). Liu et al (2008) showed that the average annual sediment yield per area has been decreased significantly in Yellow River over the past 10 years mainly due to impacts of human activities, including the operation of hydropower stations/ reservoirs, construction of dams, as well as soil conservation programs. Liu et al. (2008) showed marked decrease in annual sediment yield at the Lijin Station on the Yellow River in 1961, 1980 and 2000. Before 1960, Yellow River was under essentially natural conditions. From 1960 to 1964, the Sanmenxia reservoir was in operation for impounding water and trapping sediment. Thus, annual sediment transport downstream decreased dramatically. From 1965 to 1973, the operating mode of the Sanmenxia reservoir was changed to provide flood detention and sediment flushing. Thus, both annual sediment transport and runoff increased during this period. From 1974 to 1985, the operating mode of the Sanmenxia reservoir was further modified to provide for "storing clear water during low flow seasons and releasing turbid water during flood periods". Since 1980, due to increased water consumption by agriculture and industry and soil and water conservation projects, both annual sediment transport and runoff on the Lower Reach of the Yellow River decreased significantly (Liu et al., 2008).

During the past 50 years, the sediment loads are in increasing trend in most of the upstream stations of the Yangtze River basin, but in decreasing trend at other stations (Zhang et al., 2006). Studies by Xu and Milliman (2009) revealed that after the impoundment of the Three Gorges Reservoir (TGR), 60% of the sediment entering the TGR was trapped in flood seasons. Downstream of the TGR, substantial channel erosion is significant. However, downstream channel erosion (70 Mt/y) has not yet counteracted TGR trapping (118 Mt/y) and sediment delivered to the Yangtze estuary will probably continue to decrease.

Amazon River, Nile River, Mississippi River and Red River are other examples where reservoirs and dam construction has changed sediment dynamics of the floodplains. Expansion of hydropower and agricultural activity have recently modified Amazon's land surface processes (Forsberg et al., 2017; Latrubesse et al., 2017; Anderson et al., 2018), which have implications on discharge and sediment flux in the Amazon River (Nobre et al 2016). Fine suspended sediments flux in the Amazon River was found to be linked to rainfall and higher coarse suspended sediment flux was related with discharge. Hence, climatic conditions that control rainfall input have profound impact on discharge and sediment flux of a river (Armijos et al., 2020).

Before the High Aswan dam, the Nile River carried an average of 124 million ton of sediment to the sea in a year, and deposited another 9.5 million tons on the flood plain. But due to construction of that dam, 98% of the sediment goes to the bottom of the Nasser reservoir (Billi, 2010). In Mississippi River, prior to 1930s, the floodplain was the major sediment source. But due to human modifications in terms of dams & reservoirs, artificial levees, dikes, concrete revetments and a series of channel cutoffs, floodplain provides only a minor amount of sediments today. Major degradation to the channel including the growth of channel bars has occurred as a result of these engineered modifications (Kesel, 2003). Similarly, the impoundment of two large reservoirs in the Da and the Lo watersheds in the 1980s has resulted in a considerable reduction (70%) of the total suspended load carried to the sea by the Red River (Le et al., 2007).

Sediment load in rivers has changed significantly due to climate change impacts and human activities like economic development, industrial restructuring, population migration, and urbanization. Urbanization rate is found negatively correlated with sediment load and cultivated land area is found positively correlated with sediment load. The decrease of cultivated land area in many river basins makes the sediment load gradually decrease (Zhong et al., 2020). About 50% of the world's rivers show a significant decline in river sediment load (Roy et al., 2017; Vigiak et al., 2017; Zhao et al., 2017; Liu et al., 2019; Shi et al., 2019), affecting the structure, processes, and functions of societies and ecosystems (Syvitski et al., 2005; Ukkola et al., 2015; Walling et al., 2003).

Generic conclusions on sediment load by Brahmaputra River system is near to impossible due to wide diurnal, seasonal and annual variations in the sediment-carrying capacity of the river (Subramanian and Ramanathan, 1996). Paucity of dependable data for the main stem and tributaries also bring lot of uncertainty to sediment quantification for the Brahmaputra River.

Sediment transport in the Brahmaputra River is highly controlled by the monsoon regime with large depositional fluctuations within the braided channels (Roy and Sinha, 2014) resulting change in morphology of the river by flood and bank erosion. The Brahmaputra valley has been facing a heavy instability of landmass due to river bank erosion, believed to be accelerated after the 1950 earthquake. After the declaration of National Policy in 1954, a huge network of flood embankments along Brahmaputra and its tributaries was erected across the state. As of December, 2018, length of embankments in the state of Assam is 4486.44 km out of which 1031.8 km is in the Brahmaputra river. Flood and erosion prevention attempts by embankments to secure floodplain communities would result in higher velocities and increased scour and erosion from a smaller cross-sectional area. Mosselman (2006) observed increased erosion rate in the Brahmaputra, particularly where bank protection measures were applied.

Climate change impact (ICIMOD, 2009) and hydropower dam initiative in upstream of Brahmaputra, i.e., Arunachal Pradesh (The Ecologist Asia, 2003), has added further complexity in the sediment flux regime of the river. Fischer et al. (2017) estimated increase of sediment load of the Brahmaputra River due to projected climate change induced high water discharge by 40% by the end of the century (2075–2100) compared to levels in 1986–1991. Again, the construction of reservoirs can considerably reduce the sediment load (Walling and

Fang, 2003), and large-scale damming of the upper Brahmaputra and its tributaries could counteract the increase in sediment delivery to the delta.

SUMMARY AND CONCLUSIONS

Sediment dynamics of the major rivers of the world are changing due to climate change impacts and anthropogenic activities particularly dam construction, population migration, agriculture, urbanization and engineered modification for channel improvement. Based on the mass balance approach, contribution of tributaries, bank erosion and scouring to suspended sediment of Brahmaputra at Indo-Bangladesh border are 52%, 27% and 21% respectively.

Major limitation of the present sediment budget for the Brahmaputra River in Assam is that, data for different components were from different sources and different periods and have different reliabilities, which might lead to the uncertainty associated with the results presented herein. River bank protection by embankments, dam initiatives in the upstream of the river and potential climate change impacts have added further complexity in sediment flux regime of the Brahmaputra River. Attention is essential on sediment management in a river to restore and rejuvenate the structure, processes, and functions of societies as well as ecosystem and management of flood & bank erosion hazards.

Acknowledgement

This paper is modified version of a part of the PhD thesis of the first author in the Department of Civil Engineering at IIT Guwahati. The author highly acknowledges Lakshminath Bezbaroa Central Library and Computer Centre of IIT Guwahati for support and facilities during his PhD programme.

References

Ahmed, A. A. (2008). Sediment in the Nile River System, UNESCO-IHP-International Sediment Initiative, Khartoum- Sudan. p. 29.

Agarwal, P. K. and Singh, V. P. (2007). Brahmaputra and Barak Basin. In Agarwal P. K., Jain S. K. and Singh V. P. (eds.), Hydrology and Water Resources of India, Springer, p. 437.

Anderson, E. P., Jenkins, C. N., Heilpern, S., Maldonado-Ocampo, J. A., Carvajal-Vallejos, F. M., Encalada, A. C. and Salcedo, N. (2018). Fragmentation of Andes-to-Amazon connectivity by hydropower dams. Science Advances, v. 4(1), eaao1642.

Armijos, E., Crave, A. Espinoza, J. C., Filizola, N., Espinoza-Villar, R. , Ayes, I., Fonseca, P., Fraizy, P., Gutierrez, O., Vauchel, P., Camenen, B., Martıınez, J. M., Dos Santos, A., Santini, W., Cochonneau, G. and Guyot, J. L. (2020). Rainfall control on Amazon sediment flux: synthesis from 20 years of monitoring. Environmental Research Communications, v. 2. 051008

Billi, P. and Ali, Omer el B. (2010). Sediment transport of the Blue Nile at Khartoum. Quaternary International, v. 226 (1-2), p.12-22.

Bull, L. J. (1997). Magnitude and Variation in the Contribution of Bank Erosion to the Suspended Sediment Load of the River Severn, UK. Earth Surface Processes Landforms, v. 22(12), p. 1109-1123.

BWDB (1972). Sediment Investigations in Main Rivers of Bangladesh, 1968 & 1969. BWDB Water Supply Paper No. 359. Bangladesh Water Development Board, Bangladesh.

Callède, J., Cochonneau, G., Alves, F. V., Guyot, J. L., Guirimães, V. S. and De Oliveira, E. (2010). Les apports en eau de l'Amazone à l'Océan Atlantique J. Water Sci. v. 23, pp. 247–73.[From Armijos et al. (2020]

Church, M. and Slaymaker, O. (1989). Disequilibrium of Holocene Sediment Yield in Glaciated British Columbia. Nature, v. 337, p. 452-454.

Coleman, J. M. (1969). Brahmaputra River: Channel Processes and Sedimentation. Sediment Geology, v. 3, p.129-239.

Dai, S. B. and Lu, X. X. (2010). Sediment Deposition and Erosion During the Extreme Flood Events in the Middle and Lower Reaches of the Yangtze River. Quaternary International, v. 226 (1-2), p. 4-11.

Darby, S. E., Dunn, F. E., Nicholls, R. J., Rahman, M. and Riddy, L. (2015). A first look at the influence of anthropogenic climate change on the future delivery of fluvial sediment to the Ganges–Brahmaputra– Meghna delta. Environ Sci Process Impacts, v. 17(9), pp. 1587–1600.

Deng, L. and Shangguan, Z.P., and Sweeney, S. (2014). "Grain for Green" driven land use change and carbon sequestration on the Loess Plateau, China. Sci. Rep., v. 4, p. 7039.

Dunne, T., Mertes, L. A. K., Meade, R., Richey, J. E. and Forsberg, B. R. (1998). Exchanges of Sediment Between the Flood Plain and Channel of Amazon River in Brazil. GSA Bulletin, v. 110 (4), p. 450-467.

Elmonshid, El. and Ahmed, S. E. (1997). Environmental effect of the Blue Nile Sediment on reservoirs and Irrigation Canals [Conference] // Int. 5th Nile 2002 Conf. -Addis Ababa-Ethiopia.

EPA (2014). Sediments. In Water: Pollution Prevention & Control. Assessed from http://water.epa.gov/ polwaste/ sediments on 22/06/2018

FAP 24 (1996). Final Report, Main Volume. Water Resource Planning Organisation, Dhaka, Bangladesh.

Fielding, L., Najman, Y., Millar, I., Butterworth, P., Ando, S., Padoan, M., Barfod, D., Kneller, B. (2016). A detrital record of the Nile River and its catchment. Journal of the Geological Society, v. 174(2), pp. 301–317.

Fielding, L., Najman, Y., Millar, I., Butterworth, P., Garzanti, E., Vezzoli, G.,Barfod D. and Kneller, B. (2018). The initiation and evolution of the River Nile. Earth and Planetary Science Letters, v. 489, pp. 166-178.

Fischer, S., Pietron, J., Bring, A. and Thorslund J. (2017). Present to future sediment transport of the Brahmaputra River: reducing uncertainty in predictions and management. Regional Environmental Change, v. 17, pp. 515-526.

Forsberg, B., Melack, J., Dunne, T., Barthem, R., Goulding, M., Paiva, R. C., Sorribas, M., Silva, U. and Weisser, S. (2017). The potential impact of new Andean dams on Amazon fluvial ecosystems. PLoS One, 128 e0182254

Garzanti, E., Andò, S., France-Lanord, C., Vezzoli, G., Galy, V. and Najman, Y. (2010). Mineralogical and Chemical Variability of Fluvial Sediments 1. Bed Load Sand (Ganga – Brahmaputra, Bangladesh). Earth and Planetary Sciences Letters, v. 299(3-4), pp. 368-381.

Gay, A., Cerdan, O., Delmas, M. and Desmet, M. (2014). Variability of Suspended Sediment Yields Within the Loire River Basin (France). Journal of Hydrology, v. 519, pp. 1225-1237.

Goodbred Jr, S. L. and Kuehl, S. A. (1998). Floodplain Processes in the Bengal Basin and the Storage of Ganges–Brahmaputra River Sediment: An Accretion Study Using Cs-137 and Pb-210 geochronology. Sedimentary Geology, v. 121(3), pp. 239-258.

Goodbred Jr, S. L. and Kuehl, S. A. (1999). Holocene and Modern Sediment Budgets for the Ganges-Brahmaputra River: Evidence for High Stand Dispersal to Floodplain, Shelf and Deep-Sea Depocenters. Geology, v. 27, pp. 559-562.

Goswami, D. C. (1985). Brahmaputra River, Assam, India: Physiography, Basin Denudation and Channel Aggradation. Water Resources Research, v. 21(7), pp. 959-978.

He, M., Zheng, H., Huang, X., Jia, J. and Li, L. (2012). Yangtze River sediments from source to sink traced with clay mineralogy. Journal of Asian Earth Sciences, v. 69, pp. 60-69.

Hossain, M. M. (1992). Total Sediment Load in the Lower Ganges and Jamuna. Journal of the Institution of Engineers, Bangladesh, v. 20(1-2), pp. 1-8.

Hu, B., Yang, Z., Wang, H., Sun, X., Bi, N. and Li, G. (2009). Sedimentation in the Three Gorges Dam and the Future Trend of Changjiang (Yangtze River) Sediment Flux to the Sea. Hydrology and Earth System Sciences, v. 13, p. 2253-2264.

Huang, L., Li, X., Fang, H., Yin, D., Si, Y. and Wei, J. (2019). Balancing social, economic and ecological benefits of reservoir operation during the flood season: A case study of the Three Gorges Project, China. Journal of Hydrology, v. 572, pp. 422–434

ICIMOD (2009). The Changing Himalayas, Impact of Climate Change on Water Resources and Livelihoods in the Greater Himalayas: preprint for discussion and comments, International Centre for Integrated Mountain Development, pp. 6-7.

Islam, M. R., Begum, S. F., Yamaguchi, Y. and Ogawa, K. (1999). The Ganges and Brahmaputra Rivers in Bangladesh: Basin Denudation and Sedimentation. Hydrological Processes, v. 13(17), pp. 2907-292.

Jin, Z., Cui, B., Song, Y., Shi, W., Wang, K. and Wang, Y. (2012). How many check dams do we need to build on the Loess Plateau. Environ. Sci. Technol, v. 46, pp. 8527–8528.

Kesel, R. H. (2003). Human Modifications to the Sediment Regime of the Lower Mississippi River Flood Plain. Geomorphology, v. 56(3-4), pp. 325-334.

Knox, J. C. (2006). Floodplain Sedimentation in the Upper Mississippi Valley: Natural versus Human Accelerated. Geomorphology, v. 79(3-4), p. 286-310.

Lane, E. W. (1959). A Study of the Shape of Channels Formed by Natural Streams Flowing in Erodible Material. Missouri River Division Sediment Series No. 9, U.S. Army Engineering Division Missouri River, Corps of Engineers, Omaha, Nebraska.

Lane, E. W. and Borland, W. M. (1951). Estimating Bed Load. Eos Trans, AGU, v. 32(1), pp. 121-123.

Latrubesse, E. (2008). Patterns of Anabranching Channels: The Ultimate End-Member Adjustment of Mega Rivers. Geomorphology, v. 101(1), pp. 130–145.

Latrubesse, E. et al. (2017). Damming the rivers of the Amazon basin. Nature, v. 546, pp. 363-369.

Lawler, D. M., Grove, J. R., Couperthwaite, J. S. and Leeks, G. J. L. (1999). Downstream Change in River Bank Erosion Rates in the Swale – Ouse System, Northern England. Hydrological Processes, v. 13(7), pp. 977-992.

Le, T. P. Q., Garnier, J., Gilles, B., Sylvain, T. and Van Minh, C. (2007). The Changing Flow Regime and Sediment Load of the Red River, Viet Nam. Journal of Hydrology, v. 334, pp. 199-214.

Li, X., Zhou, Y. X., Zhang, L. P., and Kuang R. Y. (2014). Shoreline Change of ChongmingDongtan and Response to River Sediment Load: a Remote Sensing Assessment. Journal of Hydrology, v. 511, pp. 432-442.

Liu, C., Sui, J. and Wan, Zhao-Yin. (2008). Sediment Load Reduction in Chinese Rivers. International Journal of Sediment Research, v. 23, pp. 44-55.

Liu, J. P., Xue, Z., Ross, K., Wang, H. Z., Yang, Z. S., Li, A. C. and Gao, S., (2009). Fate of Sediments Delivered to the Sea by Asian Large Rivers: Long-Distance Transport and Formation of Remote Alongshore Clinothems. The Sedimentary Record, v. 7(4), pp. 4-9.

Liu, C., Walling, D.E. and He, Y. (2018). Review: The International Sediment Initiative case studies of sediment problems in River basins and their management. Int. J. Sediment Res. v. 33, pp. 216–219

Liu, J.J., Zhou, Z.H., Yan, Z.Q., Gong, J.G., Jia, Y.W., Xu, C.Y. and Wang, H. (2019). A new approach to separating the impacts of climate change and multiple human activities on water cycle processes based on a distributed hydrological model. Journal of Hydrology, v. 578, pp. 1–13.

Martinelli, L. A., Victoria, R. L., Devol, A. H. et al. (1989). Suspended sediment load in the Amazon basin: An overview. GeoJournal v. 19, pp. 381–389.

Martinez, J. M., Guyot, J. L., Filizola, N. and Sondag, F. (2009). Increase in Suspended Sediment Discharge of Amazon River Assessed by Monitoring Network and Satellite Data. Catena, v. 79(3), pp. 257-264.

Maurice-Bourgoin, L, Bonnet, M. P., Martinez, J. M., Kosuth, P., Cochonneau, G., Moreira-Turcq, P., Guyot, J.L., Vauchel, P., Filizola, N. and Seyler, P. (2007). Temporal Dynamics of Water and Sediment Exchanges Between the Curuaí Floodplain and Amazon River Main Stream, Brazil. Journal of Hydrology, v. 335, pp. 140-156.

Miao, C. (2010). Recent Changes of Water Discharge and Sediment Load in the Yellow River Basin, China. Progress in Physical Geography, v. 34(4), pp. 541-561.

Milliman, J. D. and Meade, R. H. (1983). World-wide Delivery of River Sediment to the Oceans. The Journal of Geology, v. 91 (1), pp. 1-21.

Milliman, J. D. and Farnsworth, K. L. (2011). River Discharge to the Coastal Ocean, A Global Synthesis. Cambridge University Press, New York.

Mosselman, E. (2006). Bank protection and river training along the braided Brahmaputra–Jamuna River, Bangladesh. In: Sambrook Smith GH, Best JL, Bristow CS, Petts GE (eds) Braided rivers: process, deposits, ecology and management. Blackwell, Oxford, pp. 277–287.

Nanson, G. C. and Croke, J. C. (1992). A Genetic Classification of Floodplains. Geomorphology, v. 4, pp. 459-486.

Nobre, C. A., Sampaio, G., Borma, L. S., Castilla-Rubio, J. C., Silva, J. S. and Cardoso, M. (2016). Land-use and climate change risks in the Amazon and the need of a novel sustainable development paradigm. Fate of the Amazon forests and the Third Way, Proceedings of the National Academy of Sciences, v. 113 (39), pp. 10759-10768.

Noe, G. B. and Hupp C. R. (2009). Retention of Riverine Sediment and Nutrient Loads by Coastal Plain Floodplains. Ecosystems, v. 12, pp. 728–746.

Ojha, C. S. P. and Singh, V. P. (2004). Introduction. In Singh V., Sharma N. and Ojha C. S. P. (Eds.), The Brahmaputra Basin Water Resources, Springer Netherlands.

Pahuja, S. and Goswami, D. (2006). A Fluvial Geomorphology Perspective on the Knowledge Base Brahmaputra. Draft paper No. 3, Study of Natural Resources, Water and the Environmental nexus for development and growth in Northeast India, World Bank and Gauhati University.

Paul, J.D., Roberts, G.G., and White, N. (2014). The African landscape through space and time. Tectonics.

Phillips, J. D. (1992). The Source of Alluvium in Large Rivers of the Lower Coastal Plain of North Caroloina. Catena, v. 19(1), pp. 59-75.

Rapp, A. (1960). Recent Development of Mountain Slopes in Kärkevagge and Surroundings, Northern Scandinavi. Geografiska Annaler, v. 42(2-3), pp. 65-200.

Roy, E. D., Nguyen, N. T., White, J. R. (2017). Changes in estuarine sediment phosphorus fractions during a large-scale Mississippi River diversion. Sci. Total Environ. v. 609, pp. 1248–1257.

Roy, N. G. and Sinha, R. (2014). Effective discharge for suspended sediment transport of the Ganga River and its geomorphic implication. Geomorphology, v. 227, pp. 18–30.

Saikia, L. (2017). Sediment properties and processes influencing key geoenvironmental aspects of a large alluvial river, the Brahmaputra in Assam. PhD Thesis, Department of Civil Engineering, Indian Institute of Technology Guwahati.

Saikia, L., Mahanta, C., Mukherjee, A., Borah, S.B. (2019). Erosion-deposition and land use/ land cover of the Brahmaputra River in Assam, India. Journal of Earth System Science, v. 128, p. 211.

Shi, P., Zhang, Y., Ren, Z .Q., Yu, Y., Li, P. and Gong, J.F. (2019). Land-use changes and check dams reducing runoff and sediment yield on the Loess Plateau of China. Sci. Total Environ. v. 664, pp. 984–994.

Slaymaker, O. (2003). The Sediment Budget as Conceptual Framework and Management Tool. Hydrobiologia, v. 494(1-3), pp. 71-82.

Steiger, J., Gurnell, A. M., Ergenzinger, P. and Snelder, D. (2001). Sedimentation in the Riparian Zone of an Incising River. Earth Surface Processes and Landforms, v. 26, pp. 91–108.

Subramanian, V. and Ramanathan, A. L. (1996). Nature of Sediment Load in the Ganges-Brahmaputra River Systems in India. In Milliman J. D. and Haq B. U. (Eds.), Sea-Level Rise and Coastal Subsidence: Causes, Consequences, and Strategies, Kluwer Academic Publisher, pp. 151-168.

Syvitski, J. P. M., Vorosmarty, C. J., Kettner, A. J., and Green, P. (2005). Impact of Human on the Flux of Terrestrial Sediment to the Global Ocean. Science, v. 308, pp. 376–380.

Ta, W., Jia, X. and Wang, H. (2013). Channel Deposition Induced by Bank Erosion in Response to Decreased Flows in the Sand-Banked Reach of the Upstream Yellow River. Catena, v. 105, pp. 62-68.

The Ecologist Asia (2003). Some Proposed and Existing Dam Projects in Northeast India. The Ecologist Asia, v. 11(1), p. 48.

Thorne, C., Harmar, O., Watson, C., Clifford, N., Biedenharn, D. and Measures, R. (2008). Current and Historical Sediment Loads in the Lower Mississippi River: Report submitted to United States Army from School of Geography, University of Nottingham, p. iii.

Ukkola, A. M., Prentice, I. C., Keenan, T. F. (2015). Reduced streamflow in water-stressed climates consistent with CO2 effects on vegetation. Nat. Clim. Chang. v. 6, pp. 75–78.

Vigiak, O., Malagó, A. and Bouraoui, F. (2017). Modelling sediment fluxes in the Danube River Basin with SWAT. Sci. Total Environ. v. 599, pp. 992–1012.

Walling, D. E. and Fang, D. (2003). Recent trends in the suspended sediment loads of the world's Rivers. Glob. Planet Chang. v. 39, pp. 111–126.

Walling, D. E. and Collins, A. L. (2008). The Catchment Sediment Budget as a Management Tool. Environmental Science & Policy, v. 11(2), pp. 136-143.

Wang, C., Dai, S. B., Ran, L. S., Jiang, L. and Li, W. T. (2015). Contribution of River Mouth Reach to Sediment Load of the Yangtze River. Advances in Meteorology, Article ID 415058, Hindawi Publishing Corporation.

Wang, H. J., Yang, Z. S., Saito, Y., Liu J. P., Sun, X. X. and Wang, Y. (2007). Stepwise decreases of the Huanghe (Yellow River) sediment load (1950–2005): impacts of climate change and human activities. Global Planet Change, 57(3), pp. 331–354.

Wang, S., Fu, B. J., Piao, S. L., Lu, Y. H., Ciais, P., Feng, X. M., et al. (2016). Reduced sediment transport in the Yellow River due to anthropogenic changes. Nat. Geosci. v. 9(1), pp. 38–41.

Wang, Z. Y., Li, Y. and He, Y. (2007). Sediment Budget of the Yangtze River. Water Resources Research, v. 43(4).

Walling, D. E. (2006). Human Impact on Land-Ocean Sediment Transfer by the World's Rivers. Geomorphology, v. 79(3-4), pp. 192 – 216.

Wasson, R. J. (2003). A Sediment Budget for the Ganga-Brahmaputra Catchment. Current Science, v. 84(8), pp. 1041-1047.

Wetzel, R. G. (2001). Limnology: Lake and River Ecosystems., San Diego, CA, Academic Press.

Woodward, J., Macklin, M., Fielding, L., Millar, I., Spencer, N., Welsby, D. and Williams, M. (2015). Shifting sediment sources in the world's longest river: A strontium isotope record for the Holocene Nile. Quaternary Science Reviews, v. 130, pp. 124-140.

Xu, Y. N., Liang, Z. Y., Wang, X. D., Li, W. W. and Du, Y. Q. (2001). Analysis on Bank Failure and River Channel Changes. Journal of Sediment Research, v. 4, pp. 41-46.

Xu, K. and Milliman, J. D. (2009). Seasonal Variations of Sediment Discharge from the Yangtze River Before and After Impoundment of the Three Gorges Dam. Geomorphology, v. 104(3-4), pp. 276-283.

Yu, Y., Wang, H., Shi, X., Ran, X. and Cui, T. (2013). New discharge regime of the Huanghe (Yellow River): Causes and implications. Cont. Shelf Res. v. 69, pp. 62–72

Zhang, Q., Xu, C., Becke, S. and Jiang,T. (2006). Sediment and Runoff Changes in the Yangtze River Basin During Past 50 Years. Journal of Hydrology, v. 331(3-4), pp. 511-523.

Zhao, G.J., Kondolf, G.M. and Mu, X. (2016). Sediment yield reduction associated with land use changes and check dams in a catchment of the Loess Plateau, China. Catena, v. 148, pp. 1–17.

Zhao, Y.F., Zou, X.Q., Liu, Q. and Yao, Y. L. (2017). Assessing natural and anthropogenic influences on water discharge and sediment load in the Yangtze River, China. Sci. Total Environ. v. 607, pp. 920–932.

Zhou, H., Van Rompaey, A. and Wang, J. A. (2009). Detecting the impact of the "Grain for Green" program on the mean annual vegetation cover in the Shaanxi province, China using SPOT-VGT NDVI data. Land Use Policy, v. 26, pp. 954–960.

Received: 3rd May, 2020
Revised Accepted: 26th December, 2021

JOURNAL INDIAN ASSOCIATION OF SEDIMENTOLOGISTS ISSN NO 2582 – 2020
Vol. 38, Issue 2, 2021, pp. 25-35
DOI: https://doi.org/10.51710/jias.v38i2.123

Aeolian transportation mechanics and mass movement of surficial beach sands – a case study on Bendi-BaruvaMineral Sand Deposit, Srikakulam District, Andhra Pradesh

Souradeep Mukherjee* and A.Yugandhara Rao
Atomic Minerals Directorate for Exploration and Research
*HomiBhabha National Institute
*souradeepm.amd@gov.in

Abstract

Surficial sediment transportation studies carried out in the beach zone of Bendi-Baruva mineral sand deposit show that sand grains are transported by wind (saltation and suspension) beyond the high water line. The sand population of the study area contains heavy mineral sands (~20%) like ilmenite, garnet and sillimanite which covers 95% of the heavy mineral distribution with subordinate amounts of monazite, rutile, and zircon whereas light mineral sands (~80%) contain mostly quartz. Due to the sorted nature of these beach and dune sands the whole spectra falls within a specific range of grain size which shows a bi-modal distribution, primary mode at 0.025cm and secondary at 0.015cm. Due to this variation in density and grain size, mass of these sand particles vary resulting in differential transportation in any energy regime. In the study area, on the beach near the frontal dunes, surficial concentration of garnet grains are observed in patches having an average thickness 0.2cm i.e. around ten times of the dominant grain diameter. This surficial enrichment of garnet grains resting on a semi-uniform sand surface is the result of differential transportation of the dominant mineral grains. As more than 80% of the grain size population show a dominant grain size of 0.025cm, the wind flow parameters for the whole population is standardized with mean grain diameter (D) of 0.025cm. Mass of dominant individual minerals arrived from the grain counting technique was tallied with the theoretical mass considering spherical shape of the grains indicates a difference of mass to be within 5%. For ease of calculation and generalization the grains were considered to be spherical and their theoretical masses were taken into consideration in calculations. Considering the whole spectra of mineralogical distribution, a theoretical mass group distribution for dominant different minerals of different dominant grain sizes were formulated and total six mass groups were identified. Because quartz (~80%), ilmenite, sillimanite and garnet (together ~20%) are the most abundant, their positions were identified specifically in the theoretical mass groups and only these are considered for further discussion. To analyse wind velocity and pressure at different heights from the surface, a sediment trap was fabricated using piezo-electric sensors. A tail was attached to orient the device parallel to the wind flow so that the piezo surfaces always face the wind flow at 90^0 angle. The device records pressure data and converts those into voltage. Using the velocity data, macroscopic physical quantities of aeolian transportation were calculated for the study area, which empirically show the effect of mass in differential transportation of the dominant minerals that gives rise to these surficial garnet patches.

Introduction

In the beach zone, beyond high water line, transportation of sand grains is driven by wind. This dynamics of transportation is aided by sea-breeze and land-breeze in a daily manner which results in transportation of sands that are less in mass, leaving heavy mass behind. Mass of individual sand grains depends upon density and grain size (~volume). Product of these two physical properties generates a mass distribution in the area which reacts to wind flow differently causing a differential transportation. Surface creeping, saltation and suspension are the fundamental modes of aeolian transportation. Of these, saltation is the dominant one that covers up to 70% of the total mass movement (Bagnold, 1941; Shao, 2009). Again the initiation of surface creep and suspension is primordially caused by impact of the particles in saltation (Anderson et al., 1991a; Bagnold, 1941; Kok and Renno, 2009). So, the main transportation mode is governed and guided by the amount of saltation in a population of sand. Saltation is a response to fluid forces working on sediment-air interface zone whenever shear velocities exceed a certain threshold (Bagnold, 1941). This transportation of grains occurs within the sediment-air interface where atmospheric parameters (e.g. wind speed, temperature and aerosol concentration) vary rapidly with height from the sediment surface, and turbulence is predominantly generated by wind shear (Shao, 2009). The relationship of wind speed with increasing height creates three types of wind profiles (parabolic, linear and hyperbolic / logarithmic). For the case at hand, this relationship is a logarithmic one, where the surface layer has the highest shear velocity (so the highest drag force) which drives the main transportation mechanism (Shao, 2009).This is why a daytime wind profile (a logarithmic one) dominates transportation of materials and most of the erosion and transportation occurs during the day (Shao, 2009).Theories have been propounded to identify and quantify macroscopic physical parameters such as wind velocity profile, transportation flux, rate of transport per unit width (Bagnold, 1941; Anderson et al., 1991;Kok and Renno, 2008). These physical parameters generate an overall idea on the distribution of energy and force on the mass groups which causes them to move. Sand grains of different masses have different frictional threshold velocities (V_{*t}) which is a measure of force imparted on the particle when it is subjected to a fluid shear (Bagnold, 1941). This paper aims to empirically define the response of the dominant mass groups present in the area to the wind flow which gives rise to surficial concentration of garnet grains. To achieve that, in this paper dominant mass groups (mineral sands of different sizes and densities) were found out by weighing and daytime wind velocities were calculated using a piezoelectric sediment trap. Using these two parameters, mechanism of sand movement was theoretically derived and the response of each mass group (sand grains of different sizes and densities) to the wind imparted force was shown empirically.

Materials and Methods

To analyse the response of different groups of sand that vary in mass, a sediment trap was build using piezo-electric sensors (PZT-5H) to track the signature of transportation at different patches of heavy mineral concentration which recorded voltage output of the sensors. A tail was attached to the stand with ball bearing to orient the device parallel to the wind flow so that the piezo surfaces always face the wind flow at a 90^0 angle. The device records pressure data and converts those into voltage. The set-up was done following a typical component flowchart of any recording equipment i.e. sensor – amplifier – processor – recorder. The circuit diagram is shown in the figure 5. In this case piezo-electric chips (PZT-5H) were used as input sensors, LM-358 Op-Amps were used as amplifiers, Doit ESP-32 as microprocessors and a laptop was used as a recorder. The sediment trap is built by mounting Piezo-electric chips (sensors) on a PVC pipe (stand) with a cardboard sail (Tail) attached to it vertically. This whole arrangement is put on a stand using ball-bearings which allows height (levels) of the sensors to fix following the log law of the wind. From the output voltage the force imparted by the wind was calculated at different levels which further were used to calculate transportation dynamics of the dominant sand grains present in the area.

Dominant mass groups

The dominant surficial mineralogy of Bendi-Baruva mineral sand deposit, India was established by collecting of sand samples up to 1.5m depth at five different profiles 5 km apart with a grid of (5000m X 100m).The individual samples were analysed to draw an idea on the macro-component distribution, which shows that in light minerals (quartz) and total heavy minerals(THM) which together covers the whole sand population (Figure 1) which is dominated by quartz, ilmenite, garnet and sillimanite (around 95% of raw sand distribution). Grain size distribution of individual heavy minerals were formulated by physical separation techniques (bromoform separation as well as electro-magnetic separation) and sieving. The grain size distribution for raw sand (i.e., sand without slime and shell content) and THM show a primary dominant mode of raw sandat 250 micron so the dominant sand diameter is taken to be of 0.025cm but contrastingly the heavy minerals have a primary dominant grain size at 150 micron. In figure 2, distribution of individual heavy minerals is shown. It is also seen that in these four dominant minerals (quartz, ilmenite, sillimanite, garnet), the grains occur in specific dominant grain sizes. The dominant sizes were selected as it covers more than 95% of the total grain size distribution and have the highest influence on grain transportation. To cover the whole population, calculation of theoretical mass of individual mineral grains were done considering sphere of equivalent diameter using the following formula (Bagnold, 1941):

$$m_s = \frac{\pi}{6}\sigma_s d^3 \qquad (1)$$

where, m_s is the mass of the sand grain, σ_s is the density and d is the grain diameter.

Data for all of the dominant mineral groups were generated according to this equation to briefly identify the mass groups present in the area. Mass of each mineral pertaining to different sizes indicates that there exist small ranges where few values cluster (Fig. 3). This is compared with the dominant mineral mass groups to identify in which group it falls. In reality as the grains vary in shape and sizes, the mass also varies from the ideal calculated value. To check how closely it matches the theoretical mass, pure fraction of individual dominant heavy mineral grains of different dominant sizes (total 7) were measured by weighing a small sample and calculating total numbers of grain present in it, with the help of an optical microscope and dividing these two parameters (Fig.4). A comparative study in table 1 shows the percentage of error in mass calculation for these dominant sand grains and it is found to be less than 5%.Thus, equivalent spherical grains were considered for fluid dynamic studies to generate a very good approximation of natural events. Quartz is the dominant light mineral. For quartz grains, the theoretical values were taken. The whole population have six dominant mass groups (Fig.3) and the dominant ones are a small subset of those (Fig.4)

Calculation of wind velocity

Aeolian sand transport is aresponse to fluid forces within the near boundary of the surface whenever shear velocities exceed a certain threshold shear velocity (v_{*t}) (Bagnold, 1941, Poortinga, 2015). As the sediments behave differently to wind flow because of their mass, shape, co-efficient of friction, etc. the large scale structures and gradation in sediment distribution forms (Bagnold, 1941). For incompressible fluid flow, Navier-Stokes equation is used to determine turbulence, a chaotic eddying motion of a fluid with rapid variation in pressure and velocity in space and time which is a typical characteristic of wind flow and has been associated with the initiation of sediments movement

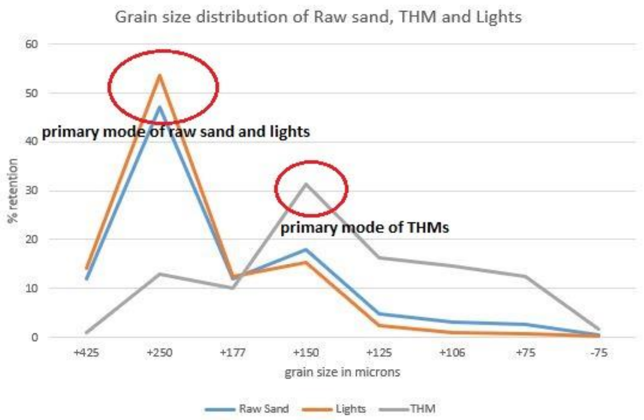

Fig.1. Grain size distribution of raw sand, THM and Light Minerals

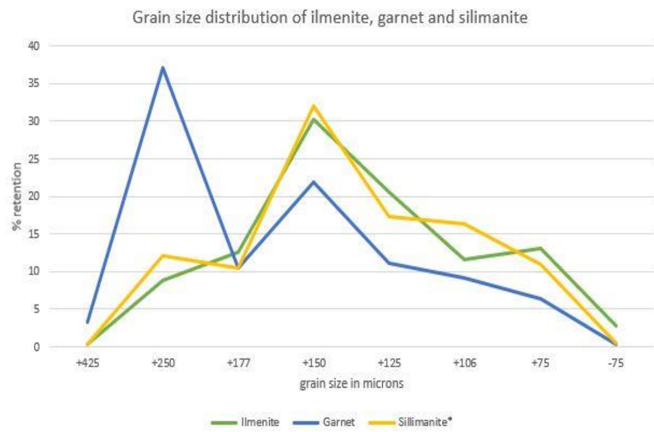

Fig.2. Grain size distribution of individual Heavy minerals

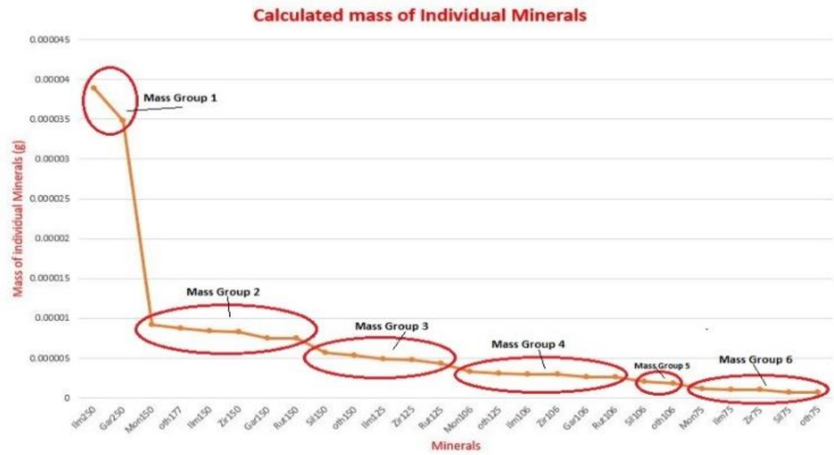

Fig.3. Calculated mass of individual minerals

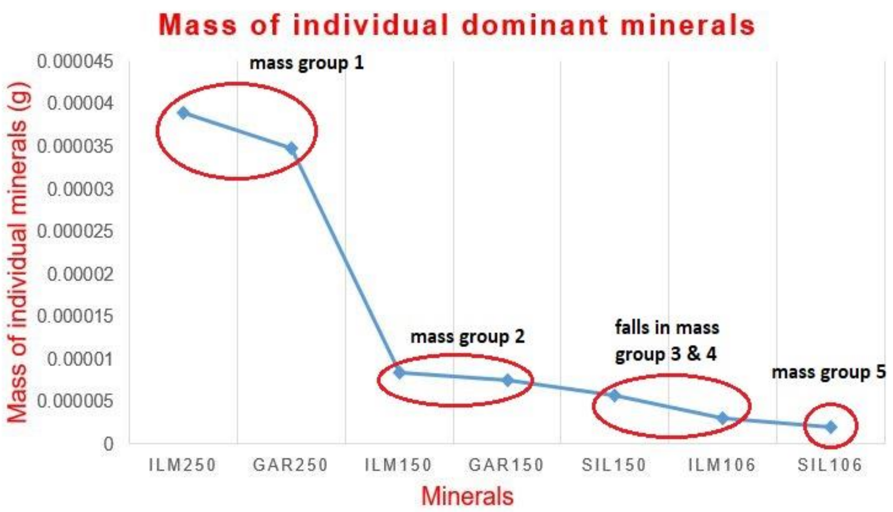

Fig.4. Mass of individual dominant minerals

(Walker, 2003). The dimensionless Reynolds Number (Reynolds, 1883, Bagnold, 1941) is derived from it and has an expression of:

$R_e = \frac{\rho l v_r}{\eta} = \frac{V_* d}{\vartheta}$(2)

For the case at hand, a PZT-5H has a value of g_{33} of 20 (10^{-3} V-m/N), thickness of 0.5mm, and a diameter of 25mm. As the processing is done by a doit ESP-32 micro-processor which operated between 0-5

Table.1 Experimental and theoretical mass of dominant mineral grains

Minerals	Density (g/cm^3)	Size (cm)	measured mass total	no of grains	individual mass	calculated volume	calculated mass	error %
Ilm250	4.75	0.025	0.0063	160	0.000039375	8.1813E-06	3.88608E-05	1.32
Gar250	4.25	0.025	0.0044	125	0.0000352	8.1823E-06	3.47702E-05	1.23
Ilm150	4.75	0.015	0.0037	425	8.70588E-06	1.7615E-06	8.39394E-06	3.71
Gar150	4.25	0.015	0.0029	371	7.81671E-06	1.7615E-06	7.51037E-06	4.07
Sil150	3.23	0.015	0.0029	493	5.88235E-06	1.7615E-06	5.70788E-06	3.05
Ilm106	4.75	0.0106	0.0028	921	3.04017E-06	6.2314E-07	2.96217E-06	2.63
Sil106	3.23	0.0106	0.0018	878	2.05011E-06	6.2614E-07	2.01427E-06	1.7

For particle size range (r) of (0.001-0.1cm), relative velocity (v_r) of (10-2000 cm/s), R_e falls in a range of 10^{-2}-10^3 which is a fuzzy area for velocity-resistance relation (Bagnold, 1941). Again wind flow imparts force on any surface it acts on, the force can be divided in two components, 1) at right angle to the surface (equation 3) and parallel to the surface (equation 4)(Bagnold, 1941).

$p = \frac{1}{2}\rho v^2$(3)

$\tau' = \rho V_*^2$(4)

where, p is force/unit area acting perpendicular to a surface,ρ is density of fluid, v is fluid velocity, τ' is the drag force and V* is drag velocity.Clearly, V∗ is not the speed of the flow but simply another expression for the momentum flux at the surface. As V∗ is a convenient description of the force exerted on the surface by wind shear, it emerges as one of the most important quantities in wind-erosion studies (Shao, 2009).For this case, to calculate wind velocity in different levels and its signature on transportation, a sediment trap using piezo-electric sensor was used where piezo surfaces face the wind flow at right angle. A piezo-electric transducer generates voltage from imparted pressure(Platt, S. et al, 2005). For this study a low power PZT-5H chip was used as input sensor for the sediment trap. When wind hits the piezo surface at a right angle it imparts pressure on the piezo chip which in turn generates a static voltage. The equation for static voltage generation for a piezo-electric transducer is given below:

$V = \frac{g_{33} F_3 h}{\pi r^2}$ (5)

where static voltage V can be calculated from piezo-electric voltage constant g_{33}, force acted on the surface F_3, thickness of the chip h and radius r. So the Force can be calculated by modifying the equation (5):

$F_3 = \frac{\pi r^2 V}{g_{33} h}$ (6)

Volts, amplification is selected on the basis of trial and error and finally set to be 50000. In this range the voltage output of the imparted pressure works properly. The pressure is calculated by dividing F_3 with the cross-sectional area (i.e. 4.908 cm^2). Now, the pressure imparted can be transformed to generate velocity data using equation (3) and this generates mass distribution in the area. The Circuit diagram of the set-up is shown in (Fig.5) and the picture of the trap is shown in (Fig.6a and 6b). The data acquisition (sampling time and repeatability) details are given in table 2. As the sampling frequency of this type of processors is very high, only the averaged value of static voltage in different levels is given in Table 3.

Wind speed vs height has been plotted and the relationship of these two parameters is exponential. The result shows a very good co-relation with a R^2 value of 0.96 (Fig.7).This type of wind profile is stated as unstable as it shows a more sheer velocity near the boundary layer which dominantly drives erosion (Shao, 2009). The wind load is also calculated from the wind velocity value by using the following expression(Bagnold, 1941):

$F = A.C_d.P$ (7)

where, F is the wind-load, A is the cross-sectional area of the piezo chips, drag-coefficient C_d and P is the calculated wind pressure. This wind load also follows the same trend when it is plotted against height.

Sediment transportation

When a sand particle moves through air, two fundamental forces have a negative impact on the flight of the particle i.e. downward force of gravity and air resistance in the direction opposite to the relative movement (Bagnold, 1941). The ratio of these two forces termed susceptibility (S). It is given by the following impression (Bagnold, 1941): $S = \frac{P}{mg}$ (8)

where, P is the force experienced by the particle horizontally which can be derived from the modification of equation (3) by introducing drag-coefficient C_d or c (in equation 9). C_d for smooth spherical grains travelling through air is to be taken as 1.8 (Bagnold, 1941). The 'm' in the denominator is to be calculated using equation (1) which gives the following expression for susceptibility

Table.2 Data acquisition details for three selected patches (each has been repeated for 5 times)

Acquisition	Lat	Long	Date	Time	Tail direction	Avg Direction
1	18°45'1.82"N	84°30'8.96"E	8th April year	11:00	336	
2	18°45'1.82"N	84°30'8.96"E	8th April	11:05	342	
3	18°45'1.82"N	84°30'8.96"E	8th April	11:10	329	332.8
4	18°45'1.82"N	84°30'8.96"E	8th April	11:15	330	
5	18°45'1.82"N	84°30'8.96"E	8th April	11:20	327	
6	18°43'5.21"N	84°28'19.27"E	12th April	09:00	319	
7	18°43'5.21"N	84°28'19.27"E	12th April	09:05	325	
8	18°43'5.21"N	84°28'19.27"E	12th April	09:10	320	319.6
9	18°43'5.21"N	84°28'19.27"E	12th April	09:15	312	
10	18°43'5.21"N	84°28'19.27"E	12th April	09:20	322	
11	18°47'17.69"N	84°32'55.06"E	20th April	11:00	349	
12	18°47'17.69"N	84°32'55.06"E	20th April	11:05	356	
13	18°47'17.69"N	84°32'55.06"E	20th April	11:10	348	351.4
14	18°47'17.69"N	84°32'55.06"E	20th April	11:15	356	
15	18°47'17.69"N	84°32'55.06"E	20th April	11:20	348	

Table.3 Calculation of wind speed from piezo data

Sensor no	channel no	Pin No	Height (cm)	Sampling frequency	Amplification	Area (sq.cm)	Voltage	Pressure (dyne/sq.cm)	Speed (cm/s)	Wind load (gm)
1	COM5	A3	5	9600	50000	4.9085	1.4694	29.389	219.5	29.534
2	COM5	A6	12	9600	50000	4.9085	1.6805	33.612	234.7	33.778
3	COM5	A7	19	9600	50000	4.9085	2.034	40.682	258.2	40.882
4	COM5	A4	26	9600	50000	4.9085	2.3101	46.203	275.2	46.431
5	COM5	A5	50	9600	50000	4.9085	2.9559	59.121	311.3	59.412
6	COM5	A8	100	9600	50000	4.9085	3.534	70.682	340.4	71.030

(Bagnold, 1941): $S = \frac{3\rho v^2 c}{4\sigma_s g d}$ (9)

values for all the dominant grains were calculated and plotted against different wind speeds at different heights. This generates a plot (Fig.8) which defines how the grains will be susceptible to transportation and if their mass and grain size play any role on it. It can be clearly seen from the plot that the susceptibility values show an exponentially decreasing trend which is quite similar to the mass group clusters. This proves the bearing of mass on transportation where silimanite$_{106}$ is more prone to travel than Ilmenite$_{250}$ mathematically which will be clearly seen when the forces for transportation will be calculated subsequently. The same mass groups show similar clustering in the susceptibility values. But for grain movement and saltation, drag force drives the whole mechanism. To tract the grain movement and their motion path, calculation of drag force is essential, and it was calculated graphically from wind speed data. Drag force is defined by equation (4) where V_* value is required. This V_* is called as drag velocity or velocity gradient which is defined by the slope of the tangent at a wind speed vs levels (in logarithmic scale) (Fig.9) diagram (Bagnold, 1941). So V_* is proportional to the tan value of the angle made by the tangent with the y-axis in the figure 9.

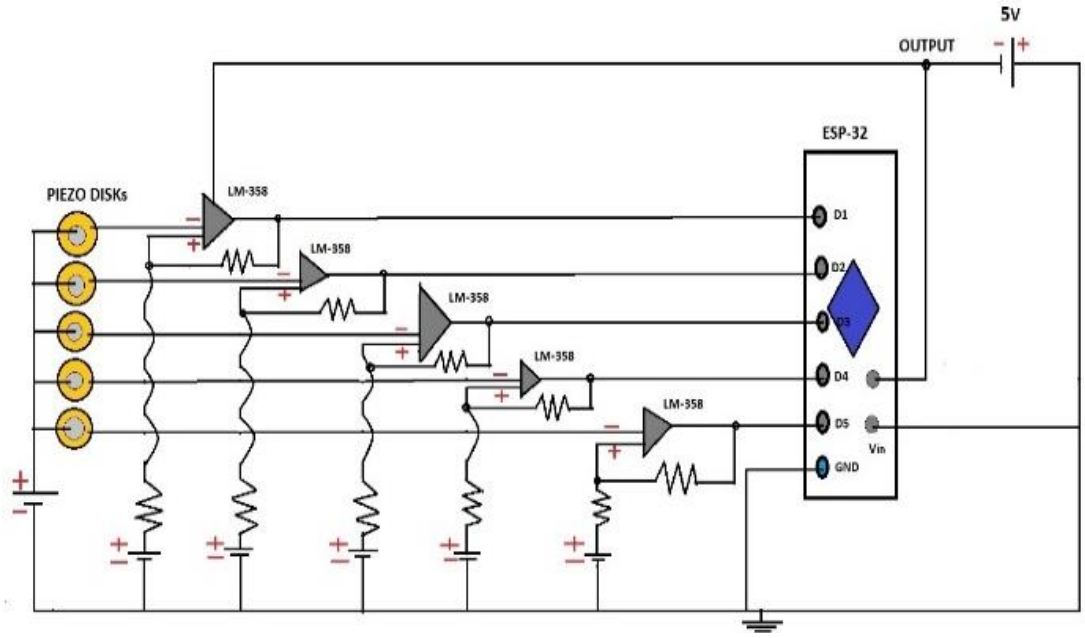

Fig.5. The Circuit diagram of Piezo-opamp-esp32 setup (only 5 piezo sensors are shown for better representation)

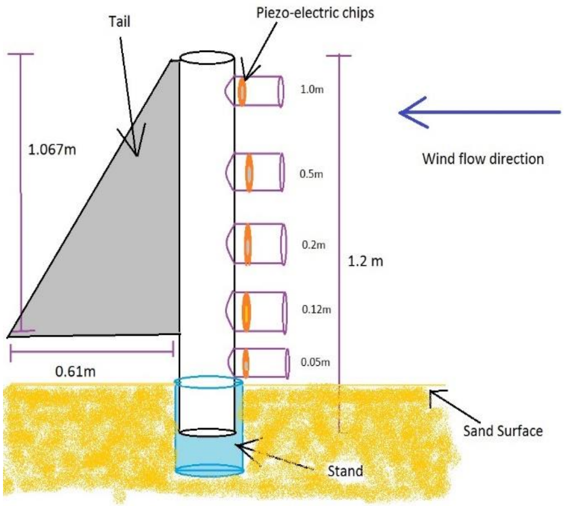

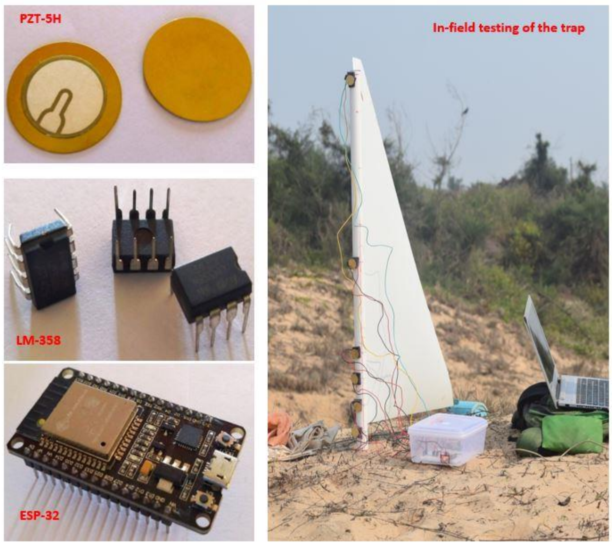

Fig.6a. The Sediment trap at work (only 5 piezo

Fig.6b, The Sediment trap at work

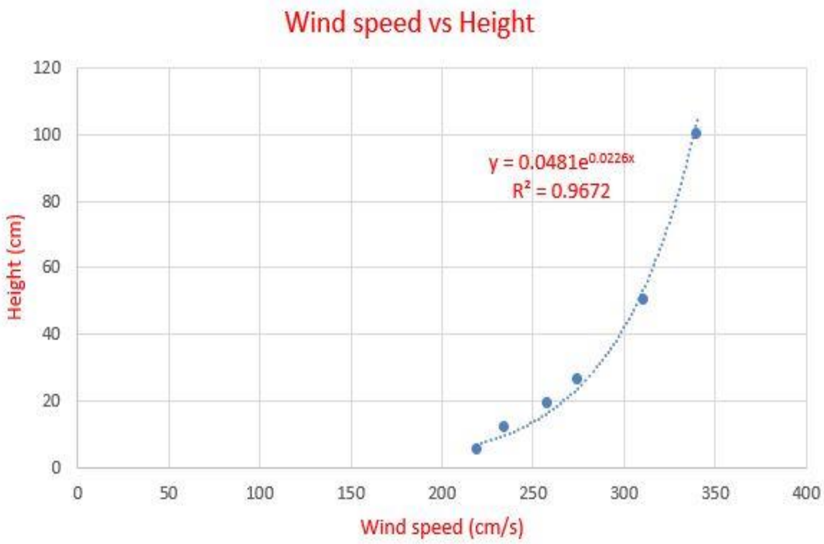

Fig.7. Wind speed vs height from the ground surface

$$V_* = \frac{AC}{CO'} tan\theta \qquad (10)$$

where θ = 64^{0}, AC= (V_{100}-V_{12}), OC' = log(z)- log(k'). Here for the calculation k' is taken as 12cm which is the height of the second sensor, and thus using equation (9), $V_*$was calculated and found to be 125.97cm/s. Roughness length (k) was calculated from the y axis intercept of the tangent and has a value of 0.47cm which defines the zero velocity height. So any saltation will takes place above that level. Now the effect of this drag force (τ') on the sediments causes them to move. The drag force was calculated using equation (4), which is found to be of 19.36 dyne.To track the response of the encountered mass groups to the wind flow, another two important parameters (Frictional threshold) were calculated- 1) Fluid threshold or static threshold and 2) impact threshold or dynamic threshold. Fluid threshold defines the minimum velocity of the fluid to act on a particle causing it to move. Fluid threshold can be calculated using the equation (Shao and Lu, 2000):

$$V_{*t} = A_s \sqrt{\frac{(\sigma_s - \rho)}{\rho} gd + \frac{\gamma}{\rho d}} \qquad (11)$$

where$\frac{\gamma}{\rho d}$ is added to modify the equation for fine particles (d < 0.008cm), but as our domain of work resides in the comparatively coarse grains (0.025cm), the normal Bagnold equation is used (Bagnold, 1941):

$$V_{*t} = A_B \sqrt{\frac{(\sigma_s - \rho)}{\rho} gd} \qquad (12)$$

$$V_{*t} = A_B . tan\theta \sqrt{\frac{(\sigma_s - \rho)}{\rho} gd} \log(\frac{z}{k'}) \qquad (13)$$

where A_s (equation 11) and A_B(equation 12, 13) are constants derived by Shao and Bagnold. Equation (13) gives V_{*t} at different levels. Using this equation static or fluid threshold for the dominant mass groups were identified (Fig.10). V_{*t} values for 1cm, 5cm, 12cm,

9cm, 26cm, 50cm, 1m are plotted serially and two types of trend were identified. The vertical curves connect the same mineral grains of different sizes and the horizontal curves connect the mass groups having similar fluid threshold values. These horizontal curves connecting different mineral grains of different sizes suggest the same range of portability for a group of minerals subjected to a fixed value of wind velocity. As with increasing height wind speed increases along with potential energy of particles, it requires more threshold velocity for transportation. Now 1 cm level is the value of k' for dune sands (Bagnold, 1941), saltation takes place just above this height. Thus the dynamic or impact threshold was calculated for 1cm height using the following equation (Bagnold, 1941):

$$V_t = A. tan\theta \sqrt{\frac{(\sigma_s - \rho)}{\rho} gd} log(\frac{k'}{k}) \qquad (14)$$

For this study, A is taken as 0.08, K' is 1 cm and roughness constant k was calculated to be 0.47cm which converts the expression to:

$$V_t = 0.0537 \sqrt{\frac{(\sigma_s - \rho)}{\rho} gd} \qquad (15)$$

Impact threshold was calculated for the dominant mass groups using equation (15), details of these threshold values are given in table 3. From figure11 an idea can be drawn on how V*t varies for different mineral grains. It is clearly seen that each mass group has a range of fluid thresholds, Sil_{106}having the least values. The less the values of V*t, more easily it will get transported because the wind flow imparted pressure will get distributed among the least V*t values (Bagnold, 1941). Figure 12 shows a plot of grain diameter in negative ϕ values with threshold velocities. As For Gar_{250} the cut off limit of grain movement (i.e. the lowest value for V_t) is found to be 15.708 cm/s, below that limit Gar_{250} is immovable. The mass groups having higher values were spotted for both the V*t and $V_t$values as they can generate collision imparted pressure on Gar_{250} for which it will move. Grains like Ilm_{250}, Ilm_{150}, Qtz_{250} and Gar_{150} can make the Gar_{250} grain move by collision, as their V*t values fall close to Vt of Gar_{250}. So it can be inferred from the values that before a Gar_{250} grain can move, a lot of other dominant minerals have already experienced Aeolian transportation (Fig.13). It is also seen from the figure 13 that the dominant mass groups of the study area fall in the saltation range. A typical uniform saltation mechanism in this domain of flow, is governed by combination of three dominant force forces - 1) Drag force on particles (F_D) which causes particles to move in the viscous layer or flow and 2) aerodynamic lift (F_L) caused by the velocity gradient which gives the lift off angle to the saltating particles and weight of the particle. So the forces to move these encountered group of particles individually (ignoring Magnus force and electric force), are calculated by these equations (Shao, 2009):

$$F_S = F_D + F_L - F_g \qquad (16)$$

Individual drag and lift were calculated using the following equations (Shao, 2009):

$$F_D = \frac{1}{2} C_d \rho A v_r . V_r \qquad (17)$$

$$F_L = \frac{1}{2} C_{ld} \rho A (\nabla V)^2 d \qquad (18)$$

For sediment transportation by saltation, the frictional threshold velocity for each mineral was considered which modifies the $v_r V_r$ values as ${V_{*t}}^2$ and ∇V defines the

gradient of v for the considered particle to move. It is seen from experimental data, C_l = $0.85C_D$. So the combined force required for saltation of sand grains is calculated from the following equation:

$$F_S = \frac{1}{2} C_{ld} \rho A {V_{*t}}^2 d + \frac{1}{2} C_d \rho A - mg \qquad (19)$$

This is the necessary equation to calculate force exerted on individual mineral grains which are subjected to saltation. The values of the different forces calculated are given in table.4.

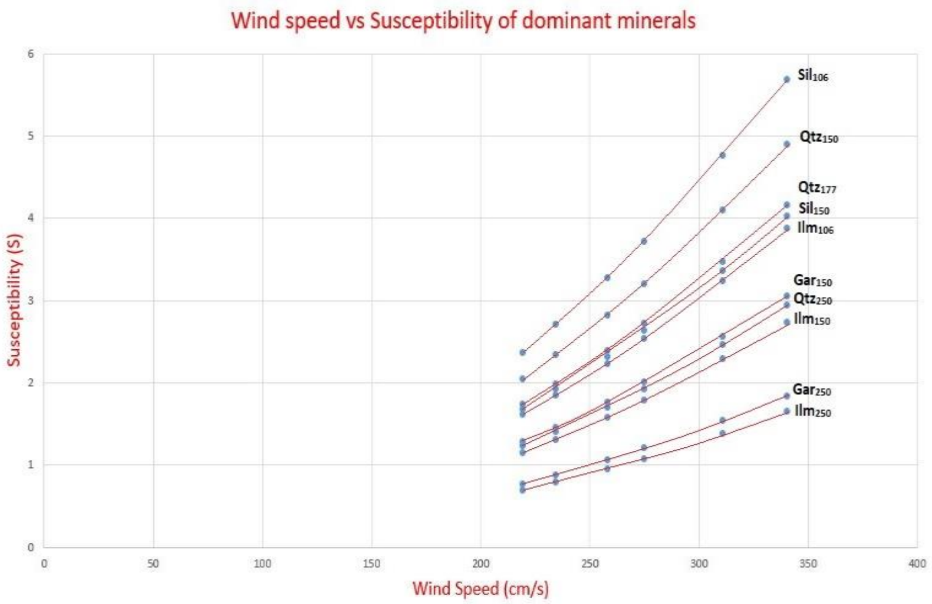

Fig.8. Wind speed vs Susceptibility

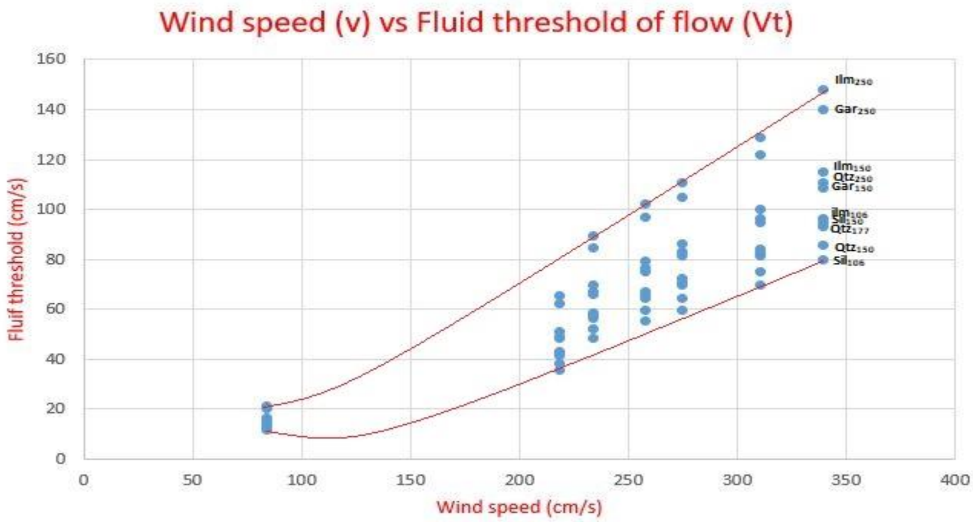

Fig.9. Calculation of V*, K

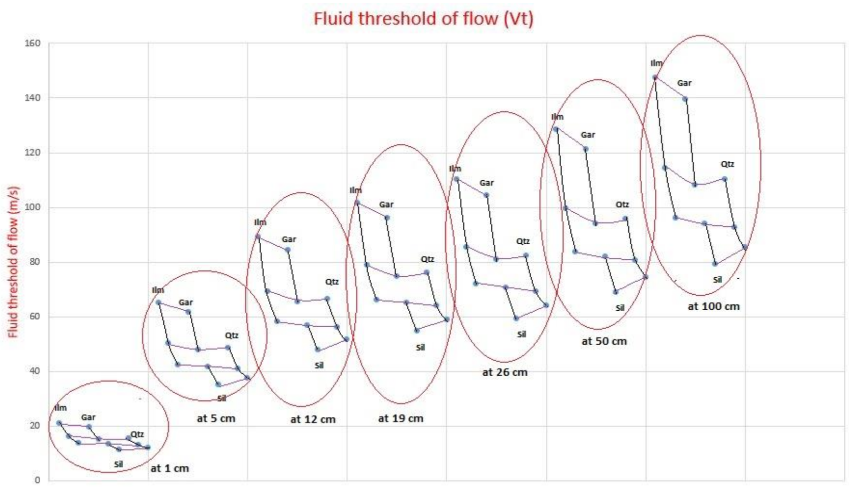

Fig.10. Fluid threshold (V_{*t}) of dominant mass groups in different heights

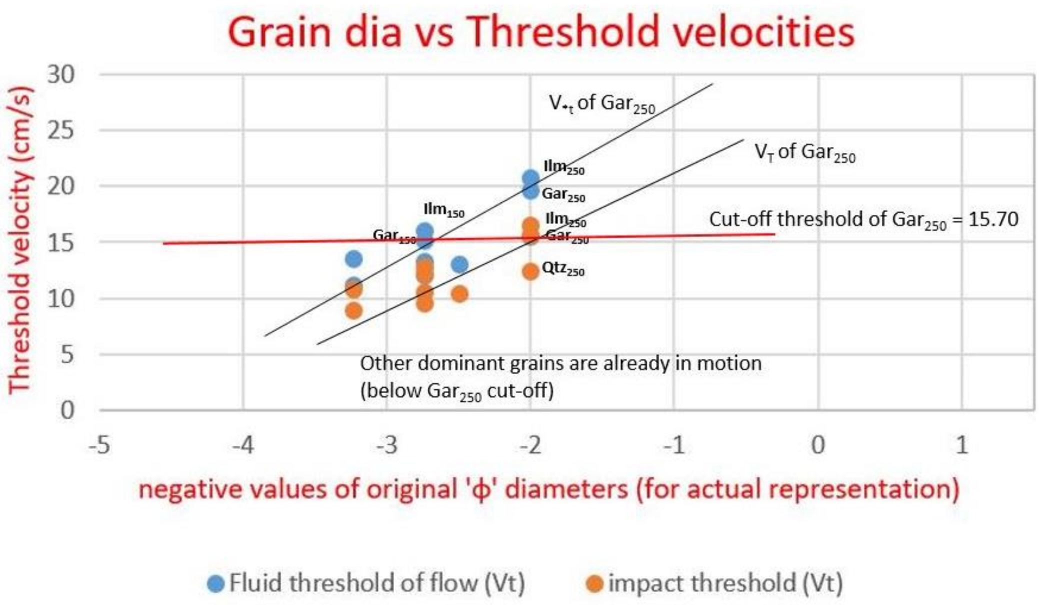

Fig.11. Wind speed vs Fluid threshold (V_{*t}) of dominant mass groups at different heights

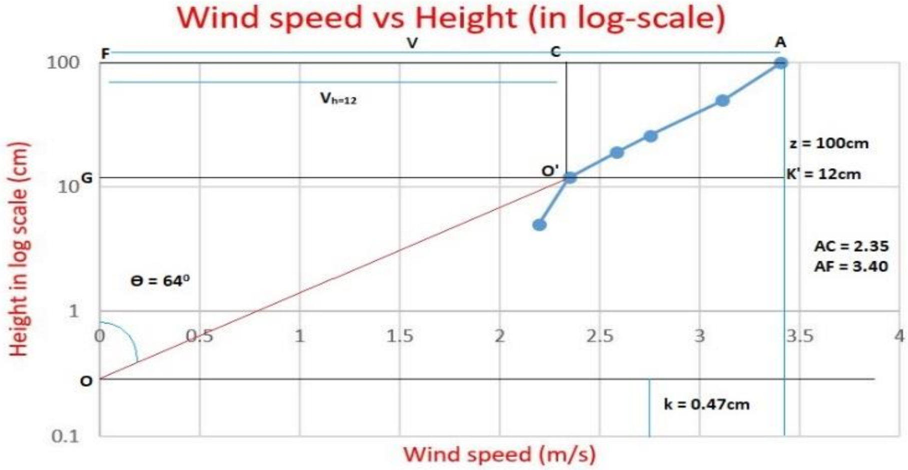

Fig.12. Grain dia vs threshold velocities (V_{*t}, V_t) of dominant mass groups at 1cm height

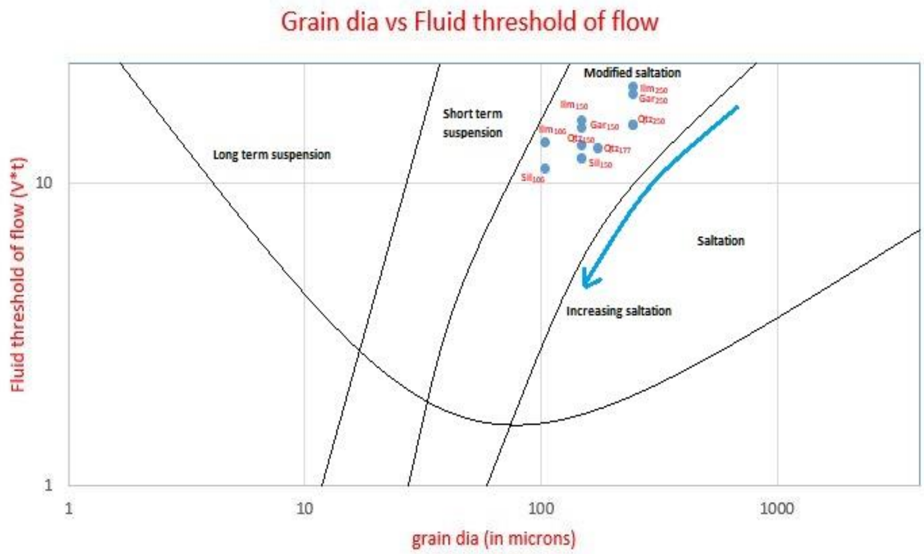

Fig.13. Frictional threshold (V_{*t}) of dominant groups plotted against grain diameter in log scale

Table.4 Calculation of Threshold velocities and forces required for saltation							
Minerals	V*t	V_T	F_D	F_l	mg	Minimun force for saltation (F)	maximum number of transported grains
Ilm250	20.758	16.607	0.904	0.01921	0.038	0.885	22
Gar250	19.635	15.708	0.724	0.01538	0.034	0.705	27
Qtz250	15.503	12.403	0.281	0.00598	0.021	0.266	73
Ilm150	16.079	12.863	0.195	0.00249	0.008	0.19	102
Gar150	15.209	12.167	0.156	0.00199	0.007	0.151	128
Qtz177	13.045	10.436	0.1	0.0015	0.008	0.094	206
Sil150	13.259	10.607	0.09	0.00115	0.006	0.086	225
Ilm106	13.517	10.813	0.069	0.00062	0.003	0.067	289
Qtz150	12.009	9.607	0.061	0.00077	0.005	0.057	340
Sil106	11.146	8.916	0.032	0.00029	0.002	0.03	645

It is clearly seen that, in the given energy regime a single grain of Ilm_{250} requires the highest amount of force to get transported (0.885 dyne) whereas a grain of Sil_{106} requires the least force (0.03 dyne). Drag force per unit width calculated from equation (4) were found to be of 19.36 dyne. Hypothetically for a uniform distribution of monomineralic sand, this force will be distributed over unit width among the grains. So, shear force in unit time and unit width can transport maximum numbers of sand grains which is calculated by dividing the total imparted force by minimum transportation force. It can now be seen that, for a constant value of $V_* = 125.97$ cm/s, only 27Gar_{250}grains can get transported in unit time compared to 646 grains of Sil_{106}. Another important relationship arises when different susceptibility values were plotted against F_s. These two parameters have a logarithmic relationship:

$$S = -A_! \ln(F_s) + B_1 \qquad (20)$$

As susceptibility is the independent variable here, the equation (20) changes to this exponential form:

$$F_s = A_2 e^{-B_2 S} \qquad (21)$$

where, A_1, B_1, A_2, B_2 are constants, A_1=0.482 and B_1=0.5198, and A_2 =2.5907, B_2 = 1.988 measured at the top limit of the saltation layer, i.e. at 5cm. This shows how the encountered mass groups of the area behave differently when they are subjected to a wind flow. Gar_{250} and Ilm_{250}has the highest requirement of force thus has a low susceptibility. These two mineral groups exist separately where rest of the values cluster, this comparative mobility of higher susceptible grains separate them from Gar_{250} and Ilm_{250}making these two relatively left out in transportation causing a local enrichment of these mineral grains in the encountered energy domain. Due to the nature of the source, Ilmenite sand occurs mostly at 0.015cm diagenetically (primary mode at +150 micron), making Gar_{250}dominating the local residue enrichment patches.

Observations and Discussion

Bendi-Baruva mineral sand deposit of North Srikakulam, shows a typical beach and dune sand regime which is subjected to daily wind flow with average velocity of 3m/s. Wind velocity of this value falls between a domain where R_e has a value (R_e= 38.11) of 10^{-2}<R_e<10^3 which is a fuzzy domain between Stoke's region (<10^{-2}) and high turbulent region where C_d is constant (>10^3). For this domain, R_e reduces with increasing C_d for a fixed grain size. The Flux-gradient relationship of atmospheric boundary layer shows an unstable wind flow profile during day time where drag force near the ground surface is maximum thus transportation and erosion takes place mostly during daytime. Hence the measurements were made during the day time. The mineralogical distribution in the area shows dominance of four minerals (Ilmenite, Garnet, Sillimanite, and Quartz) of specific grain sizes. The overall grain size distribution of the raw sand has an average diameter of 0.025cm, and 0.015cm for the most of heavy minerals (except Garnet). The wind flow in the beach zone imparts drag force on the particles which causes transportation of these particles. Different particles behaves differently to the imparted drag force (τ'=19.36 dyne) because of their mass, volume, grain size. Partition of force on sand grains is guided by the velocity gradient (V_*) of the flow and frictional threshold velocities (V_{*t}) of the particle which is an impression of minimum force for transportation. V_{*t}values of dominant mass groups fall in the region of saltation when it is plotted against grain diameter, which proves the dominant mode of transportation is saltation. The maximumheight for saltation for a standard aeolian transportation process in dune sands is about 5cm so V_{*t} values were calculated at this height where drag force is maximum for saltation. This sets the upper limit of exerted force for saltation.Ilm_{250} and Gar_{250} having the highest V_{*t} requires maximum amount of drag force for getting transported. Individual minimum force required for saltation using equation (19) also gives out an identical picture. Susceptibility (S) which is a measure of ease of lateral movement of particles in a flow, when plotted against the minimum force required for saltation, shows an exponential decrease in susceptibility value with increasing requirement of saltation force. This clearly separates out Gar_{250} grains from the other dominant mineral groups as relatively immobile one(Ilm_{250} is not considered as its primary mode of grain size is 0.015cm so Ilm_{150} is the dominant grain size for Ilmenite followed by its finer fractions). Due to this fraction of relative immobility in this energy domainGar_{250} is relatively left out during transportation causing a local surficial enrichment of these grains which is visible as patches on the beach zone. This signature is more prominent at Srikurmam, 70km southward of Bendi-Baruva which shows one of the highest surficial enrichment of coarse garnet grains in India.

Acknowledgement

I express my sincere gratitude to the Director, Atomic Minerals Directorate for Exploration and Research and Head, Beach Sand and Off-shore Investigation group, for their constant encouragement, permission and support to make this work a successful completion.

Funding: No funding.
Conflict of interest: The authors do not have any conflict of interest.

References

Anderson R S, Haff P. K. (1988). Simulation of aeolian saltation. *Science,* 241(4867): 820–823.

Anderson R. ., Sorensen M., Willetts B. B. A review of recent progress in our understanding of aeolian sediment transport. *ActaMechSuppl*, 1991, 1: 1–20.

Bagnold R. A. (1941). The Physics of Blown Sand and Desert Dunes. London: Methuen

Kok J. F., Renno N. O. (2009). A comprehensive numerical model of steady state saltation (COMSALT). *Journal of Geophysical Research: Atmospheres,* 114(D17): D17204.

Platt, S. R., Farritor, S. M., andHaider, H. (2005). On Low-frequency electric power generation with PZT ceramics. *IEEE/ASMETransactions on Mechatronics*, 10(2), 240-252.

Poortinga. Ate. (2015). Beach Sand Dynamics: measurements, models and scales *Wageningen: Wageningen University*.

Reynolds, O. (1883). An experimental Investigation of the Circumstances Which Determine Whether the Motion of Water Shall Be Direct or Sinuous, and of the Law of Resistance in Parallel Channels, *Philosophical Transactions of the Royal Society of London*, Vol. 174, pp. 935-982

Shao, Y., Lu, H., (2000). A simple expression for wind erosion threshold friction velocity. *J. Geophysics*. Res. 105, 22437–22443.

Shao. Y. (2009). Physics and Modelling of Wind Erosion. Germany.

Walker, I.J. and W.G. Nickling. (2003). Simulation and measurement of surface shear stress over isolated and closelyspaced transverse dunes in a wind tunnel. *Earth Surface Processes and Landforms* 28(10), 1111–1124.

Wyngaard JC (1990) Scalar fluxes in the planetary boundary layer –theory, modelling and measurement. Boundary-Layer *Meteorol*50: 49–75

Yamada T., Mellor G. L. (1975) A simulation of the Wangaraatmospheric boundary layer data. *J AtmosSci* 32: 2309–2329.

Received: 23rd June, 2020
Revised accepted: 6th October, 2021

The Editor-in-Chief, Professor Abhijit Basu and the Editorial Board of the Journal of the India Association of Sedimentologists (IAS), and the Executive Council of the Association mourn sad and untimely demise of Professor A. H. M Ahmed, Treasurer of the Association (IAS) and, Professor Indra Bir Singh, Doyen of Indian sedimentology. We send our condolences to their family members and, near and dear ones.

Professor G. N. Nayak
President IAS

JOURNAL INDIAN ASSOCIATION OF SEDIMENTOLOGISTS ISSN NO 2582 – 2020
Vol. 38, Issue 2, 2021, pp. 37-48
DOI: https://doi.org/10.51710/jias.v38i2.133

Lithofacies and petrochemical characterization of volcano-sedimentary sequence of Chandil Formation around Kharidih-Bareda area, Seraikela-Kharsawan District, Jharkhand: implications for uranium mineralization

Biswajit Panigrahi[1], S. P. Upadhyay[1], A. K. Sharma[1], Anirban Saha[1] and D. K. Sinha[2]
Atomic Minerals Directorate for Exploration and Research
[1]Jamshedpur [2]Hyderabad

Abstract

Mesoproterozoic Chandil Formation (ca. 1600 Ma) of North Singhbhum Mobile Belt record numerous features of felsic volcaniclastics and felsic to intermediate volcanics preserved in the central sector of the fold belt around Kharidih-Bareda area, Seraikela-Kharsawan district, Jharkhand. The felsic volcanic rocks exhibit flow bands, autoclasts and layering of crystal mushes revealing viscous nature of eruptives. The volcaniclastic sediments comprise of significant proportion of volcanic epiclasts and accidental lithic fragments. These volcaniclastics have been categorized into five prominent lithofacies viz, stratified lapilli tuff, banded tuff, tuff with penecontemporaneous deformation, welded lapilli stones, vitric tuff and volcanic bombs by field and petrographic studies of outcrops and subsurface borehole cores. The welded lapilli tuffs display fiamme and eutaxitic texture. Interlayering of the volcaniclastics, which are most often pyrite-rich, with psamo-pelitic lithology like carbonaceous phyllite, variegated phyllite, quartzite and minor limestone is suggestive of marine euxenic depositional environment.

Petrographic study of the volcaniclastics indicated presence of glass shards, garnet phenocrysts, spherules of tremolite, ovoid to lenticular accretionary lapilli along with devitrified glassy material. Compositionally these felsic volcanics and volcaniclastics are rhyodacitic to andesitic in nature with peraluminous to meta aluminous in character. A/CNK values vary from 0.52 to 2.42 in felsic volcanics and from 0.12 to 1.63 in volcaniclastics. Signatures of arc magmatism is indicated by low concentration of HFS elements such as Nb (5-17 ppm), Ga (11-17 ppm) and Y (5-28 ppm).

Elevated intrinsic content of uranium (3-8 ppm), Th/U ratio ranging from 1.2 to 13.2, presence of metamict allanite and zircon in volcanics and volcaniclastics reveal their suitability as a prospective source for search of uranium mineralization. The volcanic-volcaniclastic-clastic association of the Chandil Formation provides an ideal situation where provenance and province both are available. Thus, suitable litho-structural locales such as the concealed shear zones sympathetic to the Dalma thrust and South Purulia Shear Zone within the volcano-sedimentary package of Chandil Formation may be targeted as preferable sites for locating concealed uranium mineralization.

Key words: Lithofacies, felsic volcanics, uranium mineralization, Chandil Formation

Introduction:

The Paleo to Mesoproterozoic mobile belt delimited by Singhbhum Craton in the south and Chhotanagpur Granite Gneissic Complex in the north is known as North Singhbhum Mobile Belt (NSMB) or North Singhbhum Fold Belt (Gupta and Basu, 2000; Mahadevan, 2002). NSMB is longitudinally divided into two parts by a median spine shaped volcanic belt known as Dalma Volcanics (Fig. 1). The metasediments of NSMB exposed to the north of Dalma volcanics is known as Chandil Formation and is considered to be Mesoproterozoic (ca. 1600 Ma) in age (Ray et al., 1996; Sengupta et al., 2000; Mazumder, 2005; Reddy et al., 2009). Chandil

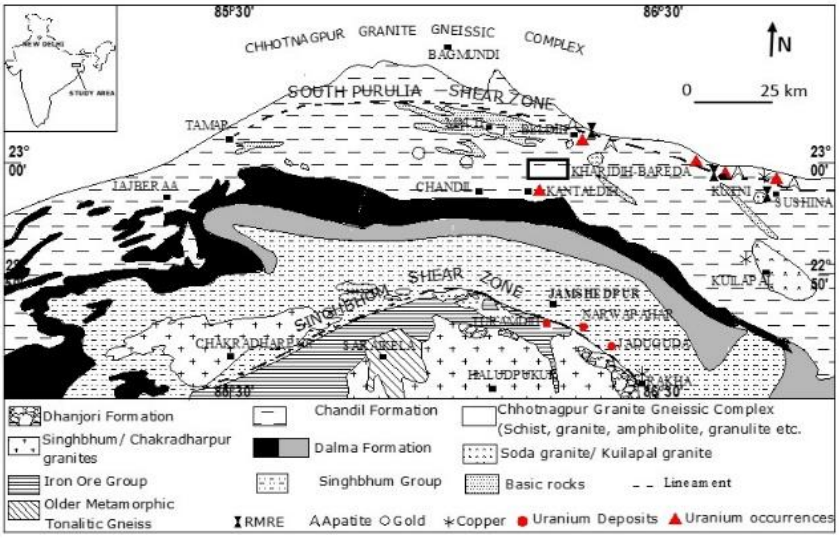

Fig. 1 Regional Geological map of North Singhbhum Mobile Belt showing location of the study area (Modified after Dunn and Dey, 1942; Mazumder, 2005)

Formation comprises lower green schist facies of rocks consisting of metapelites, metapsammites, basic intrusives and acid volcanics. Occurrences of acid volcanic rocks, viz, tuffs and rhyolites in this domain have been reported by several workers (Sengupta et. al., 2000). Isotopic data (Rb-Sr age 1484±44 Ma) of the acid volcanics of this belt suggests the presence of a Mesoproterozoic volcano-sedimentary basin in Singhbhum Craton (Sengupta et. al., 2000) which was subsequently upheld by various workers (Mazumder, 2005; Chatterjee et al., 2013; Mazumder et al., 2015). Geological and geochemical study of a part of these felsic volcanics and volcaniclastic units exposed along the South Purulia Shear Zone (SPSZ), occurring at the interface between Chandil Formation and Chhotanagpur Granite Gneissic Complex, has been described by Acharya et al. (2006). However, the information on the felsic volcanics and associated volcaniclastics still remains sparse and the data accrued are from a few selected localities. Detailed geological, lithofacies and geochemical characterization of rocks is lacking from many sectors of Chandil Formation.

In the present study, the authors focus on characterization of different lithofacies of the felsic volcaniclastic and volcanic rocks exposed in the central sector of Chandil Formation, around Kharidh-Bareda, which lies about 15 km south of SPSZ and hitherto unstudied. Field, petrographic, geochemical and radiometric criteria have been utilized to characterize the rocks and highlight their potential as a suitable source as well as a host rock for uranium mineralization.

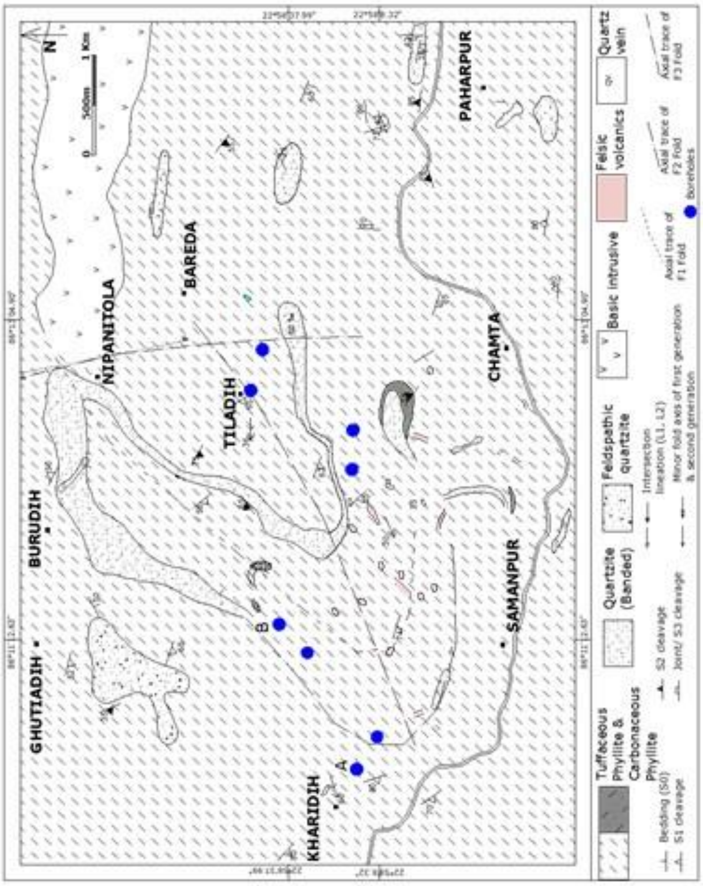

Fig. 2. Geological map of Kharidih Bareda area, Seraikela-Kharsawan District, Jharkhand showing complex outcrop pattern due to polyphase folding. Solid blue dots indicate the borehole locations where concealed felsic volcanics and volcaniclastics were recorded in subsurface. A and B represent the boreholes, the lithologs of which are shown in Fig. 12.

Geological Setting

The name Chandil Formation was given by Ray et al. (1996) to the lithopackage dominated by acid tuffaceous rocks exposed in the north of Dalma Volcanic belt. The tuffs were identified as vitric, lithic and crystal lithic tuffs (Ray et al.,1996). This meta-sedimentary belt is categorized under the northern most domain (domain V) of North Singhbhum Fold Belt by Gupta and Basu (2000). The general stratigraphy of the area is given in Table-1.

The Chandil Formation consists of meta-pelitic and psamo-pelitic sequence with felsic tuffs, acid volcanics, carbonaceous phyllite, minor interlayers of quartzite and occasional carbonate rocks showing low grade of metamorphism (Fig. 1). These are further intruded by younger basic sills and dykes.

Detailed mapping in the central sector of Chandil Formation, around Kharidih-Bareda, reveals tuffaceous phyllite covers a large part of the area (Fig. 2). These are variegated in nature with the colour varying from grey, light grey, buff to light greenish. Intercalations with bands of carbonaceous phyllite are observed in the south of Paharpur and Tilaidih. Two types of quartzite are exposed in the area. Fine grained, grey to dark grey coloured, banded quartzites are observed in the northern part, near Nipanitola and Burudih. These are cherty at places and intercalated with tuffaceous layers near Paharpur. Medium to coarse grained feldspathic quartzites showing intermittent silicification and ferugenisation are exposed in separate hillocks in the western part of the area around Ghutiadih.

Felsic volcanic are exposed as discontinuous bands within tuffaceous phyllite. These are massive, grey to dark grey in colour, fine grained, equigranular, hard, compact and form concordant lenses within the metasediments. An E-W trending amphibolite body extending over

Table 1 Generalized stratigraphy of Singhbhum Mobile Belt (Modified after Gupta and Basu, 2000 and Mazumder, 2005)

Age	Group	Formations	Lithology
	Acidic - Alkaline rocks		Ultramafics, magnetite-apatite rocks
Middle - Upper Proterozoic		Chandil Formation	Phyllite ($\pm$carbonaceous), tuff, felsic volcanic, quartzite
	Dalma Group	Upper Dalma Lower Dalma	Not represented
	Singhbhum Shear Zone Assemblage (>1.6 Ga)		
Lower Proterozoic	Singhbhum Group (>2.2 Ga)	Dalbhum	Quartzite, schist, phyllite
		Chaibasa	Medium grade Basic and pelitic schists
	Dhanjori Group (2.4 Ga)	Upper Dhanjori Lower Dhanjori	Conglomerate., Quartzite, basic volcanics and schists
Archean	Cratonic basement		Older Metamorphic gneiss, Older Metamorphic Tonalitic Gneiss, Singhbhum Granite, Iron Ore Group and other granitoids

Fig. 3 Layering of crystal mushes in rhyodacitic flow shown between black dotted lines. Seen near Samanpur in Fig. 2

3.4km strike length with 600-900m width intrudes into these metasediments in the northeastern part. It is greenish black coloured, melanocratic, medium to fine grained and massive in nature. It has faulted contact with the metasediments in the west (Fig. 1).

The area has undergone three phases of folding. First generation of folds are tight, isoclinal and reclined in nature. These are refolded by second

Fig. 4 Flow bands of rhyodacitic rock observed in borehole at location A, shown in Fig. 2.

generation folds having ENE-WSW axial trend, which mostly controls the outcrop pattern. A major synformal closure of second generation having moderate plunge due SSW is identified near Kharidih in the western part. Broad open folds having near N-S axial trend define the third generation of folds. Fold interference has resulted in a complex outcrop pattern. Lateral discontinuity, polyphase folding and inadequate surface exposures are the hindrances in the mapping of individual volcaniclastic facies on a large-scale map.

VOLCANIC AND VOLCANICLASTIC ROCKS OF CHANDIL FORMATION

Felsic flows

Felsic flows are interlayered with argillites and volcaniclastic rocks. Interspersed outcrops occur intermittently in different parts of the area which is attributed to polyphase folding and peneplanation. These rocks are grey to dark grey coloured, fine grained, massive to crudely foliated in nature and break with a conchoidal fracture. Some of these exhibit development of mushes of feldspar crystals which impart crude layering to the rock (Fig. 3). Flow layers and bands are also discernible in borehole cores (Fig. 4).

Volcaniclastic rocks

The detailed mapping of the outcrops and

Fig. 5 Stratified lapilli tuff (Outcrop photo width 0.50m)

study of boreholes cores of key locations revealed different lithofacies of volcaniclastic rocks. On the basis of field relationship, petrographic studies, grain size, textural and structural features, the volcaniclastics have been classified into the following five facies: stratified lapilli tuff, banded tuff, welded lapilli stones, tuff with

Fig. 6 Stratified lapilli tuff horizon in borehole cores of location A in Fig. 2. Photo width 1m

penecontemporaneous deformation features and spheroidal volcanic bombs, arranged in decreasing order of preponderance. Non-mappable outcrops of individual facies preclude inference of any genetic

Fig.7 Outcrop photo showing foliation in welded lapilli stone

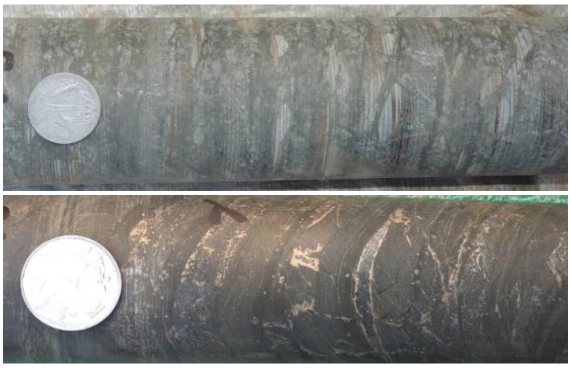

Fig. 8. Photographs of borehole cores at location B shown in Fig. 2. Top: Fiamme texture. Bottom: Pyrite encircles the lapilli clasts and also fills the cross fractures

connotation for these volcaniclastics. Thus, they are generalized under volcanic epiclasts and accidental lithoclasts. Grain size terminology used for classifying these volcaniclastics has been taken from Fischer (1966).

Stratified Lapilli Tuff

These facies comprise of predominantly tuffaceous material intermittently strewn with subangular to subrounded lapilli clasts. The size of the clasts varies from 3 mm to 5 cm (Fig. 5). Thick

Fig. 9 Banded tuff showing parallel lamination. Inset shows angular feldspar clasts set in argillaceous matrix

horizons ranging from 25m to 60m of this lithofacies have been recorded at several places in borehole columns. Stratification planes defined by tuffaceous and argillaceous layers are distinctly discernible giving the rock a layered appearance (Fig. 6).

Welded Lapilli stone

This facies is characterized by the distribution of lapilli of different sizes within the highly silicic matrix. The rock is very hard, compact

Fig. 10 Penecontemporaneous deformation feature in tuffaceous phyllite

and welded in appearance. Intermittent exposures of this facies are seen in the high lands in close proximity to the felsic to intermediate flows. The lapilli are lenticular in shape and strongly aligned along the plane of deformation (Fig. 7). Elongated lenses of lapilli clasts are compacted and strongly welded to define fiamme texture (Fig. 8).

Banded Tuff

Grey buff to light yellowish coloured, fine grained, thinly laminated rocks define this facies. It comprises abundant quartz and sericite with the frequent distribution of wedge shaped glass shards. It has a distinct banded appearance (Fig. 9). A close examination of fresh and weathered surfaces reveals that the rock is constituted of coarse to fine sand sized subangular feldspar clasts set in argillaceous matrix. Sporadic exposures are best seen north of Chamta in the southeastern part and around Ghutiadih in the northwestern part of the studied area.

Fig. 11 Spheroidal to ellipsoidal shaped volcanic bombs bound by silicified matrix observed near Tilaidih area shown in Fig. 2

Tuff showing penecontemporaneous deformation

This facies occurs intermittently within the tuffaceous phyllites and lapilli tuff zone. These are exposed in the northern part of the area to the west of Nipanitola. It is characterised by 20-50 cm thick zone of convolute laminations and contorted bedding of coarser arenaceous layers within the tuffaceous phyllite (Fig. 10). Intraformational breccia zones recorded within the tuffaceous units in a few boreholes are also categorised under this facies. These features usually originate by palaeo seismicity events and can be attributed to volcanic activity in the study area.

Volcanic bomb

A few localized occurrences of welded bomb sized (> 64 mm) aggregates are observed as a plug like body, west of Tilaidih (Fig. 11). These silica rich clasts are spheroidal in nature and embedded in siliceous matrix. The bomb clasts are flattened due to deformation. Prima facie analogy with other lithotypes of the area suggests that the rocks may be juvenile fragments of semisolid magma ejected during eruptional activity.

Subsurface lithology observed in boreholes comprises of interlayering of stratified lapilli tuff, tuffaceous phyllite, psamopellitic rocks, rhyodacitic flow, welded lapilli stone, banded tuff and psamopelitic variants (Fig. 12). The shape of the lapilli varies from highly angular to subrounded. Chloritic bands along bedding and foliation planes as

Table 2 Major and trace element concentration of felsic volcanic rocks of Kharidih Bareda area

Samp	1	2	3	4	5	6	7	8	9	10	11	12	13	14	15	16
SiO_2	62.6	65.93	60.65	63.18	62.11	66.2	66.82	64.75	59.57	68.2	66.04	62.45	64.26	61.96	61.71	60.74
TiO_2	0.6	0.51	0.63	0.64	0.71	1.02	1.04	1.02	0.45	0.54	0.58	0.68	0.62	1.22	1.21	0.72
Al_2O_3	9.47	8.03	9.43	11.83	12.76	10.04	12.41	15.08	8.25	10.08	11.38	12.43	13.46	12.71	15.92	8.61
$Fe_2O_{3(T)}$	11.38	9.38	13.43	10.45	11.19	12.95	10.67	10.83	19.55	7.31	9.46	12.46	7.52	12.29	11.13	17.4
MgO	3.23	3.41	3.76	3.78	3.13	2.69	2.74	2.6	3.24	3.79	3.7	3.53	3.75	3.7	3.37	3.03
MnO	0.37	0.44	0.29	0.29	0.49	0.42	0.12	0.12	0.56	0.26	0.43	0.18	0.21	0.16	0.11	0.43
CaO	2.95	4.13	2.65	1.93	0.99	0.67	0.38	0.47	1.92	3.54	2.53	0.89	2.26	0.6	0.61	0.83
Na_2O	1.91	2.41	2.72	1.91	1.91	0.98	0.5	0.53	0.56	0.03	0.66	0.75	0.13	0.03	0.03	0.25
K_2O	4.51	3.65	4.8	5.95	5.9	4.17	4.51	5.41	3.59	4.08	4.32	4.74	6.12	4.42	4.99	4.78
P_2O_5	0.14	0.11	0.11	0.1	0.1	0.22	0.09	0.11	0.13	0.08	0.05	0.06	0.06	0.12	0.11	0.21
Total	97.16	98	98.47	100.06	99.29	99.36	99.28	100.92	97.82	97.91	99.15	98.17	98.39	97.21	99.19	97
A/CNK	0.71	0.52	0.65	0.90	1.13	1.37	1.94	1.99	0.99	0.92	1.10	1.56	1.23	2.15	2.43	1.21
A/NK	1.18	1.01	0.98	1.23	1.34	1.64	2.18	2.24	1.72	2.26	1.98	1.95	1.97	2.63	2.92	1.54
V	75	60	77	77	89	130	128	150	nd	59	63	88	64	157	171	nd
Cr	87	83	108	82	91	201	201	165	nd	62	79	127	57	199	204	nd
Co	36	30	40	33	36	48	41	37	nd	28	33	47	25	40	39	nd
Ni	32	33	25	31	37	49	60	61	nd	36	35	38	28	50	67	nd
Cu	<10	<10	<10	82	19	41	<10	<10	nd	12	11	<10	14	20	<10	nd
Zn	78	80	94	76	103	95	105	123	nd	82	70	115	78	41	58	nd
Ga	13	12	11	14	14	12	14	16	nd	13	13	13	15	14	16	nd
Rb	130	121	133	142	155	105	120	125	nd	126	116	111	183	99	131	nd
Sr	11	34	<10	21	<10	<10	11	11	nd	30	26	50	22	<10	10	nd
Y	13	5	16	16	21	16	15	17	-	5	5	5	25	5	28	nd
Zr	53	52	57	73	66	122	142	117	nd	85	83	74	95	191	154	nd
Nb	35	15	13	11	5	10	17	10	-	5	5	5	5	12	5	nd
Ba	1118	812	1220	1585	1257	479	523	840	nd	1014	1060	994	1152	574	708	nd
Ce	176	131	162	151	158	165	137	140	nd	84	121	138	94	150	160	nd
Pb	<10	<10	<10	<10	<10	<10	<10	13	nd	<10	21	33	<10	<10	<10	nd
Zr/SiO_2	0.011	0.009	0.010	0.009	0.011	0.009	0.012	0.014	0.011	nd	0.016	0.014	0.011	0.015	0.016	0.013

Analytical values of the major oxides are given % and trace element are given in ppm well as fracture planes of volcaniclastics are noteworthy. A significant amount of pyrite and minor chalcopyrite is associated with the lapilli-dominant sediments as well as the banded tuff (Fig. 8). Brownish to pinkish colour garnet are developed as specks and clots at many places suggesting that the metasediments have attained almandine facies metamorphism. Pyrite-bearing carbonaceous phyllite and intercalatory quartzite bands are also observed in some boreholes. Concealed bands of calcareous layers in the form of limestone and calcareous quartzite are noted in the boreholes drilled in the southwestern part of the area.

Table 3 Major and trace element concentration of volcaniclastic rocks of Kharidih Bareda area

Samp	18	19	20	21	22	23	24	25	26	27	28	29	30	31	32	33	34	35	36	37
SiO_2	67.79	61.29	60.95	62.65	58.19	48.64	47.05	53.8	56.79	44.81	49.93	49.15	54.51	53.96	55.66	58.83	55.35	58.54	52.5	47.7
TiO_2	0.69	0.47	0.52	0.71	0.43	0.52	0.43	0.55	0.66	0.18	0.42	0.24	0.36	0.33	0.62	0.56	0.53	0.4	0.39	0.55
Al_2O_3	11.29	8.7	10.06	11.86	7.87	7.08	5.26	6.17	10.1	0.88	4.1	1.96	3.64	5.41	8.75	11.93	10.98	7.34	7.68	10.19
$Fe_2O_{3\,(T)}$	6.98	14.92	16.34	11.06	17.97	27.15	26.49	23.75	19.27	31.57	26.73	28.28	24.44	26.49	20.67	15.45	18.78	19.31	24.61	23.64
MgO	2.18	3.5	3.1	3.34	3.96	4.11	4.38	3.68	3.24	2.38	3.82	3.74	2.98	4.04	4.46	3.09	3.92	3.99	4.5	5.14
MnO	0.06	0.28	0.21	0.5	0.27	0.91	0.76	1.89	0.5	0.63	0.96	1.12	1.37	0.67	0.49	0.15	0.48	0.57	0.58	0.2
CaO	0.81	2.89	0.97	1.37	2.85	2.48	3.97	1.97	0.82	3.13	2.96	6.63	3.77	3.41	3.19	0.71	0.96	2.38	2.32	1.14
Na_2O	3.26	0.03	0.87	3.37	1.01	1.35	0.91	0.72	1.09	0.27	0.6	0.38	0.57	0.56	3.49	0.55	0.97	0.96	0.9	2.16
K_2O	7.47	3.87	3.72	5.59	3.22	4.34	3.56	3.11	5.3	0.95	2.6	1.59	2.16	2.27	0.39	4.71	4.83	3.92	3.8	0.91
P_2O_5	0.08	0.1	0.1	0.1	0.14	0.21	0.21	0.89	0.2	0.15	0.43	0.31	1.36	0.17	0.17	0.09	0.16	0.19	0.29	0.24
Total	100.61	96.05	96.84	100.55	95.91	96.79	93.02	96.53	97.97	84.95	92.55	93.4	95.16	97.31	97.89	96.07	96.96	97.6	97.57	91.87
A/CNK	0.76	0.92	1.39	0.84	0.76	0.62	0.42	0.76	1.12	0.12	0.45	0.14	0.36	0.56	0.73	1.64	1.28	0.72	0.78	1.54
A/NK	0.84	2.05	1.84	1.02	1.53	1.02	0.98	1.36	1.34	0.60	1.08	0.84	1.11	1.60	1.42	1.99	1.61	1.26	1.37	2.25
V	102	nd	nd	82	nd	nd	nd	nd	nd	nd	nd	nd	nd	nd	nd	nd	nd	nd	nd	nd
Cr	121	nd	nd	93	nd	nd	nd	nd	nd	nd	nd	nd	nd	nd	nd	nd	nd	nd	nd	nd
Co	32	nd	nd	34	nd	nd	nd	nd	nd	nd	nd	nd	nd	nd	nd	nd	nd	nd	nd	nd
Ni	74	nd	nd	35	nd	nd	nd	nd	nd	nd	nd	nd	nd	nd	nd	nd	nd	nd	nd	nd
Cu	10	nd	nd	<10	nd	nd	nd	nd	nd	nd	nd	nd	nd	nd	nd	nd	nd	nd	nd	nd
Zn	19	nd	nd	40	nd	nd	nd	nd	nd	nd	nd	nd	nd	nd	nd	nd	nd	nd	nd	nd
Ga	14	nd	nd	13	nd	nd	nd	nd	nd	nd	nd	nd	nd	nd	nd	nd	nd	nd	nd	nd
Rb	168	nd	nd	127	nd	nd	nd	nd	nd	nd	nd	nd	nd	nd	nd	nd	nd	nd	nd	nd
Sr	13	nd	nd	25	nd	nd	nd	nd	nd	nd	nd	nd	nd	nd	nd	nd	nd	nd	nd	nd
Y	17	nd	nd	14	nd	nd	nd	nd	nd	nd	nd	nd	nd	nd	nd	nd	nd	nd	nd	nd
Zr	105	nd	nd	75	nd	nd	nd	nd	nd	nd	nd	nd	nd	nd	nd	nd	nd	nd	nd	nd
Nb	5	nd	nd	13	nd	nd	nd	nd	nd	nd	nd	nd	nd	nd	nd	nd	nd	nd	nd	nd
Ba	585	nd	nd	1258	nd	nd	nd	nd	nd	nd	nd	nd	nd	nd	nd	nd	nd	nd	nd	nd
Ce	65	nd	nd	150	nd	nd	nd	nd	nd	nd	nd	nd	nd	nd	nd	nd	nd	nd	nd	nd
Pb	<10	nd	nd	<10	nd	nd	nd	nd	nd	nd	nd	nd	nd	nd	nd	nd	nd	nd	nd	nd

Analytical values of the major oxides are given % and that of trace element are given in ppm
Nd: Not determined by XRF due to presence of higher content of Fe

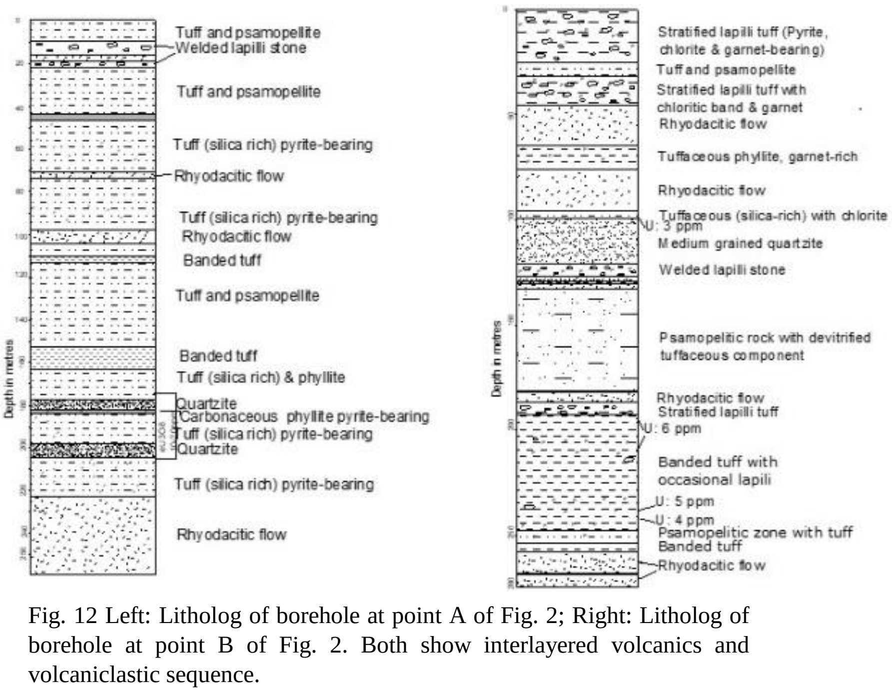

Fig. 12 Left: Litholog of borehole at point A of Fig. 2; Right: Litholog of borehole at point B of Fig. 2. Both show interlayered volcanics and volcaniclastic sequence.

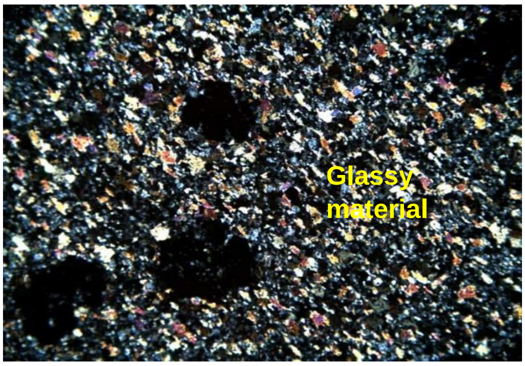

Fig. 13 Clots of glassy material within rhyolite (quartz, sericite and biotite)

Petrography

The felsic and intermediate flows are mainly composed of quartz, biotite, sericite and feldspar. Feldspars are altered to sericite invariably. Clots of glassy matters are often observed in these rocks (Fig. 13). Lapillis within the volcaniclastics are mostly identified as quartzite, consisting of quartz grains entirely (Fig. 14). These are commonly seen scattered in the tuffaceous horizon as observed in borehole cores. In some tuffaceous rocks, lapillis are constituted of fine to medium grained quartz and some sericite indicating rhyolitic composition (Fig. 15).

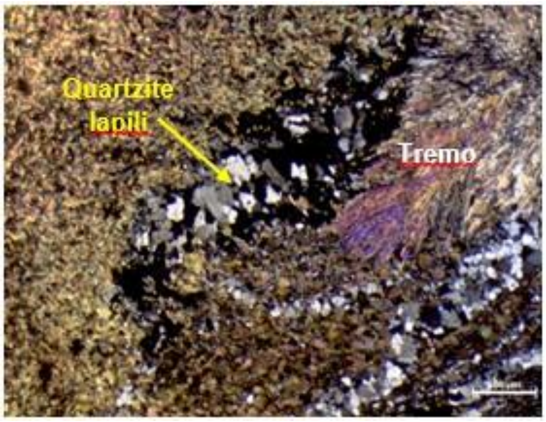

Fig. 14 Quartzite lapilli and spherulitic tremolite with quartz veining

Fig. 15 Rhyolitic lapilli (RL) within tuffaceous matter

Spherulitic structures are quite prominently developed within the lapilli bearing tuffs and tuffaceous sediments depending upon the composition of the parent rocks. The matrix part is composed of tuffaceous as well as non-volcanic components like carbonaceous matter, quartz, biotite and sericite. Radial growth of tremolite and garnet are observed within the recrystallised tuffaceous and pelitic matrix (Fig. 14, 16 and 17). These are later aligned along the schistosity of quartz and sericite grains, which define the regional foliation. Quartz tourmaline veins also traverse through the matrix containing carbonaceous matter and quartzite lapilli containing muscovite (Fig. 18). Chlorite also forms a minor part of the matrix at places. It occurs as an alteration product of garnet and biotite as well. Infiltrations of carbonate materials as veins are also noticed occasionally within the matrix part.

Meramec allanite and zircon have been observed in the volcaniclastics and volcanics by petrological studies (Fig. 19 and 20). Pleochroic haloes are observed in the biotite due to the presence of inclusions of metamict allanite (Fig. 21).

Table 4: Intrinsic U and Th content in felsic volcanics and volcaniclastics of Kharidih-Bareda area (Radiometric Assay)

Rock type	eU_3O_8 ppm	Ra eU_3O_8 ppm	ThO_2 ppm	Th/U
Tuffaceous rocks (n=42)	<2 - 35	<5 - 7	<10 - 40	2.7 – 11.2
Felsic volcanic (n=25)	2 – 38	<5 -9	<10 – 48	3.2-13.2
Carbonaceous Phyllite (n=12)	13 - 28	<5 - 10	<10 - 21	1.7-8.4

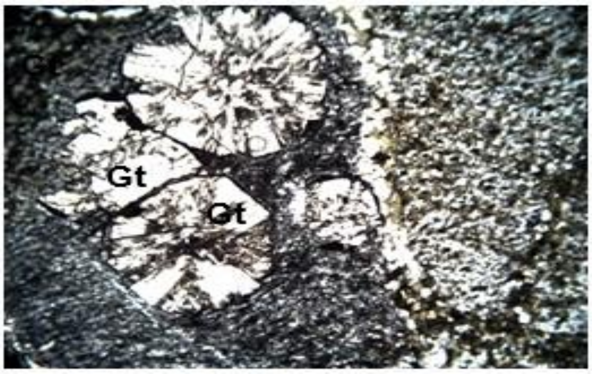

Fig. 16 Spherulitic garnet (Gt) in tuffaceous and argillaceous matrix

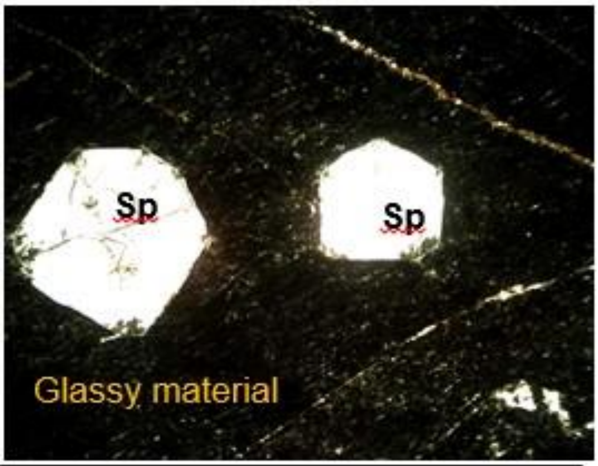

Fig. 17 Spherulitic matter (Sp) in glassy material

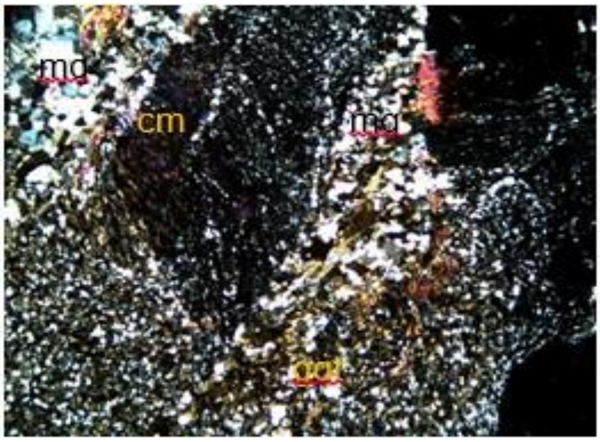

Fig. 18 Carbonaceous matter (cm) garnet quartz tourmaline (gqt) band with muscovite quartzite (mq)

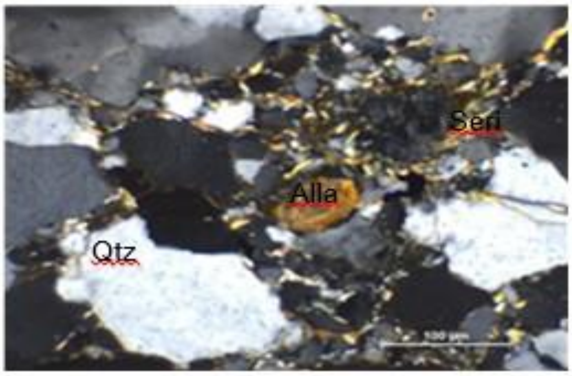

Fig. 19 Metamict allanite (Alla) in quartz-sericite rich rock

Geochemistry

Geochemical analysis of the borehole core samples of volcaniclastics and volcanic rocks were carried out by Wavelength Dispersive X-ray

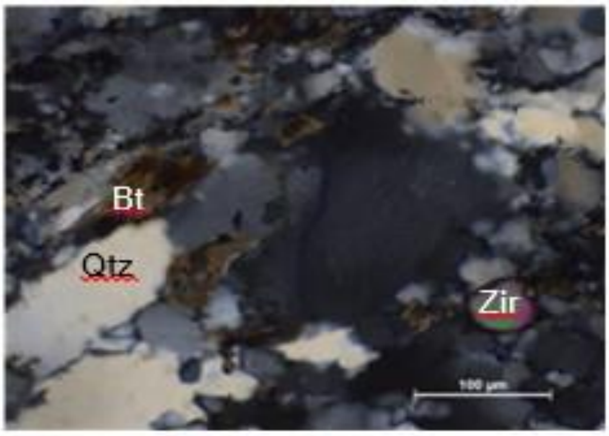

Fig. 20 Metamict zircon (Zir) in quartz and biotite-rich metasediments

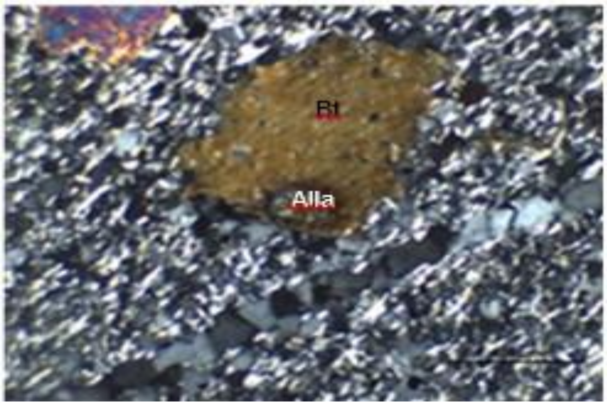

Fig. 21 Pleochroic halo in biotite due to allanite seen in sericite-biotite-quartz-rich rhyolitic rock. Quartz vein is also seen

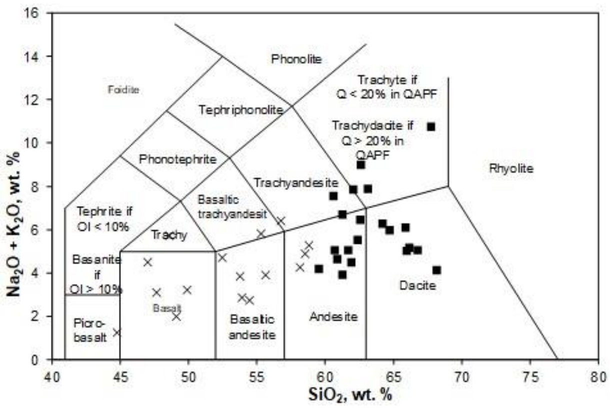

Fig. 22 Total alkali silica plot after Le Bas et al. (1986). From Fig. 22 to Fig. 26 samples of volcaniclastics and felsic volcanics are represented by cross symbols and solid squares, respectively.

fluorescence (WDXRF) at the XRF Laboratory of Atomic Minerals Directorate for Exploration and Research, Nagpur. Felsic volcanic flows have analysed SiO_2: 59.57-68.20%, TiO_2: 0.45-1.22%, Al_2O_3: 8.03-15.92%, Fe_2O_3(t): 7.31-19.55%, MgO: 2.6-3.79%, CaO: 0.38-4.13%, Na_2O: 0.03-2.72%, K_2O: 3.59-6.12% and P_2O_5: 0.05-0.22% (Table 2). The volcaniclastics show wide variation in major elemental concentration viz., SiO_2: 44.81-67.79%, TiO_2: 0.18-0.71%,, Al_2O_3: 0.88-11.93%, Fe_2O_3(t): 6.98-31.57%, MgO: 2.18-5.14%, CaO: 0.71-6.63%,

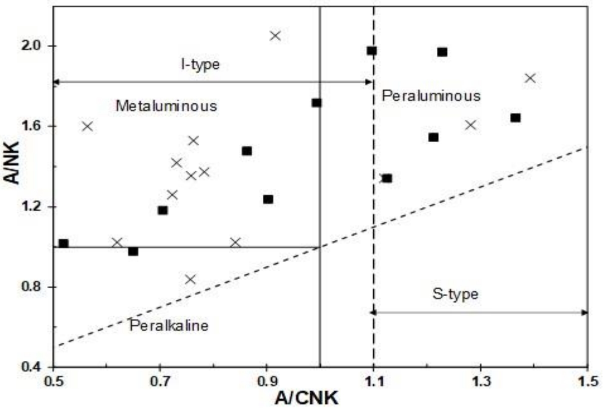

Fig. 23 A/CNK and A/NK plot after Maniar and Picoli (1989)

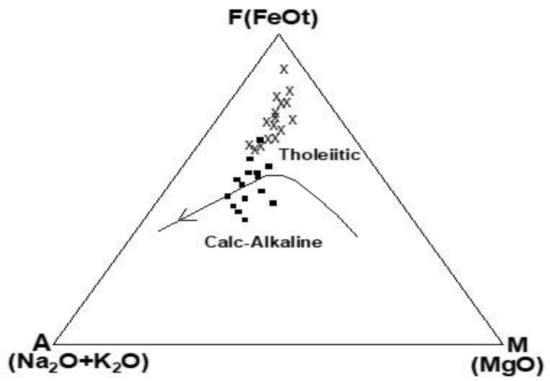

Fig. 24 AFM plot after Irvine and Barangar (1971)

Na_2O: 0.03-3.49% and K_2O: 0.39-7.47%, P_2O_5: 0.08-1.36% (Table 3).

On total alkali vs silica plot of Le Bas et al. (1986) the felsic volcanics mostly fall in andesite-

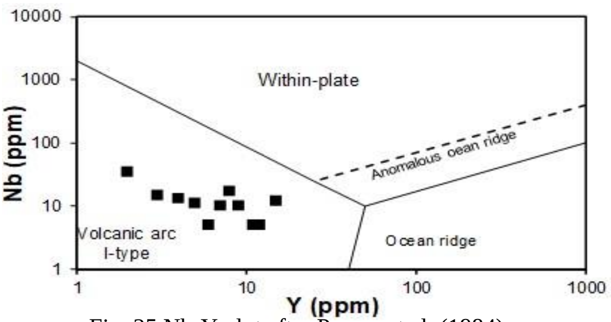

Fig. 25 Nb-Y plot after Pearce et al. (1984)

dacite field whereas the volcaniclastics straddle across basalt to basaltic andesite field (Fig. 22). A/CNK and A/NK plot (Maniar and Picoli, 1989) indicate the spread of felsic volcanics from metaluminous to peraluminous compositional range (Fig. 23). But the volcaniclastics fall in meta-aluminous field. This is also corroborated mineralogically by the occurrence of both hornblende and garnet associated with the rock suites. Similar

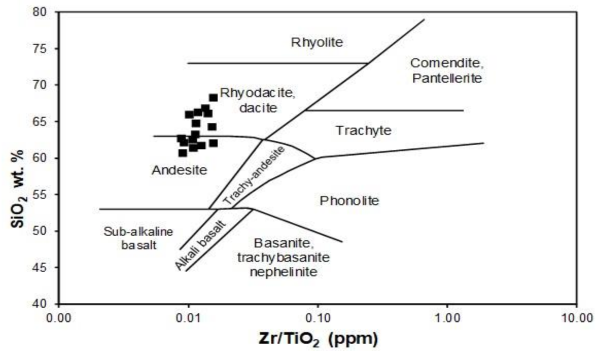

Fig. 26 Zr/TiO_2 vs SiO_2 plot after Winchester and Floyd (1977)

observation showing clear separation of both the suites of lithotypes is also indicated by AFM plot (Irvine and Barangar, 1971) (Fig. 24). In felsic volcanic, Ba content varies from 479 ppm to 1585 ppm, Zr 52 ppm to 191 ppm, Ce 84 ppm to 245 ppm. Nb vs Y plot (Pearce et al., 1984) shows volcanic arc signature of the rocks (Fig. 25). Zr/TiO_2 vs SiO_2 (Winchester and Floyd, 1977) plot of the felsic volcanic suggests that the samples clustered around andesite to rhyodacite-dacite field (Fig. 26).

Suitability of Chandil Formation as prospective uranium source rock

Felsic volcanic and volcaniclastics have radiometrically assayed intrinsic uranium content ranging <5- 7 ppm (n=42) and <5-9 ppm (n=25) respectively (Table 4). Thorium content in felsic volcanic and volcaniclastics rocks vary from <10 ppm to 40 ppm and <10 ppm to 48 ppm. Elevated intrinsic uranium concentration in these rocks is indicative of good source rock characteristics for uranium mineralization. Metamict allanite and zircon are indicative of the presence of labile uranium in source rocks which can easily contribute uranium into the system (Cuney, 2014). Another important fertile source rock for uranium is carbonaceous phyllite in which high intrinsic uranium content up to 10 ppm (n=12) have been analyzed radiometrically. Gamma ray (ppm) logging of the boreholes drilled in the area indicated intrinsic radioactivity (eU_3O_8) of 10 - 53 ppm, mostly between 10-20 ppm. Therefore, the volcanic-volcaniclastic-argillite litho-assemblage represents a prospective source for uranium.

Discussion and Conclusion

The presence of felsic volcaniclastic rocks in Chandil Formation, preponderantly tuffaceous phyllite, was reported earlier along the SPSZ by Acharya et. al. (2006). However, Kharidih-Bareda area, located about 15 km further south of SPSZ, exposes a variety of volcaniclastic rocks as well as felsic flows indicating that the middle part of Chandil Formation was the prime horizon for felsic volcanism. Earlier researchers argued for fluvial origin of the lower part of Chandil Formation on the basis of compositional and textural immaturity along with lenticular geometry and unimodal orientation of cross-strata of certain patches of sandstones (Mazumder, 2005; Chaterjee et al., 2013; De et al., 2016). However, detailed geological mapping in this key sector indicated sheet-like fine to medium grained quartzite bodies extending up to a kilometer co-folded with volcaniclastics and meta-argillites. The occurrence of interlayers of carbonaceous slate/phyllite and profuse syngenetic pyrite-bearing zones within lapilli-rich volcaniclastics suggests euxenic depositional condition. Concealed horizons of limestone and calcareous formations in association with carbonaceous and pyrite-bearing horizons intercepted in boreholes corroborate marine shelf depositional condition. Lava flow, pyroclastic fall, ash fall deposits suggest effusive activity with an intermittent mild explosion. Thus, three modes of transport viz, flow, traction and suspension are decipherable from the lithotypes and structures of the felsic volcanic rocks.

Geochemistry of volcaniclastics and volcanics of Chandil Formation in Kharidih-Bareda sector shows that the volcaniclastic rocks have a wide variation in silica content (44.81-67.79%) as compared to felsic volcanics (59.57-68.20%). Higher $Fe_2O_{3(T)}$ content (6.98-31.57%) recorded in volcaniclastics is attributed to the profuse presence of pyrite as compared to the volcanic flows (7.31-19.55%). Both syngenetic pyrite, encircling the grain boundaries of lapilli clasts and bedding planes and epigenetic pyrite occupying the fracture and foliation planes are discernible. Major element geochemistry indicates rhyodacitic - andesitic and peraluminous to meta aluminous nature of the volcanics and volcaniclastics. Although there are differences in the geochemical signatures of both felsic volcanics and volcaniclastics, their spatial closeness suggests that these rocks might have been genetically related. Geochemical signatures of HFS elements like Nb, Zr, Y indicate arc-related magmatism of the felsic volcanics.

Granites and rhyolites are considered as primary uranium sources for the formation of uranium deposits. Large uranium deposits such as Streltsovka, Russia, Dornod complex, Mongolia and Olympic Dam, Australia are associated with acidic volcanic and plutonic complexes (Cuney, 2009). Studies by Cuney (2014) have highlighted four types of felsic magmatics, viz, peralkaline, high-K metaluminous calc-alkaline, L-type peraluminous and anatectic pegmatoids, which can be sufficiently enriched in U to represent a significant source for the genesis of U deposits. The presence of uraninite or U in the glassy matrix of the volcanic equivalent of these rock types offers the best possible source. When uranium-bearing accessory minerals are available in metamict state, the high-K calc-alkaline plutonic rocks also becomes a promising U source (Leroy and George-Aniel, 1992; Cuney, 2009). Hydrothermal fluids passing through these minerals can scavenge uranium and carry them to suitable reduction traps. Studies also emphasize the capacity of highly saline, very acidic high temperature oxidizing solution to release uranium even from refractory minerals (Cuney and Mathieu, 2000). Nevertheless, acid volcanics like rhyolite, welded tuff and ignimbrites which contain readily leachable uranium present in the glassy matrix are considered to be ideal sources (Maithani and Srinivasan, 2011).

The Chandil Formation of NSMB is replete with felsic eruptives and effusive components. Based on elevated uranium concentration (up to 9 ppm) in the felsic volcaniclastics and carbonaceous metapelites, a potentially economic source of uranium for volcanic-related hydrothermal uranium deposits is envisaged in the basin. The presence of metamict allanite and zircon, and pleochroic haloes in the peraluminous to metaluminous felsic volcanics and volcaniclastics supports source rock favourability for uranium. Anomalous zones of uranium mineralization showing polymetallic signature (U-Cu-Au-Ag-REE), hosted by ferrugenised brecciated carbonaceous and cherty phyllite, has been reported at Kantaldih area, at the southern contact of Chandil Formation with Dalma Volcanics (Mishra et al., 1999; Mishra, 2002). Evidence of uranium mineralization in carbonatite-alkali ultramafite environment has been reported from the SPSZ at the northern contact of Chandil Formation with CGGC (Singh, 1977; Katti et al., 2010). Hence, based on such signatures of mineralisation, efficient remobilization of uranium by hydrothermal fluids is envisaged within Chandil Formation Thermal effect for such mobilization can be imparted by felsic and basic intrusives. Structural conduits like concealed shear and fracture zones sympathetic to Dalma thrust and SPSZ would provide passage for movement of uranium bearing fluid. Intercalatory bands of carbonaceous metapelite, ferruginous material and pyrite-bearing horizons can form reduction zones along suitable structural traps. Thus, the study suggests that Chandil Formation represents an environment wherein suitable provenance and host rock for uranium mineralization exists within the same geological domain, which necessitates further research.

Acknowledgement

The authors are thankful to Director, Atomic Minerals Directorate for Exploration & Research (AMD) for permitting to publish the paper. Encouragement provided by Additional Director (Op-I) is thankfully acknowledged. Thanks are due to the scientists of different laboratories for providing analytical support.

References

Acharya, A., Ray, S., Choudhuri, B.K., Basu, S.K., Bhadhuri, S.K. and Sanyal, A.K. (2006), Proterozoic rock suites along South Purulia Shear Zone, Eastern India: Evidence for rift – related setting: Jour. Geol. Soc. Ind, v. 68, p. 1069-1086.

Chatterjee, P., De, S., Ranaivoson, M., Mazumder, R and Arima, M (2013), A review of the ~1600 Ma sedimentation, volcanism, and tectono-thermal events in the Singhbhum craton, Eastern India: Geosci. Front., v. 4 (3), p. 277-287.

Cuney, M. and Mathieu, R. (2000), Extreme light rare earth element mobilization by diagenetic fluids in the geological environment of the Oklo natural reactor zones, Franceville basin, Gabon: Geology, v. 28, p. 743-746.

Cuney, M. (2009), The extreme diversity of uranium deposits: Miner. Dep. v. 44, p. 3-9.

Cuney, M. (2014), Felsic magmatism and uranium deposits: Bulletin de la Societe Geologiquue de France, v. 185 (2), p. 75-92.

De, S., Mallik, L., Mazumder, R., Chatterjee, P., Ohta, T., Saito, S. and Chiarenzelli, J. (2016), Sedimentation history of the Paleoproterozoic Singhbhum Group of rocks, Eastern India and its implications: Earth-Science Reviews, v. 163, p. 141-161.

Dunn, J.A. and Dey, A.K., (1942), Geology and petrology of Eastern Singhbhum and surrounding areas: Geol. Surv. Ind. Mem., v. 69 (2), p. 281-456.

Fisher, R. V. (1966), Rocks composed of volcanic fragments: Earth Science Review, v. 1, p. 287–298.

Gupta, A and Basu, A. (2000), North Singhbhum Proterozoic Mobile Belt, Eastern India- a review: Geol.Surv. Ind. Spl. Pub.,v. 55, p. 195-226.

Irvine, T.N. and Barangar, W.R.A. (1971), A guide to the chemical classification of the common volcanic rocks: Canadian Jour. of Earth Sci., v. 8, p. 523-548.

Katti, V.J., Sen,Joydip and Bhatt, A. K. (2010), Uranium potentiality of South Purulia Shear Zone. Paper presented in Technical committee meeting on low grade uranium deposits at IAEA, Vinnea, March 29-31.

Le Bas, M.J., Le Maitre, R.W., Streckeisen, A. and Zanettin, B. (1986), A chemical classification of volcanic rocks based on the total alkali-silica diagram: Journal of Petrology, v. 27, p. 745-750.

Leroy J. and George-Aniel B. (1992), Volcanism and uranium mineralisations: the concept of source rock and concentration mechanism: J. Volcan. Geotherm. Res, v. 50, p. 247-272.

Mahadevan, T. M. (2002), Geology of Bihar and Jharkhand: Geol. Soc. Ind., 563pp.

Maithani, P.B. and Srinivasan, S. (2011), Felsic volcanic rocks, a potential source of uranium - An Indian Overview: Energy Procedia, v. 7, p. 163–168.

Maniar, P.D. and Piccoli, P.M. (1989), Tectonic discrimination of granitoids: Geol. Soc. Am., v. 101, p. 635-643.

Mazumdar, R. (2005), Proterozoic sedimentation and volcanism in the Singhbhum crustal province, India and their implications: Sed. Geol., v. 176, p. 167-193.

Mazumder, R., De, S., Ohta, T.,D. Flannery, Mallik, L., C haudhury, T.,Chatterjee, P., Ranaivoson, M.A. and Arima,M. (2015), Palaeo-Mesoproterozoic sedimentation and tectonics of the Singhbhum Craton, Eastern India, and implications for global and craton-specific geological events: Geol. Soc. Lond., v. 43 (1), p. 139-149.

Mishra, K.S., Gupta, K.R., Bagchi, A.K. and Singh, Jagmer (1999), Proterozoic Iron Oxide (Cu-Ni-U-REE) type mineralization in the environs of Dalma Volcanics, West Singhbhum District, Bihar, A new horizon for exploration for polymetallic ores: Jour. Geol. Soc. Ind., v. 54, p. 491-494.

Mishra, K.S. (2002), Geochemistry of Proterozoic carbonaceous metasedimentaries from the northern part of Dalma metavolcanics belt, West Singhbhum district, Jharkhand: Implications for its provenance: Jour. of Applied Geochemistry, v. 4(2), p. 212-227.

Pearce, J.A., Harris, N.W. and Tindle, A.G. (1984), Trace element discrimination diagrams for the tectonic interpretation of granitic rocks: Journal of Petrology. v. 25, p. 956-983.

Ray, K. K., Ghosh Roy, A. K. and Sengupta, S. (1996), Acid volcanic rocks between the Dalma volcanic belt and the Chhotanagpur Gneissic Complex, East Singhbhum and Purulia Districts of Bihar and West Bengal: Ind. Mineral., v. 50, p. 956-983.

Reddy, S. M., Clarke, C. and Mazumder, R., (2009), Temporal constraints on the evolution of the Singhbhum Crustal Province from U-Pb SHRIMP data. In Saha, D.,Mazumder, R., (Eds.), Paleo-proterozoic Super Continents and Global Evolution: International Association for Gondwana Research Conference Series, Abstract v. 9, p. 17-18.

Sengupta, S., Sarkar, G., Ghosh-Roy, A. K., Bhaduri, S. K., Gupta, S. N. and Mandal, A. (2000), Geochemistry and Rb-Sr Geochronology of acid tuffs from the northern fringe of the Singhbhum craton and their significance in the Precambrian evolution: Ind. Miner., v. 54, p. 43-56.

Singh, G (1977), Status of exploration for atomic minerals in Purulia district, West Bengal and future possibilities, In: Sem. Vol. Mineral resources and mineral-based industries in Purulia district, W. B- Prospects and perspectives: Mines, Metals and Fuels. Special Publn. p. 61-65.

Winchester, J.A. and Floyd, P.A. (1977), Geochemical discrimination of different magma series and their differentiation products using immobile elements: Chem. Geol., v. 20, p. 325-343.

Received: 12th July, 2020
Revised Accepted: 13th August, 2021

JOURNAL INDIAN ASSOCIATION OF SEDIMENTOLOGISTS ISSN NO 2582 – 2020
Vol. 38, Issue 2, 2021, pp. 49-62
DOI: https://doi.org/10.51710/jias.v38i2.134

Geochemistry and tectonic setting for the deposition of IOG siliciclastics at the western margin of Bonai Granite, Singhbhum-Orissa Craton, India

Ashim Jana[1*] and D. K. Sinha[2]
Atomic Minerals Directorate for Exploration and Research, Jamshedpur- 831 002[1]; Hyderabad- 500 016[2], India
*Email: ashimjana.amd@gov.in

Abstract

Bagiyabahal and Birtola areas are located in the south-western extension of the Noamundi-Koira Iron Ore Group (IOG) basin. Rock types exposed in the area comprises of siliciclastics and volcanics which occurs unconformably over the basement tonalite-trondhjemite granite-gneiss (Bonai Granite Phase-I). The cover rocks show sheared contact with the porphyritic Bonai Granite Phase-II. The IOG basin margin is suggested to be a part of a 'volcanic passive margin' as indicated by the geochemical behaviour of the siliciclastics as well as massive emplacements of mafic intrusives (doleritic sill, dyke and gabbro) and extrusives (basaltic lava flow) along faulted continental blocks. The siliciclastics comprise of U and Au bearing quartz-pebble conglomerate (QPC) and quartzite succession. It was deposited along the western margin of the Bonai granite (phase I) in anoxic conditions as indicated by their low Th/U ratios and presence of detrital uraninite grains. Repeated cycles of sedimentation and volcanism led to the formation of alternate layers of siliciclastics and basic bodies in the area. Major, trace and rare earth elements (REE) geochemical data suggests a semi-humid to humid palaeo-climatic environment of during the deposition in the passive continental margin setting characterized by fault-controlled sedimentation over a rift related faulted continental crust and shelf. Geochemical data suggests chemically weathered provenance dominated by clay minerals. Higher content of U, Th, Au, Cr, REE, platinum group of elements (PGE) and other geochemical ratios suggest a mixed provenance for the deposition of the siliciclastics comprising a predominantly acidic/granitic source possibly from the Bonai Granitic Complex (BGC) along with granite derived reworked quartzose sediments, minor basic and ultrabasic sources of Older Metamorphic Group (OMG). This paper attempts to characterize the geochemical behaviour, tectonic setting and provenance of the siliciclastics of Birtola and Bagiyabahal areas by analyzing drill core and surface samples.

Keywords: Siliciclastics, Provenance, QPC, Diagram, Tectonic

INTRODUCTION

Geochemistry is a useful tool for determination of the provenance and tectonic setting for the deposition of sedimentary rocks (Bhatia, 1983; Bhatia and Crook, 1986, Roser and Korsch, 1986, 1988, Nesbitt et al., 1996). The Singhbhum Orissa Craton hosts several granite-greenstone assemblages with overlying metasediments as IOG rocks (Saha, 1994). The Noamundi-Koira IOG rocks are situated at the western part of the Singhbhum Orissa Craton. The geology and stratigraphy of the area to the north-west of BGC have been studied by several workers (Mahalik, 1987; Sengupta et al., 1991; Sarkar and Saha, 1992; Chakrabarti et al., 2001, Naik, 2001, Saha et al., 2004, Kundu and Matin, 2007; Kumar et al., 2009). The Noamundi-Koira IOG is also favourable for U-Au-Ag-PGE-REE bearing QPC lithounits at the base of IOG (Kumar et al., 2009, Kumar et al., 2011, Jana et al., 2016) in the Singhbhum-Orissa Craton. The geochemical characteristics as well as the tectonic setting for deposition of QPC and quartzite lithounits of the Noamundi-Koira IOG basin in this part of Singhbhum-Orissa Craton around Bagiyabahal and Birtola areas have remained the least studied so far. In this study we have carried out geochemical analysis of drill core and surface samples of Makarchua-Balisura tract (comprises of Bagiyabahal sector and Birtola sector) in order to understand the geochemical characteristics, provenance of the siliciclastics and establish the tectonic model for its deposition along the basin margin.

Regional Geology

Geologically the study area of entire Makarchua-Balisura tract is situated along the western margin of Bonai Granite in the western part of Singhbhum-Orissa Craton and it is thought to be the south-western extension of the Noamundi-Koira IOG basin. The IOG rocks rest unconformably over the Archaean basement of tonalite-trondhjemite (migmatitic at places) variety of Bonai Granite Phase-I (3369±57 Ma) (Sengupta et al., 1991) and intruded by porphyritic granite/granodiorite variety of Bonai Granite Phase-II (3163±126 Ma) (Sengupta et al., 1991, Sarkar and Saha, 1992) which is evidenced by the presence of large enclaves of IOG quartzite, pelitic metasediments, meta-lava and amphibolite within the porphyritic Bonai Granite (Saha, 1994).The volcano-sedimentary succession of IOG is unconformably overlain by the Darjing Group of rocks in the north

(Mahalik, 1987). The 2.8 Ga old Tamperkola Granite intruded both the Darjing and IOG rocks (Bandyopadhyay et al., 2001). U–Pb LA-ICPMS age from the acid volcanics of western IOG suggests an age of 3.29 Ga (Basu et al., 2008). The IOG rocks are whereas the few enclaves of Bonai Granite Phase-I are exposed as small patches within the Bonai Granite Phase-II.

IOG Siliciclastics

The IOG siliciclastic rocks of Bagiyabahal and Birtola area consist of intermittently exposed polycyclic, matrix supported, oligomictic, radioactive QPC bands hosted in matured quartzite (Jana et al., 2016) (Fig. 2). Apart from the radioactive basal QPC band (which is prominently exposed and comparatively thicker), several thin interlayered radioactive QPC layers and lenses of varying dimensions have also been located within the IOG quartzite suggesting a palaeochannel controlled cyclic deposition of sediments. The thickness of the QPC bands varies from 30cm to 3m. The QPC is matrix supported, oligomictic, comprising slightly stretched, sub-rounded to well-rounded clasts of vein quartz, greyish black coloured smoky quartz pebbles with iron oxide stains (Fig. 4a, b). Matrix is mostly siliceous and micaceous (sericite, chlorite, fuchsite, biotite and muscovite) with goethite at places and with pyrite. Sericite and chlorite are the most dominant flaky minerals in matrix along with quartz exhibiting crude schistosity (S_1) which is parallel to the strike of the

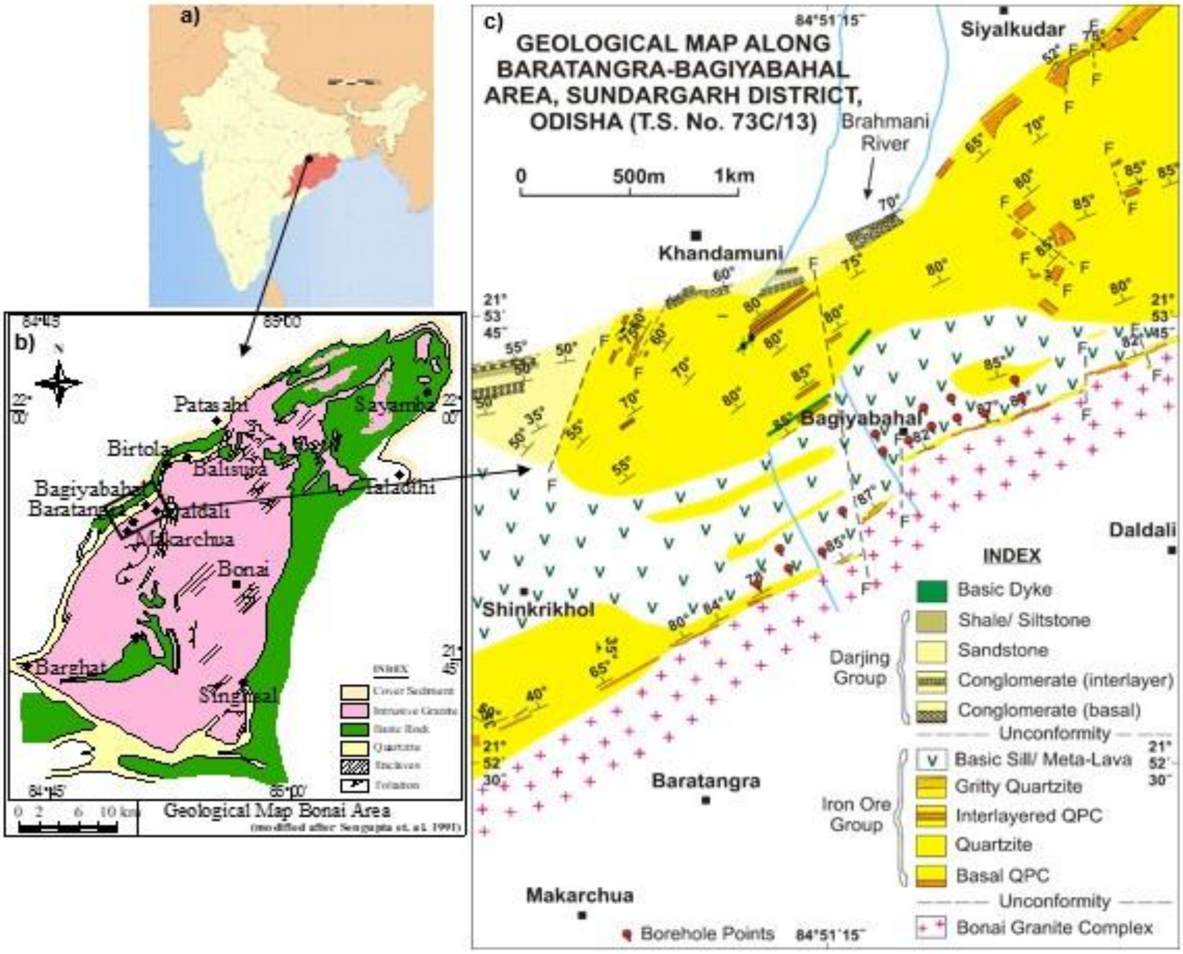

Fig. 1a)- Study area shown in India map, b) Geological Map along entire Makarchua- Balisuratract and c) along Makarchua – Daldali tract showing borehole points around Bagiyabahal, Baratangra areas, Sundargarh district, Odisha

devoid of iron ore and mostly represented by QPC, quartzite, quartz-sericite schist and intercalated meta-basic lavas exposed in a series of hills trending in NE-SW to ENE-WSW direction with dips 40º-80º due NW/NNW all along the western margin of BGC. The IOG metasediments are intruded by several younger basic dykes and sills (Fig. 1a, b, c, Table. 1). The QPC-quartzite succession is exposed over a strike length of approximately 8km from Makarchua in the west to Balisura in the east over the BGC (Kumar et al., 2009, Jana et al., 2016) (Fig. 1b). The QPC-quartzite succession of the Makarchua-Balisura tract is displaced by a regional N-S fault along the Birtola-Daldali section which bifurcates the entire succession into two parts (i) Bagiyabahal sector (Makarchua-Bagiyabahal-Daldali tract) and (ii) Birtola sector (Birtola-Balisura tract) (Fig. 1b, c). Darjing Group is represented by Birtola, Kumakela and Jalda Formation (Mahalik, 1987). Bonai Granite Phase-II covers the vast area of the terrain

Table. 1- Stratigraphic succession of Baratangra-Bagiyabahal area (after Sarkar and Saha, 1992)	
Birtola Formation (Darjing Group)	Feldspathic quartzite and conglomerate
	Green schist conglomerate and greenish quartzite
	Conglomerate and quartzite
Unconformity	
Dolerite dykes, basic sills, ultrabasics, aplite and pegmatitic veins	
Bonai Granite II (Potassic porphyritic granite, 3.16 Ga)	
Iron Ore Group (Conglomerate, quartzite and metabasic lava)	
Unconformity	
Bonai Granite I (Tonalitic grey gneiss, 3.3 Ga)	

QPC-quartzite bedding (S_0). Pebble-matrix ratio is approx. 1:4 (by volume). Reduction in clast size (7.5cm to 0.3cm) and increase in the content of vein quartz clast are observed from the basal QPC to interlayered QPC lithounit towards the top of the succession. Sub-rounded, detrital uraninites are associated with other subrounded to rounded heavy minerals, viz. monazite, magnetite, pyrite, rutile, ilmenite and zircon in the QPC matrix as palaeoplacers (Jana et al., 2016) (Fig. 4c).

Fig: 2- Radioactive basal QPC exposed in Brahmani riverbed near Baratangra

Fig: 3- Trough cross-stratified quartzite of IOG exposed near Khandamuni

Quartzite is the major siliciclastics of the 'iron ore barren' IOG which is exposed in a series of hills of Bagiyabahal and Birtola areas trending in NE-SW to ENE-WSW direction with dip of 40º-88º due NW/NNW. The quartzite shows steep dipand shearing near the contact zone with granite but dip decreases towards the centre of the basin. Quartzite occurs in

Fig. 4a, b: Stretched smoky quartz pebble in the radioactive QPC core samples, Baratangra and
c: Detrital, broken uraninite grains (U) in QPC, Bagiyabahal. TL, 1N, 10X

different varieties e.g. fuchsitic sericitic, pure massive, fine grained, gritty and also as fine layers/bands at places. Deformation and higher amount of chlorite and mica (sericite and fuchsite) minerals often turned the quartzite to quartz-chlorite-sericite schist and quartz-sericite schist (± fuchsite). These two varieties are dominantly exposed at the surface as well as intercepted in the drill cores. Foliation parallel to the regional strike of the formation (S_0) (N65°E- S65°W) is present in quartzite.In Bagiyabahal - Baratangra sector, the quartzite is massive near the lower part of the succ-

Major Oxides

The major elemental parameters of QPC and quartzite have been used to understand the tectonic settings of different sedimentary environments (Bhatia, 1983, Roser and Korsch, 1986). The QPC drill core samples have been sub-divided into two categories according to matrix composition (especially on the content of phyllosilicate minerals as well as Al_2O_3) e.g. i) QPC with sericitic matrix and ii) QPC with siliceous matrix.

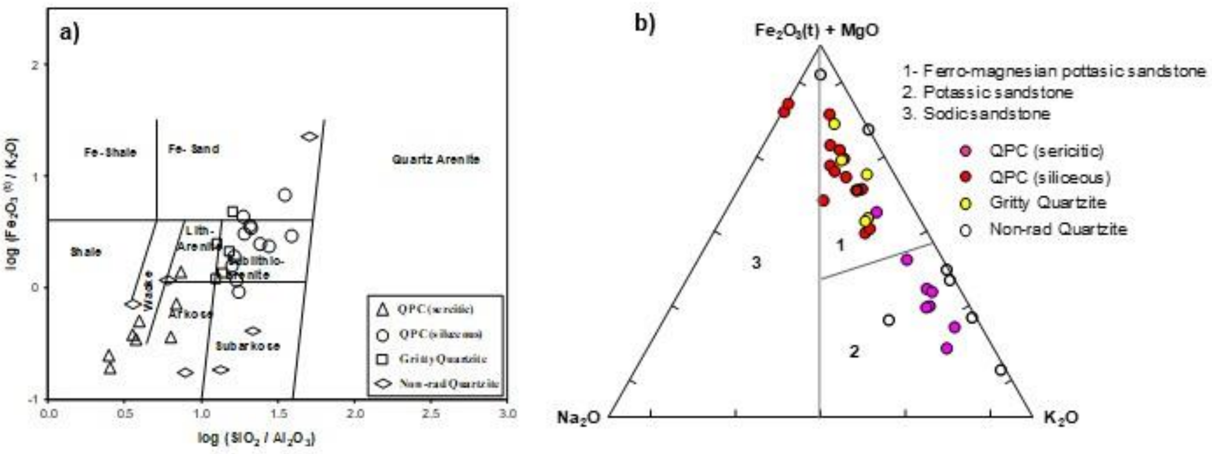

Fig. 5 Classification diagrams a) - log(Fe_2O_3(t)/K_2O) vs log(SiO_2/Al_2O_3) diagram of radioactive QPC (with siliceous and sericitic matrix), gritty quartzite and non-radioactive quartzite of Bagiyabahal and Birtola Blocks (after Heron, 1988) and b)- Fe_2O_3(t)+MgO vs Na_2O vs K_2O ternary diagram for classification of radioactive QPC (with siliceous and sericitic matrix), gritty quartzite and non-radioactive quartzite of Bagiyabahal and Birtola Blocks (after Blatt, 1972)

ession and almost devoid of any primary sedimentary feature due to intense silicification. Few crudely developed plane bedding, low angle planar cross bedding in quartzite and crude graded bedding in basal QPC band have been observed at places indicating high energy flow regime. From middle to upper part of the succession massive to mostly trough cross bedded quartzite was deposited with scattered palaeoflow directions in the braided streams with thin interlayered pebbly quartzite/conglomerates near Khandamuni area (Fig. 3). Quartzites are mostly non-radioactive in nature.

GEOCHEMISTRY

Major oxides, trace elements and REE data have been utilized in the interpretation of the tectonic setting of sedimentary rocks. The surface as well as borehole core samples of QPC and quartzite of the Birtola and Bagiyabahal sectors have been analysed. Trace elements and REE analysis of core and surface samples have been carried out by Flame-AAS and ICP-AES at Chemistry Laboratory, AMD, Jamshedpur. The procedures are normalised and validated by analysing certified reference materials. Major oxides and some of the trace elements of core samples have been analysed by XRF Spectrometry at AMD, Nagpur.

The quartzite samples also have been categorised into two, based on their radio-elemental concentration e.g. i) radioactive gritty quartzite and ii) non-radioactive massive quartzite. A total of 35 samples have been analysed, viz. radioactive QPC with siliceous matrix (n=14), QPC with sericitic matrix (n=8), gritty quartzite (n=5) and massive quartzite (n=8) (Table. 2).

The binary plot of log(Fe_2O_3(t)/K_2O) vs log(SiO_2/Al_2O_3) (Heron, 1988, Fig. 5a) shows a wide distribution of siliciclastics in different fields. QPC having sericitic matrix mostly falls in wacke field (>60% sample) as well as arkose fields with a solitary sample in the lith-arenite field. QPC having siliceous matrix (Fig. 5a) falls mostly in sub-lithic arenite field (>70% sample) with very few samples in Fe-sandstone and sub-arkose fields. The radioactive gritty quartzite samples too mostly fall in the sub-lithic arenite field with a few samples distributed in the boundary regions of lith-arenite and Fe-sandstone with sub-lithic arenite field. The non-radioactive massive quartzite samples show a scattered distribution in arkose, sub-arkose, wacke and Fe-sandstone fields indicating their variation in composition and a probable mixed provenance (Fig. 5a). The geochemistry of the siliciclastics broadly varies from sub-lithic arenite to wacke to arkosic category.

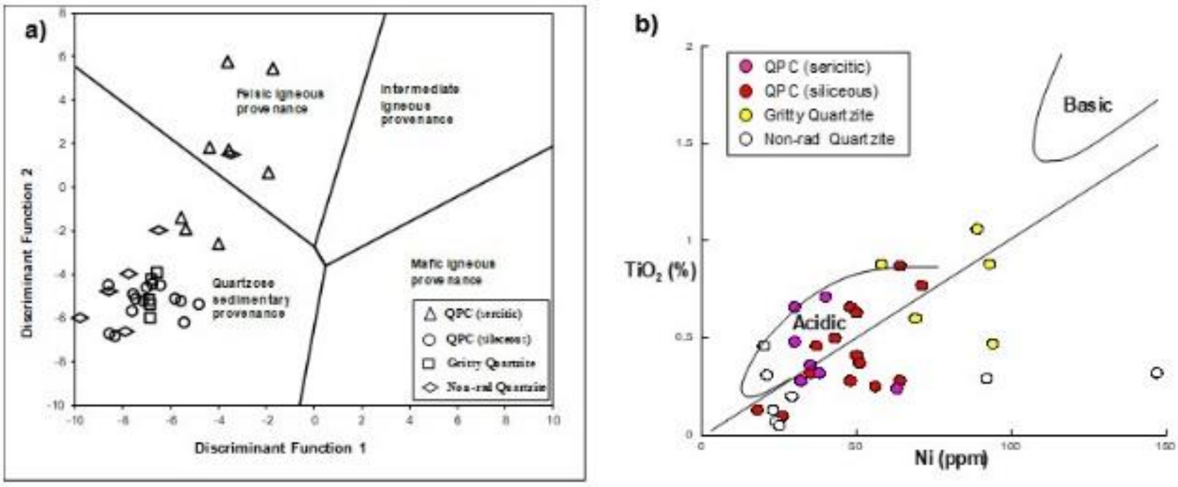

Fig. 6 Provenance diagrams a)- Provenance study of radioactive QPC (with siliceous and sericitic matrix), gritty quartzite and non-radioactive quartzite of Bagiyabahal and Birtola Blocks (after Roser and Korsch, 1988) through discriminant functions and b)- TiO_2 vs. Ni sedimentary provenance discriminant diagram of radioactive QPC (with siliceous and sericitic matrix), gritty quartzite and non-radioactive quartzite of Bagiyabahal and Birtola Blocks for fields for acidic and basic source materials (after Floyd et al. 1989)

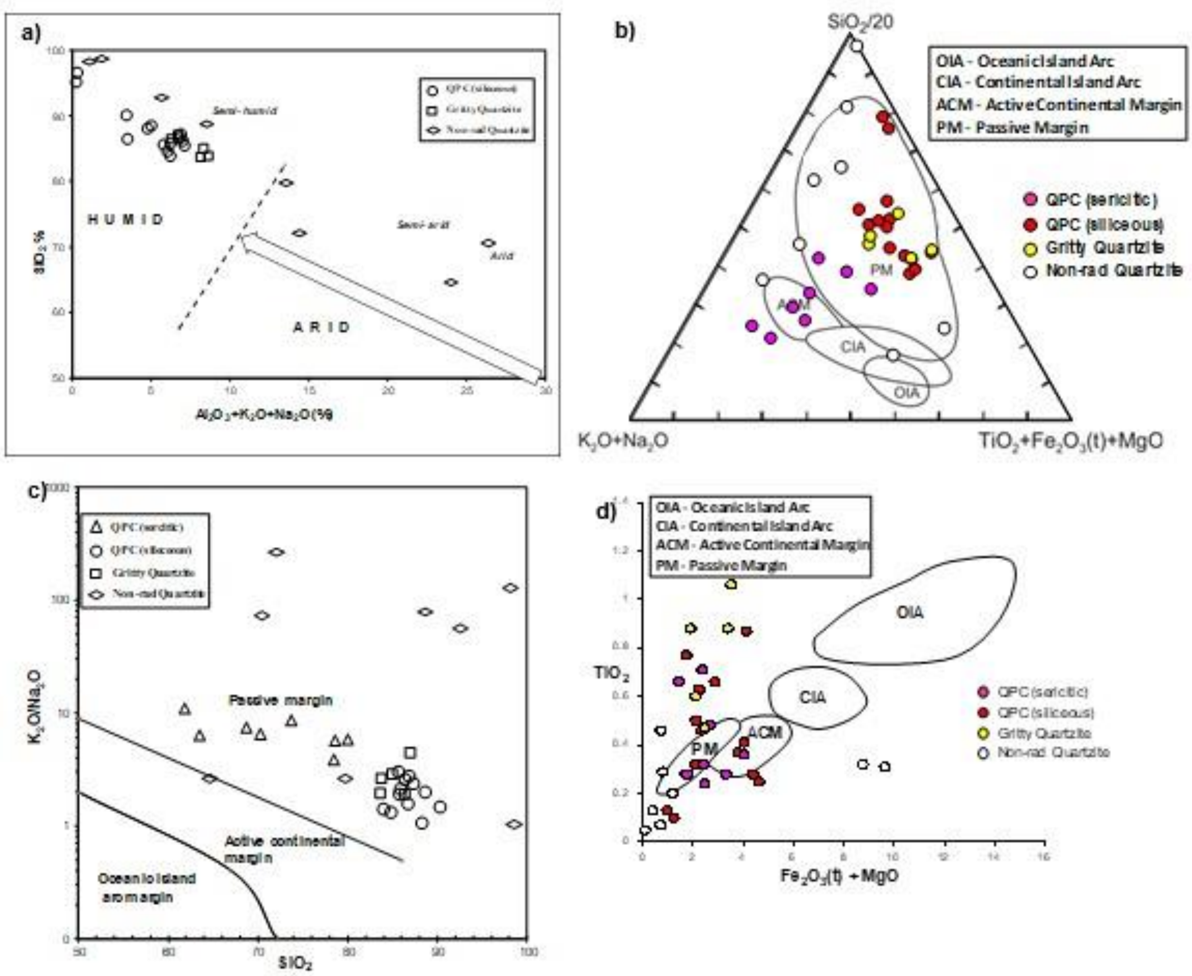

Fig. 7 Climate diagram a)- SiO_2 (%) vs Al_2O_3+K_2O+Na_2O (%) diagram of radioactive QPC (with siliceous and sericitic matrix), gritty quartzite and non-radioactive quartzite of Bagiyabahal and Birtola Blocks (after Suttner and Dutta, 1986) and Tectonic Setting Diagrams b)- SiO_2/20 vs K_2O+Na_2O vs TiO_2+Fe_2O_3(t)+MgO ternary diagram for tectonic setting of radioactive QPC (with siliceous and sericitic matrix), gritty quartzite and non-radioactive quartzite of Bagiyabahal and Birtola Blocks (after Kroonenberg, 1994), c)- K_2O/Na_2O vs SiO_2 diagram for tectonic setting of radioactive QPC (with siliceous and sericitic matrix), gritty quartzite and non-radioactive quartzite of Bagiyabahal and Birtola Blocks (after Roser and Korsch, 1986) and d)- Fe_2O_3(t)+MgO vs TiO_2 plot on tectonic setting discrimination diagram of radioactive QPC (with siliceous and sericitic matrix), gritty quartzite and non-radioactive quartzite of Bagiyabahal and Birtola Blocks (after Bhatia, 1983)

Table. 2- Analysis of major oxides and 'Ni' of the drill-core samples of the QPC and quartzite of Bagiyabahal and Birtola areas (all values are in percentage except 'Ni' which is in 'ppm' and the ratios are unitless)

Sample No.	Lithology	SiO_2	TiO_2	Al_2O_3	FeO(T)	MgO	MnO	CaO	Na_2O	K_2O	P_2O_5	Ni	SiO_2/Al_2O_3	MgO/Al_2O_3	K_2O/Al_2O_3	K_2O/Na_2O
BGL-1/B2/9	QPC (siliceous)	85.50	0.66	5.28	2.63	0.25	0.02	0.16	0.45	1.37	0.08	48	16.19	0.047	0.259	3.044
BGL-1/B2/10		85.64	0.41	4.14	3.83	0.21	0.02	0.18	0.54	1.05	0.07	50	20.69	0.051	0.254	1.944
BGL-1/B2/11		84.65	0.87	4.01	3.88	0.25	0.02	0.19	0.85	1.13	0.11	64	21.11	0.062	0.282	1.329
BGL-2/B2/10		87.19	0.77	5.04	1.15	0.59	<0.01	0.13	0.52	1.26	0.07	71	17.30	0.117	0.250	2.423
BGL-2/B2/14		83.93	0.25	4.47	4.31	0.32	<0.01	0.12	0.71	1.00	0.05	56	18.78	0.072	0.224	1.408
BGL-3/B2/26		88.52	0.46	3.68	2.13	0.23	0.02	0.19	0.43	0.87	0.08	37	24.05	0.063	0.236	2.023
BGL-4/B1/16		86.21	0.63	5.50	1.65	0.61	0.02	0.22	0.40	1.05	0.09	50	15.67	0.111	0.191	2.625
BGL-2A/B2/34		86.68	0.28	5.11	1.43	0.27	<0.01	0.12	0.44	1.22	0.03	48	16.96	0.053	0.239	2.773
BGL-2A/B2/35		88.09	0.50	3.18	1.86	0.27	<0.01	0.12	0.74	0.79	0.05	43	27.70	0.085	0.248	1.068
BGL-2A/B2/36		90.16	0.32	2.33	1.88	0.20	<0.01	0.12	0.43	0.64	0.04	35	38.70	0.086	0.275	1.488
BGL-2A/B2/37		85.73	0.37	4.49	3.51	0.28	<0.01	0.14	0.53	1.14	0.05	51	19.09	0.062	0.254	2.151
BGL-4/B2/22		95.23	0.13	<0.01	0.88	0.10	<0.01	0.21	0.21	<0.01	0.03	18	-	-	-	-
BGL-4/B2/23		96.60	0.10	<0.01	1.14	0.11	<0.01	0.19	0.23	<0.01	0.03	26	-	-	-	-
BGL-4/B2/24		86.56	0.28	2.48	4.26	0.14	<0.01	0.31	0.39	0.62	0.12	64	34.90	0.056	0.250	1.590
BGL-1/B2/12	QPC (sericitic)	63.49	0.28	25.07	1.30	0.48	0.01	0.16	1.06	6.79	0.06	32	2.533	0.019	0.271	6.41
BGL-2/B2/19		70.21	0.24	18.84	1.73	0.75	0.01	0.16	0.78	5.06	0.05	63	3.727	0.040	0.269	6.49
BGL-2/B2/31		68.71	0.28	19.38	2.09	1.24	0.02	0.18	0.75	5.58	0.05	32	3.545	0.064	0.288	7.44
BGL-2A/B3/4		78.44	0.36	10.57	3.59	0.45	<0.01	0.16	0.68	2.62	0.06	35	7.421	0.043	0.248	3.85
BGL-2A/B3/5		61.77	0.48	24.57	1.90	0.77	0.02	0.18	0.70	7.68	0.08	30	2.514	0.031	0.313	10.97
BGL-3/B2/25		80.00	0.66	12.70	1.06	0.39	<0.01	0.15	0.51	2.96	0.07	30	6.299	0.031	0.233	5.80
BGL-4/B2/21		78.58	0.71	11.48	1.96	0.42	<0.01	0.42	0.48	2.77	0.11	40	6.845	0.037	0.241	5.77
BGL-4/B2/25		73.68	0.32	18.77	2.16	0.28	<0.01	0.22	0.50	4.31	0.04	38	3.925	0.015	0.230	8.62
BGL/B1/13	Gritty Quartzite	86.42	1.06	5.35	2.94	0.58	0.05	0.17	0.33	0.62	0.09	89	16.15	0.108	0.116	1.88
BGL/B1/17		86.94	0.88	5.68	1.76	0.15	0.05	0.16	0.19	0.83	0.09	58	15.31	0.026	0.146	4.37
BGL-2/B2/30		84.98	0.47	6.16	2.16	0.32	0.01	0.18	0.56	1.60	0.08	94	13.80	0.052	0.260	2.86
BGL-2A/B1/30		83.81	0.60	6.76	1.65	0.47	0.07	0.19	0.53	1.38	0.07	69	12.40	0.070	0.204	2.60
BGL-3/B1/22		83.58	0.88	6.66	2.53	0.88	0.06	0.20	0.52	1.01	0.12	93	12.55	0.132	0.152	1.94
BRT-1/72.55	Massive Quartzite	79.71	0.20	10.16	0.42	0.78	<0.01	0.29	0.96	2.44	0.08	29	7.85	0.077	0.240	2.54
BRT-1/133.25		70.43	0.46	21.42	0.22	0.51	<0.01	0.16	0.07	4.96	0.04	20	3.29	0.024	0.232	70.86
BRT-4/30.25		72.05	0.32	11.84	2.98	5.77	<0.01	1.02	0.01	2.57	0.09	147	6.09	0.487	0.217	257.00
BRT-5/65.1		64.58	0.31	17.91	3.10	6.54	0.02	0.34	1.76	4.42	0.10	21	3.61	0.365	0.247	2.51
BRT-4/6		92.60	0.29	4.26	0.55	0.25	<0.01	0.13	0.025	1.35	0.04	92	21.74	0.059	0.317	54.00
BRT-3/11		88.62	0.07	6.60	0.35	0.36	<0.01	0.17	0.025	1.92	0.03	24	13.43	0.055	0.291	76.80
BRT-1/29		98.16	0.13	0.49	0.23	0.18	<0.01	0.19	<0.01	0.62	0.03	23	200.33	0.367	1.265	-
BRT-1/30		98.55	0.05	1.92	0.11	<0.01	<0.01	0.11	<0.01	<0.01	0.02	25	51.33	-	-	-

The presence of higher Al_2O_3 and K_2O in QPC having sercitic matrix indicates an acidic provenance. In Fe_2O_3(t) + MgO vs Na_2O vs K_2O diagram (Blatt, 1972, Fig. 5b), QPC with siliceous matrix mostly falls under ferromagnesian potassic sandstone and few samples in sodic sandstone field, whereas QPC with sericitic matrix mostly shows potassic nature with a few samples having ferromagnesian potassic characteristics. The gritty quartzite samples fall in ferromagnesian potassic sandstone whereas the massive quartzites are widely distributed both in the ferromagnesian potassic sandstone and potassic sandstone category indicating its mixed provenances. So, the siliciclastics can be categorized in an overall ferromagnesian potassic to potassic sandstone field (Fig. 5b).

Discriminant function analysis (Roser and Korsch, 1988, Fig. 6a) using the major oxides reveals a quartzose sedimentary provenance for most of the siliciclastics of Bagiyabahal and Birtola areas. However, a few QPC samples with sericitic matrix and a solitary massive quartzite sample plot in felsic igneous provenance.

The TiO_2vs Ni binary provenance discriminant diagram (Floyd et al., 1989, Fig. 6b) shows the concentration of all the samples in the field of the acidic source. Thus, two sources of provenance for the siliciclastics consisting of granite and granite derived reworked quartzose sediment especially for QPC is suggested based on geochemical characteristics.

The implication of climatic conditions on the chemical maturity of the siliciclastics was also inferred. The siliciclastics of Bagiyabahal and Birtola areas were deposited under a semi-humid to humid paleo-climate as indicated by a plot of SiO_2 vs Al_2O_3 + K_2O + Na_2O (Suttner and Dutta, 1986, Fig. 7a). The siliciclastics of Bagiyabahal and Birtola areas were deposited in a passive continental margin setting as inferred from the SiO_2 vs K_2O/Na_2O binary diagram. A solitary massive quartzite sample falls in the boundary of passive and active continental margin setting (Roser and Korsch, 1986, Fig. 7c). SiO_2 vs K_2O + Na_2O vs TiO_2 + Fe_2O_3 (t) + MgO diagram (Kroonenberg, 1994, Fig. 7b) also shows the same passive marginal setting for all the samples except a few QPC samples with sericitic matrix and a solitary massive quartzite sample which falls in active continental margin setting. Similarly, Fe_2O_3(t) + MgO vs TiO_2 binary diagram on tectonic setting discrimination diagram (Bhatia, 1983, Fig. 7d) shows that the majority of samples spread over passive continental margin setting with a few QPC samples with both sericitic and siliceous matrix falling within active continental margin tectonic setting. Thus, it can be suggested that the siliciclastics of Bagiyabahal and Birtola were deposited broadly in a passive continental margin setting. This is supported by the quartzose sedimentary source rock and quartz-rich nature of the sediments which were deposited in close proximity to the provenance.

Critical ratios of certain major oxides have also been studied to understand the source rock chemistry and nature of weathering (Table. 2). TiO_2 content in QPC ranges from 0.10 to 0.87 whereas in quartzite, it varies from 0.05-1.06, which may be due to the presence of more titanium bearing minerals in the siliciclastics such as rutile, ilmenite and anatase. These minerals have also been identified by petrographic study.

The K_2O/Al_2O_3 ratio is an indicator to identify the original composition of terrigenous sediments (Cox et al., 1995). The low ratios (<0.3) of K_2O/Al_2O_3 in both the QPC (avg. 0.253, n=21) and quartzite (avg. 0.22, n=21) (Table. 2) suggests the dominance of clay minerals (illite and chlorite) in the siliciclastics. Granite derived quartz clasts formed the siliceous matrix of the QPC and the reworking of clasts led to attaining the high chemical maturity whereas QPC with sericitic matrix showed low SiO_2/Al_2O_3 ratio (2.51-7.42, n=8) (Table. 2) indicating the presence of alumina-rich sediments dominated by clay minerals (Naqvi et al., 1988). Gritty quartzite shows a moderate SiO_2/Al_2O_3 ratio (12.40-16.15) (Table. 2) whereas the massive quartzites show varying ratio. K_2O/Na_2O ratio in sandstones is another important chemical parameter that depends on both the composition of source and intensity of weathering (Lindsey, 1999). A high K_2O/Na_2O ratio (>1) in all the siliciclastics suggests a chemically weathered provenance with presence of clay minerals (e.g. illite).

Trace Elements

The trace element of QPC surface samples (n=30) indicates high Th content ranging from 32 ppm to 330 ppm (avg. 108 ppm) and Cr content ranging from 195 ppm to 1900 ppm (avg. 818 ppm) compared to the average crustal concentration of 8.5 ppm and 126 ppm respectively (Wedepohl, 1995) (Table. 3, Fig. 8). Th and Cr are high mainly due to the presence of monazite and fuchsite in the matrix respectively. Higher Cr/Th ratio (range: 0.95 - 32.91; avg: 10.98) indicates the ultramafic provenance. Pb (5 to 1175 ppm) is also high. Earlier, Au was reported up to 2250 ppb in QPC (Jana et al., 2016). Similarly, 1527 ppb Au and 692 ppb Pt were also reported in quartzite (Kumar et al., 2011). Rh and Ru contents have now been analysed up to 102 ppb and 100 ppb respectively in QPC (Table. 4). QPC is also reported to contain up to 0.34% U_3O_8 with detrital uraninite grains (Jana et al., 2019). Quartzite is mostly non-radioactive except few gritty layers within the quartzite.

Radioactive core samples of gritty quartzite and QPC contain 68ppm to 375ppm U and 31ppm to 146ppm Th. Th/U ratios in the lithounits ranged from 0.186 to 1.515 which is lower in comparison to crustal

Table. 3- Analysis of trace elements of the surface samples of radioactive QPC of Bagiyabahal and Birtola areas (values are in ppm)

Location	Li	Cu	Cr	Zn	Pb	Co	Ni	Sr	V	Th	Cr/Th
Baratangra	5	79	865	20	751	11	<5	10	27	67	12.91
	9	43	1574	57	195	36	<5	17	50	165	9.54
	9	20	1362	100	272	26	7	26	60	93	14.65
	8	34	1100	32	275	17	5	20	27	134	8.21
	6	19	1060	8	988	7	<5	18	23	101	10.50
	13	24	1590	18	425	13	<5	42	64	194	8.20
	12	9	1900	48	362	19	<5	26	67	153	12.42
	11	27	650	34	689	7	<5	19	38	92	7.07
	7	48	1053	73	1175	14	5	28	35	32	32.91
	21	28	900	28	375	13	<5	14	35	78	11.54
	5	43	790	78	117	11	5	15	25	48	16.46
	8	10	195	12	53	<5	<5	51	5	206	0.95
	<5	24	1080	27	99	21	<5	15	49	68	15.88
Bagiyabahal	<5	11	735	9	99	<5	<5	8	24	104	7.07
	<5	15	855	10	50	7	<5	8	30	49	17.45
	<5	18	1095	<5	117	<5	<5	3	18	161	6.80
	<5	<5	650	<5	168	<5	<5	7	19	69	9.42
	<5	14	530	<5	89	<5	<5	12	14	48	11.04
	<5	<5	465	<5	68	<5	<5	9	12	35	13.29
	<5	6	370	<5	74	<5	<5	11	17	75	4.93
	5	64	1050	13	45	12	39	18	25	102	10.29
	6	74	1122	20	55	16	51	19	28	330	3.40
	5	46	980	19	1140	14	8	42	26	111	8.83
	<5	42	840	<5	320	6	<5	10	10	85	9.88
	<1	62	520	<1	130	<1	12	8	46	N.A.	N.A.
	<1	2	482	<1	36	<1	4	<1	12		
Birtola	<5	13	131	<5	5	<5	34	<5	5		
	<5	32	234	13	31	8	38	<5	18		
	<5	26	208	82	55	5	29	<5	22		
	<1	14	158	10	116	<1	20	<1	<1		

rocks (average Th/U ratio ~4) and indicate deposition under anoxic conditions.

High U and Th in QPC indicate a granitic source more specifically the Bonai Granite Complex. The presence of higher Cr and PGE indicates an ultrabasic provenance component. Higher Au content suggests basic sources which probably might be the amphibolite suites of OMG. So, the geochemical characteristic of the siliciclastics suggests an overall mixed provenance.

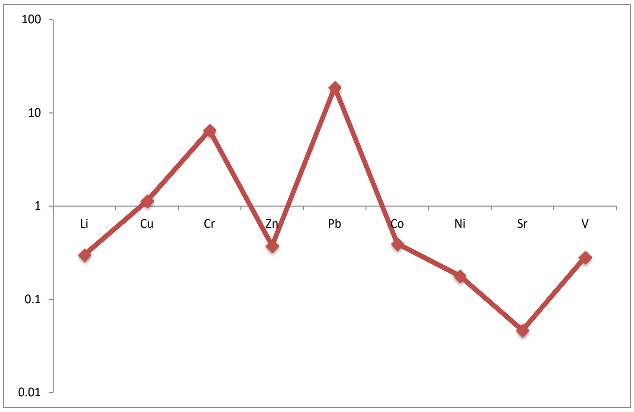

Fig. 8- Average value of trace elements of radioactive QPC of Bagiyabahal and Birtola with respect to continental crust

Table-4: Analysis of PGE of core QPC samples of Bagiyabahal-Baratangra tract (values are in ppb)

Sample No.	Pd	Rh	Ru
BGL-2/B-2/10	15	58	100
BGL-2/B-2/19	<10	95	84
BGL-2A/B-2/34	<10	88	70
BGL-2A/B-2/35	<10	102	92
BGL-2A/B-3/4	<10	23	41
BGL-2A/B-3/5	<10	<10	<10
BGL-2A/B-3/33	<10	<10	<10
BGL-4/B-2/21	<10	<10	<10
BGL-4/B-2/22	<10	<10	<10
BGL-4/B-2/23	<10	<10	<10
BGL-4/B-2/24	<10	<10	<10
BGL-4/B-2/25	<10	<10	<10
BGL-2A/B-1/30	<10	79	52

Rear Earth Elements

REE content of the surface QPC samples of Bagiyabahal area ranges from 303.50 ppm to 2680 ppm with a very high LREE/HREE (31.09) ratio (Table. 5, Fig. 9) and for core QPC samples, it ranges from 254 ppm to 999 ppm with moderately high LREE/HREE (18.30) ratio (Table. 6, Fig. 10). LREE enrichment in QPC are also reflected by their high values of $(La/Sm)_{CN}$ with an average value of 5.04 in surface QPC and 4.86 in core QPC samples. HREE depletion is reflected in surface QPC samples by $(Gd/Yb)_{CN}$ value of 6.60 whereas a nearly flat HREE pattern is observed in core QPC samples with $(Gd/Yb)_{CN}$ value of 2.50. QPC show fractionated
REE pattern with $(La/Yb)_{CN}$ value varying from 16.78 to 52.31 from the core to surface QPC samples. The Eu anomaly in sedimentary rocks is usually interpreted as being inherited from igneous source rocks (McLennan and Taylor, 1991, Taylor and McLennan, 1985). Strong negative Eu anomaly (Eu/Eu*: 0.30) characterises both the surface and core QPC samples. Negative Eu anomaly has been attributed to the presence of plagioclase depleted felsic igneous rocks in the provenance such as granites. Higher content of total REE and negative Eu anomaly is characteristic of QPC. QPC samples yield higher concentration LREE mainly due to the presence of monazite in the matrix which have been derived from the pegmatite and granite sources. LREE fractionation, HREE depletion, higher LREE/HREE and strong negative Eu anomaly indicate derivation of sediment from the highly evolved granitic source.
REE were also used by different workers to decipher provenance study and tectonic setting of the sedimentary rocks (Taylor and McLennan, 1985, Cullers, 1994, Cullers, 2000, McLennan 1989, McLennan and Taylor, 1991). On La-Th-Sc ternary diagram (Bhatia and Crook, 1986, Fig. 11), the radioactive QPC surface samples plot near passive and active continental margin fields along the La-Th line, mostly towards La. REE concentration with trace element signatures such as high Th/Sc (25.45), La/Sc (60.54) ratio also supports granitic provenance for QPC samples (Condie, 1993). High REE and Th concentrations and low Sc (2–10 ppm) indicate derivation of QPC from felsic igneous

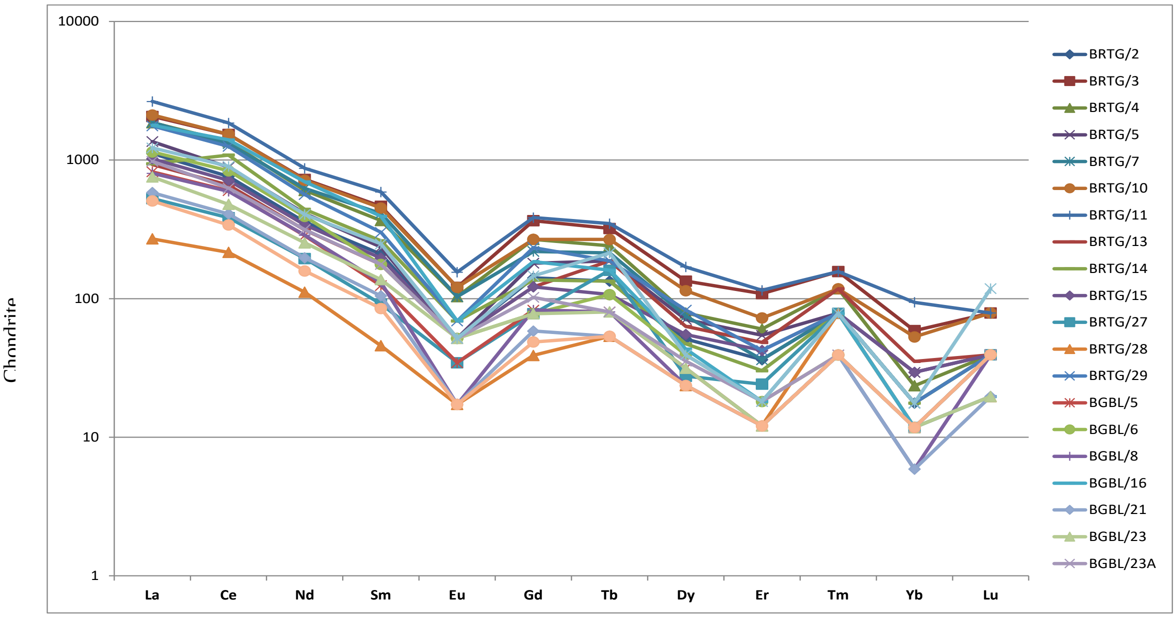

Fig. 9- REE distribution pattern of radioactive QPC surface samples (chondrite normalized)

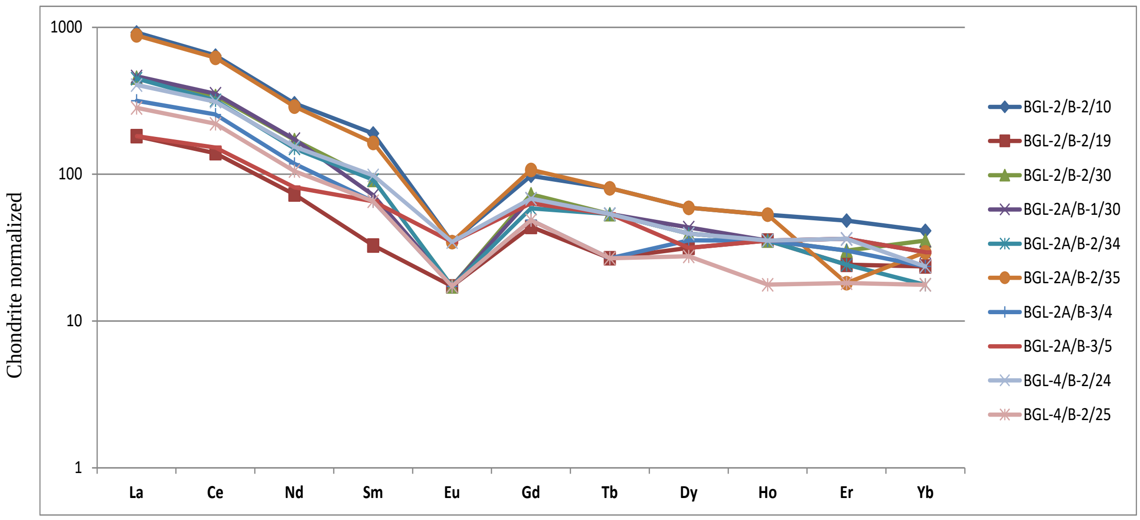

Fig. 10- REE distribution pattern of radioactive QPC core samples (chondrite normalized)

Table. 5- REE content of the surface samples of QPC of Bagiyabahal and Baratangra areas (values are in ppm)

QPC	LREE								HREE								
	Sc	La	Ce	Pr	Nd	Sm	Eu	Gd	Y	Tb	Dy	Ho	Er	Tm	Yb	Lu	La/Sc
BRTG/2	4	264	466	13	167	32	3	29	48	5	13	2	6	2	3	1	66.0
BRTG/3	8	489	936	34	339	71	7	75	121	12	34	6	18	4	10	2	61.1
BRTG/4	8	441	829	20	282	56	6	55	64	9	20	4	10	3	4	1	55.1
BRTG/5	5	322	543	18	192	36	3	37	68	7	18	3	9	2	5	1	64.4
BRTG/7	6	443	803	19	292	63	6	45	53	8	19	3	6	2	3	1	73.8
BRTG/10	10	501	939	29	334	69	7	55	112	10	29	6	12	3	9	2	50.1
BRTG/11	10	627	1133	43	407	90	9	79	187	13	43	8	19	4	16	2	62.7
BRTG/13	4	220	403	16	146	27	3	25	84	7	16	4	8	3	6	1	55.0
BRTG/14	2	223	665	12	206	40	4	28	14	5	12	2	5	2	3	1	111.5
BRTG/15	5	242	436	14	159	30	3	25	60	4	14	2	7	2	5	1	48.4
BRTG/27	4	125	235	7	91	14	2	16	25	6	7	1	4	2	2	1	31.3
BRTG/28	3	64	132	6	52	7	1	8	18	2	6	1	2	2	2	<1	21.3
BRTG/29	5	418	768	21	263	46	4	48	68	7	21	2	7	2	3	1	83.6
BGBL/5	4	195	368	8	133	19	2	17	23	3	8	<1	2	1	2	1	48.8
BGBL/6	5	271	512	10	183	27	3	16	34	4	10	<1	3	1	2	1	54.2
BGBL/8	3	190	364	6	134	20	1	17	18	3	6	<1	2	1	1	1	63.3
BGBL/16	4	423	856	11	325	60	4	38	26	6	11	<1	3	2	2	<1	105.8
BGBL/21	2	138	250	6	92	16	1	12	17	2	6	<1	2	1	1	<1	69.0
BGBL/23	4	179	293	8	118	21	3	16	25	3	8	<1	2	1	2	<1	44.8
BGBL/23	4	232	384	9	147	27	3	21	31	3	9	<1	3	1	2	1	58.0
BGBL/66	3	290	551	10	189	38	3	30	33	8	10	1	3	2	3	3	96.7
DLDL/67	3	120	208	6	74	13	1	10	25	2	6	<1	2	1	2	1	40.0
Average	4.82	291.68	548.82	14.82	196.59	37.36	3.59	31.91	52.45	5.86	14.82	2.23	6.14	2.00	4.00	1.14	62.04
∑REE	303.5 - 2680																

Table. 6- REE content of the drill-core samples of QPC of Bagiyabahal and Baratangra areas (values are in ppm)

QPC	LREE								HREE							
	Sc	La	Ce	Pr	Nd	Sm	Eu	Gd	Y	Tb	Dy	Ho	Er	Tm	Yb	Lu
BGL-2/B-2/10	1	219	394	38	142	29	2	20	116	3	15	3	8	1	7	1
BGL-2/B-2/19	2	43	85	<10	34	<10	1	9	50	<2	8	2	4	<1	4	<1
BGL-2/B-2/30	1	108	209	20	80	14	1	15	61	2	10	2	5	<1	6	<1
BGL-2A/B-	2	110	216	22	81	11	1	14	290	2	11	2	6	1	5	<1
BGL-2A/B-	1	106	195	19	70	14	1	12	43	2	10	2	4	<1	3	<1
BGL-2A/B-	1	209	380	35	135	25	2	22	92	3	15	3	3	<1	5	1
BGL-2A/B-3/4	2	75	156	16	55	10	1	10	56	<2	9	2	5	<1	4	<1
BGL-2A/B-3/5	3	43	93	<10	38	10	2	13	71	2	8	2	6	<1	5	<1
BGL-4/B-2/24	1	96	191	18	72	15	2	14	51	2	10	2	6	<1	4	<1
BGL-4/B-2/25	2	67	135	13	49	10	1	10	41	<2	7	<2	3	<1	3	<1
Average	1.6	107.6	205.40	19.10	75.60	14.30	1.40	13.90	87.1	1.9	10.3	2.1	5	-	4.6	-
∑REE	254 - 999															

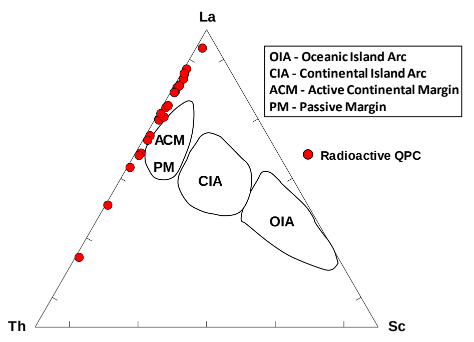

Fig. 11- La-Th-Sc ternary diagram for tectonic setting of radioactive QPC of Bagiyabahal and Birtola (after Bhatia and Crook, 1986)

source rocks. Higher La/Sc and Th/Sc relative to the well-known Archaean sediments suggest derivation from the fractionated and evolved crustal sources as well.

TECTONIC SETTING

The overall geochemical behaviour shows the siliciclastics of Bagiyabahal and Birtola were deposited mostly in a passive continental margin setting with an indication of the active regime of the continent in a few samples (inferred from SiO_2 vs K_2O/Na_2O diagram, SiO_2 vs K_2O + Na_2O vs TiO_2 + Fe_2O_3 (t) + MgO diagram, Fe_2O_3(t) + MgO vs TiO_2 diagram and La vs Th vs Sc diagram). This is supported by the quartzose sedimentary source rock along with granite derived reworked quartz clasts which were deposited in close proximity to the provenance. So, the western part of the Noamundi-Koira IOG basin around the Bagiyabahal and Birtola area is probably a part of ancient 'volcanic rifted passive margin' indicated by the massive emplacements of mafic extrusive and intrusive rocks along the series of faulted continental crust and the geochemical behaviour of the metasediments (Fig. 12a, b, c, d). Passive continental margins are generally developed when the continental blocks are separated by continental rift systems (Frisch et al., 2010) and this is evidenced by the repeated downthrown blocks of siliciclastics towards the WNW direction due to rift related parallel normal faults (slightly oblique to the basin margin) along Daldali-Bagiyabahal-Khandamuni tract (Fig. 12c). In volcanic rifted passive margin, rifting is accompanied by significant mantle melting with volcanism occurring before and/or during the continental breakup and the volcanism is characterized by a huge volume of basaltic lava flows and numerous emplacements of doleritic sill, dykes and gabbro which are present all along the Gurundia-Baratangra-Bagiyabahal tract and Birtola-Balisura tract within the subsided continental crust (Fig. 12a, b, c, d). The passive basin margins are also characterized by thick accumulations of sediments over the continental shelf. The deposition of thick sediments over the relatively thin continental crust led to the gradual subsidence of the crust and increases the slope of the basin margin.Repeated cycles of sedimentation and volcanism led to the formation of alternate layers of basic bodies in the area (Fig. 12a, b, c, d). So, it can be suggested that the deposition of sedimentary succession was controlled by fault-controlled sedimentation over the faulted continental siliciclastics and crust and shelf.

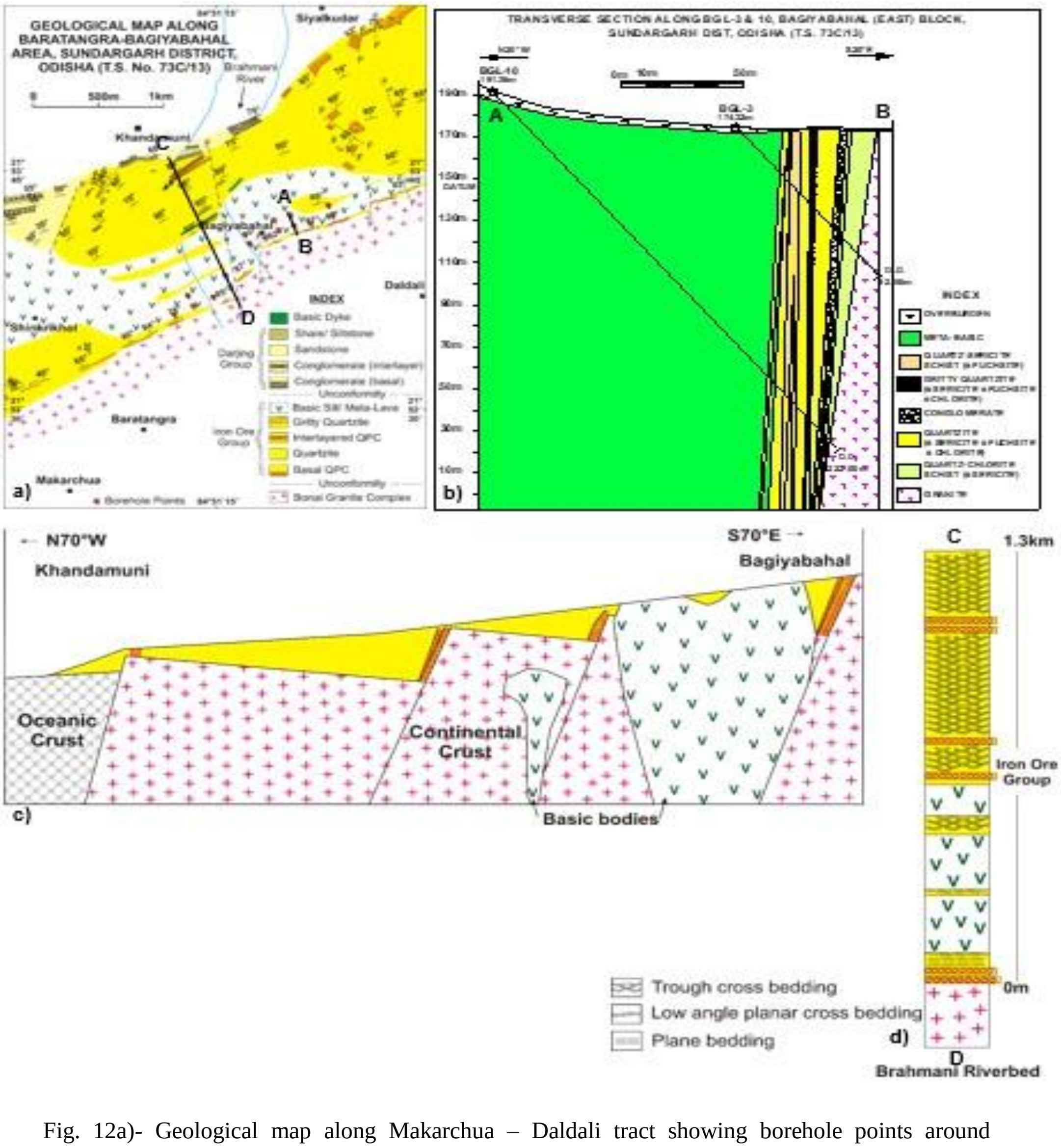

Fig. 12a)- Geological map along Makarchua – Daldali tract showing borehole points around Bagiyabahal, Baratangra areas, b) Transverse section along borehole BGL-3 and 10 of Bagiyabahal sector (along A-B line), c) Schematic diagram showing the deposition of sediments and volcanism in passive margin setting along Khandamuni – Bagiyabahal tract and d) Vertical section along Brahmani river-bed showing IOG meta-sedimentary succession (along C-D line)

The entire volcanoclastic succession has subsequently been deformed and the deformation and tilting resulted in the occurrence of higher inclination of beds (sub-vertical to vertical) near Bagiyabahal and Birtola areas. The boundary between Bonai Granite and the IOG meta-sediments is also sheared in nature as evidenced by highly sheared QPC with stretched pebbles, deformed granite and quartz-sericite schist at contact.

DISCUSSION & CONCLUSION

The geochemical parameters of the polymetallic QPC and quartzite horizon at the south-western margin of the Noamundi-Koira IOG basin have been utilized to understand the tectonic settings of different sedimentary environments. The siliciclastics were deposited along the western margin of Bonai granite in anoxic conditions as indicated by their low Th/U ratios and presence of detrital uraninite grains. Critical elemental ratio with high Th/Sc and La/Sc indicates granitic provenance for the QPC samples. The TiO_2 vs Ni diagram also indicates the acidic source. The presence of higher Al_2O_3 and K_2O in QPC with sericitic matrix indicates an acidic provenance too. However, discriminant function analysis shows a quartzose sedimentary provenance for all the siliciclastics except few QPC samples with sericitic matrix which show a felsic igneous provenance. So, a possible first cycle of granitic source and a subsequent granite derived reworked quartzose sedimentary source is suggested for the siliciclastics. A chemically weathered provenance dominated by clay minerals has been suggested for the siliciclastics from the critical ratios of major oxides like low K_2O/Al_2O_3 ratio (<0.3) and high K_2O/Na_2O ratio (>1). High SiO_2/ Al_2O_3 ratio in all the quartzite and QPCs with siliceous matrix indicates high chemical maturity of the sediments and a felsic provenance. Granite derived quartz clasts formed the siliceous matrix of the QPC and the reworking of clasts led to attaining the high chemical maturity of the lithounit. The geochemical ratios, as well as the higher contents of U, Th, Au, Cr and PGE suggest an overall mixed provenance for the deposition of the siliciclastics comprising predominantly acidic/granitic source possibly from the BGC along with some reworked quartzose sediments and minor basic and ultrabasic sources of Older Metamorphic Group (OMG). Higher content of total REE, LREE fractionation, HREE depletion, higher LREE/HREE ratio and strong negative Eu anomaly analysed in the QPC also indicate derivation of sediment from the highly evolved granitic source. The higher LREE content is due to the presence of monazite and uraninite in the matrix which have been derived from the pegmatite and granite sources. LREE enrichment in QPC is also reflected by the high values of $(La/Sm)_{CN}$ whereas near flat to depleted HREE pattern is reflected by $(Gd/Yb)_{CN}$.

The study area is suggested to be a part of an ancient volcanic passive margin where deposition of sediments was characterized by fault-controlled sedimentation over the rift related faulted continental crust and continental shelf. This has been evidenced by the presence of (i) repeated downthrown blocks of siliciclastics towards the WNW direction due to a series of rift related normal faults from Daldali to Khandamuni, (ii) huge basaltic lava flows as well as prolific emplacements of doleritic sill, dykes and gabbro due to mantle melting accompanying volcanism along the faulted and separated continental blocks and (iii) the overall geochemical behaviour of the metasediments. The huge pile of sediments over the subsided continental shelf led to the gradual subsidence of the crust and increases the slope of the basin margin. Repeated cycles of sedimentation and volcanism led to the formation of alternate layers of siliciclastics and basic bodies in the area.

Acknowledgement

The authors are highly grateful to the Director, AMD, Hyderabad for according permission to publish this paper. We are thankful to the Incharges of XRF Laboratory, AMD, Nagpur and Chemical Laboratory, AMD, Jamshedpur for the analysis of samples. We are also thankful to the Regional Director, AMD, Jamshedpur for his constant encouragement and support. We also thank the reviewers for their critical reviews and valuable suggestions for enhancing the quality of the paper.

References

Bandyopadhyay, P. K., Chakrabarti, A. K., Deomurari, M. P. and Misra, S. (2001), 2.8 Ga old Anorogenic granite-acid volcanic association from western margin of Singhbhum-Orissa craton, eastern India: Gondwana Research, v. 4, p. 465-475.

Basu, A. R., Bandyopadhyay, P. K., Chakraborti, R. and Zou, H. (2008), Large 3.4 Ga algoma type BIF in the Eastern Indian Craton. Goldschmidt Conference, Vancouver (Canada): Geochimica Cosmochimica Acta, Abstract v. 72, (12S), p. A59.

Bhatia, M. R. (1983), Plate tectonics and geochemical composition of sandstones: Journal of Geology, v. 91, p. 611-627.

Bhatia, M. R. and Crook, K. A. W. (1986), Trace elements characteristics of greywackes and tectonic setting discrimination of sedimentary basins: Contributions to Mineralogy and Petrology, v. 92, p. 181-193.

Blatt, H. (1972), Origin of Sedimentary Rocks. Englewood Cliffs, N.J.: Prentice-Hall, 634p.

Chakrabarti, A., Bandyopadhyay, P. K. and Chakrabarti, A. K. (2001), Rounded fresh feldspar in the Late Archaean nearshore deposits around Patasahi, Orissa: Glacial activity?: Indian Journal of Earth Sciences, v. 25, p. 94-107.

Condie, K. C. (1993), Chemical composition and evolution of the upper continental crust. Contrasting results from surface samples and shales: Chemical Geology, v. 104, p. 1-37.

Cox, R., Lowe, D. R. and Cullers, R. L. (1995), The influence of sediment recycling and basement composition on evolution of mudrock chemistry in the southwestern United States: Geochimica Cosmochimica Acta, v. 59(14), p. 2919-2940.

Cullers, R. L. (1994), The controls on the major and trace element variation of shales, siltstone and sandstones of Pennsylvanian–Permian age from uplifted continental blocks in Colorado to platform sediment in Kansas, USA: Geochimica Cosmochimica Acta, v. 58, p. 4955-4972.

Cullers, R. L. (2000), Geochemistry of the Mesoproterozoic Lakhanda shales in southeastern Yakutia, Russia: implications for mineralogical and provenance control and recycling: Precambrian Research, v. 104, p. 77-93.

Floyd, P. A., Winchester, J. A. and Park, R. G. (1989), Geochemistry and tectonic setting of Lewisian clastic metasediments from early Proterozoic Loch Maree Group of Gairloch, N.W. Scotland: Precambrian Research, v. 45, p. 203-214.

Frisch, W., Meschede, M. and Blakey, R. (2010), Passive continental margins and abyssal plains: Plate Tectonics, p. 43-57.

Heron, M. M. (1988), Geochemical classification of terrigenous sands and shales from core and log data: Journal of Sedimentary Petrology, v.58, p. 820-829.

Jana, A., Sarkar, B. C., Kumar, S., Kumar, A., Yadav G. S. and Kumar P. (2016), Gold and uranium occurrences in quartz-pebble conglomerate of Iron Ore Group, Bagiyabahal–Baratangra area, Sundargarh district, Odisha, India: Current Science, v. 111, no. 12, p. 1917-1921.

Jana, A., Sarkar, B. C., Akhila, V. R., Shrivastava, V. K., Saha, A., Sinha, D. K. and Verma, M. B. (2019), The characteristics of IOG meta-sedimentary rocks along the western margin of Bonai Granite in Bagiyabahal - Birtola sector, Sundargarh District, Odisha, India, National Seminar on 'Sedimentary Researches' and 35th Convention of Indian Association of Sedimentologists, p. 84-85.

Kroonenberg, S. B. (1994), Effects of provenance, sorting and weathering on the geochemistry of fluvial sands from different tectonic and climatic environments: Proceedings of the 29th International Geological Congress, Part A, p. 69-81.

Kumar, A., Birua, S. N. S., Pande, D., Nath, A. R., Ramesh Babu, P. V. and Pandit, S. A. (2009), Radioactive quartz-pebble conglomerates from western margin of Bonai granite pluton, Sundargarh district, Orissa- A New Find: Journal of Geological Society of India, v. 73, no. 4, p. 537-542.

Kumar, A., Venkatesh, A. S., Ramesh Babu, P. V. and Nandakishore, S. (2011), A note on the presence of Au-REE ± Ag-Pt in uraniferous Archean Iron Ore Group sediments, western margin of Bonai Granite Pluton, Eastern India: Exploration and Research for Atomic Minerals, v. 21, p. 9-19.

Kundu, A. and Matin, A. (2007), Sedimentary and tectonic environment of deposition of the Archaean Birtola Formation of Singhbhum Orissa Craton, Sundergarh District, Orissa: Indian Journal of Geology, v. 79, no. 1-4, p. 22-34.

Lindsey, D. A. (1999), An evaluation of alternative chemical classifications of sandstones. U.S.G.S. Open File Report 99-34, 23p.

Mahalik, N. K. (1987), Geology of rocks lying between Gangpur Group and Iron Ore Group of the horse shoe syncline in North Orissa: Indian Journal of Earth Sciences, v. 14, no.1, p. 73-83.

McLennan, S. M. (1989), Rare earth elements in sedimentary rocks- Influence of provenance and sedimentary processes: Review of Mineralogy, v. 21, p. 169-200.

McLennan, S. M. and Taylor, S. R. (1991), Sedimentary rocks and crustal evolution: Tectonic setting and secular trends: Journal of Geology, v. 99, p. 1-21.

Naik, A. (2001), A revision of the stratigraphy of Chandiposh area in eastern part of Sundargarh district, Orissa: Indian Journal of Geology, v. 73, no. 2, p. 119-137.

Naqvi, S. M., Sawarkar, R. H., Subba Rao, D. V., Govil, P. K. and Gnaneswar Rao, T. (1988), Geology, Geochemistry and Tectonic Setting of Archean greywackes from Karnataka Nucleus, India: Precambrian Research, v. 39, p. 193-216.

Nesbitt, H. W., McLennan, S. M. and Keays, R. R. (1996), Effects of chemical weathering and sorting on the petrogenesis of siliciclastic sediments with implications for provenance studies: Journal of Geology, v. 104, p. 525-542.

Roser, B. P. and Korsch, R. J. (1986), Determination of Tectonic Setting of Sandstone-Mudstone Suites Using SiO_2 Content and K_2O/Na_2O Ratio:Journal of Geology, v. 94, no. 5, p. 635-650.

Roser, B. P. and Korsch, R. J. (1988), Provenance signatures of sandstone- mudstone suites determined using discriminant functions analysis of major element data: Chemical Geology, v. 67, p. 119-139.

Saha, A., Basu, A. R., Garzione, C. N., Bandyopadhyay, P. K. and Chakrabarti, A. (2004), Geochemical and petrological evidence for subduction-accretion processes in the Archean Eastern Indian Craton: Earth and Planetary Science Letters, v. 220, p. 91-106.

Saha, A. K. (1994), Crustal evolution of Singhbhum-North Orissa, eastern India: Geological Society of India Memoir, v.27, p. 341.

Sarkar, S. N. and Saha, A. K. (1992), Aerial photo-interpretation and ground check of the Bonai Granitic Complex and the associated supracrustals: Indian Journal of Geology, v. 64, no. 2, p. 223-233.

Sengupta, S., Paul, D. K., de Laeter, J. R., McNaughton, N. J., Bandyopadhyay, P. K. and de Sweth, J. B. (1991), Mid-Archaean evolution of the Eastern Indian Craton: geochemical and isotope evidence from the Bonai pluton: Precambrian Research, v. 49, p. 23-37.

Suttner, L. J. and Dutta, P. K. (1986), Alluvial Sandstone Composition and Palaeoclimate Framework Mineralogy: Journal of Sedimentary Petrology, v. 56, no. 3, p. 329-345.

Taylor, S. R. and McLennan, S. M. (1985), The continental crust: its composition and evolution, Blackwell, Oxford, U.K., 349p.

Wedepohl, K. H. (1995), The composition of the continental crust, Ingerson Lecture, Geochimica et Cosmochimica Acta, v. 59, no. 7, p. 1217-1232.

Received: 19th July, 2020
Revised Accepted: 5th July, 2021

JOURNAL INDIAN ASSOCIATION OF SEDIMENTOLOGISTS ISSN NO 2582 – 2020
Vol. 38, Issue 2, 2021, pp. 63-78
DOI: https://doi.org/10.51710/jias.v38i2.141

Changing Tropical Estuarine Sedimentary Environments with Time and Metals Contamination, Cest Coast of India

G. N. Nayak
Marine Sciences, School of Earth, Ocean and Atmospheric Sciences, Goa University,
Goa - 403 206, India
gnnayak@unigoa.ac.in / gnnayak57@gmail.com

Abstract

Estuaries are one of the major sub-environments of the coastal zone wherein freshwaters interact and mix with saline waters, and facilitate deposition of finer sediments, organic matter, and metals. Intertidal mudflat and mangrove sediment cores collected from estuaries along the central west coast of India were investigated for various sedimentological and geochemical parameters to understand the changes in the sedimentary depositional environments and various factors influencing the processes. Additionally, estuarine biota was examined to understand the bioaccumulation of metals with respect to bioavailability. The results indicated considerable changes in the depositional environments with time owing to sea-level changes; geomorphology of the estuaries; rainfall and river runoff; anthropogenic activities including construction of dams and bridges. The sediments in the estuaries are considerably polluted by metals and pose toxicity risks to the estuarine biota due to high metal bioavailability. Marine gastropods and mangrove plants act as prospective bio-indicators, and the bioremediation potential of mangroves for contaminated sediments was identified. Metal bioaccumulation in edible benthic biota can be harmful to the human health.

Introduction

The Indian subcontinent has a large coastline of 7,517 km and spans along the Arabian Sea from the coastline of the Gulf of Kutch to Cape Comorin that comprises the West Coast of India and extends further on until the eastern shoreline near the Sundarbans comprising the East Coast of India. The west coast is around 1400 km in length and is intersected by many short swift rivers that form estuaries on encountering the waters of the Arabian Sea. A large number of ports are located along the west coast due to its broken and indented features. Further, many economically important activities are carried out in the catchment areas of these estuaries. These estuaries are important for their ability to filter sediment and contaminants from the water before it flows into the oceans. They are also vital habitats for thousands of marine species because the protected environments and abundant food which provide an ideal location for marine organisms to reproduce.

Estuaries are important zones of mixing of freshwater with saline water (Fig. 1) and sediment transfer between fluvial and marine systems, often forming sinks for material moving downstream, alongshore or landwards, and consequently for dissolved and particulate contaminants (Ridgway and Shimmield, 2002). Despite high hydrodynamics, estuaries are sites of accumulation of fine-grained sediments, organic matter and metals originated from various marine and terrestrial sources including those of human-induced. Estuaries constitute many different habitats such as river deltas, shallow open waters, salt marshes, mud- and sand flats, sandy beaches, rocky shores, sea-grass beds, mangrove forests, and tidal pools. Out of these mudflats and mangroves are an important habitat for wildlife, food, and recreation and very effective in coastal protection. They also respond to sea-level changes and therefore have received considerable attention in the recent years.

Mangroves are forested wetlands living along coasts within low latitudes. Mangroves occur in a variety of coastal settings dominated by rivers, tides, and waves and develop and persist over timescales in which morphological evolution of coastlines occurs; they are pioneers colonizing newly formed mudflats, but they can also shift their intertidal position in the face of environmental change (Alongi, 2016). Mangroves are of great importance economically to coastal inhabitants and ecologically as an integral part of the coastal zone and are a prime source of wood for fuel and construction; chemicals for traditional medicine; food; breeding grounds and nursery sites for many terrestrial and marine organisms; sites of accumulation of sediments, carbon, nutrients, and contaminants; as well as offering some protection from erosion and catastrophic events, such as tsunami and cyclones (Alongi, 2008). The mangrove trees are known to supply large amounts of organic matter, which is being consumed by many small aquatic animals. These organisms in turn provide food for fish and other higher organisms.

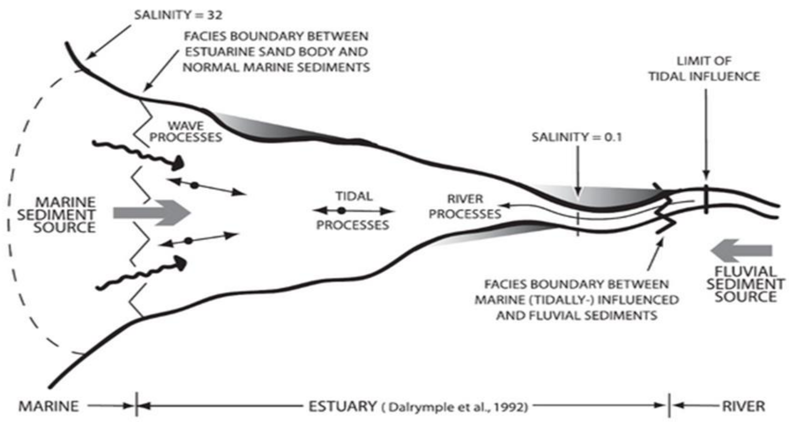

Fig. 1: Schematic diagram of an estuary showing various processes, and marine and fluvial sediment sources.

Likewise, Mudflats are sedimentary intertidal habitats formed by deposition in low energy coastal environments. Their sediment consists mostly of silts and clays with high organic matter content. They commonly are present between subtidal channels and vegetated salt marshes and hence, tend to dissipate wave energy, thus reducing the risk of eroding salt marshes, damaging coastal defenses, and flooding the low-lying lands. The mud surface also plays an important role in nutrient chemistry. In areas receiving pollutants, the sediments sequester contaminants and thus, may contain high concentrations of heavy metals. The surface of the mudflat sediment is often apparently devoid of vegetation, although mats of benthic micro-algae are common that produce mucilage (mucopolysaccharides) that binds the sediment (Maddock, 2008).

The estuaries are known for sediment deposition and act as a sink for metals in the environment. The estuary receives metals from both the natural processes as well as anthropogenic activities (Fig. 2) and are transferred from solution to sediment by adsorption onto suspended particulate matter, and are further deposited and trapped in the sediments (Spencer et al., 2003). The metals get assimilated along with organic matter, Fe/Mn oxides, sulfide, and clay in the sediment, and undergo geochemical modifications resulting in their species. The sediment characteristics such as pH, cation exchange capacity, organic matter content, redox conditions, chloride content, and salinity determine metal sorption and precipitation processes, which are associated with metal mobility, bioavailability, and potential toxicity (Du Laing et al., 2002). After deposition and burial, metals are affected by a variety of physical, chemical, and biological processes that are responsible for mixing and remobilizing metals into the water column (Lee and Cundy, 2001). Some metals or parts of the metal may be immobilized in the sediments and undergo compaction and diagenesis eventually. The sediment-associated metals have the potential to become ecotoxic due to their mobility and bioavailability, and this in turn affects both ecosystems and life through a process of bioaccumulation and biomagnification (Buccolieri et al., 2006; Ip et al., 2007).

The study of estuarine sediments helps us to understand contamination on the one hand and changing depositional environments on the other. The surface sediment interacts and exchanges with suspended materials, thereby involving in the release of metals to the overlying water (Zvinowanda et al., 2009). The top few centimeters of the sediments, therefore, reflect the continuously changing degree of contamination of present times. The bottom sediments, however, record its history (Seshan et al., 2010). The metal concentration in sediment core profiles provides information on the palaeo-weathering processes and post-depositional mobility of metals (Subramanian and Mohanchandran, 1994).

Several researchers have investigated the metal geochemistry to understand the metal source, contamination, mobility and bioavailability of metals in estuarine mangrove and mudflat sediments along the west coast of India (Nayak et al., 2016; Fernandes and Nayak, 2016, 2015; Fernandes et al., 2014; Noronha D'Mello and Nayak, 2015; Nasnodkar and Nayak, 2015; Pande and Nayak, 2013a, 2013b; Siraswar and Nayak, 2013, 2012, 2011; Singh and Nayak, 2009, 2006; Fernandes and Nayak, 2016, 2014, 2013,2012, 2010, 2009; Fernandes et al., 2011; Volvloikar and Nayak, 2015, 2014a, 2014b, 2013a, 2013b; Singh et al., 2014, 2013, 2008). Besides, studies on bioaccumulation and bioremediation potential in estuaries have also been assessed (Noronha-D'Mello and Nayak, 2016; Dias and Nayak, 2016; Cruz et al., 2020). Further, studies have been carried out employing various proxies such a sediment grain size, clay minerals, diatoms, isotopes to understand the past-climate variations (Pande et al., 2015; Volvloikar et al., 2014).

Fig. 2: Various anthropogenic metal sources input to the estuary.

The objective of this review is to understand the changes in the depositional environments in the mangroves and mud flats within estuaries along the west coast of India (Fig.3). Also, the bioavailability of metals in the sediments and the bioaccumulation and bioremediation potential of estuarine biota have been examined.

Methodology

Sediment cores collected (Fig. 4B) from the estuarine mudflats (Fig. 4A) and mangroves from the Maharashtra, Goa, and Karnataka coast, along the west coast of India, were sub-sampled at 2 cm interval using a plastic knife and transferred to plastic bags to avoid metal contamination. The sub-samples were then transferred to the laboratory and refrigerated at 4°C until further analysis. The samples were oven-dried and divided into two portions. One part of the sub-samples was used grain size analysis following the method by Folk (1974). Further, clay was separated and was used for the analysis of clay minerals using X-ray diffraction. Magnetic susceptibility measurements of the sediments were carried out using a Bartington MS2 system for various magnetic parameters. A second dried portion of the sub-sample was ground using an agate pestle and mortar and was used for the analysis of total organic carbon (Walkley and Black, 1934), total Nitrogen (Grasshoff, 1999), and total phosphorous (Murphy and Riley, 1962). Digestion of the ground sediments for total metal analysis was carried out using the protocol proposed by Jarvis and Jarvis (1985). Further, the chemical speciation of metals was also carried out using the sequential extraction procedure by Tessier et al. (1979). The metals were analyzed on a flame atomic absorption spectrophotometer, Varian AA240FS model using an air –acetylene mixture for trace metals and nitrous oxide acetylene mixture for selected major elements. ^{210}Pb dating was carried out on the sediments following the standard radiochemical procedure given by Flynn (1968). Also, stable carbon isotope ratios of total organic carbon ($\delta^{13}C_{org}$) and total organic carbon to total nitrogen (TOC/TN) were analyzed on an elemental analyzer coupled with a continuous flow stable isotope ratio mass spectrometer (IRMS). Further, diatom analysis was done following the method detailed by Battarbee (1986) in estuaries along the Maharashtra coast. Gastropod samples from the estuarine environments were collected and analyzed for metals following the procedure of Yüzereroğlu et al. (2010) in Zuari estuary, Goa. Mangrove pneumatophore samples were also analyzed for metal content following the procedure given by MacFarlane and Burchett

(2002) in Zuari estuary, Goa. Microbiological studies were carried out on the mudflat sediments using heterotrophic bacterial counts In Mandovi estuary, Goa.

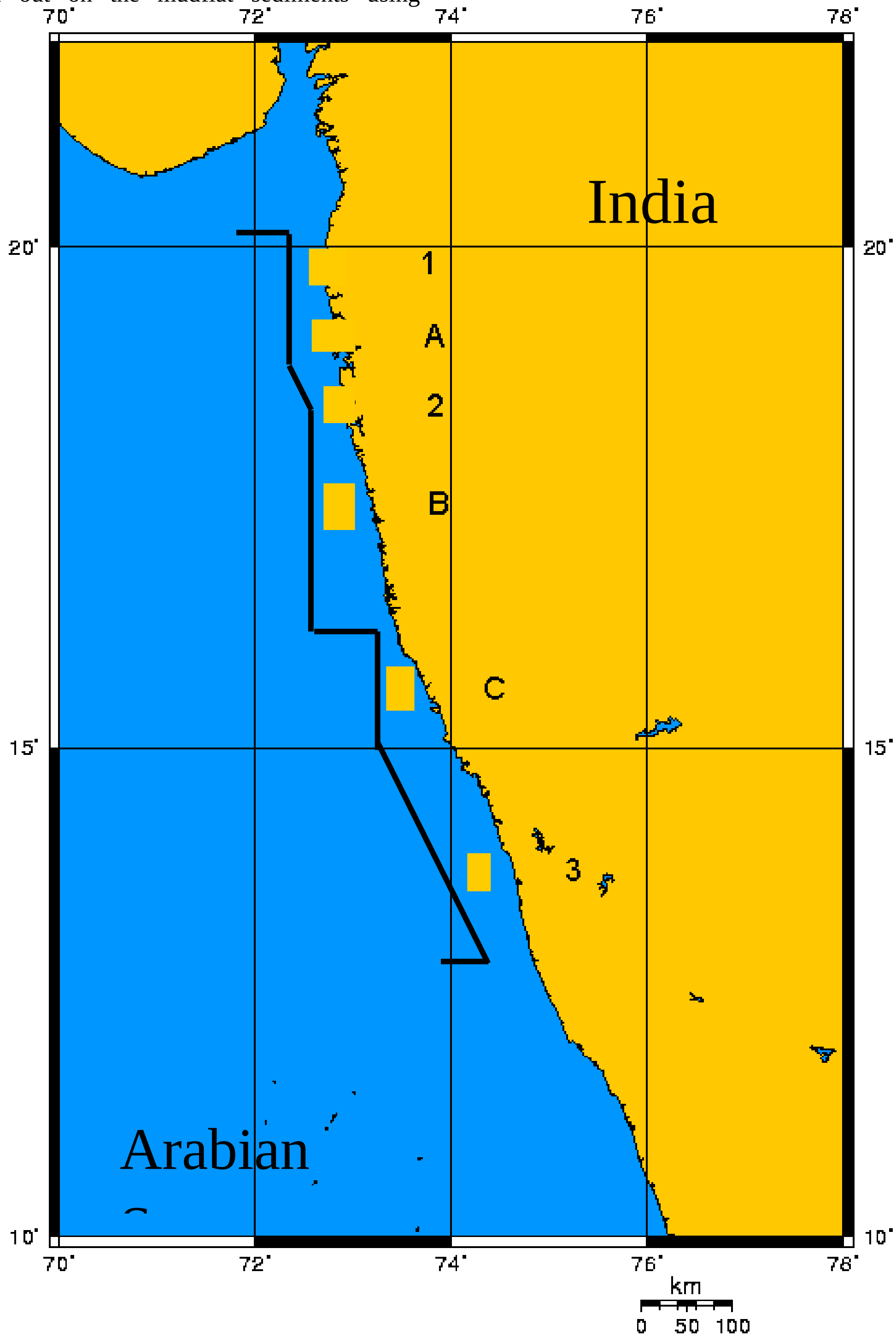

Fig. 3: Sediment core samples were collected from mangroves and mudflats within estuaries of Maharashtra, Goa and Karnataka coasts - marked area.

A

B

Fig.4: Mudflat exposed during low tide (A), Sediment core collected from a mudflat sedimentary environment (B).

Results and Discussion

Estuarine sedimentation as a record of sea-level changes and monsoon variations

In estuarine intertidal regions, sedimentation and erosion processes are controlled by a combination of sediment availability, sediment property, local morphology, hydrodynamics parameters including tidal cycles, river flow, and wind-generated waves, and biological activity (Deloffre et al., 2007). Studies carried out by various researchers indicated the potential use of mudflats and mangroves as a record of past climate due to their high sedimentation rates, their ability to preserve various sediment components, and their response to changing environmental conditions.

Singh et al. (2013) studied sediment cores collected from the estuarine mudflats of the central west coast of India namely Kolamb creek (Malvan), Mandovi estuary (Panaji), and Tadri creek (Gokarn), and highlighted on variations in sediment characteristics with time. They recorded a higher sedimentation rate for the upper portions of the cores corresponding to increased deposition of finer sediment components, magnetic minerals, organic matter, and metals which were related to geology and/or human activities in the catchment area and variation in rainfall (Fig.5). Another factor accountable for variations in sedimentation is the local sea-level rise, which is directly related to the morphology and sedimentation pattern in the estuary and creeks. According to the fourth assessment report of the Inter-Governmental Panel on Climate Change (IPCC, 2007), the global average sea-level (Fig. 5) rose at an average rate of 1.8 (1.3 to 2.3) mm per year from 1961 to 2003. The rate was faster from 1993 to 2003, i.e. about 3.1 (2.4 to 3.8) mm per year. The average sea-level rise for India has been reported as 2.5 mm/year since the 1950s (Das and Radhakrishna, 1993). Agarwal (1990) considered the west coast of India to be an emergent type and identified a rise in sea level to the order of 0.3 m during the past 57 years. Therefore, many of the large estuaries along the west coast would be most affected by the sea level rise. The rise in sea level may have facilitated the deposition of the increased amount of sediments released through anthropogenic activities such as mining in the hinterland (Singh et al., 2014).

Further, research carried out on the sediments of the Vaitarna estuary, Northern Maharashtra coast of India (Volvloikar and Nayak, 2014a; Volvloikar et al., 2014) using sediment components, grain size (Fig. 6), metals, and $\delta^{13}C_{org}$, revealed significant changes in the sedimentary depositional environment over time. The study on the sediment cores revealed that the sediments of the core at deeper parts had a considerable amount of terrestrial material whereas the recent sediments had more marine characteristics. Also, it was reported that organic matter of terrestrial origin was received during heavy rainfall regimes in the past and the sedimentological and geochemical data corresponded well to the high rainfall between the years 1954 and 1961. Notably, the Vaitarna estuary is dammed in the upstream region that may have resulted in a reduced freshwater influx into the estuary and hence increased seawater influx. Also, the higher deposition of clay fraction bound metals in recent years has been suggested as the result of increased marine inundation which resulted in greater flocculation and facilitated deposition of metals and finer clay particles. The gradual increase in Cu, Zn, Mn, and Al concentration towards the surface of the cores strongly suggested an increase in marine inundation. Volvloikar and Nayak (2013a) also analyzed sediment cores collected from mangroves within macro-tidal Dudh creeks, Northern Maharashtra coast, India. It was found that in the Dudh creek core, a higher percentage of coarser sediments were recorded in the middle section of the core and was attributed to the washing of finer particles and deposition of coarser sedimentary particles from surrounding catchments under the influence of heavy rainfall recorded in the past (1953–1960) in this region. The decrease in precipitation in successive years favored the deposition of finer particles in recent years.

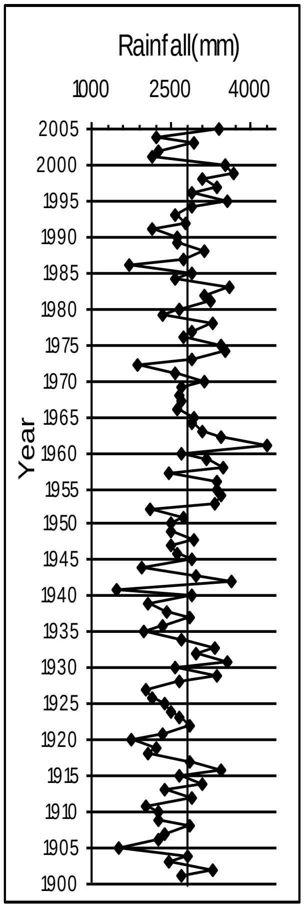

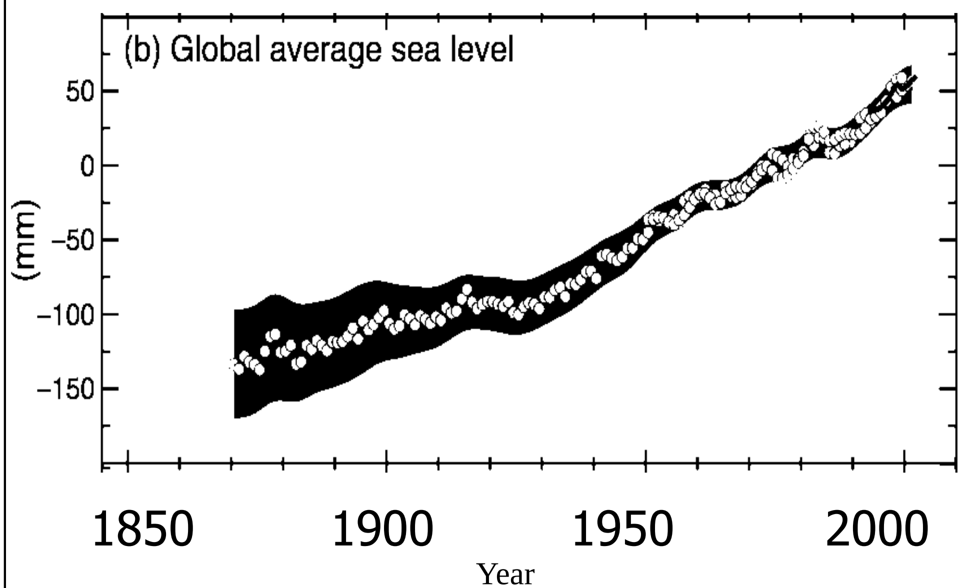

Global average sea level rise (after 4th report, IPPC, 2007)

a b

Fig. 5: Variation of annual rainfall in Goa during last 100 years (a), and global average sea level after IPPC (b)

VAITARNA ESTUARY

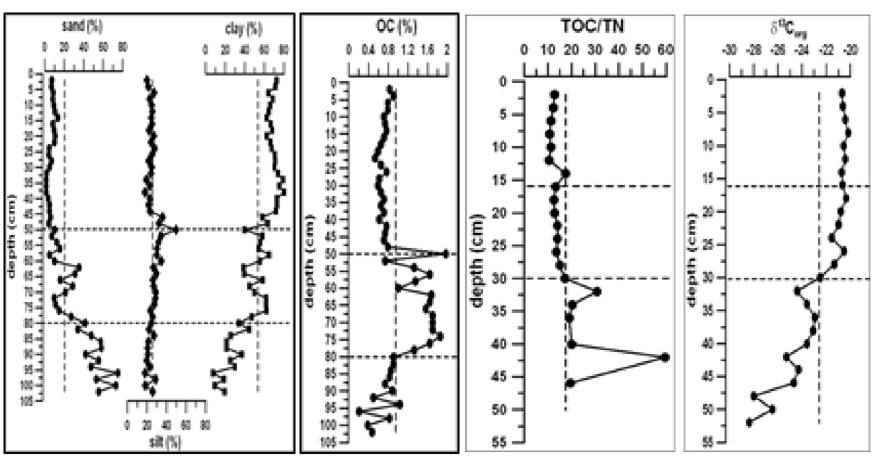

Fig. 6: Down core variation in sediment components of Vaitarna Estuary, Maharashtra (Volvoikar and Nayak, 2014a; Volvoikar et al., 2014).

Sediment cores collected from a tidally influenced Manori creek (Fernandes et al., 2011) were analyzed to understand the metal distribution, thereby understanding the depositional environments of the region. The results showed that coarse sediments were higher in the lower portion of both the cores which decreased up to the mid-core section and the increased input of sand might have resulted from increased precipitation during that period of deposition. Additionally, the C:N ratio helped in identifying marine and terrestrial influence in the two sediment cores. The TOC/TN ratio in the deeper sediments of the core indicated greater input of eroded material from the surrounding land that was concluded from the high sand percentage observed in the lower portion of the cores. The core collected from the upstream region indicated an irregular profile of ^{210}Pb activity that may be explained by complex hydrodynamics, changing sedimentary environments, or rapid changes in sediment supply, source, or energy conditions. Fernandes and Nayak (2014) collected sediment cores from the intertidal regions of Thane creek and Ulhas estuary, located along the southeastern part of Mumbai, and analyzed for sediment components and metal content. In the Ulhas estuary core, a distinct part of the core was characterized by higher sand content and was attributed to high monsoonal runoff and may have led to the lower concentration of some of the elements wherein the sandy type sediments being organically poor have little ability to retain the metal ions. Further, a higher sedimentation rate was also reported in the Ulhas estuary (Fernandes and Nayak, 2012a; Ram et al., 2003) in the recent years.

Further, Pande et al. (2015) examined sediment cores of Mandad River and the Rajapuri creek, central west coast of India, to reconstruct the recent environmental changes using geochemical and diatom records. A change over from river-dominated to the marine dominated depositional environments over the years was reported. The relatively higher sand percentage, elevated TOC/TN ratio, and predominance of freshwater diatoms revealed greater river runoff in the past, while, decrease in TOC/TN ratio and increased dominance of marine diatoms supported marine influence in recent years. Sediment cores collected from the Dharmatmar creek and Amba river mudflats (Pande and Nayak, 2013b) exhibited higher sand in the lower portion of the cores that indicated, both varying rainfall and runoff may have been responsible for the formation of sediment beds with coarser sediments between finer sediments. Investigation on the distribution of sediment components, organic carbon, and metals both spatial and depth-wise in tidal flats of Kundalika Estuary, central west coast of India (Pande and Nayak, 2013b) revealed that strong flood and ebb currents during spring tides, high river discharge or during extreme events such as storm surges may have affected the depositional environments in the past.

Further, Nayak et al. (2016) analyzed the sediment cores collected from the Vaghotan estuary and related the sedimentological data to the rainfall. It was noted that the peak of sand percentage corresponded with high rainfall. It was concluded that during the period of high rainfall, the movement of coarser material transported from the upstream region towards the mouth of the estuary was obstructed on encountering the large marine influx from the Vijaydurg bay which resulted in the deposition of the coarser material in the estuary.

Noronha D'Mello and Nayak (2015) also examined sediment cores collected from the Zuari estuary and found the sediments were deposited under varying depositional environments with time. Rao et al. (2015), used clay mineralogy to understand the provenance and estuarine process. Nasnodkar and Nayak (2015), studied sediment cores collected from the Mandovi, Sharavathi, and Gurupur, west coast of India. Form their sedimentological data it was found that there was a considerable change in the depositional environments of the sediments over time. A major dam was constructed in the mid-1960s on the Sharavathi River and smaller dams on tributaries of Mandovi, for diversion and use of river water for drinking and irrigational purposes in the recent years. This had caused a decrease in freshwater runoff and this in turn enhanced tidal surge regulating changed mixing processes leading to the deposition of fine-grained sediments in recent years. Additionally, considerable finer sediments were added in recent years due to the anthropogenic activities like mining, industrial discharge, agricultural practices, and domestic wastes along with natural processes within their catchment area. It was also reported that an increase in coarser sediments was observed in recent years in the Gurupur estuary due to changes in estuarine geomorphology over time. Fernandes et al. (2014) investigated the depositional environments of mudflats and Mangroves of the Shastri estuary, west coast of India, and found considerable changes in depositional environments from the past to the present.

Overall, from the above case studies, it can be concluded that there were considerable variations in the depositional environments with time. The geomorphology of the estuaries, rainfall, river runoff, construction of dams, bridges, and other anthropogenic activities have considerably influenced the depositional environments. It is prominently noted from the above studies, that there is a strong transition in the estuarine environments from freshwater dominated in the past to marine inundated in recent times. These changes were mainly attributed to the rise in sea level, decrease in rainfall and the construction of dams in recent times that was evident from the higher percentage of coarser sediments in the deeper part of the cores and finer sediments in recent times. In heavy rainfall regimes, the rate of erosion of rocks in the catchment area was considerably high and this material was carried by the runoff by streams into the rivers. The movement of coarser material transported from the upstream region towards the mouth of the estuary was obstructed by encountering the large marine influx from the sea into the estuary. During a deposition in the calm estuarine intertidal environments, the coarser material tends to settle down faster while the finer sediments are washed off and transported in suspension. Thus, the presence of coarser material in the sediment cores could be indicative of periods of high rainfall. This is also supported by the geochemical data wherein less metal concentrations were found along with the high sand content and high metal content in the upper part associated with high clay and organic matter (Singh et al., 2014) (Fig. 7).Further, anthropogenic activities in the catchment areas of the estuaries have considerably affected sedimentation. Activities like mining and transportation of ores added a considerable amount of material into the estuaries. Further, many of the estuaries such as Vaitarna, Rajapuri, Zuari, Sharavathi are dammed in the upstream regions for diversion and use of river water for drinking and irrigational purposes in the recent years that resulted in a reduced freshwater runoff. This in turn enhanced the tidal surge into the estuary and hence more saline water intrusion towards the upper reaches of the estuaries in the recent times. Thus, the mixing processes were affected leading to increased flocculation and deposition of fine-grained sediments in recent years. Additionally, increased anthropogenic activities in the catchment area that discharge a considerable amount of contaminants has caused increased flocculation of material.

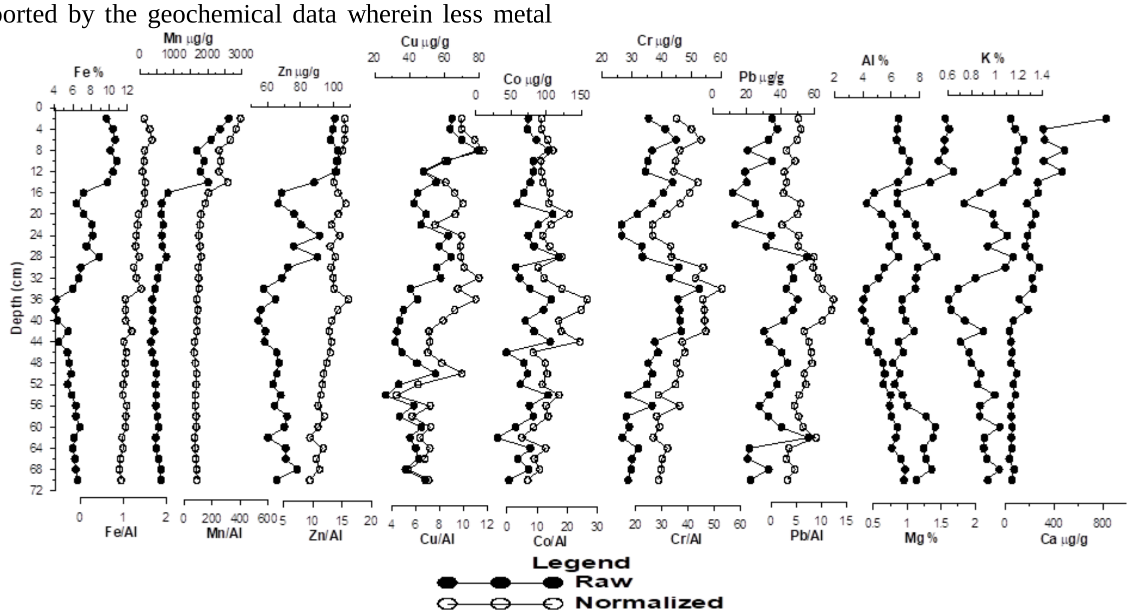

Fig. 7: Down core variation of metals in Mandovi Estuary, Goa (Singh et al., 2014)

Records of contamination history, bioindicator and bioremediation potential

Estuarine sediments are one of the largest repositories of metal pollutants. When discharged into aquatic ecosystems, metals can be absorbed on to suspended solids, and then accumulate into sediments. The sediments act as sinks, and may in turn act as sources of metals (Tang et al., 2014). The contamination of the aquatic system by metals, especially in the sediment, has become one of the most challenging pollution issues owing to the abundance, persistence, toxicity, and subsequent bio-accumulation of these metals. Contaminated sediments pose a potential risk to aquatic environments and human health because they release recalcitrant chemicals that can harm organisms and enter aquatic food chains that lead to humans (Paller and Knox, 2013). Estuarine mangroves and mudflats are thus important in contaminant monitoring studies as they are habitats for several macro-faunal species.

Total metal concentrations do not necessarily correspond with metal availability for biota. To differentiate between natural and anthropogenic loads of metal it is necessary to understand the sedimentology and geochemistry of the region (Herut and Sandler, 2006). Speciation of metals in the sediments allows identifying the percentage of metals supplied from a natural and anthropogenic source. Bioavailability is defined as the degree to which chemicals present in the sediment/soil are absorbed or metabolized by ecological receptors or is available for interactions with biological systems (ISO, 2005). It depends on the specific target organism, contaminant, and sedimentary environments and includes exposure time, transfer of contaminants from sediment to organisms, their accumulation in the organisms, and the subsequent effects of the contaminants (Paller and Knox, 2013). Only the contaminant fraction is available for biological uptake and has the potential to cause harm to human health or ecological risks. To understand bioavailability and bioaccumulation, selective chemical leaches of sediment and plant materials and organism tissues were be analyzed and the results compared.

Several studies were carried out on the estuarine mudflats and mangroves along the west coast of India, to assess the contamination and fate of metals and their bioavailability. Volvoikar and Nayak (2013a, b) studied the sediments of the mudflats and mangroves of the Khonda and Dudh creek and found that the Dudh creek sediments are highly deteriorated by human activities. An increase in metal concentration towards the surface of the core was regarded as the outcome of enhanced anthropogenic activities in recent years. High metal concentrations in the Dudh creek were mainly impacted by industrial effluents while in the Khonda creek it was attributed to the addition of metals from domestic and agricultural wastes. Further, speciation of metals carried out indicated a high concentration of metals in the bioavailable fractions supporting anthropogenic input and therefore suggested a risk of toxicity to sediment-associated biota of Dudh creek (Volvoikar and Nayak, 2015). Geochemical studies carried out on the sediments of the Vaitarna estuary (Volvoikar and Nayak, 2014a) revealed considerable inputs of metals in recent times, and most metals were enriched in bulk sediments, indicating an association with coarser particles and Fe-Mn oxyhydroxides.

Further, studies carried out on the sediments of the Ulhas estuary and Thane creek, Mumbai (Fernandes and Nayak, 2012a; 2014) indicated that metals in the sediments of both sites were greatly influenced by anthropogenic sources that included the use of fertilizers and herbicides, municipal sewage and industrial effluents. An enhanced rate of human activities coupled with the direct discharge of untreated sewage and effluents from the multifarious industries situated in the upper stretch of the creek and estuary had resulted in an increase of metal in the coastal region. Besides, there was a risk of the second cycle of pollution in Ulhas estuary due to routine dredging which released metals by sediment disturbance and/or changes in sediment chemistry. Further, a study carried out on sediment cores from the mangrove ecosystem of the Mumbai region, indicated that the sediments are moderately polluted with Pb and Cu in Manori creek and with Mn in Thane creek (Fernandes and Nayak, 2012b). In the Manori creek, mechanized boats for fishing have led to the emission of Pb and its deposition at a local scale whereas the increasing use of Cu as an anti-fouling agent on fishing trawlers and other commercial boats may have been one of the reasons for the increase in Cu concentration in the recent years. However, in the Thane creek, the increasing amount of organic pollutants has considerably affected metal geochemistry in the sediments. Further, a speciation study carried out on the sediments of the two regions showed a low risk to the aquatic environments, except for Mn in the creek sediments (Fernandes and Nayak, 2014).

The sediments of the Kundalika estuary (Pande and Nayak, 2013a) exhibited recent input of anthropogenic contaminants owing to extensive use of fertilizers, population growth, and urban waste. Also, the sediment of the Dharmatmar creek and Amba River were found to be moderately polluted with metals (Pande and Nayak, 2013b). Sediments of the Vaghotan estuary were also found to be contaminated by metals due to enhanced human-induced activities in the catchment area in recent times and concentration of Co posed a higher risk to biota (Nayak et al., 2016) in the mudflat sediments. The mudflat sediments of the Kolamb creek, Mandovi estuary, and Tadri creek exhibited an increase in finer sediments and metals in recent times which were attributed to an increase in human activities like agriculture, alteration of land use patterns, mining, construction, and development in the catchment area, in the recent years (Singh et al., 2014). The Zuari estuary mudflats and the adjoining Cumbharjua canal were studied by Singh et al. (2013) and reported enrichment of metals revealing a high degree of contamination and reflected mining and industrial sources. Further, studies on the Zuari estuarine mangrove (Noronha-D'Mello and Nayak, 2015) and mudflat (Gadkar et al., 2019) sediments revealed enrichment of Fe, Mn, and Cr in mangroves and, Mn, Cu and Co in mudflat sediments and fractionation of metals indicated that Mn posed a considerable risk to biota.

Along the Karnataka coast, bioavailability studies carried out on the sediment of the Sharavathi River (Fernandes M. et al., 2014) revealed a higher concentration of Mn in bioavailable phases related to increased addition of material from anthropogenic sources. Mn and Co concentrations in the sediments when compared with sediment quality guidelines exceeded the apparent threshold level indicating their toxicity to the environments of Sharavathi estuary.

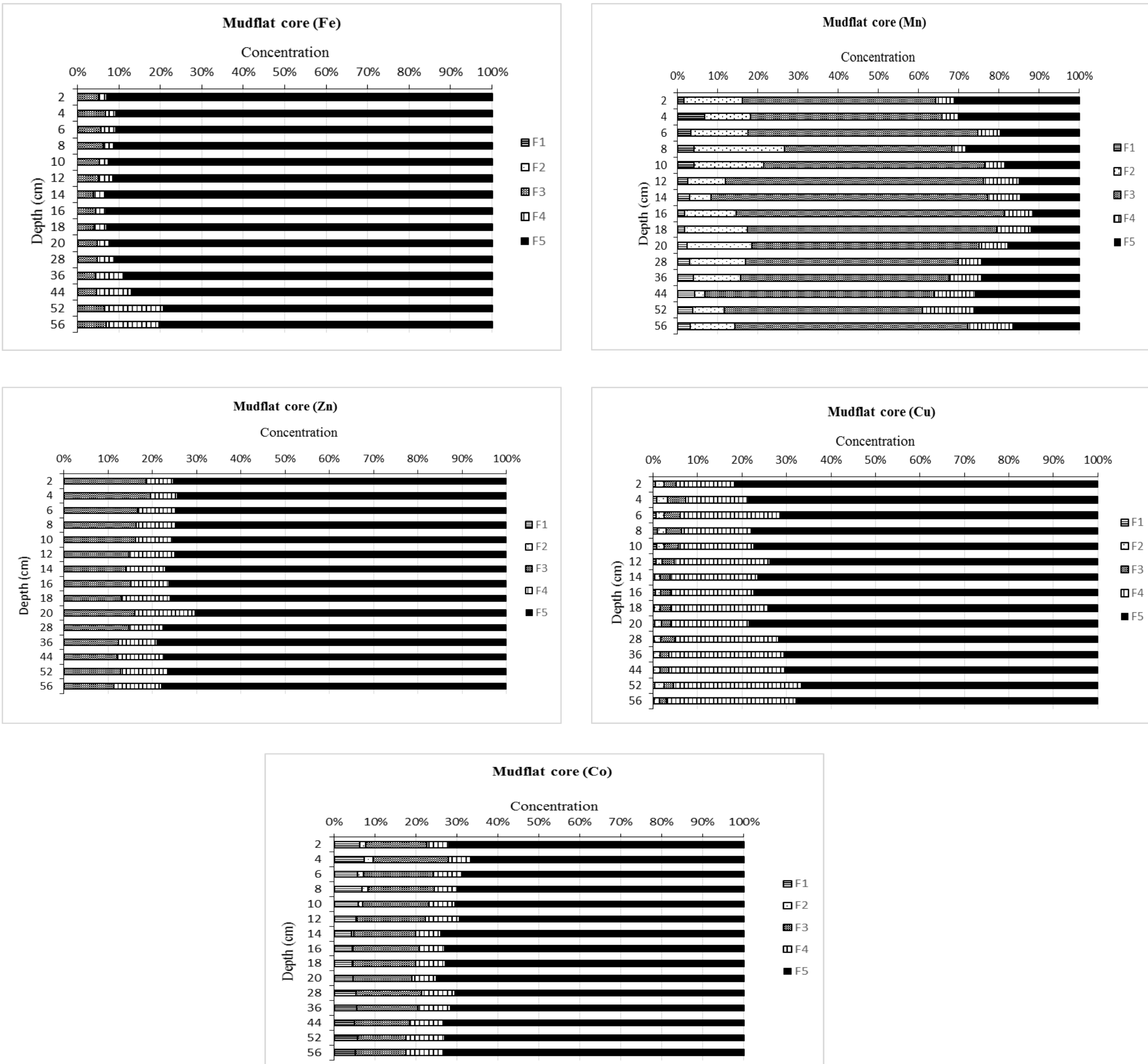

Fig. 8: Different chemical phases of Fe, Mn, Zn, Cu and Co separated using sequential extraction procedure (Gadkar et al., 2019)

The mudflat sediments of the Swarna and Gurpur estuaries were investigated (Fernandes M. and Nayak, 2015) to understand the bioavailability of metals and their toxicity. They reported that Mn, Ni, Cu, and Co show bioavailability in Gurpur estuary and are of anthropogenic addition in the recent years whereas in Swarna estuary, metals showed diagenetic remobilization and diffusion to the water column from surface sediments. Also, Co and Cr in bulk sediments of both estuaries exceeded the apparent threshold level value, and Co in the bioavailable fractions in Swarna exceeded the AET, indicating its toxicity to the environments of Swarna estuary. Fernandes and Nayak (2016) investigated cores from the mudflats and mangroves of the Sharavathi estuary for metal content in the different grain size fractions and reported that the pollution load index computed for both the cores indicated higher metal enrichment in the clay fraction.

Thus, estuaries have been the focal point for a wide variety of human activities and have become sites of a major port, industrial, urban, and recreational development. From the above studies, the sediments of intertidal mudflats and mangroves along the west coast of India considerably hold a high concentration of metal contaminants received through inputs from agricultural fertilizers, industrial and domestic waste discharges, mining transportation, and recreational activities in the catchment areas of the estuaries. These metals in the sediment posed considerable toxicity risk to the biota due to their high concentrations in the bioavailable fractions which the organisms can readily take up. Also, a physical disturbance resulting in sediment re-suspension may increase desorption of contaminants from sediment particles to water and thus increase the bioavailability of contaminants to water column organisms. Thus, there is an increasing concern about pollutants entering the aquatic environments which can have detrimental effects by finding its way into estuarine waters and affecting biotic communities. The metals assimilated by the organisms can further undergo bioaccumulation in the organism tissues and biomagnification. However, some organisms have the ability to concentrate a high amount of metals in their tissues and can be used as bioindicators whereas other organisms can affect the geochemistry of metals in the sediments and be useful for bioremediation purposes. Further, the behavior of trace metals in an environment is critically dependent on their chemical form, which influences mobility, bioavailability, and toxicity to the organisms (de Andrade Passoset al., 2010). Therefore the sediment geochemistry and biology of the particular organism must be understood in order to explain the mechanisms that control metal bioaccumulation (Griscom and Fisher, 2004).

Marine bivalves and gastropods are sedentary, filter-feeders, feeding on suspended particles coupled with their ability to accumulate metals have made them as important candidates to study metal pollution (Phillips, 1980). Most importantly, the concentration of many pollutants in the tissue of bivalves appears to be proportional to the concentration of pollutants in the surrounding water (Amiard et al., 1987). Several authors have reported trace metal concentration in estuaries and studied bioaccumulation in tissues of bio-indicator organisms. Studies by Gawade et al. (2013) on edible clam *Polymesodaerosa* from Mandovi estuary, west coast of India showed that bivalves accumulate higher metal concentration compared to fish indicating that feeding habits, habitat, size, and regulatory ability play important roles in bioaccumulation. Dias and Nayak (2016) made an attempt to understand the relation between bioavailability in sediments and bioaccumulation of metals in tissues of mollusks along the Zuari estuary. They reported that the order of mobility from most to least bioavailable forms was Mn>Zn >Cu > Ni > Co > Fe and Zn showed higher toxicity level and bioavailability. Bioaccumulation of Cu and Zn was higher than bioavailability in both gastropods and bivalves (Table 2) which indicated their preference in metal accumulation over their life span period. Further, metal concentrations were comparatively higher in gastropods. The uptake of metals by mollusks, however, did not exceed the recommended levels. Metals were bound to different fractions with different bonding strengths influencing mobility and bioavailability. Thus, the interactions between metal geochemistry and animal physiology determine the differences in bioavailability among heavy metals (Wang et al., 2002).

Table 1: Concentration of metals in the soft tissues of organisms (ppm). Class Gastropoda (stations — M1, S2, M3 and M5) and Class Bivalvia (stations — S4 and S6)(Dias and Nayak, 2016)

Station Species name	Fe (ppm)	Mn (ppm)	Cu (ppm)	Zn (ppm)	Ni (ppm)	Co (ppm)
(M1) Neritina (Dostia) violaceae	3248.15	958.45	43.70	221.35	14.45	14.65
(S2) Telescopiumtelescopium	5981.55	679.65	106.15	197.10	41.65	3.70
(M3) Cerathideacingulata	1738.80	238.30	40.65	136.15	16.90	18.90
(S4) Katelysiaopima	1363.10	105.50	11.80	150.10	6.00	2.50
(M5) Cerathideacingulata	725.45	609.00	76.25	133.25	11.55	9.05
(S6) Polymesodaerosa	2405.05	153.45	9.40	147.50	11.50	7.10

Mangroves have the ability to sequester or partition metals in their substratum, which protects coastal environments from contamination. However, high metal concentrations in sediment may be deleterious to plants in these ecosystems due to bio-accumulation in tissues (Jin-Eong, 1995; Harty, 1997; Birch et al., 2015). The metals deposited in sediment may be re-mobilized through plant uptake and eventually transported by plant detritus thus increasing the possibility of heavy metals entering the coastal food chain (Subramanian et al., 2001). Earlier research found that the sediment of the mangrove environments could sink a substantial quantity of toxic contaminants, particularly heavy metals, without much damage to the vegetation (Badarudeen et al., 2014). The special ability of mangrove plants' to survive in high-salt and anoxic conditions and high tolerance to contaminant stress contribute to their potential use in preventing dispersion of anthropogenic pollutants into aquatic ecosystems (Alongi et al., 2004; Yang et al., 2008). The factors affecting metal accumulation by plants can be biological like species, growth stage, generation, and non-biological like temperature, season, salinity, pH, metal concentration (Bonanno and Giudice, 2010). The assessment of metals in mangrove sediment is therefore of prime importance as sediment is a useful indicator of metal flux in developing areas and their study helps in initiating management strategies. The contamination and bioavailability of metals in sediments and the metal bioaccumulation in mangrove plants (pneumatophores) were assessed in the sediments of the Zuari estuary, west coast of India (Noronha –D'Mello and Nayak, 2016). They reported that the high content of Mn in the bioavailable fraction of sediment was potentially toxic to biota. Further, mangrove plants accumulated bioavailable Fe, Cu, and Zn in the pneumatophores (Table 2) as compared to other analyzed parts of plants that suggested their potential phytoremediation ability. In general, the phytoextraction of contaminants from sediments involves translocation from root to other plant parts and hyper-accumulation of contaminants requires species tolerance to high bioavailable metals concentrations (MacFarlane et al., 2007). Such conditions were found to be presented by the mangrove plants and thus have a high potential for bioremediation of contaminated sediments. Also, the mangrove plants were able to accumulate metals following the metal content available in the underlying sediment therefore reflect as bioindicator potential. Nath et al. (2014) reported a strong positive correlation between metals in sediment and pneumatophores and suggested the potential use of pneumatophore tissues as a bio-indicator of estuarine contamination.

Table 2: Bioaccumulation in mangrove Pneumatophores (Noronha –D'Mello and Nayak, 2016)

	Avicennia Officinalis	*Snnertiaalba*
Unit	µg/g	
Fe	4015.0	840.0
Mn	1045.0	75.0
Cr	10.0	3.9
Co	3.6	2.7
Ni	4.7	2.4
Cu	17.0	7.8
Zn	52.0	14.4

Bioaccumulation in mangrove is very significant. Bacteria also play a key role in nutrient recycling and the transfer of energy and material to higher trophic levels and thus are at the base of the food chain. Further, benthic invertebrates are known for the link in the transfer of metals to higher trophic levels due to their close association with sediments and also for their ability to accumulate metals (Morillo et al., 2002). Further, they are a major component in the diet of many fish (Summers, 1980). The high content of bioavailable metals may cause deleterious effects on aquatic life because of their high toxicity. This sensitivity of bacteria to metals is an important attribute in environmental indicators as impacts may be assessed earlier in the system before the loss of biodiversity and healthy functioning of the food chain. Besides, bacteria have a rapid generation time which is advantageous in facilitating early-detection of ecosystem stress (Ford et al., 1998). Also, bacterial communities in the sediments provide greater potential for detecting the effects of anthropogenic contaminants across different estuarine areas. Siraswar (2014) investigated the impact of bioavailable metals on bacterial structure from the sediments of the Mandovi estuary, west coast of India. It was found that bioavailable Mn and Pb concentrations posed a high toxicity risk to sediment-dwelling biota. The bacterial population structure was affected by changes in sediment grain size and organic carbon. Further, a metal tolerance study (Mn and Pb) on heterotrophic bacteria suggested that the microbial populations were highly sensitive to metal concentration and could be used as bio-indicators of stress conditions. Also, the bacteria showed high metal tolerance to Pb and Mn at 1000 ppm in the laboratory experiments, which indicated they have developed metal resistance mechanisms over the years. In terms of sensitivity, efficiency and ecological relevance, bacterial communities, therefore, present an attractive alternative to macro-faunal communities for use as indicators of sediment health. Hence, it was concluded that mudflats could serve as avenues for the transformation of native bacterial flora to strains with increased heavy metal tolerance, acting as sinks for bacteria potential bioremediations of heavy metals.

Conclusions

Various studies carried out on the tropical estuaries along the central west coast of India on intertidal mangrove and mudflat sedimentary environments revealed considerable variations in sedimentation pattern and metal deposition with time. The sedimentation in the estuaries along the coast was considerably impacted by the geomorphology of the estuaries, rainfall, river runoff, construction of dams, bridges, and other anthropogenic activities. The role of sea-level changes, rainfall variations, and human activities was well recorded in the sediment cores of the estuaries. Increased marine inundation in recent times was noted in most of the estuaries. Besides, an increase in anthropogenic influence in recent times was evident from the metal abundance in the upper parts of the cores. Furthermore, speciation analysis of metals in the sediment helped in estimating the metal bioavailability and their toxicity to biota. Additionally, marine bivalves, mangrove plant pneumatophores, and heterotrophic bacteria in the sediments were identified as prospective bio-indicators, and mangrove plants have the potential for bioremediation of contaminated sediments. Further bioaccumulation of metals in edible benthic biota can be harmful to the human health.

Acknowledgment

The author thanks the Council of Scientific and Industrial Research (CSIR) for awarding the Emeritus Scientist position and thanks Ministry of Earth Sciences for financial support to carry out studies on mudflats and mangroves within estuaries along west coast of India.

References

Agarwal, J.M. (1990). Sea level variation-through bathymetric data example-Azhikkal on west coast of India.Sea Level Variation and Its Impact on Coastal Environment.Tamil university Press, Thanjavur, pp. 1–6.

Alongi, D. M. (2016).Mangroves. In: Kennish, M. J. (2016). Encyclopedia of estuaries (Ed.) Springer Netherlands. pp.393-404.

Alongi, D. M. (2008). Mangrove forests: resilience, protection from tsunamis, and responses to global climate change. Estuarine, Coastal and Shelf Science, 76, 1-13.

Alongi, D.M., Wattayakorn, G., Boyle, S., Tirendi, F., Payn, C. and Dixon, P. (2004).Influence of roots and climate on mineral and trace element storage and flux in tropical mangrove soils. Biogeochemistry, 69(1), 105-123.

Amiard, J.C., Amiard-Triquet, C., Berthet, B. and Metayer, C.(1987). Comparative study of the patterns of bioaccumulation of essential (Cu, Zn) and non-essential (Cd, Pb) trace metals in various estuarine and coastal organisms. Journal of Experimental Marine Biology and Ecology, 106(1), 73-89.

Badarudeen, A., Sajan, K., Srinivas, R., Maya, K. and Padmalal, D. (2014).Environmental significance of heavy metals in leaves and stems of Kerala mangroves, SW coast of India. Indian Journal of Marine Sciences, 43, 1021-1029.

Battarbee, R.W. (1986).Diatom analysis. In: Berglund BE (ed) Handbook of holocenepalaeoecology and palaeohydrology. Wiley, Chichester, pp 527–570.

Birch, G., Nath, B. and Chaudhuri, P. (2015).Effectiveness of remediation of metal-contaminated mangrove sediments (Sydney estuary, Australia).Environmental Science and Pollution Research, 22(8), 6185-6197.

Bonanno, G. and Giudice, R.L. (2010).Heavy metal bioaccumulation by the organs of Phragmitesaustralis (common reed) and their potential use as contamination indicators.Ecological indicators, 10(3), 639-645.

Buccolieri, A., Buccolieri, G., Cardellicchio, N., Dell'Atti, A., Di Leo, A. and Maci, A. (2006).Heavy metals in marine sediments of Taranto Gulf (Ionian Sea, southern Italy).Marine chemistry, 99, 227-235.

Cruz, T.C., Nayak, G.N., Tiwari A.K. and Nasnodkar, M.R. (2020). Assessment of metal pollution and bioaccumulation of metals by edible bivalve Polymesodaerosa in the Zuari Estuary, west coast of India.Marine Pollution Bulletin, 158, 111415.

Dalrymple, R.W., Zaitlin, B.A. and Boyd, R. (1992). Estuarine facies models: conceptual basis and stratigraphic implications. Journal of Sedimentary Petrology 62,1130-1146.

Das, P.K. andRadhakrishna, M. (1993). Trends and the pole tide in Indian tide gauge records. Proceedings Indian Academy of Sciences (Earth Planetary Sciences) 102, 175–183.

de Andrade Passos, E., Alves, J.C., dos Santos, I.S., Jose do Patrocínio, H.A., Garcia, C.A.B. and Costa, A.C.S. (2010). Assessment of trace metals contamination in estuarine sediments using a sequential extraction technique and principal component analysis. Microchemical Journal, 96(1), 50-57.

Deloffre, J., Verney, R., Lafite, R., Lesueur, P., Lesourd, S. and Cundy, A.B. (2007). Sedimentation on intertidal mudflats in the lower part of macrotidal estuaries: sedimentation rhythms and their preservation. Marine Geology, 241(1), 19-32.

Dias, H.Q. and Nayak, G.N. (2016).Geochemistry and bioavailability of mudflats and mangrove sediments and their effect on bioaccumulation in selected organisms within a tropical (Zuari) estuary, Goa, India.Marine pollution bulletin, 105(1), 227-236.

Du Laing, G., Bogaert, N., Tack, F.M., Verloo, M.G. and Hendrickx, F. (2002).Heavy metal contents (Cd, Cu, Zn) in spiders (Piratapiraticus) living in intertidal sediments of the river Scheldt estuary (Belgium) as affected by substrate characteristics. Science of the Total Environment, 289, 71-81.

Fernandes, L. and Nayak, G.N.(2009).Distribution of sediment parameters and depositional environment of mudflats of Mandovi estuary, Goa, India. Journal of Coastal Research, 25(2), 273-284.

Fernandes, L., Nayak, G.N., Ilangovan, D. and Borole, D.V. (2011). Accumulation of sediment, organic matter and trace metals with space and time, in a creek along Mumbai coast, India. Estuarine, Coastal and Shelf Science, 91(3), 388-399.

Fernandes, L.L and Nayak, G.N. (2010).Sources and factors controlling the distribution of metals in mudflat sedimentary environment, Ulhas Estuary, Mumbai. Indian Association of Sedimentologists, 29, 71-83.

Fernandes, L.L. and Nayak, G.N. (2012).Geochemical assessment in a creek environment in Mumbai, West Coast of India. Environmental Forensics, 13(1), 45-54.

Fernandes, L.L. and Nayak, G.N. (2012).Heavy metals contamination in mudflat and mangrove sediments (Mumbai, India). Chemistry and Ecology, 28(5), 435-455.

Fernandes, L.L. and Nayak, G.N. (2012).Geochemical assessment in a creek environment in Mumbai, West Coast of India. Environmental Forensics, 13(1), 45-54.

Fernandes, L.L. and Nayak, G.N. (2013).Assessment of Metal Pollution in Ulhas Estuary, Mumbai, India.In On a Sustainable Future of the Earth's Natural Resources.Springer Berlin Heidelberg, pp. 395-409.

Fernandes, L.L. and Nayak, G.N. (2014).Characterizing metal levels and their speciation in intertidal sediments along Mumbai coast, India.Marine pollution bulletin, 79(1), 371-378.

Fernandes, L.L. and Nayak, G.N. (2016). Geochemical assessment and fractionation of trace metals in estuarine sedimentary sub-environments, in Mumbai, India. Environmental Nanotechnology, Monitoring & Management, 6, 14-23.

Fernandes, M.C. and Nayak, G.N. (2015).Speciation of metals and their distribution in tropical estuarine mudflat sediments, southwest coast of India.Ecotoxicology and environmental safety, 122, 68-75.

Fernandes, M.C. and Nayak, G.N. (2016).Role of sediment size in the distribution and abundance of metals in a tropical (Sharavati) estuary, west coast of India. Arabian Journal of Geosciences, 9(1), 1-13.

Fernandes, M.C., Nayak, G.N., Pande, A., Volvoikar, S.P. and Dessai, D.R.G. (2014).Depositional environment of mudflats and mangroves and bioavailability of selected metals within mudflats in a tropical estuary. Environmental Earth Sciences, 72(6), 1861-1875.

Flynn, W. (1968).The determination of low levels of polonium-210 in environmental samples.AnalyticaChimicaActa, 43, 221-227.

Folk, R.L. (1974).In Petrology of sedimentary rocks. Austin, Texas: Hemphill. pp 182.

Ford, T., Sorci, J., Ika, R. and Shine, J. (1998).Interactions between metals and microbial communities in New Bedford Harbor, Massachusetts.Environmental Health Perspectives, 106, 1033.

Gadkar, N.S., Nayak, G.N. and Nasnodkar, M.R. (2019) Assessment of metal enrichment and bioavailability in mangrove and mudflat sediments of the tropical (Zuari) estuary, west coast of India.Environmental Science and Pollution Research, 26(2),24998–25011.

Gawade, L., Harikrishna, C.N.V., Sarma, W., Ingole, B.S. (2013). Variation in heavy metal concentrations in the edible oyster Crassostreamadrasensis, clam Polymesodaerosa and grey mullet Liza aurata from coastline of India. Indian Journal of Science, 2 (4), 59–63.

Grasshoff, K. (1999). Methods of Seawater Analysis, VerlagChemie, Weinheim, 205p.

Griscom, S.B. and Fisher, N.S. (2004). Bioavailability of sediment-bound metals to marine bivalve molluscs: an overview. Estuaries, 27(5), 826-838.

Harty, C. (1997).Mangroves in New South Wales and Victoria.Vista Publications, Melbourne.

Herut, B. and Sandler, A. (2006). Normalization methods for pollutants in marine sediments: review and recommendations for the Mediterranean. IOLR Report H, 17.

Ip, C.C., Li, X.D., Zhang, G., Wai, O.W. and Li, Y.S. (2007). Trace metal distribution in sediments of the Pearl River Estuary and the surrounding coastal area, South China. Environmental Pollution, 147, 311-323.

IPCC, Inter Governmental Panel on Climate Chang, (2007). The Physical science basis. Contribution of working group I to the fourth assessment report of the intergovernmental panel on climate change.

ISO.(2005). 11074: Soil-quality-Vocabulary. ISO, Geneva, Switzerland.

Jarvis, I.J. and Jarvis, K. (1985). Rare earth element geochemistry of standard sediments: a study using inductively coupled plasma spectrometry. Chemical Geology, 53, 335-344.

Jin-Eong, O. (1995). The ecology of mangrove conservation and management.Hydrobiologia 295, 343–351.

Lee, S.V. and Cundy, A. B.(2001).Heavy metal contamination and mixing processes in sediments from the Humber Estuary, Eastern England.Estuarine Coastal and Shelf Science, 53(5),619-636.

MacFarlane, G.R. and Burchett, M.D. (2002). Toxicity, growth and accumulation relationships of copper, lead and zinc in the grey mangrove Avicennia marina (Forsk.) Vierh. Marine Environmental Research, 54(1), 65-84.

MacFarlane, G.R., Koller, C.E. and Blomberg, S.P. (2007). Accumulation and partitioning of heavy metals in mangroves: a synthesis of field-based studies. Chemosphere, 69(9), 1454-1464.

Maddock, A. (2008). Intertidal Mudflats From: UK Biodiversity Action Plan; Priority Habitat Descriptions. BRIG.

Morillo, J., Usero, J. and Gracia, I. (2002).Partitioning of metals in sediments from the Odiel River (Spain). Environment International, 28, 263–271.

Murphy, J. and Riley, J. P. (1962).A modified single solution method for determination of phosphate in natural waters.AnalyticaChimicaActa, 26, 31-36.

Nasnodkar, M.R. and Nayak, G.N. (2015).Processes and factors regulating the distribution of metals in mudflat sedimentary environment within tropical estuaries, India. Arabian Journal of Geosciences, 8(11), 9389-9405.

Nath, B., Birch, G. and Chaudhuri, P. (2014). Assessment of sediment quality in Avicennia marina-dominated embayments of Sydney Estuary: the potential use of pneumatophores (aerial roots) as a bio-indicator of trace metal contamination. Science of the Total Environment, 472, 1010-1022.

Nayak, G.N., Noronha-D'Mello, C.A., Pande, A. and Volvoikar, S.P. (2016). Understanding sedimentary depositional environments through geochemical signatures of a Tropical (Vaghotan) estuary, West Coast of India. Environmental Earth Sciences, 75(2), 1-15.

Noronha-D'Mello, C.A. and Nayak, G.N. (2015).Geochemical characterization of mangrove sediments of the Zuari estuarine system, West coast of India. Estuarine, Coastal and Shelf Science, 167, 313-325.

Noronha-D'Mello, C.A. and Nayak, G.N. (2016). Assessment of metal enrichment and their bioavailability in sediment and bioaccumulation by mangrove plant pneumatophores in a tropical (Zuari) estuary, west coast of India. Marine Pollution Bulletin, 110(1), 221-230.

Paller, M.H. and Knox, A.S. (2013).January.Bioavailability of Metals in Contaminated Sediments.In E3S Web of Conferences (Vol. 1).EDP Sciences.

Pande, A. and Nayak, G.N. (2013a). Understanding distribution and abundance of metals with

space and time in estuarine mudflat sedimentary environment. Environmental earth sciences, 70(6), 2561-2575.

Pande, A. and Nayak, G.N. (2013b). Depositional environment and elemental distribution with time in mudflats of dharamtar creek, west coast of India.

Pande, A., Nayak, G.N., Prasad, V. and PrakashBabu, C. (2015).Geochemical and diatom records of recent changes in depositional environment of a tropical wetland, central west coast of India.Environmental Earth Sciences, 73(9), 5447-5461.

Phillips, D.J.H. (1980). Quantitative Biological Indicators.Applied Science Publishers, London, pp. 23–27.

Ram, A., Rokade, M.A., Borole, D.V. and Zingde, M.D. (2003).Mercury in sediments of Ulhas estuary. Marine Pollution Bulletin, 46(7), 846-857.

Rao, V.P., Shynu, R., Singh, S.K., Naqvi, S.W.A. and Kessarkar, P.M. (2015). Mineralogy and Sr–Nd isotopes of SPM and sediment from the Mandovi and Zuari estuaries: Influence of weathering and anthropogenic contribution. Estuarine, Coastal and Shelf Science, 156, 103-115.

Ridgway, J. and Shimmield, G. (2002).Estuaries as repositories of historical contamination and their impact on shelf seas. Estuarine, Coastal and Shelf Science, 55(6), 903-928.

Seshan, B.R.R., Natesan, U. and Deepthi, K. (2010).Geochemical and statistical approach for evaluation of heavy metal pollution in core sediments in southeast coast of India. International Journal of Environmental Science and Technology, 7, 291-306.

Singh, K.T. and Nayak, G.N. (2006).Distribution and Depositional environment of sediment components in mudflats of Kalinadi River, Karwar, Central West Coast of India. Jour. Indian Association of Sedimentologists, 25, 37-44.

Singh, K.T. and Nayak, G.N. (2009).Sedimentary and geochemical signatures of depositional environment of sediments in mudflats from a microtidalKalinadi estuary, central west coast of India. Journal of Coastal Research, 25(3), 641-650.

Singh, K.T., Nayak, G.N. and Fernandes, L.L. (2013).Geochemical evidence of anthropogenic impacts in sediment cores from mudflats of a tropical estuary, Central west coast of India. Soil and Sediment Contamination: An International Journal, 22(3), 256-272.

Singh, K.T., Nayak, G.N., Borole, D.V., Basavaiah, N. (2008).Understanding sedimentary processes and degree of pollution through geochemistry and magnetic properties of mudflat sediments from a tropical micro tidal estuary, Central West Coast of India pages.International symposium on sediment management. 353 – 369.

Singh, K.T., Nayak, G.N., Fernandes, L.L.,Borole, D.V. and Basavaiah, N.(2014). Changing environmental conditions in recent past—Reading through the study of geochemical characteristics, magnetic parameters and sedimentation rate of mudflats, central west coast of India. Palaeogeography, Palaeoclimatology, Palaeoecology, 397, 61-74.

Siraswar, R. and Nayak, G.N.(2012).Distribution of Sediment Components and Metals in Recent Sediments within Tidal Flats along Mandovi Estuary. Jour. Indian Association of Sedimentologists, 31(1&2), 33-44.

Siraswar, R. and Nayak, G.N. (2011).Mudflats in lower middle estuary as a favorable location for concentration of metals, west coast of India.Indian Journal of Marine Sciences, 40(3), 372.

Siraswar, R. (2014). Speciation and Bioavailability of metals in Mudflats and Mangroves of Mandovi Estuary, Goa. (Ph.D. thesis) Department of Marine Sciences, Goa University.

Siraswar, R.R. and Nayak, G.N. (2013). Role of Suspended Particulate Matter in Metal Distribution Within an Estuarine Environment: A Case of Mandovi Estuary, Western India. In On a Sustainable Future of the Earth's Natural Resources, Springer Berlin Heidelberg. pp. 377-394.

Spencer, K.L., Cundy, A.B. and Croudace, I.W. (2003).Heavy metal distribution and earlydiagenesis in salt marsh sediments from the Medway Estuary, Kent, UK. Estuarine, Coastal and Shelf Science, 57, 43-54.

Subramanian, S., Eswaramoorthi, S., Periakali, P., Saravana-Kumar, K. and Lakshmi-Narasimhan, C.L. (2001). Major and trace elements (Fe, Mn, Al, Cu, & Hg) in Pichavaram Mangrove sediments, Tamil Nadu, east coast of India. Journal of Applied Geochemistry, 3(1), 6-12.

Subramanian, V. and Mohanchandran, G. (1994).Deposition and Fluxes of Heavy Metals in the Sediments of three major Peninsular Estuaries. In: Dyer, K.R. and Orth, R.J.(eds), Changes in Fluxes in Estuaries, Olsen and Olsen Pub., Denmark, 97-106.

Summers, R.W. (1980).The diet and feeding behaviour of the flounder Platichthysflesus (L.) in the Ythan Estuary, Aberdeenshire, Scotland. Estuarine, Coastal and Shelf Science, 2, 217–232.

Tang, W., Shan, B., Zhang, H., Zhang, W., Zhao, Y., Ding, Y., Rong, N. and Zhu, X. (2014).Heavy metal contamination in the surface sediments of representative limnetic ecosystems in eastern China. Scientific reports, 4.

Tessier, A., Campbell, P.G. and Bisson, M. (1979). Sequential extraction procedure for the speciation of particulate trace metals. Analytical chemistry, 51, 844-851.

Volvoikar, S.P. and Nayak, G.N. (2013b). Evaluation of impact of industrial effluents on intertidal sediments of a creek. International Journal of Environmental Science and Technology, 10(5), 941-954.

Volvoikar, S.P. and Nayak, G.N. (2013a). Depositional environment and geochemical response of mangrove sediments from creeks of northern Maharashtra coast, India. Marine pollution bulletin, 69(1), 223-227.

Volvoikar, S.P. and Nayak, G.N. (2014a). Factors controlling the distribution of metals in intertidal mudflat sediments of Vaitarna estuary, North Maharashtra coast, India. Arabian Journal of Geosciences, 7(12), 5221-5237.

Volvoikar, S.P. and Nayak, G.N. (2014b). Reading source and processes with time from mangrove sedimentary environment of Vaitarna estuary, west coast of India. Indian J Geo-Mar Sci, 43, 1063-1075.

Volvoikar, S.P. and Nayak, G.N. (2015).Impact of industrial effluents on geochemical association of metals within intertidal sediments of a creek.Marine pollution bulletin, 99(1), 94-103.

Volvoikar, S.P., Nayak, G.N., Mazumdar, A. and Peketi, A. (2014). Reconstruction of depositional environment of a tropical estuary and response of δ 13 C org and TOC/TN signatures to changing environmental conditions. Estuarine, Coastal and Shelf Science, 139, 137-147.

Walkley, A. and Black, I.A. (1934).An examination of the degtjareff method for the determining organic matter and a proposed modification of the chromic acid titration method. Soil Science, 37, 29-38.

Wang, W.X., Yan, Q.L., Fan, W. and Xu, Y. (2002). Bioavailability of sedimentary metals from a contaminated bay. Marine Ecology Progress Series, 240, 27-38.

Yang, Q., Tam, N.F., Wong, Y.S., Luan, T.G., Su, W.S., Lan, C.Y., Shin, P.K. and Cheung, S.G. (2008). Potential use of mangroves as constructed wetland for municipal sewage treatment in Futian, Shenzhen, China. Marine Pollution Bulletin, 57(6), 735-743.

Yüzereroğlu, T.A., Gök, G., Coğun, H.Y., Firat, Ö. Aslanyavrusu, S., Maruldalı, O. and Kargin, F. (2010).Heavy metals in Patella caerulea (Mollusca, Gastropoda) in polluted and non-polluted areas from the Iskenderun Gulf (Mediterranean Turkey).Environmental monitoring and assessment, 167(1-4), 257-264.

Zvinowanda, C.M., Okonkwo, J.O., Shabalala, P.N. and Agyei, N.M. (2009).A novel adsorbent for heavy metal remediation in aqueous environments. International Journal of Environmental Science and Technology, 6, 425-434.

Received: 17th September, 2020
Revised accepted: 27th December, 2021

JOURNAL INDIAN ASSOCIATION OF SEDIMENTOLOGISTS ISSN NO 2582 – 2020
Vol. 38, Issue 2, 2021, pp. 79-84
DOI: https://doi.org/10.51710/jias.v38i2.147

Grain size variation in sand column along Chhatrapur coast, Ganjam district, Odisha – A clue to the depositional environment

Indrajit Patra[1], William Prasad[1] and A. Y. Rao[2]
1: BSOI, AMD, Visakhapatnam; 2: Since retired
E-mail: indrajitpatra.amd@gov.in

Abstract

The concentration of heavy mineral placer deposits along the coastal tracts are function of various favourable factors i.e. hinterland geological formations, prevalence of favourable climatic condition, their transportation through intricate drainage systems and various coastal processes, which operated during the geological past. Textural analysis of the available unconsolidated sediments from the present deposits is of vital importance to decode the prevailing depositional environment while grain size analysis is the major parameter used. Present study highlights the grain size analysis of the identified sand column from Chhatrapur Mineral Sand Deposit along the coastal tract of Odisha to infer the environment of deposition of heavy mineral bearing sand and their heavy mineral content variation. Standard procedure of sampling, data analysis and interpretation techniques were adopted. Result shows that, sands from frontal and rear dune are characterized by distinct bi-modal distribution, medium to fine, moderately to well sorted with good positive skewness, whereas, sand from Inter-dunal region shows dominant unimodal, medium to coarse grain, moderately poorly sorted nature and slightly positive skewness. The better heavy mineral concentration (10 to 25 % grade) in frontal and rear dunes is attributed to prevalence of aeolian dune deposition accompanied by good sorting. In contrast, the low concentration of heavy mineral (3 to 6 %) in inter dune region is due to occasional fluvial regime and poor sorting of sediments. Thus, grain size analysis can be an effective tool to decipher local prevailing depositional environment, which has a bearing on heavy mineral concentration as well.

Key Words: Grain size, depositional environment, texture, heavy mineral concentration.

Introduction

India, endowed with a coastline of over 6000 km, hosts some of the largest and richest shoreline placers comprising of ilmenite, rutile, leucoxene, garnet, zircon, monazite and sillimanite (Ali et al., 2001). The coastline of Odisha has got a special place in heavy mineral inventory of India with mostly uniform composition dominantly in beach & dune complex and minor inland (Rao et al., 2001). The concentration of heavy minerals (HM) suite is a function of hydro-dynamic conditions like sediment influx from hinterland, wave energy and its velocity, long-shore current and wind speed, which control the littoral transport, sorting and deposition of placer minerals in suitable locale (Rao et al., 2001). Therefore, textural studies from grain size analysis have been a key factor to decode these events and have been applied worldwide and in Indian coast (Mason and Folk, 1958, Elshahat, 2018, Sundararajan et al., 2009, Pradhan et al., 2020).

Grain-size analysis can be used to distinguish among sedimentary environments as well as to identify water or wind conditions that shaped the deposition environment and are widely used to determine and compare aeolian, marine, lacustrine, and fluvial environments. Grain size distribution is affected by other factors such as distance from the shoreline, distance from the source (river), source material, topography and transport mechanisms (Zhu et al., 2014, Abuodha, 2003). The mode of transportation and the energy conditions of the transporting medium are the two most important factors interpreted from grain size study and hence is applied with ease (Friedman, 1961, 1962, 1967). Moreover, the methodology to interpret the depositional environment from granulometric analysis is well established in the field of sedimentology by standard procedures (Folk and Ward, 1957, Folk, 1968 and Friedman, 1967).

The present area of investigations forms a part of well-known high grade Beach Sand Minerals (BSM)deposit i.e. Chhatrapur Mineral Sand Deposit, Ganjam district, Odisha. This is located along the southern sector of coastal Odisha and is under active exploration by Odisha Sand Complex (OSCOM), IRE (India)Ltd. (Rao et al., 2001).Moreover, Atomic Minerals Directorate for Exploration & Research (AMD)carried out HM investigations from time to time, along this coastal tract. Earlier (Rao et al, 1993) carried out textural studies along three geomorphic domains i.e. frontal-inter-rear and interpreted an increase ingrain size from top to bottom based on limited number of samples. In the present case, very detailed studies have been attempted in a small area, depending on the variation in lithology of sand column with an objective to interpret the grain size variation to depositional environment and its bearing on HM content as well. The work includes, drilling, sampling of sand column, sieving of selected samples, estimating univariate statistics, plotting of grain size data and bi-variate plot etc.

Geology / Geomorphology

Geologically, Chhatrapur deposit, is a well known beach-dune and ridge complex oriented along N50^0 - 55^0 E direction, almost parallel to the coastal trend in this part. This area forms part of the well known Central Migmatic Zone (Ramakrishna et al., 1998) of EGMB (Eastern Ghat Mobile Belt). The central migmatitic zone contains rock types subjected to extensive anatexis and migmatisation i.e. migmatitic hornblende ortho-gneisses and leptinites associated with charrnockites, garrnetiferous granite gneisses occur as domes) and khondalites as enclaves within granitic rocks, besides presence of younger phases of alkaline rocks, anorthosites etc. The weathered derivatives are invariably present, and the above rock types with soil cover are present all along the major Rushikulya drainage basin, which is the feeder to the HM suite to Chhatrapur Mineral Sand Deposit. The Quaternary Formations in the area are represented by laterites, red sediments, alluvium and dune sands. According to Devdas and Meshram (1990), the Quaternary deposits (coastal/river valley) is divided into four Formations namely Lower Naira Fm. (sand, gravel and ash bed), followed by Balgarh Fm. (laterite), Kaimundi Fm. (sandy), Bankigarh Fm. (deltaic deposits) overlain by Recent alluvium. The present deposit belongs to Kaimundi Fm. and is represented by sand dunes (yellowish brown), well sorted, medium to fine grained, disposed parallel to the coast. In regard to geomorphology, the Rushikulya River with its narrow coastal plain, form estuarine type of Delta. The dune belt has been divided into i) frontal dune (close to the shore), ii) rear dune (the landward side) and iii) inter dune, the intervening area between frontal and rear dune (Rao, 1989). The Tampara Lake is the major geomorphic feature at the landward boundary of the deposit. The simplified geological map with location of study area is furnished in figure 1.

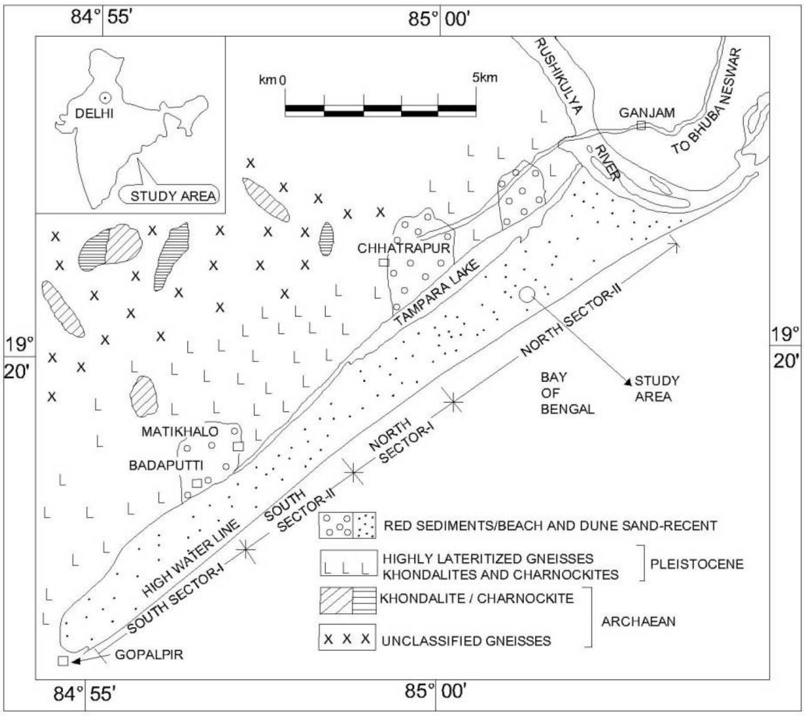

Figure 1: Generalized geological map aroundChhatrapur deposit showing study area

Methodology

The basic objective is to study the grain size parameters to infer the depositional environment and theirbearing on heavy mineral concentration. In the study area, there are development of different geo-morphic domains i.e. Frontal - Inter - Rear dunes with varying widths. Manual drilling (Dormer) indigenously developed by AMD was employed for sampling in the area. Samples were drawn at every 1.5 m interval lalong the run of the boreholes. Auger sampling was done up to the water table and Dormer drilling below water table. Detailed litho-logging in the area was carried out to understand the lithological variation depth wise and domain wise, which can be related to prevailing depositional conditions. The area in general shows the dominance of fine to medium sand (yellowish to brownish) all along the three domains.

In the frontal dune area, fine to medium sand is dominant with variation in colour from yellowish brown to brownish black due to variation in heavy mineral content. In the interdunal zone, although the lithology is mostly same i.e. yellowish brown fine to medium sand, but a distinct zone of medium to coarse sand (whitish to light yellow colour) is observed at 7.0m depth with angular fragments. This may be due to changing depositional environment. In the rear dune part in the top part, there is dominance of fine size, but the overall lithology is fine to medium sand. Sticky clay was intercepted around 9.0 to 10.0 m depth in Rear dune part. Therefore, representative samples (50-70 gm approx.) was collected from 1 borehole in frontal dune (FD) and rear dune (RD) area and 3 boreholes in Interdunal (ID) areas. From the borehole in FD region, systematic close sampling (0.5 m interval; 16 samples) was done to record minor variation.

From rear dune area, samples at 1.5m interval was collected. In the inter-dune area, only one sample each was collected from coarse sand unit from three boreholes in interdunal region, as such unit was absent from Frontal and Rear dune areas. The detailed map showing these four boreholes is given in figure 2 and the lithological section across the area is given in figure 3. The samples were dried and sieved using ASTM sieve (10 minute shaking time) with sieves of 425, 250, 177, 150, 125,106, 75 micron sizes to get a total of 08 fractions. The initial weight of the samples and the weight in the respective sieves was recorded. The sieving data is shown in table 1. Weight % of material in each sieve were converted into %retention in each sieve. In the present study, cumulative frequency curves (also, smooth curves) were drawn manually from cumulative weight of sediment and phi units using graph paper. Phi units (ϕ5, ϕ 16,ϕ 25, ϕ 50, ϕ 75, ϕ 84 and ϕ 95) were determined manually from smooth curves. Then the Mean, Standard Deviation and Skewness of each sediment sample were calculated by Graphic Method using standard formulas. This method is widely accepted owing to its ease and easy interpretation methodology (Folk and Ward, 1957, Krumbein, 1934). Simple plots of grain size (μ) versus % retention was attempted to decipher the modal distribution. Bivariate plot was also attempted to distinguish between depositional environments.

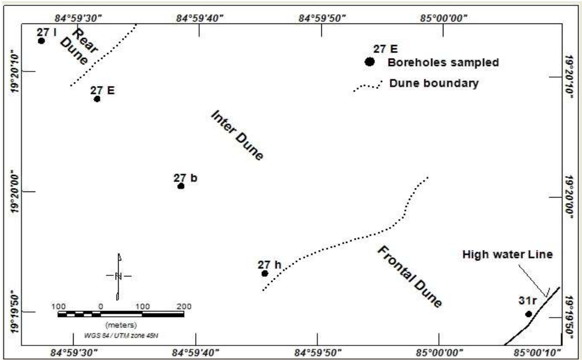

Figure 2: Area in parts of Chhatrapur Deposit showing the locations of boreholes.

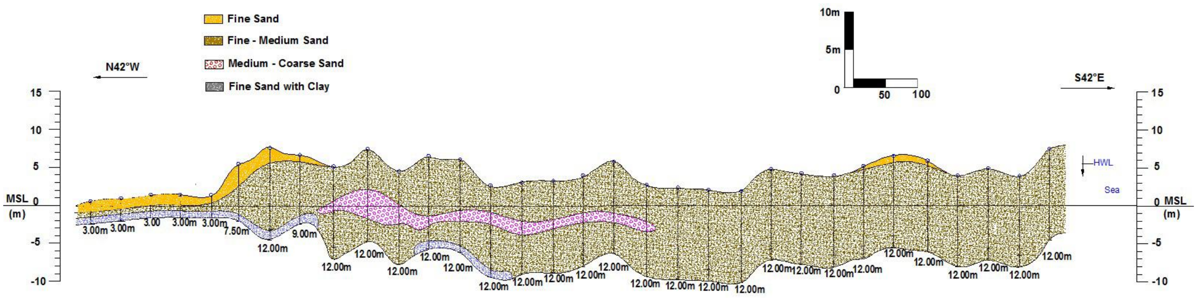

Figure 3: Detailed litholog in the study area

Table 1: Grain size data by sieving (n=26; 16 from FD, 03 from ID & 07 from RD

Size (micron)	425+	250+	177+	150+	125+	106+	75+	75	Total Wt (gm)
Seive (Mesh)	40	60	80	100	120	140	200	200	
FRONTAL DUNE (n=16; BH No. 31 r)									
RD/31r/1	15.871	31.586	3.648	3.769	1.157	0.221	0.285	0.071	56.607
RD/31r/3	14.462	25.228	4.383	5.521	1.686	0.732	0.577	0.170	52.759
RD/31r/5	19.933	30.948	4.726	6.410	1.790	0.931	0.451	0.161	65.350
RD/31r/7	20.303	20.127	3.646	4.794	1.858	1.104	0.806	0.249	52.886
RD/31r/9	29.082	19.711	2.597	3.541	1.019	0.476	0.249	0.420	57.094
RD/31r/11	13.594	22.523	3.333	4.621	2.137	0.360	0.475	0.230	47.272
RD/31r/13	9.623	28.485	4.366	7.432	2.267	1.204	0.634	0.204	54.214
RD/31r/15	13.687	30.938	5.107	6.852	1.956	1.251	0.534	0.232	60.555
RD/31r/17	10.313	31.851	6.889	10.307	2.439	1.549	1.081	0.180	64.608
RD/31r/19	14.698	34.370	4.894	6.475	1.760	0.813	0.266	0.311	63.587
RD/31r/21	14.565	24.386	4.052	5.961	1.754	1.197	0.575	0.216	52.706
RD/31r/23	19.795	29.856	4.627	7.461	2.820	0.687	0.722	0.447	66.414
RD/31r/25	10.433	30.921	6.839	10.712	3.037	1.095	0.688	0.661	64.385
RD/31r/27	17.703	33.569	3.446	3.477	1.028	0.733	0.491	1.178	61.625
RD/31r/29	10.372	29.628	6.776	2.412	9.686	1.659	1.209	1.990	63.732
RD/31r/31	14.176	29.988	5.599	6.369	1.659	1.110	0.783	0.985	60.668
INTER DUNE (n=03; BH No.27 b, h & E)									
27b/3	64.10	10.80	0.81	0.81	0.16	0.10	0.01	0.12	76.91
27E/5	31.54	17.44	1.44	1.43	0.27	0.12	0.08	0.31	52.63
27h/3	49.80	17.50	2.00	2.31	0.45	0.25	0.05	0.75	73.11
REAR DUNE (n=07; BH No.27 l)									
27 l/1	11.40	26.46	3.50	7.45	2.93	2.37	1.75	0.56	56.42
28 l/2	10.32	23.76	3.49	8.49	3.60	2.80	1.13	0.17	53.76
28 l/3	14.03	21.79	4.83	6.22	1.36	0.71	0.70	0.12	49.75
29 l/4	15.50	22.26	4.96	8.08	1.23	1.80	1.17	0.75	55.74
29 l/5	16.39	23.01	2.30	5.75	2.15	0.79	0.51	0.31	51.22
30 l/6	20.71	22.93	1.85	6.36	1.27	0.60	0.49	0.11	54.31
30 l/7	15.06	18.74	3.90	5.35	1.31	0.81	0.55	0.24	45.96

Results & Discussions

Based on the results of the above methodology, following relevant points are highlighted: .Modal Distribution: The grain size data (Table 1) was utilized to prepare plots (Figure 4, 5 and 6) of modal distribution FD, ID and RD areas. Besides, percentage of coarse, medium, fine and very fine population is given in pie-diagrams (Figure 7, 8, & 9).

The three modes of transport (suspension, saltation and surface creep) are developed as separate population in a grain size distribution and the distribution pattern is strongly dependent on provenance, sedimentary processes and dynamics. Hence, analysis of these parameters is the basis for determining the process response characteristics of individual sand units (Visher, 1969 and Sahu, 1964). Modality of a distribution reflects the dominance of a particular size class/classes within the mixture and bi-modal distribution and is characteristics of many depositional environments (Taira and Scholle, 1979).Figure 4 (for FD) exhibits a distinct bi-modal (at 250 μ and 150 μ) pattern suggesting dominance of saltation process over suspension, during their transportation. The variation in grain size indicates their deposition under varying energy condition. Wentworth (1922), classified sands into five categories i.e.very coarse (2000-1000 μ), coarse (1000-500 μ), medium (500 -250 μ), fine (250 -125

μ) and very fine (125-63 μ), based on sizes. Pie diagram (figure 6) also suggests that, more than 90 % of sediments are within medium to fine sand range. The dominance of medium to fine sand also indicates dunal environment (Reddy et al., 2013). The grain size plot for RD exhibits similar characteristics to that of Frontal Dune. However, in the bi-modal pattern, the secondary mode is clearer than Frontal Dune. In comparison to Frontal Dune, the quantum of fine to very fine sand is marginally higher in Rear Dune (Fig. 9).

Figure 5 (for ID) exhibits two modes, but the prime mode is 450+ μ which is coarse sand, and the secondary mode is poorly developed at 150 μ. Unlike FD, here more than 90 % is contributed by coarse to medium sand (Fig. 8). The grains are mostly angular in nature and the relatively coarser size indicating their deposition under higher energy condition. The dominance of traction process over saltation during transportation is inferred from the data. This energy condition is typical of fluvial origin (Friedman, 1967).

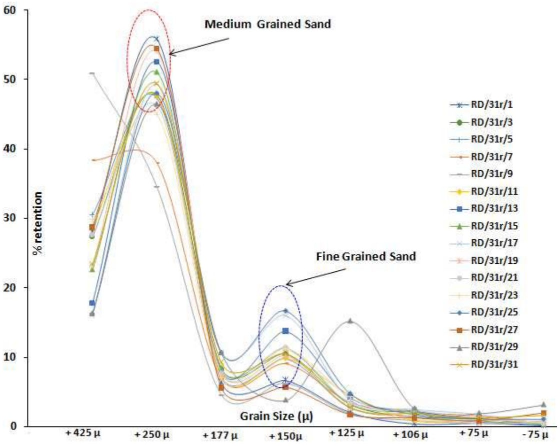

Figure 4: Grain size plot of sand samples (n=16) from BHNo.31r, Frontal Dune, showing distinct bi-modal pattern

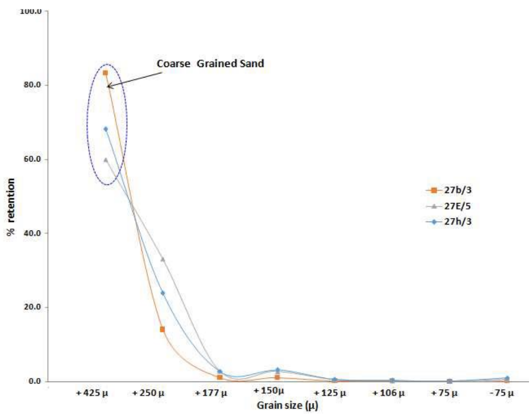

Figure 5: Grain size plot of sand samples (n=03) from

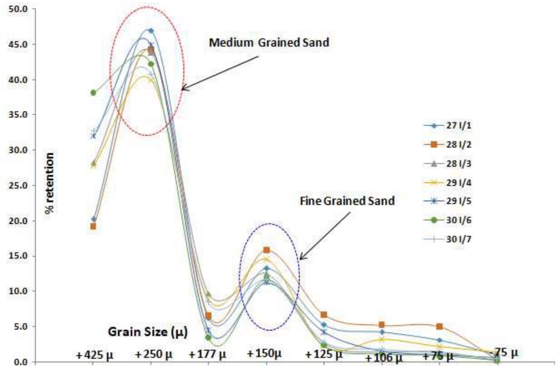

Figure 6: Grain size plot of sand samples (n=07) fromBH 27 I, Rear Dune

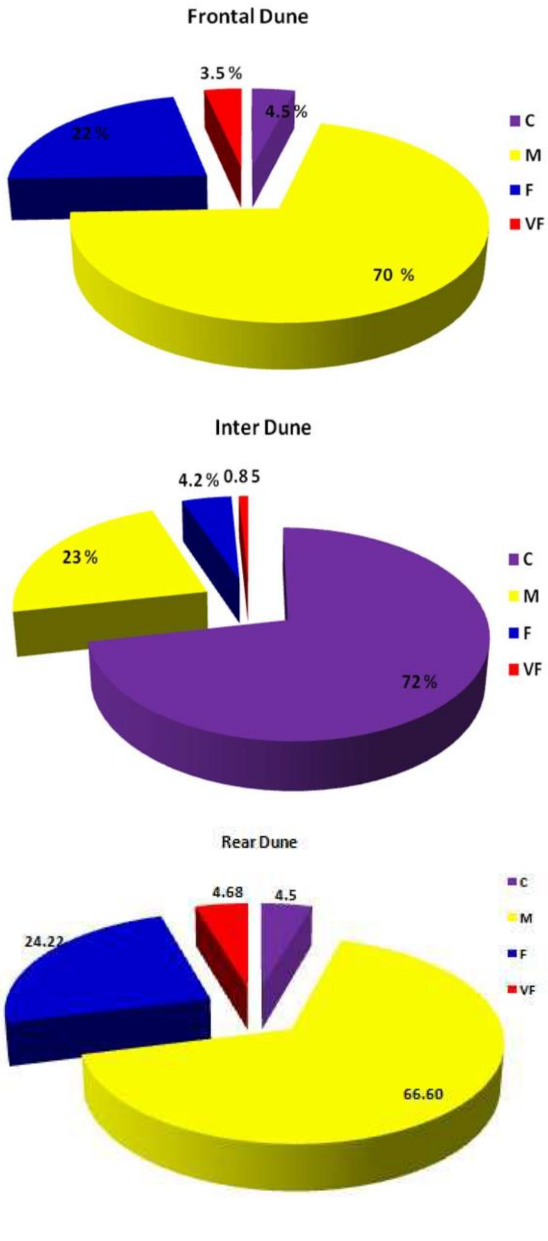

Figure 7, 8 & 9: Pei diagrams showing % of coarse, medium, fine and very fine sand in Frontal-Inter-Rear Dunes.

Univariate statistics

Textural attributes of sediments like, Mean, standard deviation and skewness are widely used to reconstruct the depositional environment of sediments and sedimentary rocks (Komar, 1998), as they have correlation between size parameters and transport processes/depositional mechanism of sediments(Folk and Ward, 1957, Friedman, 1967 , Visher, 1969). The mean size of the sediments indicates average size of the sediments which is influenced by the source of supply, environment and the average kinetic energy (velocity) of the depositing agent (Sahu, 1964). Standard deviation is a useful measure of dispersion of a distribution around the mean. It indicates the difference in energy associated with two modes of deposition. Sorting is inversely proportional to standard deviation. Skewness is a measure of frequency distribution that indicates the position of the mean with respect to the median and, is geometrically independent of sorting nature of the sample.

In the FD, the sediments are well to moderately well sorted (S.D. range from 0.48 to 0.70; n=16) and show strongly positive to positive skewness (Range: 0.29 to 0.40). The characteristic grain size (medium to fine), sorting (well to moderately well sorted) and positive skewness indicates their deposition in aeolian environment. No systematic variation of grain size with respect to depth is observed. In the Rear Dune, similar characteristics is observed except marginal higher sorting (S.D. ranging from 0.38 to 0.60).In the ID, the grain size for this unit vary from 0.30 to 0.72 ϕ (n=3) and are moderately to poorly sorted(S.D.: ranging from 0.72 to 1.20) with slightly positive (Range: 0.05 to 0.1) skewness. The coarser grain size, poorly sorting and slightly positive skewness nature of sand indicate their deposition under fluvial environment.

Wind and river transportation results from unidirectional flow and may be responsible for the generally positive skewness of dune and river sands (Friedman, 1961). As more and more fine sands are added to the dunes due to wind activity, the resulting skewness is slightly positive as compared to river.

Bivariate plot

The mean and standard deviation are the prime variables to differentiate dune - beach -River depositional environment, although overlaps are observed at various occasions (Friedman, 1967). The simple Mean - SD plot for present study is shown to distinguish between dune and river environment (Figure 10) , where these occur as two separate clusters. The sorting in case of dune is better as compared to river and the mean size also is more in case of river.

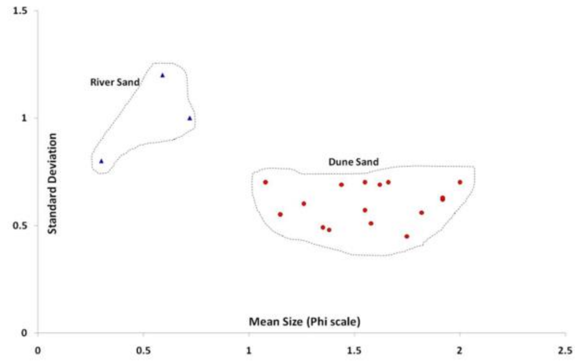

Figure 10: Bi-variate plot of mean vis-à-vis standard deviation todistinguish between dune and river sand from Chhatrapur area

Conclusion

Detailed grain size analysis of sands collected from frontal, inter and rear -dune regions of parts of Chhatrapur deposit, clearly reflects contrasting depositional environment. Sands from frontal/rear dune are characterized by medium to fine grained, moderately well sorted and strong positive skewness suggesting a typical case of dunal deposition. These conditions are very essential for heavy mineral deposition, which is corroborated by good grades of heavy minerals in this zone (i.e. 10 to 25 % grade).The heavy mineral suite essentially comprise of ilmenite, garnet, sillimanite, monazite, zircon and rutile as economic minerals and EGMB is the provenance for these heavy minerals. This unit at top is exposed to aeolian action, which is an effective sorting agent for which higher heavy mineral grade is observed in this unit. In contrast, sands at depth from Inter-dunal region are medium to coarse grained, poorly sorted with slightly positive skewness. This suggests, local prevalence of fluvial environment, and hence is reflected by less heavy mineral content (3 to 6 %), due to less sorting. Hence, study of grain size data is helpful to infer the deposition history as first-hand information on relative heavy mineral distribution in aparticular area.

Acknowledgements

The authors are grateful to the Director, AMD for giving permission to publish this work. Thanks are dueto Head, BSOI & MR Groups, AMD for encouragement during preparation of this manuscript. Authors thank Shri N. K. Panda, AMD for suggestions during interpretation stage. Authors also duly acknowledge, the critical suggestions given by the reviewers to modify the manuscript.

References

Abuodha, J.O.Z. (2003). Grain size distribution and composition of modern dune and beach sediments, Malindi Bay coast. Kenya Journal of African Earth Sciences, v.36, p. 41–54.

Ali, M. A., Krishnan, S. and Banerjee, D. C. (2001). Beach and Inland Heavy Mineral Sand Investigations and Deposits in India – An overview. Exploration and Research for Atomic Minerals, v.13, p. 1-21.

Devdas, V. and Meshram, S. N. (1990). Report on Quaternary ash beds in river basins of south and central Orissa. Geological Survey of India Progress Report for F. S. 1989 – 90 (Unpublished).

Elshahat, O. R. (2018). Heavy minerals distribution and granulometric studies of the surficial placer wadi deposits in Gabal Ambagi area, central eastern desert, Egypt. Annals Geological Survey Egypt. v. XXXV, p. 117 – 139.

Friedman, G.M. (1961). Distinction between dune, beach, and river sands from their textural characteristics. Journal of Sedimentary Research, v.31, no.4, p. 514–529.

Friedman, G.M. (1962) on sorting coefficient and the log normality of grain size distribution in sandstones. Journal of Geology, v.70, p. 737-753.

Friedman, G.M. (1967). Dynamic processes and statistical parameters compared for size frequency distributions of beach and river sands. Journal of Sedimentary Petrology, v. 37, p. 327– 354.

Folk, R. L. and Ward, W. (1957). Brazos River Bar : Study on the significance of grain size parameters. Journal of Sedimentary Petrology, v.27, p.3-26.

Folk, R.L. (1968). Petrology of Sedimentary Rocks: Austin, Texas, Hemphill, 169 p.

Gajapathi Rao, R., Sahoo, P. and Panda, N. K. (2001). Heavy Mineral sand Deposits of Orissa. Exploration & Research for Atomic Minerals, v.13, p.23 – 52.

Komar, P. D. (1998). The analysis of grain size measurements by sieving and setting tube techniques. Journal of Sediment Petrology, v. 54, p.603–61.

Krumbein, W. C. (1934). Size Frequency Distribution of Sediments. Journal of Sedimentary Petrology, v. 4, no. 2, p. 65-77.

Mason, C. C. and Folk, R. L. (1958) Differentiation of Beach, Dune and Aeolian Flat Environments by Size Analysis, Mustang Island. Texas. Journal of Sedimentary Research. v. 28, p. 211-226.

Pradhan, A.K., Sahoo, R. K., Pradhan, S., Mohanty, P. K. and Mishra, P. (2020). Textural Analysis of Coastal Sediments along East Coast of India. Journal of the Geological Society of India. v.95, p. 67 – 74.

15. Ramakrishnan, M., Nanda, J. K. and Augustine, P. F. (1998). Geological evolution of the Proterozoic Eastern Ghats Mobile Belt. Geological Survey of India. Special Publications, .no.44, p. 1-21.

Rao, K. B. (1989). Origin and evolution of the sand dune deposits of Ganjam coast, Orissa, India. Exploration and Research for Atomic Minerals, v.2, p. 133 – 146.

Reddy, D. V., Singaraju, V., Mishra, R., Kumar, D., Thomas, P. J., Rao, K. K., Singhvi, A. K. (2013). Luminescence chronology of the inland sand dunes from SE India. Quaternary Research, v.80, p. 265–273.

Sahu, B. K. (1964). Depositional mechanism from the size analysis of clastic sediments. Journal of Sedimentary Petrology, v.34, no.1, p.73– 83.

Sundararajan, M., Natesan, U., Babu, N. and Seralathan, P. (2009). Sedimentological and Mineralogical Investigation of Beach Sediments of a Fast Prograding Cuspate Foreland (Point Calimere), Southeast Coast of India. Research Journal of Environmental Sciences, v. 3, p. 134-148.

Taira, A. and Scholle, P. A. (1979). Origin of bimodal sands in some modern environments. Journal of Sedimentary Research, v.49, no.3, p. 777–786.

Visher, G. S. (1969). Grain size distribution and depositional processes. Jour. of sedimentary Petrology, v. 39, no.3, p. 1074 – 1106.

Wentworth, C.K., (1922). A scale of grade and class terms for clastic sediments. Journal of Geology, v. 30, p. 377–392.

Yugandhar Rao, A., Gajapathi Rao, R., Ravi, G. S. and Ali, M. A. (1993). Sorting conditions and their control on heavy mineral concentration in the dunal system : A case study from Chatrapur sand deposit, Orissa, India. Journal of Atomic Minerals Science, v.1, p.87-91.

Zhu, B.Q., Yu, J.J., Rioual, P. and Ren, X.Z., (2014). Particle size variation of aeolian dune deposits in the lower reaches of the Heihe River Basin, China. Sedimentary Geology. v.301, p.54–69.

Received: 27th October, 2020
Revised accepted: 6th July, 2021

JOURNAL INDIAN ASSOCIATION OF SEDIMENTOLOGISTS ISSN NO 2582 – 2020
Vol. 38, Issue 2, 2021, pp. 85-88
DOI: https://doi.org/10.51710/jias.v38i2.156

Exploitation of Beach Sand Minerals in the Offshore Areas – Legal perspective in the light of MMDR Act, 1957 and OAMDR Act, 2002

Iqbal Basha J. M.[1], Rohit Jaiswal[1], Rajan Chopra[1], Eric D'Cruz[1], M. B. Verma[1, 2]
[1]Atomic Minerals Directorate for Exploration and Research
[1, 2]Retired since
E-mail id: iqbalbasha.amd@gov.in

Abstract

Beach Sand Minerals (BSM) form by weathering and erosion of the rocks in the hinterland which are liberated, disintegrate by various processes and, are transportation by the streams to the sites of deposition (coastal plains). These minerals get concentrated along the coastal areas due to constant winnowing by wave action. It is well documented that sea level changes have occurred along the coastal areas at different points of time whose signatures on land can be seen in the form of palaeo-strandline occurring up to 15-20 km from the present day coast. On a similar analogy and in view of bathymetric profile of the sea floor, BSM deposits are expected in the offshore areas as well, in continuity to onshore deposits, which possibly are the submerged onshore deposits of the past.

Mineral Concessions in respect of onshore BSM deposits are governed with the Mines and Minerals Development and Regulation (MMDR) Act, 1957 and those in the offshore are governed as per the Offshore Areas Mineral Development and Regulation (OAMDR) Act, 2002 and the rules thereunder respectively. This paper deals with various provisions of these Acts and recent policies of the Government to harmonize mineral concession in offshore areas in line with the onshore BSM deposits.

Keywords: MMDR Act, OAMDR Act, Beach Sand Minerals (BSM), Threshold Value, Heavy Minerals, Monazite Resources

Introduction

Beach Sand Minerals (BSM) represent a group of seven economic heavy minerals(HM) (having specific gravity >2.89), viz. ilmenite, leucoxene, rutile(titanium minerals),monazite(thorium and REE mineral), zircon,garnet (abrasive) and sillimanite which co-exists in the coastal and inland placers. Amongst these minerals, monazite is a prescribed substance under the Atomic Energy Act, 1962 and thorium is envisaged as a fuel in the 3rd Stage of the Nuclear Power Programme of the country. The mainland of Indian subcontinent is endowed with a coastal length of 6000km. The occurrence of BSM in the form of placer deposits of varied dimensions and grade has been proved by the Atomic Minerals Directorate for Exploration and Research (AMD) from various parts of the coastal and inland tracts of the country. The mineralogical composition in these deposits is the reflection of hinterland geology whereas their concentration depends up on the coastal processes operating along the coast.

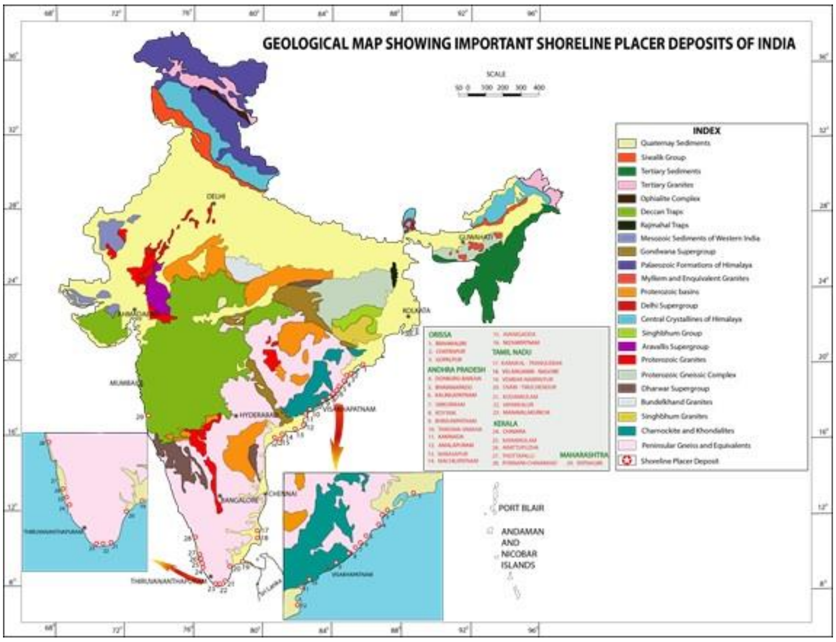

Fig. 1: Heavy Mineral Deposits of India explored by AMD (Source: http://amd.gov.in)

Coastal Heavy Mineral Deposits

The shoreline BSM deposits are of varied dimensions having their width up to 3km from the present day coastline. The heavy mineral content in these deposits varies from 1 to 49%. AMD, Department of Atomic Energy (DAE), Government of India is a pioneer organization having mandate for exploration of atomic minerals. Systematic exploration and evaluation by AMD have established heavy mineral resource of 1231 million tonnes (mt) of which12.73 mt is the monazite resources. The monazite content in these placer deposits range from 0.02-5% in Total Heavy Minerals (THM). (Heavy Mineral Resources of India, 2020, AMD). Khondalites, charnockites, leptynites, granites, pegmatites, Deccan Traps, etc. are the host rocks for BSM which are found in the hinterland. These deposits are formed by weathering and erosion of these hinterland rocks, liberation, disintegration and transportation by the streams to the sites of deposition (coastal plains). These minerals get concentrated along the coastal areas due to constant winnowing by wave action. BSM deposits occur abundantly along the coastal tracts in Andhra Pradesh, Odisha, Tamil Nadu, Kerala and a few small deposits in Karnataka, Maharashtra and West Bengal along the eastern and western coastal plains of the country.

Offshore Heavy Mineral Deposits

The offshore areas extend up to the territorial waters [12 nautical miles (NM) from low tide line (LTL)] and exclusive economic zone (EEZ) [200 NM from territorial waters]. India enjoys exclusive economic rights to map, assess, explore and harness the mineral wealth of the seabed up to EEZ in the offshore [Ministry of Mines (MoM) Report on 12th Five Year Plan].

The Geological Survey of India (GSI) and the CSIR-National Institute of Oceanography (CSIR-NIO) are the pioneering agencies involved in the exploration of the nearshore and offshore regions of India. The source of sediments/minerals in the nearshore or offshore areas is the same hinterland rocks viz. khondalites, charnockites, leptynites, granites, pegmatites, Deccan Traps etc. as in the case of inland deposits. The rivers drain through the rocks containing these heavy minerals and deposit in the sea and are preserved due to sea level changes that occurred along the coastal areas over a period of time. [India Bureau of Mines (IBM), Indian Minerals Year Book (2012) and Merh (1992).The Marine and Coastal Survey Division, GSI has been acquiring geoscientific data on the sea bed sediments, seabed morphology, mineral resource, geochemistry and geophysical parameters. GSI has identified offshore mineral-rich tracts and obvious geological potential areas for detailed exploration and scientific exploitation. [S.K. Wadhawan, GSI, 2016].

Further exploration in the potential offshore areas has been reported for the mineral assemblage of ilmenite, sillimanite, garnet, monazite, zircon, rutile and others (amphibole and pyroxene, etc). The grades of heavy minerals as reported from the offshore blocks of Bhimunipatnam (Andhra Pradesh), Palur-Malud (Odisha), Cochin and Quilon (Kerala) varies from 0.030% to 8.50%. Preliminary investigations carried out by GSI and CSIR-NIO in the offshore areas indicated monazite content varying from 1-4%in THM. The exploration and analytical data on heavy mineral resource in theseoffshore blocks are not available in public domain.

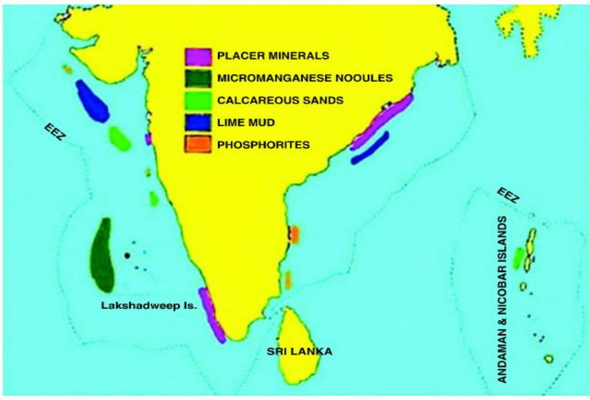

Fig. 2: Offshore mineral-rich tracts constitute obvious geological potential areas, S.K. Wadhawan, GSI

Legal perspective

The Government of India (Allocation of Business) Rules, 1961,delegates powers to various ministries, departments, etc. to administer the business of the Government. As per the said Rules, the Ministry of Mines (MoM) has been delegated powers to make legislation/laws made by the Parliament for regulation of mines and development of minerals within the territory of India, including mines and minerals underlying the ocean within the territorial waters or the continental shelf, or the EEZ and other maritime zones of India.

Exercising above powers, MoM has notified various Acts and Rules thereunder for regulation and development of mineral resources of the country. As a part of our study, we restrict to the provisions of two major Acts and the rules made thereunder which are:

1. The Mines and Minerals (Development and Regulation) [MMDR] Act, 1957
2. The Offshore Areas Mineral (Development and Regulation) [OAMDR] Act, 2002.

Salient features of MMDR and OAMDR Acts-Comparative study

MMDR Act, 1957

It is an Act under the control of the Union which extends to the whole of India and is enacted by the Parliament of India. MMDR Act, 1957 notified by MoM has enabled powers to the Central Government (viz. MoM) to make separate rules for grant of mineral concessions, for conservation and development of mineral resources, etc. It has also enabled powers to the State Governments to make rules for minor minerals and to make rules for preventing illegal mining, transportation and storage of minerals. Exercising these powers, several rules have been made. Reconnaissance Permit (RP), Prospecting Licence (PL) and Mining Lease (ML) are the mineral concessions mainly dealt under this Act on the principle of "First Come First Serve" basis. Mineral concessions were granted based on the applications system and the holder of RP and PL will have preferential rights for obtaining PL and ML as the case may be. The atomic minerals are listed under Part-B of First Schedule of MMDR Act, 1957.

MMDR Act has been amended from time to time based on the industrial and other strategic policies of the country. Major amendments were made in the parent Act and MMDR (Amendment)Act, 2015 was notified on 12.01.2015 with the concept of grant of mineral concessions through competitive bidding and e-auction along with other amendments.

Exercising powers under Section 11B of the MMDR (Amendment) Act, 2015, MoM vide notification dated 11.07.2016 issued the Atomic Minerals Concession Rules (AMCR), 2016 with the concept of Threshold Values for atomic minerals and also brought BSM under Part-B 'Atomic Minerals'. The Threshold for BSM was initially notified as 0.75% monazite in THM. For the purpose of conservation and in the national interest, Government of India has revised the threshold value for BSM from 0.75% to 0.00% monazite content in THM vide notification dated 20.02.2019.

OAMDR Act, 2002

The Government of India notified the Offshore Areas Minerals (Development & Regulation) Act, 2002 (OAMDR)for development and regulation of mineral resources in the territorial waters, continental shelf, EEZ and other maritime zones of India and for matters connected thereto. The Act is applicable to all minerals in offshore areas including minerals prescribed under the Atomic Energy Act, 1962, but excludes oils and related hydrocarbons. The Act and the rules made thereunder viz. the Offshore Areas Mineral Concession (OAMC) Rules, 2006, deals with the mineral concessions viz. Reconnaissance Permit (RP), Exploration Licence (EL) and Production Lease (PL) which came into effect w.e.f. 15.1.2010.

MMDR Act, 1957	OAMDR Act, 2002
It extends to the whole of India for all minerals except mineral oils, petroleum and natural gas	It extends from low tide line to territorial waters and EEZ of India for all minerals in the offshore areas including prescribed substances, except mineral oils and hydrocarbons
RP, PL, PL-Cum-ML and ML are the mineral concessions	RP, Exploration Licence and Production Lease are the mineral concessions
State Government is the Authority for Grant of Mineral Concessions	ADG, National Mission Head-II, GSI is the Administering Authority
RP, PL and ML are granted for a period not exceeding 2, 3 and 30/50 years respectively	RP, EL and PL are granted for a period not exceeding 2, 3 and 30 years respectively
Royalty shall be paid to the State Govt. as per the scheduled rates notified by Central Govt.	Royalty shall be paid to the Central Govt. as per scheduled rates notified by Central Govt.
No RP, PL or ML in respect of atomic minerals **without "Previous Approval" of Central Govt. (NOC from DAE)**	**No Production Lease** in respect of atomic minerals or prescribed substance **without consultation with DAE**

AMCR, 2016	OAMC Rules, 2006
Applicable to atomic minerals (AM) having grades= or > than the Threshold Value	Applicable to all minerals including AM and prescribed substances. No threshold concept
Govt. agencies permitted under Section 4 of the Act can undertake exploration for AM	Any person (Indian) or company registered in India can undertake exploration
Above Threshold, ML to Govt. agency. Below Threshold, ML only through Auction.	Mineral concessions to any person granted by the Administering Authority (No Auction)
RP, PL, ML for atomic minerals in consultation with DAE/AMD	RP, EL, PL **in** consultation with MoM, Defence, MoEFCC, Home Affairs, Fisheries, NIO, Shipping, Petroleum and Natural Gas

Comparative study: MMDR Act, 1957 Vs OAMDR Act, 2002

AMCR, 2016 Vs Offshore Rules, 2006

Under OAMDR Act or OAMC Rules, provision for consultation with DAE is mentioned at the stage of grant of production lease but not during grant of RP and EL. The Government has taken several measures to address these issues.

Post amendment of threshold value, all BSM deposits (onshore/inland placers) in association with monazite are notified as above threshold, irrespective of monazite grade. Hence mining leases shall be granted at the instance of DAE to a Government Company/Corporation as per the provisions of AMCR, 2016.However, in spite of containing appreciable concentration of monazite in the near shore and offshore areas, the legislation under OAMDR Act is different from MMDR Act. Technically, atomic minerals occurring in offshore areas (governed by OAMDR Act) cannot be treated differently from the atomic minerals in inland/onshore areas (governed by MMDR Act). Hence legislation for grant of reconnaissance permit, exploration licence or production lease in the offshore areas shall be in line with the minerals laws in force for inland/onshore areas i.e. AMCR, 2016.

Recent policies of the Government to harmonize the grant of mineral concessions in offshore areas:
As per the above study, it is understood that:

- Source of BSM in the near-shore or offshore areas are hinterland rocks, same as in the case of inland/onshore BSM deposits.

- Offshore BSM deposits are in immediate vicinity of onshore BSM deposits and appear to be continuation of same placer assemblages.
- Appreciable concentrations of monazite in near shore and offshore areas.
- For conservation of strategic mineral resources viz. monazite, zircon etc. and in the national interest, mineral concessions of onshore BSM deposits are granted to Government Company or Corporation owned or controlled by the Government. However, there is no such concept in the OAMDR Act/Rules.

The Government of India has brought certain amendments in OAMC Rules, 2006 to harmonize the provisions of grant of mineral concession in offshore areas in line with those of onshore BSM deposits. The MoM vide notification dated 23.08.2019 has made certain amendment i.e. the Offshore Areas Mineral Concession (Amendment) Rules, 2019, as per which, no reconnaissance permit, exploration licence or production lease of atomic minerals shall be granted to any person, except the Government or a Government Company or a Corporation owned or controlled by the Government.

The provision for grant of production lease in the offshore areas is also governed as perSection 6 'Grant of Operating Rights' of OAMDR Act, 2002. As per Section 6, provisions for consultation with DAE exists for grant of production lease in respect of atomic minerals or prescribed substance, but not for the reconnaissance or exploration licence. For effective governance, amendment in Section 6 of OAMDR Act, 2002 is required to the effect that, operating rights i.e. reconnaissance permit, exploration licence or production lease in respect of atomic minerals or prescribed substance shall be granted to the Government or a Government Company or a Corporation owned or controlled by the Government, with the prior approval of DAE.

Conclusion

The Government has harmonized the provisions of grant of mineral concessions in the offshore areas in line to the mineral concessions of onshore BSM deposits, for conservation of strategic mineral resources by amending OAMCR Rules, 2006 vide notification dated 23.08.2019.However, for effective governance, Section 6 of OAMDR Act, 2002 also need to be amended in line to the provisions of mineral concessions under MMDR Act, 1957 and the rules made thereunder so as to have uniform/similar mineral concession policies in respect of atomic minerals and/or prescribed substances irrespective of whether it occurs in the inland or in the offshore areas.

References

Government of India, Ministry of Mines, Acts and Rules, *The Mines and Minerals (Development and Regulation) Act, 1957; MMDR (Amendment) Act, 2015 and the Atomic Minerals Concessions Rules, 2016* Government of Indiahttp://mines.gov.in

Government of India, Ministry of Mines, Acts and Rules, *The Offshore Areas Mineral (Development and Regulation) Act, 2002; OAMDR (Amendment) Act, 2019 and the Offshore Areas Mineral Concession Rules, 2006* Government of Indiahttp://mines.gov.in

Government of India, Ministry of Mines, Publications, *Report of the Working Group on Mineral Exploration &Development (other than coal & lignite) for the twelfth five year plan*Government of India http://mines.gov.in

Government of India, Indian Bureau of Mines, *Indian Minerals Year Books, 2012,2014,2017, 2018*Government of Indiahttp://ibm.gov.in

Government of India,Atomic Minerals Directorate for Exploration and Research, *Heavy Mineral Resources of India, 2020*Government of India http://amd.gov.in

Merh S S, FNA, Department of Geology, M. S. University of Baroda, India Quaternary Sea Level Changes along Indian Coast - Review Article (1992) *Proc. Indian National Science Academy* 58, A,No. 5, 1992. pp. 461-472.

Wadhawan,S. K.., Former Director General, Geological Survey of India, Kolkata, India, *Marine Geology and Coastal Surveys for Seabed Mapping and Mineral Resource Evaluation in India – An Overview, Proc. Indian National Science Academy, 82 No. 3 July Spl. Issue 2016 pp. 675-683.*

Received: 30 October, 2020
Revised Accepted: 6th August, 2021

JOURNAL INDIAN ASSOCIATION OF SEDIMENTOLOGISTS ISSN NO 2582 – 2020
Vol. 38, Issue 2, 2021, pp. 89-100
DOI: https://doi.org/10.51710/jias.v38i2.189

Evaluating the source and Quality of River and Groundwater using hydrochemistry and stable isotopes in Tawi Watershed, Jammu District, Jammu and Kashmir, India

Meenu Sharma[1*], Sundeep K. Pandita[1], Rajwant[2]
[1]Department of Geology, University of Jammu, Jammu- 180006 (India)
[2]Scientific and Engineering Research Board, Department of Science and Technology, New Delhi-110019 (India)
*Email: meenu25ju@gmail.com

Abstract

Hydrogeochemical and isotopic composition of river and groundwater in Kandi and Sirowal belts of Jammu District in the Union Territory of Jammu and Kashmir was carried out to understand the recharge source and chemical nature of these waters for drinking water quality criteria. Physical parameters (temperature, pH, Total dissolved solids, total hardness and electrical conductivity), major cations and anions (Ca^{2+}, Mg^{2+}, Na^{+}, K^{+}, HCO_3^-, Cl^-, SO_4^{2-}, NO_3^-) and stable isotopes ($\delta^{18}O$ and $\delta^{2}H$) inTawi river and groundwater samples from hand pumps and tube wells were measured. The dominant cation is Ca^{2+} and the dominant anion HCO_3^- implyingCaHCO3type water in both river and groundwater. To assess the quality of water for drinking purposes, Groundwater Quality Index (GWQI) has been calculated. The GWQI indicates that Kandi and Sirowal belts are showing "Excellent" to "Good" category for drinking purposes. The stable isotopic composition of river water and groundwater is indicative of meteoric origin and enrichment before groundwater recharge. The stable isotopes in water suggest that the active canals in Sirowal belt,and rainfall and river water near the banks in Kandi belt contribute to ground water recharge.

Keywords: Kandi, Sirowal, Tawi river, Isotope hydrology, Hydrogeochemical.

Introduction

Groundwater is an important natural resource which is recharged by direct infiltration of precipitation and surface water or by subsurface flow. These surface water bodies such as streams, rivers, springs etc. are connected to groundwater in most types of landscapes, being integral part of groundwater flow systems (Romanelli et al., 2011). During the last four decades, environmental isotope techniques have been commonly and largely used in the overall domain of water resource development and management (Fritz and Fontes, 1980). Oxygen and hydrogen isotopic ratios in water have been used to determine the origin and recharge of local ground waters (Burgman et al., 1979; Weyer et al., 1979). These ratios are usually reported relative to an international standard reference such as Standard Mean Ocean Water (SMOW) (Craig, 1961). In the Indian context, there are numerous studies dealing with isotope application in groundwater as summarized by Gupta and Deshpande (2005) and Deshpande et al. (2012). Studies using hydrochemistry and stable isotopes have to understand the interaction between lake water and groundwater in Dal Lake (Saleem and Jeelani, 2017), stable isotopes to identify the sources of groundwater recharge in a karstified landscape of Western Himalaya (Jeelani et al., 2018), quantification of groundwater-surface water interactions using environmental isotopes in Bringi watershed of Kashmir Himalayas (Bhat and Jeelani, 2018).

Jammu district is the highly populated area in the Union Territory of Jammu and Kashmir where geographic factors play dominant role in the development of groundwater and surface water. The Jammu district is drained by Tawi River in addition to Ranbir canal and its distributaries (Fig. 1). The River Tawi gets bifurcated into Nikki Tawi and Wadi Tawi near Jammu city. The socio-economic activities of the region predominantly depend on the groundwater and surface water (River Tawi and canal system) and these are the only water sources which sustain the irrigational as well as domestic needs. The increase in population and urbanisation is severely affecting the water resources of the district. Continuous extraction of groundwater, deforestation and degradation of soil and agricultural resources has affected the recharging of water resources resulting in depletion of groundwater. The quality of water also degrades due to the dumping of garbage and sewage along Tawi River.

Kumar (2013) in a study around Kandi belt, Jammu district suggested that the groundwater is recharged by rain as well as river passing through the area. Kanwar et al. (2014) studied the groundwater levels and water quality in the Kandi and Sirowal belts in Jammu region. However, no study has been carried out to understand the role of surface water in recharging the groundwater in Kandi and Sirowal belts of Tawi watershed in the Jammu district.

The present study has been carried out in part of Tawi watershed in the Jammu district to understand the hydrogeochemistry and isotope hydrology of the river water and groundwater to enhance the understanding of the hydrogeochemical and isotopic characteristics of the river and ground water. This study helps in locating various suitable sites for groundwater development and management in the study area.

STUDY AREA

Physiography and Meteorology

The Jammu District can be divided into two physiographic units namely northern hilly terrain and outer plain area. The hilly terrain constitutes the rocks of Siwalik Group where the terrain is mostly showing rugged topography. The outer plain area comprises of Kandi and Sirowal belts (CGWB, 2013) (Fig. 1). The Kandi belt is dry semi-hilly tract, prone to soil erosion due to high runoff which results in sizeable loss of soil and nutrients (Gupta et al., 2010). The Kandi area is highly porous and capable of allowing in-situ percolation of large quantities of rain and surface water, but is deprived of the water because of substantial runoff due to steep topographic gradient (Thakur et al., 2014). This area shows an undulating topography with irregular steep slope and badly dissected terrain having number of gullies which comprise of boulder beds, gravels and pebbles with ferruginous clay matrix. The outer plain area shows well graded pattern from north to south direction with sediments becoming finer downwards.

The transition zone of Kandi and Sirowal belt lies near Jammu-Pathankot National Highway, Ranbir canal and then along the Pratap canal to the line of actual control on the Munawar Tawi (Kumar et al., 2004). Swampy conditions prevail at places because of immense auto flow of groundwater along the spring line marking the contact between the Kandi in north and the Sirowal in the south (CGWB, 2013).

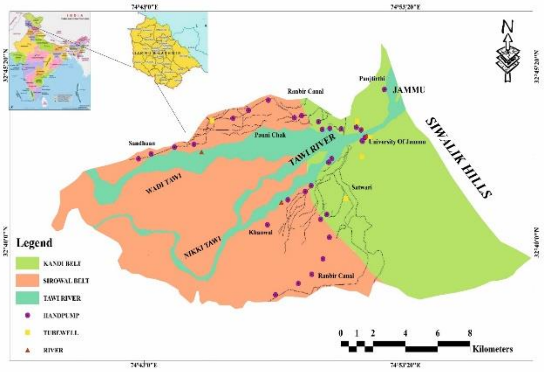

Figure 1: Location map and Physiography of the study area in Tawi watershed in Jammu District (modified after Kanwar et al., 2014).

In Jammu district, the climate is described as sub-humid to sub-tropical type. The months of July and August show maximum rainfall due to south-west monsoon. The district receives annual rainfall of 1246mm. The temperature ranges from 4°C (January) to 41°C (June), June being the hottest month while January is the coldest (CGWB, 2013).

Geology and hydrogeology

The Siwalik Group of rocks consists of conglomerate, sandstone, siltstone and shale and is divided into three subgroups namely lower, middle and upper. The outer plain area comprises of Kandi and Sirowal belts (CGWB, 2013) (Fig. 1). The Kandi belt runs along the foothills and is comprised of unconsolidated to semi-indurated conglomerate, sandstone and clay. Towards the south, the Kandi belt grades into low lying Sirowal belt. Stratigraphically the Sirowal belt is comprised of unconsolidated sand and clay in the upper part and conglomerate, sand and clay at depth. The form and condition of groundwater in the Kandi belt reveal unconfined and deeper ground water table whereas, in the Sirowal belt, the water table is in shallow and confined conditions. The direction of groundwater flow is broadly from north-east to south-west viz from Kandi to Sirowal belt and corresponds roughly with the topographic slope (Kanwar et al., 2014). Due to deeper water table, there are few tube wells and dug wells in the Kandi belt and people mostly rely on the surface water and precipitation.

Materials and Methods

In the present study, 3 and 37 number of samples were collected from Tawi river water and groundwater (hand pumps and tube wells) respectively during Pre-monsoon season corresponding with the month of May and June in 2015. Samples were collected from different locations covering urban and rural areas in the Tawi watershed in Jammu district (Fig. 1). Groundwater sampling sites were mostly located near the Tawi river and were selected based on their frequent use for drinking and domestic purposes. During the collection of samples, global positioning system was used to map the well locations. Field parameters such as temperature using water mercury thermometer, pH using handheld HANNA PH meter HI 96107 water tester while TDS and EC using HM Digital EC/TDS hydrotester were measured at the time of collection of samples. The samples were collected in 250 ml bottles of PVC (Polyvinyl chloride) for measuring the chemical constituents while for stable isotopes, 60 ml capacity bottles were used. The major cations and anions were measured by using Metrohm Ion Chromatograph (IC) model 850 integrated with Compact Autosampler (model 863). This facility was provided by Department of Environmental Sciences, University of Jammu. HCO_3^- was measured in the laboratory using volumetric titration method.

The isotopic (δD and $\delta^{18}O$) results were measured using Isotope Ratio Mass Spectrometer (IRMS) at Physical Research Laboratory, Ahmedabad by adopting the standard equilibration method in which water samples were equilibrated with CO_2 (or H_2) and the equilibrated CO_2 (or H_2) gas was analysed by Delta V Plus isotope ratio mass spectrometer (IRMS) in continuous flow mode using a Gas bench II preparation and introduction system (Maurya et al., 2009).

Groundwater Quality Index

In order to assess the chemical data for water quality, Groundwater Quality Index (GWQI), is used and compared with the drinking water quality standards of Bureau of Indian Standards (BIS, 2012). The steps which are important to calculate GWQI (Horton, 1965) are:

- **Step: 1** To assign weight (wi)- The weight is assigned to the parameter considered for the study. The weight of each parameter depicts their harmfulness when present in water.
- **Step: 2** To calculate relative weight (Wi)- The relative weight has been calculated using the following equation:

  $$Wi = wi / \sum_{i}^{n} wi$$

  Where "Wi" is the relative weight, "wi" is the weight assigned to each parameter, and "n" is the number of parameters.

- **Step: 3**Quality rating (Qi)- The quality rating of each parameter has been computed with its concentration in the groundwater sample by its respective BIS standard and then multiplied by 100. The equation is

  $$Qi = (Ci/ Si)*100$$

  Where Ci= concentration of each groundwater quality parameter
  Qi= quality rating
  Si= recommended value for each parameter.

- **Step: 4** Sub-index (SIi) and GWQI- The sub index and GWQI have been computed using the following equation:

  $$SIi = Wi \times Qi$$
  $$GWQI = \sum_{i=0}^{n} SIi$$

Where SIi is the sub-index of the i^{th} parameter and Qi is the quality rating based on the i^{th} parameter and 'n' is the total number of parameters.

The parameters selected for the assessment of water quality are based on their competence towards deteriorating the water quality. Nine quality parameters were selected to infer the GWQI which includes pH, TDS, Calcium, Magnesium, Sodium, Potassium, Sulphate, Chloride and Nitrate. The GWQI and the water quality status and the usage for drinking purposes are summarized in table 1. The standard values of selected parameters recommended by BIS (2012), their ideal values and the unit weights are presented in table 2.

Table 1: Recommended Ground Water Quality Index (GWQI) (Ramakrishna et al., 2009) and observed water quality status in the study area.
.

S. No	Ground Water Quality Index (GWQI)	Water Quality Status	Number of samples	% of samples
1	< 50	Excellent	12 (Kandi) and 13 (Sirowal)	66.6 % (Kandi) and 68.4 % (Sirowal)
2	50-100	Good	6 (Kandi) and 6 (Sirowal)	33.3 % (Kandi) and 31.5 % (Sirowal)
3	100-200	Poor	-	-
4	200-300	Very Poor	-	-
5	> 300	Unsuitable for drinking	-	-

Table 2: Groundwater quality parameters, the assigned weights and computed relative weights with BIS standards in the study area.

S. No	Parameters	BIS standard value	Weight (wi)	Relative weight (Wi)
1	pH	8.5	4	0.129032
2	Total dissolved solids	1500	5	0.161290
3	Calcium	200	3	0.096774
4	Magnesium	150	4	0.129032
5	Sodium	200	5	0.161290
6	Potassium	12	3	0.096774
7	Sulphate	400	3	0.096774
8	Chloride	600	2	0.064516
9	Nitrate	45	2	0.064516
		Total	31	1

Table: 3Chemical composition (mg/L) of groundwater and river water in the study area

Physio-graphic division	S. No.	Latitude	Longitude	Type	Ca	Mg	Na	K	HCO3	Cl	SO4	NO3
GROUNDWATER												
Kandi	MS1	32°43'29.1"	74°51'22.9"	H/P	87.7	14.3	8.3	3.2	120	5.0	2.6	5.2
Kandi	MS2	32°43'24.5"	74°51'34.4"	H/P	76.8	23.2	14.0	2.1	102	11.9	10.2	1.8
Kandi	MS3	32°43'04.7"	74°51'36.6"	H/P	65.4	13.4	24.4	0.9	106	1.5	11.2	1.9
Kandi	MS4	32°43'03.6"	74°51'38.0"	H/P	74.5	27.1	14.5	1.9	119	11.8	9.0	1.8
Kandi	MS5	32°43'11.3"	74°51'44.1"	H/P	94.1	3.3	4.2	0.7	105	1.4	0.9	1.0
Kandi	MS8	32°43'39.3"	74°49'53.0"	H/P	100.5	29.2	29.4	2.0	116	24.3	21.7	25.3
Kandi	MS9	32°43'25.4"	74°50'02.1"	H/P	97.8	5.3	8.5	2.5	105	7.8	7.0	2.3
Kandi	MS10	32°43'27.3"	74°50'20.2"	H/P	91.3	11.0	27.1	3.3	111	12.4	18.6	17.5
Kandi	MS11	32°42'32.0"	74°50'24.6"	H/P	62.6	15.5	16.8	2.7	111	2.8	3.1	0.5
Kandi	MS12	32°42'25.3"	74°50'17.2"	H/P	99.8	4.8	8.9	1.5	107	3.5	1.8	2.0
Kandi	MS13	32°41'42.8"	74°49'36.0"	H/P	80.7	17.9	11.1	1.6	123	5.3	3.2	2.4
Kandi	MS20	32°40'50.7"	74°50'13.2"	H/P	97.7	13.4	23.0	10.1	107	16.5	20.8	8.1
Kandi	MS25	32°44'38.3"	74°52'29.7"	H/P	99.3	7.8	11.3	3.3	114	6.5	19.6	3.5
Kandi	MS47	32°43'26.2"	74°50'47.2"	H/P	78.9	12.3	13.1	3.9	103	6.0	9.6	2.2
Kandi	MS7	32°43'10.9"	74°51'56.0"	T/W	65.5	23.2	14.6	2.4	112	2.8	3.8	2.9
Kandi	MS58	32°41'19.2"	74°50'58.3"	T/W	77.0	30.7	25.6	2.2	82	19.8	2.9	34.6
Kandi	MS61	32°42'35.7"	74°51'36.1"	T/W	83.2	24.6	11.4	3.0	109	7.9	11.9	12.2
Kandi	MS62	32°43'40.4"	74°51'24.4"	T/W	88.2	16.5	32.6	16.4	128	11.5	12.6	19.0
Average value					84.5	16.3	16.6	3.5	110	8.8	9.5	8.0
Sirowal	MS14	32°41'32.2"	74°49'21.8"	H/P	78.2	18.3	20.9	11.0	101	10.9	16.5	4.9
Sirowal	MS16	32°40'31.5"	74°47'52.2"	H/P	85.2	21.6	11.0	1.7	106	4.0	12.2	0.4
Sirowal	MS17	32°41'17.1"	74°48'40.5"	H/P	71.2	9.7	23.6	2.6	96	3.1	9.9	12.5
Sirowal	MS18	32°40'08.9"	74°50'19.2"	H/P	91.7	11.9	12.1	2.2	99	14.0	15.9	10.7
Sirowal	MS19	32°40'41.7"	74°49'58.7"	H/P	58.8	24.5	21.6	2.6	103	5.9	6.4	8.9
Sirowal	MS21	32°39'29.6"	74°50'04.1"	H/P	71.6	7.2	19.4	1.5	98	8.5	10.9	3.8
Sirowal	MS22	32°39'01.7"	74°49'37.6"	H/P	60.7	15.2	15.4	11.0	90	6.5	8.9	5.1
Sirowal	MS23	32°38'44.8"	74°49'05.8"	H/P	81.3	7.0	17.3	1.1	106	7.9	9.1	4.8
Sirowal	MS24	32°38'24.1"	74°48'11.6"	H/P	69.7	10.0	12.3	10.9	98	4.5	5.8	6.2
Sirowal	MS48	32°43'50.3"	74°49'13.0"	H/P	75.3	21.1	6.1	1.4	98	8.3	2.8	12.0
Sirowal	MS49	32°43'46.4"	74°48'55.7"	H/P	68.0	23.9	10.0	1.6	103	6.6	3.6	9.9
Sirowal	MS50	32°44'18.3"	74°47'53.6"	H/P	78.4	15.7	19.6	5.2	119	9.4	2.2	4.0
Sirowal	MS51	32°43'59.6"	74°47'06.8"	H/P	70.7	13.6	11.9	7.4	108	5.6	4.1	7.1
Sirowal	MS52	32°43'45.3"	74°46'29.8"	H/P	67.1	18.2	22.0	1.8	117	7.3	4.0	3.4
Sirowal	MS53	32°42'57.6"	74°44'57.4"	H/P	50.5	21.0	7.9	10.4	99	3.7	7.8	1.0
Sirowal	MS54	32°42'52.4"	74°44'11.1"	H/P	55.5	20.0	26.8	1.7	109	5.0	3.8	8.5
Sirowal	MS55	32°42'40.2"	74°43'15.6"	H/P	72.1	23.1	8.5	2.1	107	5.6	2.2	11.2
Sirowal	MS57	32°42'31.1"	74°42'45.7"	H/P	86.9	16.0	11.5	1.4	97	4.0	20.9	2.9
Sirowal	MS60	32°43'41.0"	74°45'40.2"	T/W	90.4	18.6	9.0	1.2	102	3.7	2.5	4.0
Average value					72.8	16.7	15.1	4.2	102.9	6.6	7.9	6.4
RIVER												
Kandi	MS6	32°43'13.9"	74°51'48.1"	R/W	45.6	27.1	26.8	12.0	105	3.5	8.1	3.6
Sirowal (NT)	MS15	32°41'12.3"	74°48'25.4"	R/W	63.0	15.7	18.4	7.7	104	2.1	1.7	2.8
Sirowal (WT)	MS59	32°42'43.2"	74°45'15.5"	R/W	102.8	6.7	12.6	2.1	115	2.3	12.3	5.3

* NT- Nikki Tawi, WT- Wadi Tawi

Table 4: Chemical composition (mg/L) and isotopic composition of river water and groundwater in Kandi and Sirowal belts in the study area

Physio-graphic division	S.No.	Latitude	Longitude	Type	Temp (°C)	pH	EC (µS)	TDS (mg/L)	TH (mg/L)	SAR	% Na	Mg^{2+}/Ca^{2+}	CAI-1=bei	d ^{18}O (‰)	d ^{2}H (‰)	d-excess
GROUNDWATER																
Kandi	MS1	32°43'29.1"	74°51'22.9"	H/P	24	7.6	381	240	278.39	0.85	10.11	0.16	-0.26	-6.12	-39.64	9.3
Kandi	MS2	32°43'24.5"	74°51'34.4"	H/P	20	7.8	253	158	287.65	1.49	13.85	0.30	-0.03	-5.96	-33.48	14.2
Kandi	MS3	32°43'04.7"	74°51'36.6"	H/P	19	7.8	249	156	218.49	2.87	24.31	0.20	-10.23	-5.81	-36.14	10.3
Kandi	MS4	32°43'03.6"	74°51'38.0"	H/P	20	7.8	245	154	297.70	1.54	13.83	0.36	-0.03	-5.38	-32.21	10.8
Kandi	MS5	32°43'11.3"	74°51'44.1"	H/P	25	8.1	260	135	248.83	0.43	4.82	0.03	-1.81	-5.90	-33.94	13.3
Kandi	MS8	32°43'39.3"	74°49'53.0"	H/P	24	7.1	850	534	371.62	2.74	19.49	0.29	-0.01	-6.46	-38.55	13.1
Kandi	MS9	32°43'25.4"	74°50'02.1"	H/P	26	7.4	442	277	266.19	0.85	9.68	0.05	-0.05	-5.70	-37.66	7.9
Kandi	MS10	32°43'27.3"	74°50'20.2"	H/P	24	7.1	735	463	273.27	2.76	22.95	0.12	-0.12	-5.46	-36.56	7.1
Kandi	MS11	32°42'32.0"	74°50'24.6"	H/P	26	8.0	234	147	220.35	2.01	20.00	0.25	-2.18	-6.24	-36.62	13.3
Kandi	MS12	32°42'25.3"	74°50'17.2"	H/P	25	7.7	327	206	269.04	0.88	9.03	0.05	-0.55	-5.24	-32.33	9.6
Kandi	MS13	32°41'42.8"	74°49'36.0"	H/P	23	7.2	502	316	275.59	1.17	11.39	0.22	-0.26	-7.53	-46.91	13.3
Kandi	MS20	32°40'50.7"	74°50'13.2"	H/P	25	6.9	741	467	299.40	2.25	22.92	0.14	-0.06	-6.39	-37.98	13.1
Kandi	MS25	32°44'38.3"	74°52'29.7"	H/P	22	7.8	405	255	280.28	1.11	12.01	0.08	-0.19	-5.98	-34.78	13.1
Kandi	MS47	32°43'26.2"	74°50'47.2"	H/P	24	7.4	444	277	247.73	1.42	15.73	0.16	-0.30	-6.69	-38.81	14.7
Kandi	MS7	32°43'10.9"	74°51'56.0"	T/W	24	7.5	279	175	259.17	1.66	16.08	0.35	-1.75	-5.14	-30.27	10.9
Kandi	MS58	32°41'19.2"	74°50'58.3"	T/W	26	7.1	766	484	318.76	2.67	20.56	0.40	-0.02	-8.13	-32.86	32.2
Kandi	MS61	32°42'35.7"	74°51'36.1"	T/W	27	7.4	675	425	309.38	1.16	11.76	0.30	-0.11	-5.68	-30.33	15.1
Kandi	MS62	32°43'40.4"	74°51'24.4"	T/W	23	7.4	553	349	288.39	3.32	31.88	0.19	-0.28	-3.55	-31.96	-3.6
Average value					24	7.5	463	290	278.35	1.73	16.13	0.20	-1.01	-6.0	-35.6	12.1
Sirowal	MS14	32°41'32.2"	74°49'21.8"	H/P	23	7.2	462	290	270.89	2.23	24.81	0.23	-0.18	-7.90	-46.40	16.8
Sirowal	MS16	32°40'31.5"	74°47'52.2"	H/P	24	7.3	318	201	301.97	1.12	10.63	0.25	-0.54	-6.23	-35.17	14.7
Sirowal	MS17	32°41'17.1"	74°48'40.5"	H/P	25	6.9	576	364	218.02	2.71	24.50	0.14	-2.36	-8.71	-59.30	10.4
Sirowal	MS18	32°40'08.9"	74°50'19.2"	H/P	24	6.9	635	400	277.97	1.22	12.13	0.13	0.00	-8.12	-51.96	13.0
Sirowal	MS19	32°40'41.7"	74°49'58.7"	H/P	25	6.8	764	481	247.98	2.57	22.52	0.42	-0.52	-5.65	-38.20	7.0
Sirowal	MS21	32°39'29.6"	74°50'04.1"	H/P	24	6.8	623	392	208.51	2.23	20.95	0.10	-0.17	-6.83	-44.55	10.1
Sirowal	MS22	32°39'01.7"	74°49'37.6"	H/P	26	6.9	537	338	214.24	1.86	25.81	0.25	-0.46	-8.46	-53.41	14.3
Sirowal	MS23	32°38'44.8"	74°49'05.8"	H/P	25	6.9	632	398	232.06	1.88	17.26	0.09	-0.17	-6.56	-43.20	9.3
Sirowal	MS24	32°38'24.1"	74°48'11.6"	H/P	27	6.8	621	391	215.40	1.43	22.57	0.14	-0.94	-7.59	-50.05	10.7
Sirowal	MS48	32°43'50.3"	74°49'13.0"	H/P	23	7.2	633	398	274.95	0.66	7.20	0.28	0.01	-8.39	-50.21	16.9
Sirowal	MS49	32°43'46.4"	74°48'55.7"	H/P	23	7.0	718	452	268.32	1.12	11.26	0.35	-0.11	-8.10	-50.30	14.5
Sirowal	MS50	32°44'18.3"	74°47'53.6"	H/P	23	6.7	572	360	260.60	2.11	20.83	0.20	-0.18	-9.06	-56.71	15.8
Sirowal	MS51	32°43'59.6"	74°47'06.8"	H/P	22	6.8	447	281	232.78	1.35	18.66	0.19	-0.43	-9.57	-58.41	18.1
Sirowal	MS52	32°43'45.3"	74°46'29.8"	H/P	22	7.4	477	300	242.63	2.51	21.77	0.27	-0.31	-8.87	-55.83	15.1
Sirowal	MS53	32°42'57.6"	74°44'57.4"	H/P	23	7.4	491	308	212.62	1.02	20.42	0.42	-1.06	-8.66	-54.82	14.5
Sirowal	MS54	32°42'52.4"	74°44'11.1"	H/P	23	7.4	484	304	221.08	3.31	27.36	0.36	-0.92	-8.64	-50.87	18.3
Sirowal	MS55	32°42'40.2"	74°43'15.6"	H/P	23	7.2	527	333	275.47	0.93	10.07	0.32	-0.16	-5.17	-47.32	-6.0
Sirowal	MS57	32°42'31.1"	74°42'45.7"	H/P	22	7.5	375	235	283.27	1.18	11.13	0.18	-0.55	-6.02	-39.20	9.0
Sirowal	MS60	32°43'41.0"	74°45'40.2"	T/W	24	7.5	497	313	302.45	0.90	8.54	0.21	-0.46	-6.75	-54.87	-0.9
Average value					24	7.1	547	344	250.59	1.70	17.81	0.24	-0.50	-7.6	-49.5	11.7
RIVER																
Kandi	MS6	32°43'13.9"	74°51'48.1"	R/W	24	8.2	147	93	225.42	3.48	34.80	0.59	-2.90	-4.46	-18.24	17.4
Sirowal (NT)	MS15	32°41'12.3"	74°48'25.4"	R/W	24	7.9	208	131	221.87	2.18	24.88	0.25	-5.55	-4.50	-27.10	8.9
Sirowal (WT)	MS59	32°42'43.2"	74°45'15.5"	R/W	23	8.0	210	134	284.48	1.22	11.83	0.07	-2.30	-6.00	-30.30	17.7

* H/P= Handpump, T/W= Tubewell, R/W= River water, EC= Electrical conductivity, TDS= Total dissolved solids, TH= Total hardness, SAR= Sodium absorption ratio, CAI= Chloro alkaline indice, WT- Wadi Tawi, NT- Nikki Tawi.

RESULTS AND DISCUSSION

Physico-chemical parameters

The chemical composition of river and groundwater is presented in Table 3, analytical calculations of physico-chemical parameters of groundwater and river are presented in Table 4 and statistical calculations of major ions (mg/L) are presented in table 5. These chemical parameters have been assessed for the Ground Water Quality Index (GWQI) and the computed results are presented in Table 6.

Table 5: Statistical summary of major ions (mg/L) of the river and groundwater samples in the Kandi and Sirowal Belts in the study area

Parameter	Groundwater Kandi Belt			Groundwater Sirowal Belt			River Water		
	Minimum	Maximum	Average	Minimum	Maximum	Average	Minimum	Maximum	Average
Ca^{2+}	62.6	100.5	84.5	50.5	91.7	72.8	45.6	102.8	70.4
Mg^{2+}	3.3	30.7	16.3	7.0	24.5	16.7	6.7	27.1	16.5
Na^{+}	4.2	32.6	16.6	6.1	26.8	15.1	12.6	26.8	19.2
K^{+}	0.7	16.4	3.5	1.1	11.0	4.2	2.1	12.0	7.3
HCO_3^-	82.0	128.0	110.0	90.0	119.0	102.9	104.0	115.0	108.0
Cl^-	1.4	24.3	8.8	3.1	14.0	6.6	2.1	3.5	2.6
SO_4^{2-}	0.9	21.7	9.5	2.2	20.9	7.9	1.7	12.3	7.3
NO_3^-	0.5	34.6	8.0	0.4	12.5	6.4	2.8	5.3	3.9

The pH value of groundwater and river water ranges from 6.7-8.1 and 7.9-8.2 respectively, which show slightly acidic to slightly alkaline nature. Total dissolved solids (TDS) in groundwater and river water ranges from 135-534 mg/L and 93-134 mg/L respectively. The TDS concentration of river and groundwater of Kandi and Sirowal belts indicates fresh water (0-1000 mg/L) category (Davis, 1966; Freeze and Cherry, 1979).

Electrical Conductivity (EC) is an index which represents the total concentration of dissolved salts present in water (Purandara, 2003). The EC of groundwater and river water ranges from 234-850 µS and 147-210 µS respectively. The low value of EC in river water may be due to recent infiltration of water which had little time to interact with rocks for mineral dissolution (Olea et al., 2019).

Sources of major ions

Various chemical ions show their presence in river and groundwater due to rock-water interaction in the study area. Calcium and sodium concentration in the groundwater ranges from 50.5 to 100.5 mg/L and 4.2 to 32.6 mg/L respectively. Calcium and sodium concentration in groundwater may be due to weathering of minerals such as pyroxene, epidote, tourmaline and feldspar found in the Siwalik sediments (Abid et al., 1983). The calcium and sodium concentration in river water ranges from 45.6 to 102.8 mg/L and 12.6 to 26.8 mg/L respectively. The magnesium concentration in groundwater and river water ranges from 3.3 to30.7 mg/L and 6.7to 27.1 mg/L respectively. Both calcium and magnesium concentration result from the weathering of carbonate bearing rocks found in the Siwaliks (Sinha et al., 2007; Hossain et al., 2008; Ullah et al., 2009) and are also contributed by river water coming from Trikuta Limestone through Jhajjar stream. Low potassium concentration in groundwater (0.7 to16.4 mg/L) and river (2.1 to 12.0 mg/L) is likely due to less dissolution of potassium salts. The concentration of Ca and Mg (alkaline earth metals) is more than that of Na and K (alkali metals) in the study area and is also reported by Kanwar and Bhatti (2014) which might be due to the presence of clay and silt in the outer plain area.

Table 6: Results of Ground Water Quality Index (GWQI) values in the study area

KANDI BELT			SIROWAL BELT		
Sample	GWQI Values	Status of Water	Sample	GWQI Values	Status of Water
			Along Ranbir Canal		
MS1	44	Excellent	MS14	53	Good
MS2	43	Excellent	MS16	42	Excellent
MS3	38	Excellent	MS17	48	Excellent
MS4	44	Excellent	MS18	51	Good
MS5	35	Excellent	MS19	53	Good
MS8	70	Good	MS21	44	Excellent
MS9	42	Excellent	MS22	49	Excellent
MS10	58	Good	MS23	45	Excellent

MS11	38	Excellent	MS24	50	Good
MS12	39	Excellent	MS48	50	Good
MS13	44	Excellent	MS49	51	Good
MS20	60	Good	MS50	48	Excellent
MS25	45	Excellent	MS51	45	Excellent
MS47	44	Excellent	MS52	45	Excellent
MS7	41	Excellent	MS53	47	Excellent
MS58	68	Good	MS54	46	Excellent
MS61	56	Good	MS55	49	Excellent
MS62	65	Good	MS57	44	Excellent
			MS60	46	Excellent

Based on the hardness classification of water by Sawyer and McCarty's (1967), the river water (221.87 to284.4 mg/L) belongs to hard class and groundwater (208.51 to 371.62 mg/L) belongs to hard and very hard categories. Stuyfzand (1989) classified the groundwater into eight categories on the basis of chloride concentration showing the source and the time length of groundwater interaction with the geological units. In the present study, the river water with chloride concentration of 2.1 to3.5 mg/L groups into Very Oligohaline (<5) and groundwater (1.4to24.3 mg/L) belongs to Very Oligohaline (<5) and Oligohaline (5-30) categories.

Sulphate concentration of groundwater and river water ranges from 0.9to 21.7 mg/L and 1.7 to 12.3 mg/L respectively whereas, the Nitrate concentration of groundwater and river water ranges from 0.4to34.6 mg/L and 2.8to5.3 mg/L. High level of nitrate concentration in groundwater might be due to application of nitrogenous fertilizers, irrigation practices and cattle population in the area (Kanwar et al., 2014).

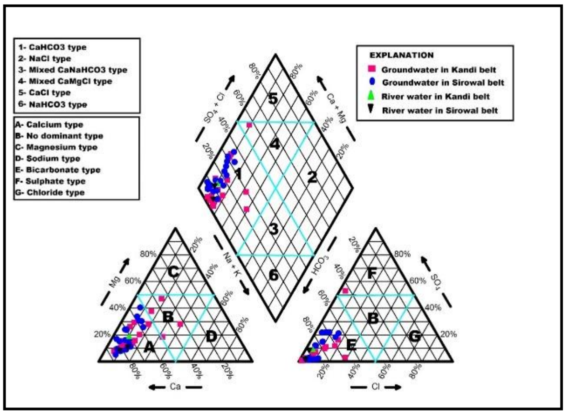

Figure 2: Piper-Trilinear plot for river water and groundwater in Kandi and Sirowal belts.

Calculation of Ground Water Quality Index (GWQI)

GWQI is divided into five categories (Ramakrishnalah et al., 2009) and the status of water quality is given in Table 1. GWQI calculated for groundwater samples are presented in Table 6. The ground water samples of Kandi and Sirowal belts show GWQI ranging from 35 to 70. In Kandi belt, 66.6% ground water samples fall in the Excellent and 33.3% in the Good category whereas, in the Sirowal belt, 68.4% ground water samples fall in Excellent and 31.5% in Good category. The GWQI suggests that the water is suitable for drinking purposes in both Kandi and Sirowal belts.

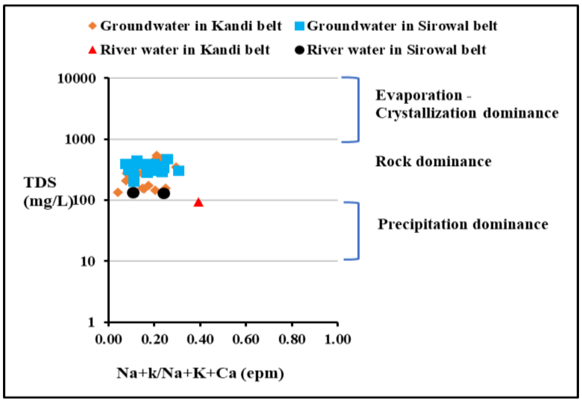

Figure 3: Gibbs diagram showing dominance of rocks for cation composition in study area

Hydrogeochemical characteristics

Piper diagram

The variation in the chemical composition of river water and groundwater was illustrated using the Piper Trilinear diagram (Piper, 1953).

The Piper Trilinear plot (Fig. 2) shows that the hydrochemical facies of groundwater in Sirowal and Kandi belts is $CaHCO_3$ water type (Zone 1). The river water of Kandi and Sirowal belts indicate that the $CaHCO_3$ water type (Zone 1) hydrochemical facies. The $CaHCO_3$ water type reflects that the rain water acts as the primary source for the groundwater recharge (Yang et al., 2019. This means that alkaline earths exceed alkalis and weak acids exceed strong acids. Dominance of HCO_3^- anion suggests bicarbonate class of groundwater (Chebotarev, 1955) in the study area indicating initial stage of groundwater evolution and presence of groundwater near the surface of earth which can be explained in the following sequence.

$HCO_3 \rightarrow HCO_3 + Cl \rightarrow Cl + HCO_3 \rightarrow (Cl + SO_4)$ or $(SO_4 + Cl) \rightarrow Cl$

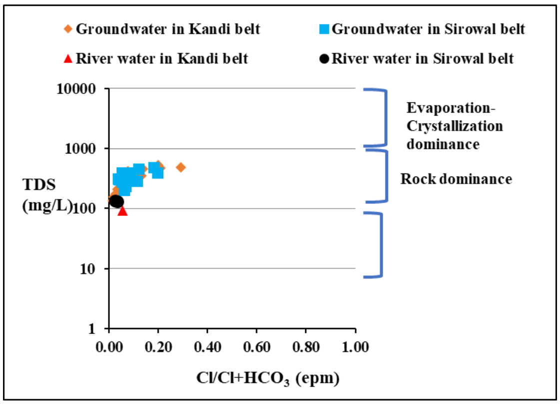

Figure 4: Gibbs diagram showing dominance of rocks for anion composition in study area.

Gibbs diagram

The Gibbs diagrams for the groundwater and river water of Kandi and Sirowal belts are shown in figures 3 and 4. Both the Kandi and Sirowal groundwater samples indicate that the ionic composition was controlled mainly by the rock-dominance. The Gibbs diagram enlightened the fact that weathering of rocks act as the major dominant process which controls the ionic composition in the groundwater of Kandi and Sirowal belts of Tawi watershed. This dominant process confirms that the rock-water interaction acts as the source for the chemical constituents in the groundwater of Kandi and Sirowal belts.

The ionic composition of river water in Sirowal belt is controlled by rock-dominance whereas, the data for river water of the Kandi belt plots at the boundary line between rock dominance and precipitation dominance.

Index of Base Exchange (between groundwater and surrounding rocks)

The "Index of Base Exchange" is used to describe the geochemical reactions taking place in groundwater and was given by Schoeller (1965). The Chloro-alkaline indices (CAI-1) is used to measure the base-exchange during the water-rock interaction. There are minerals in the rocks such as clay etc. which absorb and exchange the ions with the groundwater.

Chloro-alkaline indices (CAI-1)

The ion exchange between groundwater and the surrounding environment has been illustrated by the (CAI-1= bei) indices using ionic concentration expressed in mg/L. The equation used to infer the base-exchange is as:

$$\text{CAI-1} = \frac{[Cl - (Na + K)] / Cl}{Cl}$$

The calculated CAI-1 values of both river water and groundwater are presented in Table 4. The negative CAI-1 values indicate normal ion exchange of Ca^{2+} or Mg^{2+} ions in the groundwater with that of Na^{+} and K^{+} in the weathered materials whereas the positive value of index represents the reverse ion exchange (Schoeller, 1965). In this study, 95% water samples show negative CAI-1 values and 5% water samples show positive values suggesting that the normal ion exchange is the dominant process.

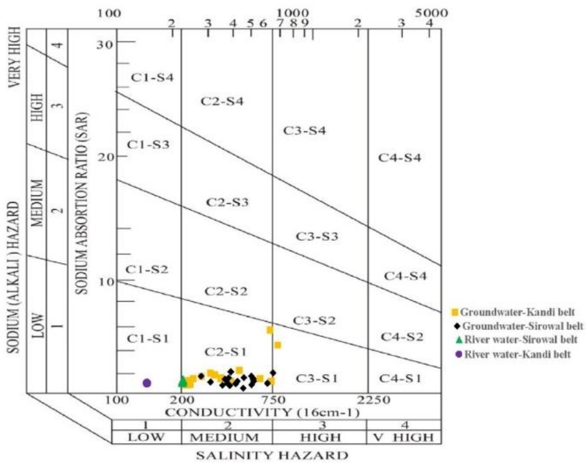

Figure 5: U.S Salinity diagram for the classification of water for irrigational use in the study area

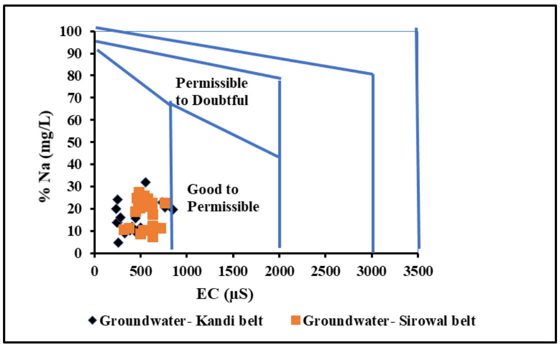

Figure 6: Ratings of groundwater samples based on electrical conductivity and sodium percentage (Wilcox, 1955) in the study area.

Suitability for Irrigational purpose

As the Kandi and Sirowal belts show steep slope and variation in topographic gradient, the study area comes under irrigation land use for the Kharif as well as Rabi crops. The Tawi River, canals as well as groundwater play major role for the irrigation pattern in agricultural land. Two parameters – Sodium absorption ratio (SAR) (Richards, 1954) and Sodium percentage (%Na) (Wilcox, 1955) were used to determine the suitability of water for irrigational use. The calculated SAR and % Na values of river and groundwater (mg/L) are presented in Table 4. Diagrams used to illustrate the groundwater suitability for irrigational use are as under:

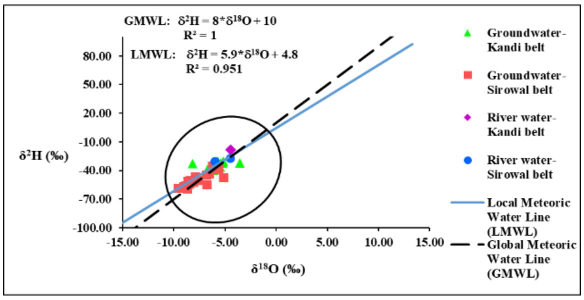

Figure 7: Regression line for LMWL, GMWL, river water and groundwater in Kandi and Sirowal belts in the study area.

A) Richard Diagram- The plot between SAR and EC in the U.S Salinity Diagram (USSL) shows that the majority of groundwater samples of Kandi and Sirowal belt fall in the category of C2S1 (Fig. 5). One groundwater sample of Kandi belt fall in the category of C3S1. The field of C2S1 represents medium salinity and low sodium water which indicates that the quality of water is good and favourable for all types of crops except least salt tolerant crops such as dry beans, soya beans, corn and field peas. C3S1 represents high salinity and low sodium water which can be used on clayey soil but the type of crop depends on the salt tolerant range prior to the cultivation (AL-Alhamdi and EL-Fiky, 2009). The SAR values of river and groundwater in the Kandi and Sirowal belts show the suitability of water for the irrigation use.

B) Wilcox Diagram- The plot between % Na and EC describe Wilcox diagram (Fig.6). High value of these parameters affects the crop growth. The groundwater samples of Kandi and Sirowal belts fall in the category of "Excellent to Good". One groundwater sample of Kandi belt falls in the category of "Good to Permissible". Thus, the groundwater of Kandi and Sirowal belts with respect to percentage Na and EC show favourable conditions for irrigational use.

Isotopic analysis

The isotopic composition of $\delta^{18}O$ and δ^2H of groundwater (hand pumps & tube wells) and river water in Kandi and Sirowal belts is presented in Table 4. These isotopic measurements are plotted in (Fig. 7).

The Global Meteoric Water Line was developed by Craig (1961) using the following equation:

$$\delta^2H = 8\times\delta^{18}O + 10. \qquad \text{(eq.1)}$$

Jeelani et al (2017) developed the Local Meteroic Water Line (LMWL) based on the precipitation data for Jammu which is represented by the equation:

$$\delta^2H = 5.9\times\delta^{18}O + 4.8 \text{ (March-April-May).} \qquad \text{(eq. 2)}$$

Isotopic composition of river water- The $\delta^{18}O$ values of river water (n=3) range from -6.00‰ to -4.46‰ and δ^2H range from -30.30‰ to -18.24‰ respectively. The $\delta^{18}O$ and δ^2H values of river water samples fall on the LMWL which indicates modern precipitation act as primary source of Tawi River (Fig. 7).

Isotopic composition of groundwater- The $\delta^{18}O$ values of groundwater in Kandi belt (n=18) range from -8.13‰ to -3.55‰ (average= -6.0‰) and δ^2H from -46.91‰ to -30.27‰ (average= -35.6‰). The $\delta^{18}O$ values of groundwater in Sirowal belt (n=19) range from -9.57‰ to -5.17‰ (average= -7.6‰) and δ^2H range from -59.30‰ to -35.17‰ (average= -49.5‰).

The isotopic composition of river water is slightly enriched than that of the groundwater in study area in equation 3 and 4 respectively:

Groundwater (*Kandi* and *Sirowal*):

$$\delta^2H = 5.3\times\delta^{18}O - 6.6 \text{ (May-June)} \qquad \text{(eq.3)}$$

River water (*Kandi* and *Sirowal*):

$$\delta^2H = 5.1\times\delta^{18}O + 0.38 \text{ (May-June)} \qquad \text{(eq.4)}$$

The slope and intercept of groundwater of Kandi and Sirowal belts are lower than that of the LMWL which indicates the evaporative enrichment effect on groundwater samples. It is being observed that the slope of groundwater samples is similar to LMWL as given by Jeelani et al. (2017). Contrary to the expectations, groundwater samples are not exclusively recharged by rain water but by river and canal also. Similar slope (Fig. 7) is mere a coincidence because the isotopic values of groundwater is depleted with an average of -6.8‰ and rainfall recharge process cannot cause isotopic depletion.

The groundwater locations along the Ranbir canal show depleted isotopic signatures compared to the river (Nikki and Wadi Tawi) and rain (eq. 1) isotopic signatures except groundwater sample MS19 and MS55. In the Kandi belt, the groundwater locations on both the banks of Tawi River show isotopic signatures similar to rain (eq. 1) except MS1, MS8, MS11, MS13, MS20, MS47 and MS58. Out of these exceptions, MS11, 13, 20, 47 and 58 are groundwater locations along the canal. The highly depleted $\delta^{18}O$ values of groundwater are observed in the Sirowal belt than that of the Kandi belt and might be due to Ranbir canal carrying snow melt cold water of Chenab River into the area and recharging the groundwater. Similar conclusions have been drawn by Ahmad et al. (2012) in the Indus basin in Pakistan.

"Deuterium excess", d-excess = $\delta^2H - 8*\delta^{18}O$ has been defined to identify the relative magnitude of kinetic fractionation in different water masses (Dansgaard, 1964). The values of d-excess for river water in Kandi belt is 17.4‰ and in Sirowal belt, the d-excess value is 8.9‰ (Nikki Tawi) and 17.7‰ (Wadi Tawi). About 72.2% of groundwater samples in Kandi belt and 73.7% in Sirowal belt have d-excess > 10‰ whereas 27.7% in Kandi and 26.3% in Sirowal belt have d-excess < 10‰. These values are close to and more than 10‰. The higher d-excess values (> 10‰) show precipitation due to Western Disturbance (Rozanski et al., 1993) and also indicate the existence of the recycled water derived from local evaporated vapour (Bowen et al., 2012; Gat et al., 1994).

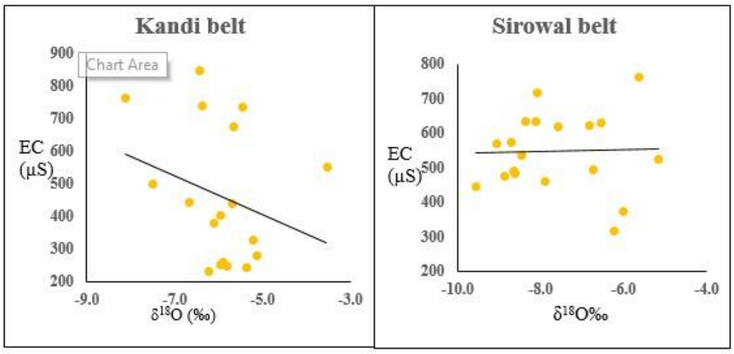

Figure 8: Scatter plot of Electrical Conductivity and $\delta^{18}O$ isotopes of groundwater in the study area.

The plot of $\delta^{18}O$ and conductivity of Kandi belt indicate negative correlation while Sirowal belt do not show any correlation which gives clear picture of no evaporation effect (Fig. 8). It has been reported that the evaporation process in water is associated with low d-excess values (Dansgaard, 1964). However, in Kandi and Sirowal belts, the groundwater has high d-excess values which may be due to the recharging by rainfall and canal water (Jeelani et al., 2017; Ahmad et al., 2012).

Groundwater recharge

In the Sirowal belt, the depleted groundwater $\delta^{18}O$ values compared to river water isotopic values suggest that there is highly depleted source present in the area. The Ranbir Canal traversing from the left bank of Chenab River drains the Sirowal belt and some parts of Kandi belt. This canal carries the snow melt cold water of Chenab River from the glaciated higher reaches and irrigates the Sirowal belt. Thus, there are two sources- highly active canal and precipitation that dominate the groundwater recharge in the study area. In the case of Kandi belt, the $\delta^{18}O$ values of groundwater are enriched and show close isotopic signatures to the river water in scatter plot (Fig. 7). Near the banks, the groundwater $\delta^{18}O$ values might get recharged due to river water. In this zone, precipitation and Tawi river water act as predominant source for the groundwater replenishment. Hence, the sources of groundwater recharge in the study area are modern local precipitation, river and canal water. At this stage, we do not give any quantification of recharge source to groundwater.

Groundwater development involves the management and sustainable use of resources for future use. In the study area, the groundwater recharge occurs mainly along the canal area and through the natural infiltration of rain and river water. The development of sites along the Ranbir canal in Sirowal belt and natural infiltration of rainwater in the Kandi belt can serve as the potential sites for groundwater development. The quantification of recharge sources can further give clear picture about the potential sites for development and sustainable use in future.

CONCLUSIONS

The conclusions drawn from the current study of hydrochemistry and isotope hydrology of river water (Tawi river) and groundwater (Hand pumps & Tube wells) in the Kandi and Sirowal belts of Tawi watershed in the Jammu district are as follow:

- The quality of river water and groundwater is good in the study area with respect to drinking and irrigational purposes.
- The river water shows alkaline nature while groundwater in Kandi belt shows slight acidic to basic nature and Sirowal belt shows acidic nature.
- The hydrochemical facies determined using the Piper-Trilinear plot revealed that both the river water and groundwater were of $CaHCO_3$ type.
- GWQI observation indicates that the quality of water mostly falls in the Excellent and Good categories in the study area.
- The stable isotopic composition ($\delta^{18}O$ and $\delta^{2}H$) of river water and groundwater is indicative of meteoric origin and enrichment before groundwater recharge. Ranbir canal is the active recharge source for ground recharge in Sirowal belt while river water contributes to ground recharge near the banks in the Kandi belts.

Acknowledgement

Thanks are due to Dr. R. D. Deshpande, Physical Research Laboratory, Ahmedabad, Gujarat for providing facility for isotopic measurements. One of the authors (MS) thank Inspire Programme of Department of Science and Technology, Govt. of India, New Delhi for providing fellowship to carry out the research work. The suggestions by two anonymous reviewers have improved the quality of manuscript.

References

Abid, I. A., Abbasi, I. A., Khan, M. A., & Shah, M. T. (1983). Petrography and geochemistry of the Siwalik sandstone and its relationship to the Himalayan orogeny. Geological Bulletin University of Peshawar, 16, 65-83.

Ahmad, M., Latif, Z., Tariq, J. A., Rafique, M., Akram, W., Aggarwal, P., & Vitvar, T. (2012). Isotope investigations of major rivers of Indus Basin, Pakistan. Monitoring Isotopes in Rivers: Creation of the Global Network of Isotopes in Rivers (GNIR), 167.

Al-Ahmadi, M. E., & El-Fiky, A. A. (2009). Hydrogeochemical evaluation of shallow alluvial aquifer of Wadi Marwani, western Saudi Arabia. Journal of King Saud University-Science, *21*(3), 179-190.

Bhat, N. A., & Jeelani, G. (2018). Quantification of groundwater–surface water interactions using environmental isotopes: A case study of Bringi Watershed, Kashmir Himalayas, India. Journal of Earth System Science, *127*(5), 1-11.

BIS (Bureau of Indian Standard) (2012) 10500, Indian standard drinking water specification, second revision, pp. 1-24.

Burgman, J. O. S., Eriksson, E., Kostov, L., & Moeller, A. (1979). Application of oxygen-18 and deuterium for investigating the origin of groundwater in connection with a dam project in Zambia. In Isotope hydrology 1978.

Bowen, G. J., Kennedy, C. D., Henne, P. D., & Zhang, T. (2012). Footprint of recycled water subsidies downwind of Lake Michigan. Ecosphere, 3(6), 1-16.

Craig, H. (1961). Isotopic variations in meteoric waters. Science, 133(3465), 1702-1703.

Chebotarev, I. I. (1955). Metamorphism of natural waters in the crust of weathering. Geochimica et Cosmochimica Acta, Vol.8, 22-48, 137-170, 198-212.

CGWB (2013). Groundwater Information Booklet of Jammu District. Ministry of Water Resources, Government of India.

Dansgaard, W. (1964). Stable isotopes in precipitation. Tellus, 16(4), 436-468.

Davis, Stanley N., and Roger JM DeWiest. (1966). Hydrogeology. No. 551.49 D3.

Deshpande, R. D., and S. K. Gupta (2012). Oxygen and hydrogen isotopes in hydrological cycle: new data from IWIN national programme. Proc. Indian Natl. Sci. Acad. Vol. 78.

Freeze, R. Allan, and John A. Cherry (1979). Groundwater. Prentice Hall, Englewood Cliffs, No. 629.1 F7.

Fritz, P., & Fontes, J. C. (1980). Vienna-Standard Mean Ocean Water. Handbook of environmental isotope geochemistry, 1, 1-19.

Gat, J. R., Bowser, C. J., & Kendall, C. (1994). The contribution of evaporation from the Great Lakes to the continental atmosphere: estimate based on stable isotope data. Geophysical Research Letters, 21(7), 557-560.

Gupta, S. K., & Deshpande, R. D. (2005). Groundwater isotopic investigations in India: What has been learned?. Current Science, 825-835.

Gupta, S. K., & Deshpande, R. D. (2005). The need and potential applications of a network for monitoring of isotopes in waters of India. Current Science, 107-118.

Gupta, R. D., Arora, S., Gupta, G. D., & Sumberia, N. M. (2010). Soil physical variability in relation to soil erodibility under different land uses in foothills of Siwaliks in NW India. Tropical ecology, 51(2), 183.

Horton, R. K. (1965). An index number system for rating water quality. J Water Pollut Control Fed, *37*(3), 300-306.

Hossain, H. M., Ulak, P. D., & Roser, B. (2008). Geochemical analyses of sandstones and mudstones from the Siwalik succession, Surai Khola, western Nepal. Geoscience Rept. Shimane University, 2727, 53-60.

Jeelani, G., & Deshpande, R. D. (2017). Isotope fingerprinting of precipitation associated with western disturbances and Indian summer monsoons across the Himalayas. Journal of Earth System Science, 126(8), 108.

Jeelani, G., Shah, R. A., & Deshpande, R. D. (2018). Application of water isotopes to identify the sources of groundwater recharge in a Karstified landscape of Western Himalaya. Journal ofClimate Change, *4*(1), 37-47.

Kumar, V., Rai, S. P., & Rathore, D. S. (2004). Land use mapping of Kandi belt of Jammu region. Journal of the Indian Society of Remote Sensing, 32(4), 323-328.

Kumar, C. P. (2013). Hydrological studies using isotopes. International Journal of Innovative Research and Development, 2(13), 8-15.

Kanwar, P., & Bhatti, R. (2014). Assessment of chemical quality of groundwater in the equivalents of Bhahbar and Taryai belts of Jammu district, J&K. Journal of Himalayan Ecology and Sustainable development, 7, 6-11.

Kanwar, P., Khan, N., & Singh, K. P. (2014). Variation and Evaluation of Ground Water Levels and Water Quality in Kandi and Sirowal Belts of Jammu District, Jammu and Kashmir, India. Environment, *3*(9).

Maurya, A. S., Shah, M., Deshpande, R. D., & Gupta, S. K. (2009, November). Protocol for $\delta 18O$ and δD analyses of water sample using Delta V plus IRMS in CF Mode with Gas Bench II for IWIN National Programme at PRL, Ahmedabad. In 11th ISMAS Triennial Conference of Indian Society for Mass Spectrometry (Vol. 314, pp. 314-317). Indian Society for Mass Spectrometry Hyderabad.

Olea-Olea, Selene, Oscar Escolero, and Jürgen Mahlknecht. (2019). Geochemical characterization of components of the groundwater flow system in the basin of Mexico. In E3S Web of Conferences, vol. 98, p. 07022. EDP Sciences.

Piper, A. M. (1953). A graphic procedure for the geo-chemical interpretation of water analysis. USGS Groundwater Note 12.

Purandara, B. K. V. N. Jayashree K. 2003. Poll Res, *22*(2), 189.

Ramakrishnalah, C. R., Sadashivaiah, C., & Ranganna, G. (2009). Assessment of water quality index for the groundwater in Tumkur Taluk, Karnataka State, India. E-Journal of chemistry, *6*(2), 523-530.

Romanelli, A., Massone, H. E., & Qutrozl, O. M. (2011). Integrated hydrogeological study of surface & ground water resources in the southeastern Buenos Aires Province, Argentina. International Journal of Environmental Research, 5(4), 1053-1064.

Richards, L. A. (1954). Diagnosis and improvement of saline and alkali soils (Vol. 78, No. 2, p. 154). LWW.

Rozanski, K., Araguás-Araguás, L., & Gonfiantini, R. (1993). Isotopic patterns in modern global precipitation. GMS, 78, 1-36.

Saleem, M., & Jeelani, G. (2017). Geochemical, isotopic and hydrological mass balance approaches to constrain the lake water–groundwater interaction in Dal Lake, Kashmir Valley. Environmental earth sciences, *76*(15), 1-18.

Sawyer, C. N., & McCarty, P. L. (1967). Chemistry for sanitary engineers (2nd ed.). New York: Mc Graw-Hill Education.

Schoeller, H. (1965). Qualitative evaluation of groundwater resources. Methods and techniques of groundwater investigations and development. UNESCO, 5483.

Stuyfzand, P. J. (1989). A new hydrochemical classification of water types: Regional Characterization of water quality (Proceedings of the Baltimore Symposium, May 1989): IAHS Publ, 182, 89-98.

Sinha, S., Islam, R., Ghosh, S. K., Kumar, R., & Sangode, S. J. (2007). Geochemistry of Neogene Siwalik mudstones along Punjab re-entrant, India: Implications for source-area weathering, provenance and tectonic setting. Current Science, 1103-1113.

Thakur, K. K., Pandita, S. K., Goyal, V. C., Singh, Y. U. D. H. B. I. R., & Kotwal, S. S. (2014). Characterisation of drainage basin morphometric parameters of Balawal Watershed, Jammu province, Jammu and Kashmir. Himalayan Geology, 35, 124-134.

Ullah, K., Arif, M., Shah, M. T., & Abbasi, I. A. (2009). The Lower and Middle Siwaliks fluvial depositional system of the western Himalayan foreland basin, Kohat, Pakistan. Journal of Himalayan Earth Sciences, 42, 61-85.

Weyer, K.U., Horwood, W.C., & Krouse, H.R. (1979). Investigation of regional geohydrology south of Great Slave Lake, Canada, utilizing natural sulphur and hydrogen isotope variations. International Atomic Energy Agency (IAEA): IAEA.

Wilcox, L. (1955). Classification and use of irrigation water. US Department of Agriculture, Washington, p 969.

Yang, K., Han, G., Song, C., & Zhang, P. (2019). Stable HO isotopic composition and water quality assessment of surface water and groundwater: a case study in the Dabie Mountains, central China. International journal of environmental research and public health, 16(21), 4076.

Received: 26th April, 20021
Revised accepted: 17th August, 2021

JOURNAL INDIAN ASSOCIATION OF SEDIMENTOLOGISTS ISSN NO 2582 – 2020
Vol. 38, Issue 2, 2021, pp. 101-114
DOI: https://doi.org/10.51710/jias.v38i2.192

Provenance, Depositional and Diagenetic Reconstruction of the Early Palaeozoic Succession in Kupwara District, Kashmir, North-western Himalaya

Ashaq Hussain Bhat[1, 2,*], S. K. Pandita[1], H. N. Sinha[3] Bindra Thusu[4] and Ahsan ul Haq[1]

1. Department of Geology, University of Jammu, Jammu and Kashmir-180006 (India)
2. Department of Geology, S. P. College, Srinagar, Jammu and Kashmir-190001 (India)
3. Department of Geology, Vinobha Bhave University, Hazaribagh, Jharkhand-825301 (India)
4. Department of Earth Sciences, University College London, Gover Street London (UK)

*Email: ahbhat.amu@gmail.com

Abstract

Early Palaeozoic succession in Kupwara district of Jammu and Kashmir, North-western Himalaya comprise of sandstone, shale, carbonates and slate. The petrological properties of these rocks were used to work out the provenance, depositional environment and their diagenetic history. The siliciclastic sediments with interbedded carbonate rocks indicate shifts in sea level and consequent changes in energy conditions of the basin as well as biogenic interferences leading to carbonate precipitation in a shallow marine depositional environment. Provenance of these rocks has been of mixed nature with monocrystalline quartz dominant in sandstones indicating greater contribution from igneous sources.

Keywords: Early Palaeozoic, Kupwara, North-western Himalaya, Depositional environment

INTRODUCTION

The Tethyan sedimentary belt of Himalaya extends from Nanga Parbat in the west to Namcha Barwa in the east overlying the central crystalline basement known as Salkhalas in Kashmir Himalaya (Wadia, 1934). The deposition of marine sediments of Phanerozoic Eon has been restricted to the Tethyan realm of Himalaya (Parcha, 2021). Among the Tethyan strata, the Palaeozoic-Mesozoic rock formations along the northern margin of the Indian plate are essentially a shelf sequence (Shah, 1991). These nearly uninterrupted sedimentary successions were deposited in four sub-basins i.e., Kashmir, Zanskar, Spiti-Kinnaur and Garhwal-Kumaon during Proterozoic to Eocene with varying thickness from 5000 to 16000m. The early and late Palaeozoic Tethyan strata are widely distributed in north-western and south-eastern parts of Kashmir basin respectively.

The majority of physico-chemical processes involved in sedimentation history of a basin are weathering in the source area, transportation, sorting, deposition and diagenesis (Roser and Korsch, 1986, 1988; McLennan et al., 1990; Eriksson et al., 1992; Weltje and Eynatten, 2004). These major processes involved during sedimentation are controlled by nature of sedimentary provenance, processes dominating in the depositional basin and sediment dispersal from provenance to basin that affects the mineralogical composition of clastic rocks. Facies and petrographic analysis of sandstones is an organized discipline in depositional and diagenetic studies.

The sandstone petrography is governed by the combined impact of provenance of the detrital input, the distance between the depositional basin and the provenance, the mode of transport of the sediments, and the prevalent environment. Plate tectonics-controlled geometry of provenance with respect to basin defines the type of sandstone deposited (Dickinson & Suczek, 1979). Quartz content in sediments has varied with the tectonic settings (Crook, 1974 and Schwab 1975). Quartz-rich rocks have been associated with passive continental margins whereas quartz-poor rocks as volcanogenic derivatives from magmatic island arcs. The rocks of intermediate quartz content are associated typically with active continental margins. Since inter-granular cement and matrix are the function of diagenesis and deposition, provenance studies focus on proportions of detrital framework grains (Dickinson, 1970). Diagenesis controls porosity of the sediments which in turn is controlled largely by framework composition of the rocks (Dickinson and Suczek, 1979).

The early Palaeozoic rocks in the north-western Kashmir have been substantially addressed for stratigraphy and palaeontology (Shah, 1968, 1972, 1982; Shah and Sudan, 1983, 1987; Shah, 1991), but a research gap exists as to the provenance, depositional and diagenetic environment of these rocks. This preliminary study is the first attempt to address that gap by carrying out facies, petrographic and diagenetic investigations in this area.

Geological Setting

The Palaeozoic-Mesozoic rocks of the "Himalayan Tethys belt" are exposed along a series of structural basins which constituted a continuous sea, separated as a result of collision tectonics of the Himalayan Range (Shah, 1991). Sedimentation in structural sub-basin of Kashmir, between the Pir Panjal Range in the southwest and Zanskar Range in northeast, has been deposited in subtidal shoreface to tidal flats (Bhargava, 2011). In the north-western Kashmir, the early Palaeozoic succession has been assigned to Pohru Group in Kupwara district, and predominantly comprises of argillaceous rocks with sub-ordinate calcareous and arenaceous bands. These successions are Cambro-Silurian with Precambrian basement referred as Salkhalas (Wadia, 1934). Wadia (1934) during mapping of the north-western sector of Kashmir recorded Trilobite-bearing Cambrian sediments and unconformities between the Silurian and middle Carboniferous, besides, an apparent gradation between Salkhala Crystallines and the ‘Dogra Slate’. Lithologically, these rocks comprise of interbedded sequence of slate, shale, greywacke, sandstone and thin-bedded limestone. Strike is due NE-SW with average dips varying from 15º-25º to 40º-50º. In the early Palaeozoic, the basal Lolab Formation is conformably overlain by Nutnus Formation comprising of thin bedded, pale to deep green shale, with the sporadic occurrence of sandy and cherty fabric and few beds of limestones. The Trehgam Formation represents green

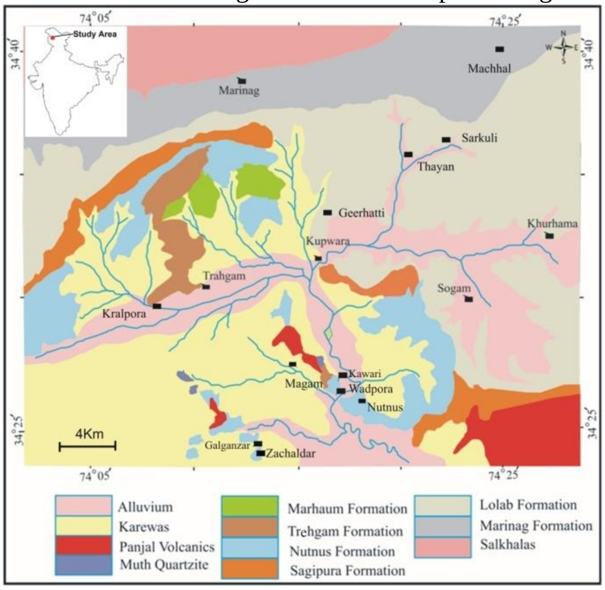

Fig-1: Geological map of study area in Kupwara district, North-western Kashmir (after Shah, 1968)

shale or siltstone alternating with limestone interbedded with minor arenaceous bands (Table 1).

The early Palaeozoic rocks in Pohru valley are exposed in a folded sequence of Cambrian, Ordovician and Silurian rocks. These are overlain by Muth Quartzite of Middle Silurian to Early Devonian (Reed, 1912 and Goel et al., 1987) and Panjal Volcanics of Permo-Carboniferous age with a discrete angular unconformity. The age of Muth Quartzite has often remained contentious due to lack of fauna (Talent et al., 1988). However, Goel et al., 1987, Webster et al., 1993, Draganits et al., 1998; suggest Middle Silurian to Early Devonian (?) age for these rocks. Larger extent of outcrops of the early Palaeozoic comprises of the Cambrian rocks, whereas the Ordovician and Silurian rocks are exposed within the Marhaum syncline and the Shamsabari syncline (Shah, 1982). Cambrian strata directly overlie Precambrian and the complete sequence rests on a schistose basement, the Salkhala Formation. Stratigraphically, Salkhalas are overlain by Marinag Formation along a faulted contact (Wadia, 1934). The dominance of Lolab Formation exposures in the Lolab Valley is due to repetition of beds by tight and often isoclinal folding (Shah, 1982). The stratigraphic nomenclature (Table-1) adopted in this work is after Shah (1968) for lucid reading. Marinag Formation has also been referred to as Dogra Slates (Wadia, 1934) and Machhal Formation (Raina and Razdan, 1975).

Table 1: Litho-stratigraphic succession of early Palaeozoics of North-western Kashmir (After Shah, 1968)

		Formation	**Lithology**	**Age**
Late Palaeozoic		Panjal Volcanics	Mafic and silicic volcanic rocks	Late Carboniferous - Early Permian
		------------------------**N O N C O N F O R M I T Y ---**		
		Muth Quartzite	Quartzite and quartzitic sandstone	Middle Silurian-Early Devonian
		------------------------**D I S C O N F O R M I T Y ----**		
		Marhaum	Greywacke and dark sandy Shale	Early Silurian-Middle Ordovician
Early Palaeozoic	**POHRU GROUP**	Trehgam	Green shale with alternating massive and oolitic limestone with carbonate component increasing towards top	Early Ordovician-Late middle Cambrian
		Nutnus	Thin bedded, pale to deep green shale, occasionally sandy and cherty	Middle Cambrian
		Lolab/ Sagipora	Thin bedded green to bluish grey shale alternating with sandstone/grey slaty shale alternating with sandstone	Early middle Cambrian – early Cambrian
Marinag/ Machhal/ Dogra Slates			Grey to dark grey phyllite and slate with bands of greywacke	Early Cambrian -- Precambrian
Salkhala			Schistose basement	Precambrian

Field Samples and Micropetrography

The field investigations resulted to map the lateral and vertical facies variations at Sarkuli and Geerhatti localities representing lower and upper parts of Lolab Formation, Zachaldar-Galganzar and Wadpora-Kawari of Nutnus Formation, and Kralpora representing Trehgam Formation. Oriented stratigraphic samples and thin sections of sandstones and limestones of the early Palaeozoic succession of Kupwara district are studied. The modal analyses of sandstones were addressed by following point counting method of Dickinson and Suczek (1979), with minimum of 300 frame work grains/thin section. Matrix contents were resolved during counting by tabulating only masses of the matrix having clear grain boundaries besides, rock fragments and reworked grains.

In this study, five different lithofacies have been identified on the basis of petrographic characters. The spatial and temporal interrelationship of different facies is helpful in interpretation of sedimentary history. With sedimentary processes through time, the boundaries between facies migrate laterally in response to transgressive-regressive events and geographically contiguous facies form temporal associations (Prothero and Schwab, 1996).

Facies

1. Lolab Formation (Thayan-Machhal Road Section)

The Lolab Formation along Thayan-Machhal Road has been studied at two localities namely Sarkuli and Geerhatti and is comprised of shale, siltstone, sandstone and low grade silty-slate or phyllite to siltstone or silty sandstone.

1A. SARKULI SECTION

Sandstone Facies

The lower part of Lolab Formation at Sarkuli section (34.61ºN, 74.37ºE) is characterised by bimodal sandstone facies (Fig 4a) at the lower part of the lithosection followed by boudinaged sandstone with tectonic fishes (Fig 4b) and shale/silty shale. This formation is composed of thin-bedded bluish green to grey shale with alternating sandstone/grey slaty shale interbedded with sandstone in its lower part and partly bimodal in its upper part at Geerhatti. These subfacies have gradational contacts and are seen laterally continuous for about 800m showing grain size and thickness variations. Some argillaceous beds in this lithosection being incompetent have yielded to sediment load giving subtle foliation to such rock beds, hence slate or slaty prefixes have been used here.

The sandstone of bimodal fabric is made up of quartz grains of two size populations floating in fine grained matrix of silica and clay minerals (Fig 4a). The quartz grains show high angularity indicating transportation from the nearby source, and fractured and corroded grains are attributes due to compaction. The diagenetic response of sandstone during progressive burial is specific to a complex set of boundary conditions (Dickinson and Suckzek, 1979). The bimodal sandstone is supposed to have a high natural tendency to hygric swelling and shrinking and, therefore, moisture-induced degradation (Blöchl et al., 1998). Bimodal distribution has been reported in sands of varied origin like fluvial, beach and desert (Folk, 1968). Such textural properties are common to sandstones from the lower Palaeozoics across different continents (Folk 1968).

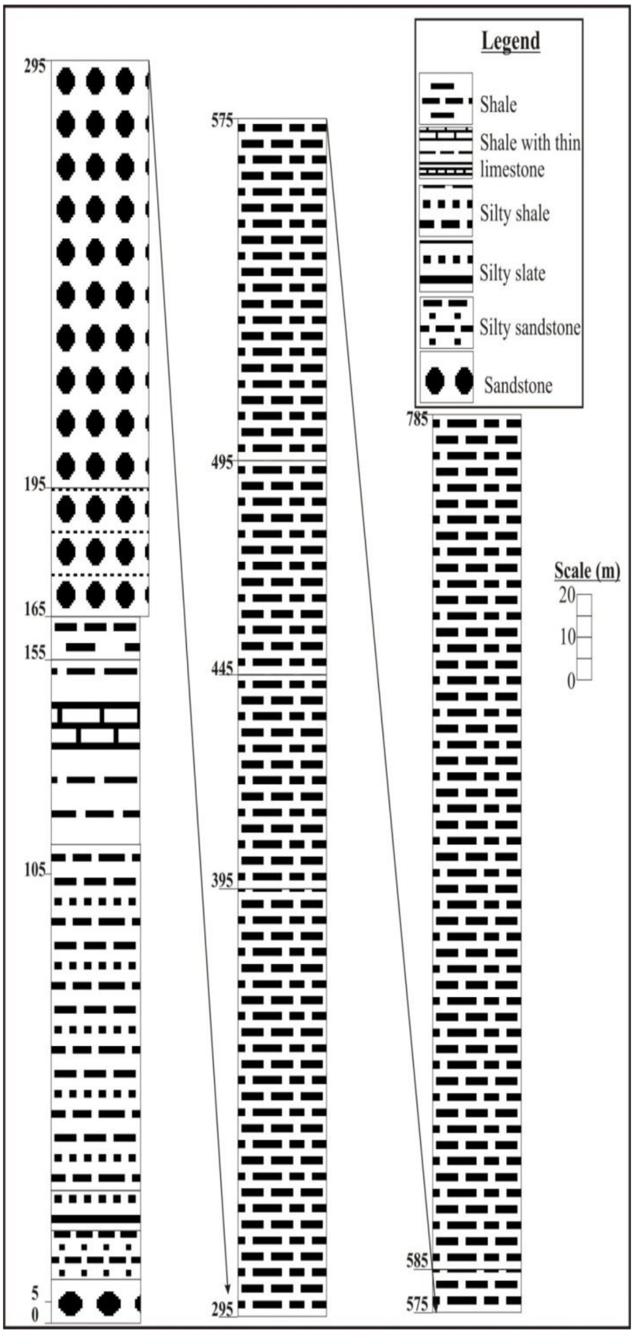

Fig-2: Litholog of lower part of Lolab Formation at Sarkuli along Thayan-Machhal Road indicating coarsening upward towards middle of the section followed by fining upward top of the section.

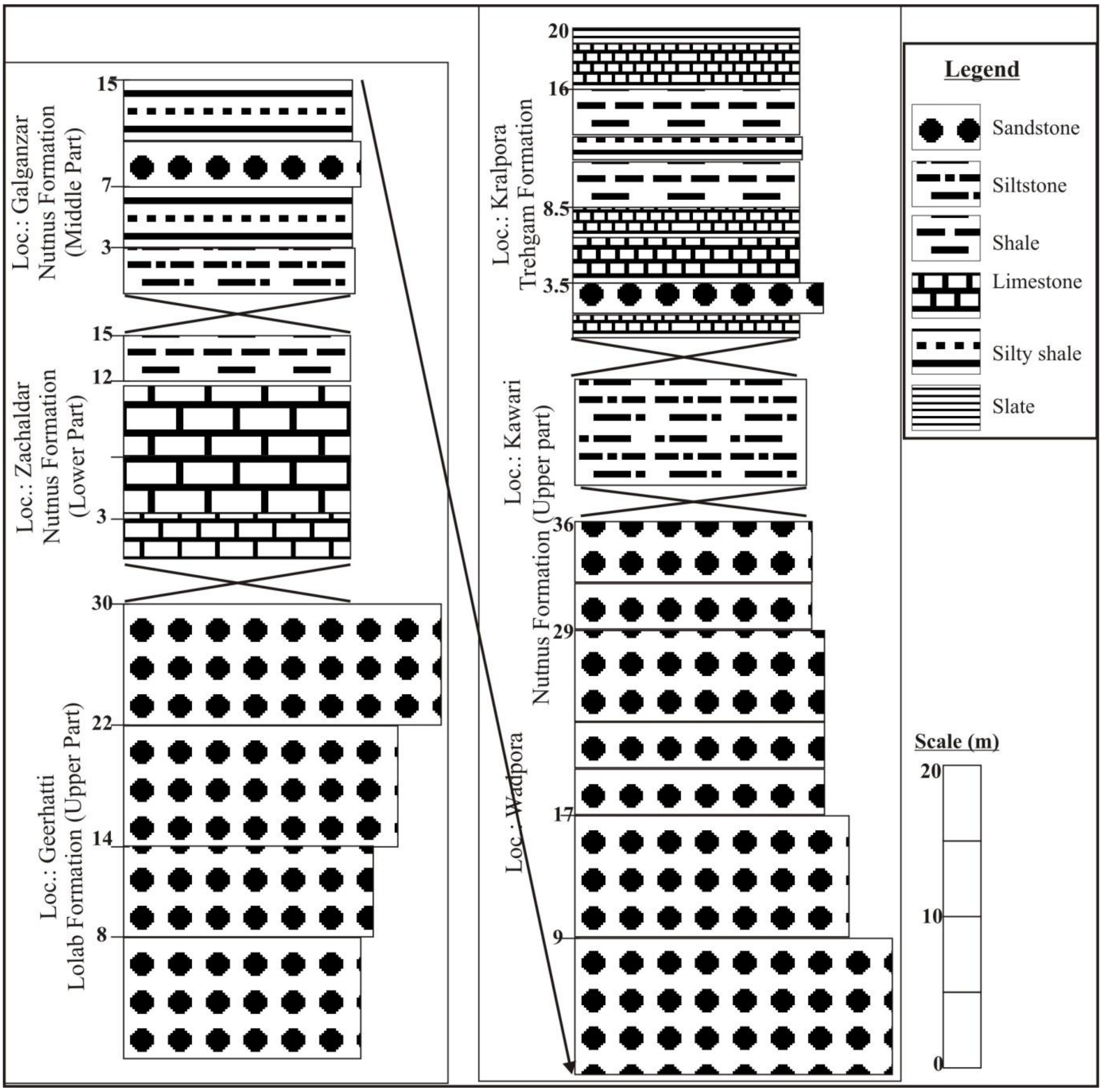

Fig-3: Litholog of Lolab Formation (upper-part), Nutnus Formation and carbonate-dominated Trehgam Formation

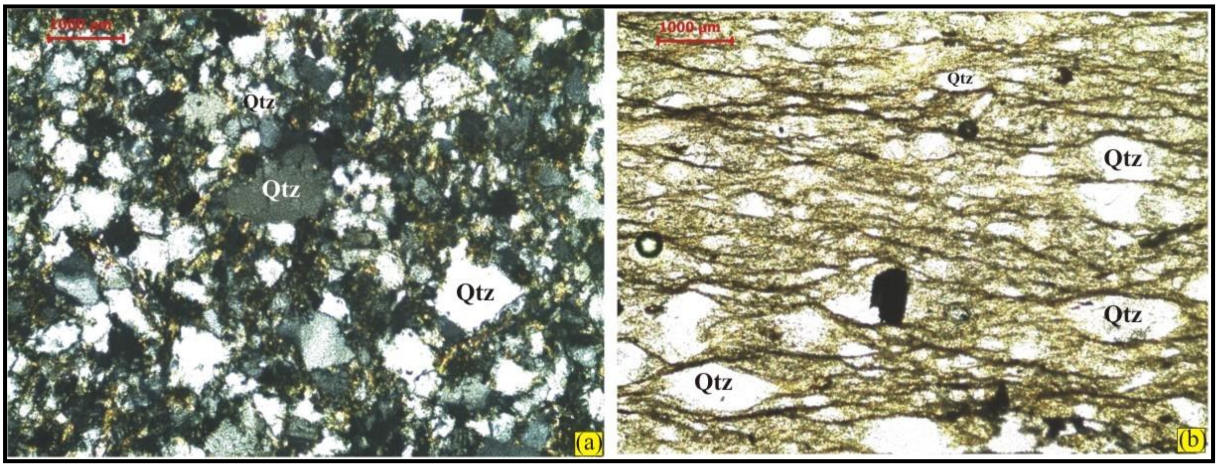

Fig: 4. Photomicrographs showing (a) Sandstone with bimodal fabric. Quart (Qtz) grains of two sizes floating in fine grained matrix of silica and clay minerals. (b) Tectonic fishes floating in fine grained ground mass of clay and silt size sediments. Boudinaged sandstone beds interbedded within the mudstone layers are indicative of extensional setup.

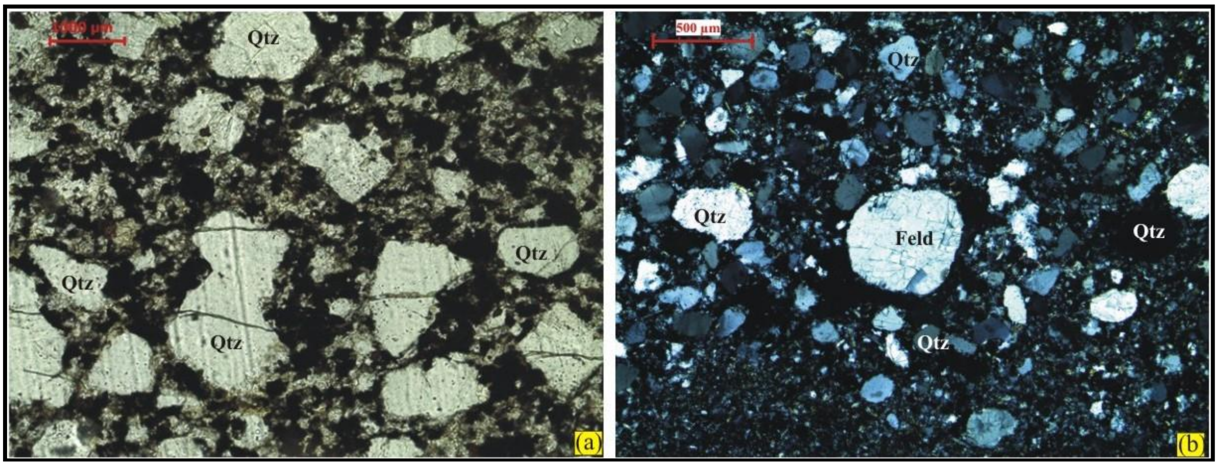

Fig: 5. Photomicrographs showing (a) Fine grained sandstone with round to subround quartz grains along with prominent quartz vein (Qv) with euhedral grains. (b) Compressional evidence where quartz vein is sheared. Recrystallization of quartz in vein due to pressure solution process in the surrounding quartz and the ground mass

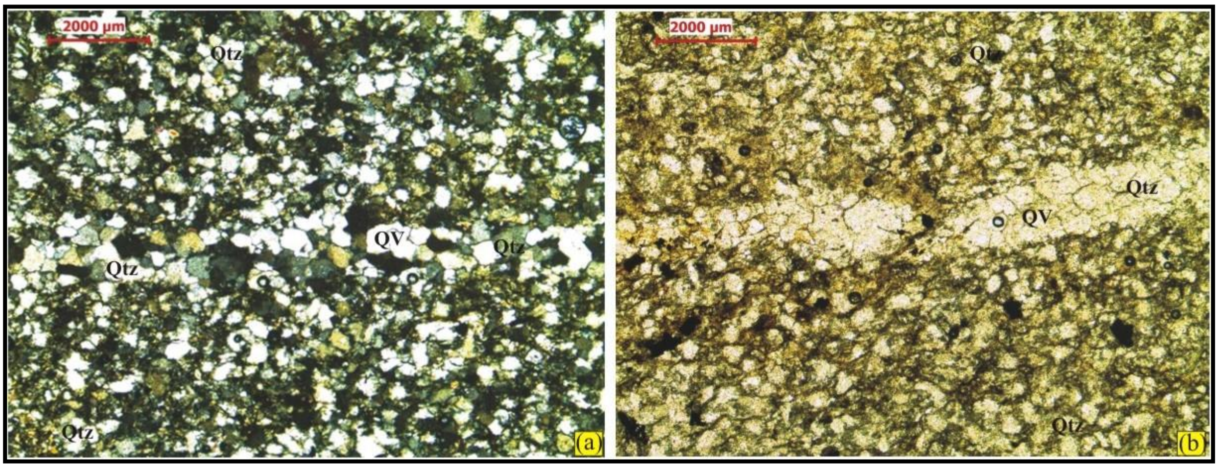

Fig: 6. Photomicrographs showing (a) Bimodal sandstone floating in fine grained ground mass. Evidences of dissolution process is reflected in residual quartz grains and fractures in larger quartz grains (b) Large feldspar (Field) grain with stress induced fractures within bimodal sandstone.

Silty Sandstone Facies

The overlying silty sandstone at lower part of the section is on an average composed of 70 - 80% monocrystalline, sub angular to sub round quartz grains with low sphericity along with 10-15% mica, characterised by tectonic fishes of muscovite floating in fine grained ground mass of clay and silt size sediments.

Besides the rock is characterised by boudinage of detrital quartz bands (Fig 4b) interbedded within the mudstone layers indicating extensional stress setup. This boudinage is reflective of limb-parallel stretching of the competent sandstone band within an incompetent mudstone. The boudinages are consistent at the limb of the fold in multilayered sequence (Ghosh and Sengupta, 1999). The extension in massive quartz result in periodic necking of the layer, giving a prominent "pinch and swell" structure followed by separation of the layer into discrete rhombic or lens-shaped boudins (Paterson & Weiss, 1968). Quartz is dominantly monocrystalline which is typically derived from volcanic source (Basu, et al; 1975) as well as from the disintegration of polycrystalline quartz in transit for long distance from a magmatic or metamorphic source (Dabbagh and Rogers, 1983), and the low sphericity indicates lower transport distance. In the middle of the Sarkuli section, the grain size grades to fine or medium sandstone characterised with quartz veins (Fig 5a, b). Moreover, the quartz veins along with the host rock have been cut across by later fractures which appear to be compressional in nature (Fig 5b). The quartz grains are round to subround in nature. Recrystallization of quartz in vein has been as a consequence of pressure solution process in the surrounding quartz of the ground mass.

The offset in quartz veins appear to be compressional as the part of vein on the left side of the fracture appears to be riding over the right hand side (Fig 5b) with bulging on either side of the fracture. However, there has been alteration of mineral where silica along the fracture zone has given rise to chlorite with free ions which are present in clay minerals. The sandstone samples (SRK1 and TM7) from lower part of Lolab Formation got plotted in lithic arenite field in QFL diagram (Fig. 12).

1B. GEERHATTI SECTION

Fine – Coarse Sandstone Facies

The Geerhatti section (N 34.50º E 74.30º) represents upper part of Lolab Formation and is dominated by range of fine to coarse sandstones and silty sandstone followed by massive coarse sandstone towards the top. This facies also shows lateral variations in grain size and thickness. The difference in silty-shale to shale-dominated lithology at Sarkuli and coarse sandstone-dominated section at Geerhatti with sandstone beds showing bimodality gives indication of depositional shift from a low energy environment suitable for fine sediments to an estuarine environment where coarse and fine sediments mix.

The coarse sandstone continues to dominate the section at Geerhatti. Bimodal sandstone is followed by sandstone with uniform grain size and is subround to round in nature (Fig 7b). The contact between siltstone and bimodal sandstone (Fig 7a) shows sharp change in the sediment size. Quartz shows evidences of compaction in the form of undulatory/wavy extinction. Quartz grains show overgrowth and compaction resulting in breakage of the grains. The contacts are sutured owing to compression and resultant pressure solution. Due to continuous compaction, the ductile grains have been squeezed out from quartz clasts. The amount of plastic deformation and framework collapse is dependent upon the amount of lithic fragments and on the time of initiation and quantity of cementation (Lander & Walderhaug, 1999). In case of more rigid grains, the mechanical compaction has caused floating and point contacts to become long as well as fracturing of rigid framework grains

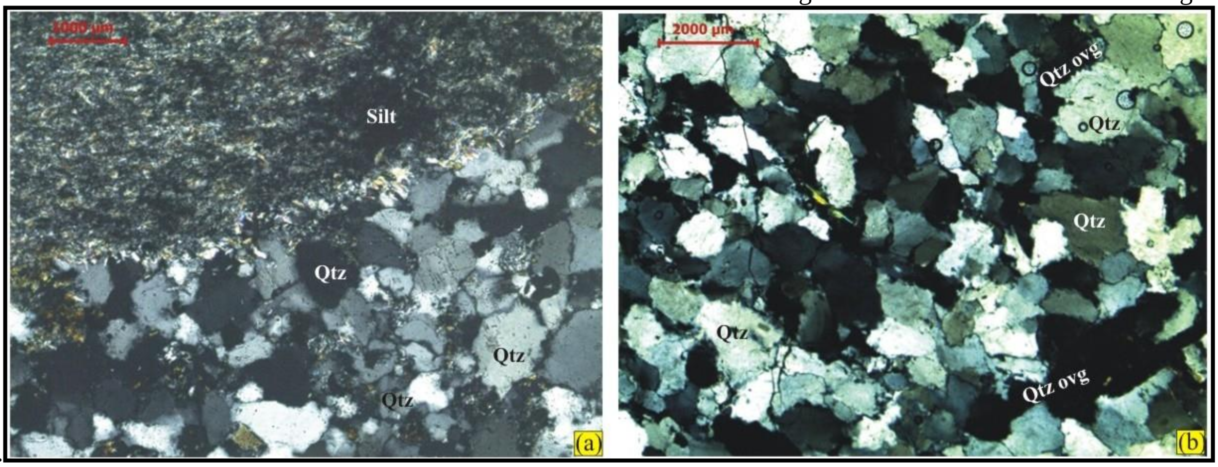

Fig: 7. Photomicrographs showing (a) Contact between sandstone and siltstone (Silt) beds (b) Sandstone with uniform grain size and sub round to round in nature. Some quartz grains show overgrowth (Qtz ovg)) and compaction resulting in breakage of the grains.

The studied section at Geerhatti shows variation in textural properties from bottom to top with bimodal silty sandstone (Fig 6a) in the lower part to low-matrix coarse grained sandstone (Fig 7b) towards the top. Undulose extinction in quartz is typical of low rank metamorphic rocks (Basu et al., 1975, Pandita and Bhat, 1995; Pandita et al., 2014). The grain contacts are predominantly sutured with few concavo–convex and pore spaces are recognizable. In sandstones, long axis grain contacts are suggestive of intermediate burial depth and concavo-convex and sutured contacts as a result of intense compaction and pressure dissolution processes during deep progressive burial diagenesis (Chima et al., 2018). Intensity of compaction is directly proportional to the overburden which results in bed thinning, expelling of intergrannular fluids (dewatering), closer packing of the grains, and reduction of porosity with advance-stage compaction transforming the concavo-convex contacts into sutured contacts (Baiyegunhi et al., 2017). The sandstone samples from the lower part of Lolab Formation are lithic arenites in nature whereas, those from upper part of the Lolab Formation belong to subarkose and sublitharenite category (Fig 12). The limited presence of sandstones in lower part of Lolab Formation with dominance of argillaceous part represented by shale implies dominance of deep and low-energy environment in comparison to sandstone dominated upper part of the formation.

2. NUTNUS FORMATION

Mixed Carbonate - Clastic Facies:

Nutnus Formation conformably overlies the Lolab Formation and is exposed in parts at Zachaldar-Galganzar locality with limestone followed by siltstone or silty sandstone and at Wadpora locality with siltstone as dominant facies and fine sandstone, whereas at Kawari it is exclusively composed of siltstone. Four exposed lithosections of Nutnus Formation were studied at Zachaldar, Galganzar, Wadpora and Kawari. A 10m lithosection at Zachaldar composed of carbonates is characterised by pelsparite facies followed by recrystallized limestone. The degree of calcite recrystallization varies between the lower and upper parts of the section. Following the dip direction to younger beds, the lithosection towards top of Nutnus Formation at Galganzar is cropping out with fine grained sandstone dominated by subround quartz grains with feldspar in fine grained ground mass followed by fine grained sandstone with uniformly distributed sub round quartz grains floating in matrix. Both sandstones are having prevalent elongated mica grains. The lower part is composed of pellet bearing carbonate (Fig 8a) containing scattered peloids cemented within calcite (Pelsparite of Folk, 1959). The overlying part of the lithosection comprises of limestone recrystallized from micritic matrix in which about 60% of matrix has got recrystallized into calcite with distinct cleavage sets (Fig 8b). Moreover, prior to recrystallization the veins of calcite have been developed. After the deposition of carbonate-rich part in calm and warm environment, the depositional environment has shifted to fluvial low energy condition leading to deposition of fine sandstone both at Zachaldar as well as at Wadpora. The three sandstone samples (from Galganzar and Wadpora lithosections) of the Nutnus Formation plotted in subarkose field in QFL diagram (Fig 12).

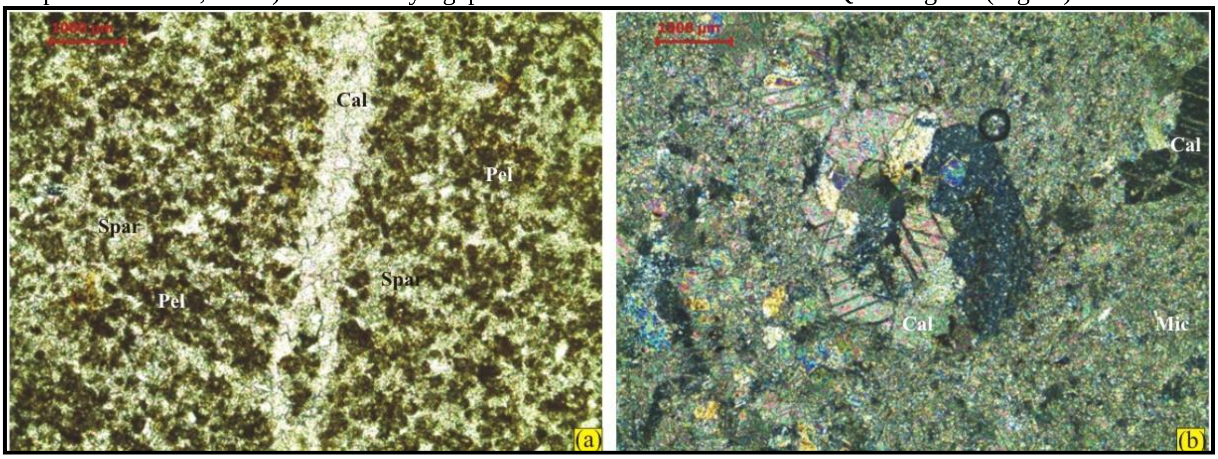

Figs: 8. Photomicrographs showing (a) Limestone beds marked by calcite (Cal) veins filled with sparry calcite. The thin section shows pelsparite having well distributed sparite (Spar) and, partially replaced pellets (Pel) due to compaction and pressure solution processes. (b) Recrystallized limestone showing well developed crystals of calcite (Neomorphism) with prominent cleavage sets. Calcitization of micrite (Mic) is prevalent uniformly throughout the thin section.

The limestone at bottom of Zachaldar section is marked by calcite veins filled with sparry calcite. The section shows pelsparite having well distributed sparite which partially replaces pellets due to compaction and pressure solution process. Variations in the intensity of the calcification being controlled by the level of calcium carbonate saturation give rise to homogeneous micrite and peloid-like bodies, producing a pelmicrite fabric. Disintegration of such fabric gives way to formation of individual peloids and reworking by currents result in a pelsparite texture (Flugel & Flügel, 2004). The comparison between lower and upper part of Zachaldar lithosection and the continuous calcite veins with recrystallization of calcite along veins and in host mass in the lower section and the upper part of the section indicates a break in diagenetic progression as it is still partially micritic in nature. This is attributed to tectonic exhumation of the section during the middle Cambrian. Since, it is difficult to differentiate between solution-precipitates and recrystallization in polarising microscope (Boggs, 1995), a term neomorphism was introduced (Folk, 1965) which includes all transformations between one mineral itself or its polymorph. This process involves all transformations between polymorphs of carbonate minerals and their recrystallization to stable forms within a given set of physico-chemical parameters of the basin.

Towards northwest of Zachaldar lithosection at a distance of about 200m, Galganzar lithosection is composed of mudstone followed by non fissile siltstone and fine sandstone with remarkable amounts of muscovite flakes (Fig 9a) which have been bent and have high order blue and green colour. Individual detrital minerals which are flexible or brittle are indicators of deformation (Adams and Mackenzie, 1998). The preferred orientation difference in different minerals is due to differential response of minerals to diagenetic stress (Reed, 1962). The siltstone is overlain by fine grained sandstone with uniformly distributed subround quartz grains floating in matrix along with prevalent elongated mica grains (Fig 9b).

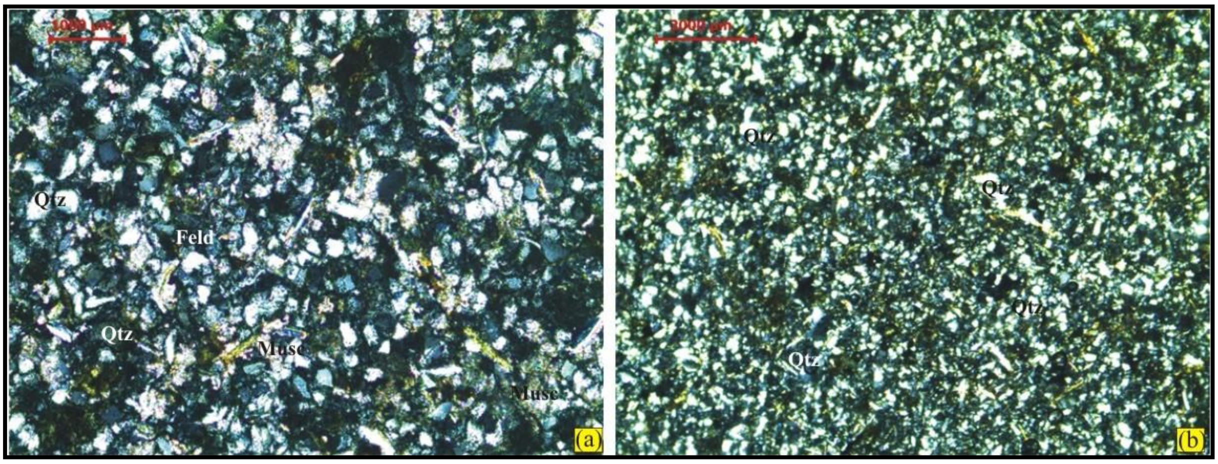

Fig: 9. Photomicrographs showing (a) Fine grained sandstone dominated by sub round quartz grains, feldspar, elongated micas (Muscovite) and fine grained ground mass. (b) Fine grained sandstone with uniformly distributed sub round quartz grains floating in matrix with elongated mica grains.

Nutnus Formation at Wadpora and abandoned quarry at Kawari is composed of siltstone, and medium to coarse sandstone with occasional alternating mudstone laminations. This attributes to as facies variant of Zachaldar-Galganzar section in vertical extension as the carbonate beds are absent. However, like interrupted diagenesis indicated by partially recrystallized calcite from carbonates in Zachaldar section, this part shows diagenetic immaturity of detrital siltstones and sandstones from their low degree of sorting and presence of clayey matrix of chlorite appearing in first order yellow interference colour in most of the samples apart from iron oxide-filled pores. The grain-coating of chlorite, inhibits quartz overgrowth in sandstone and reflects the original porosity in deeply buried sandstones (Worden, et al., 2020). The upper part of lithosection at Wadpora is represented by siltstone with dispersed quartz grains (Fig 10a). The quartz grains are comparatively large in size. The small quartz grains are aligned in one direction giving rise to subtle foliated fabric of the rock.

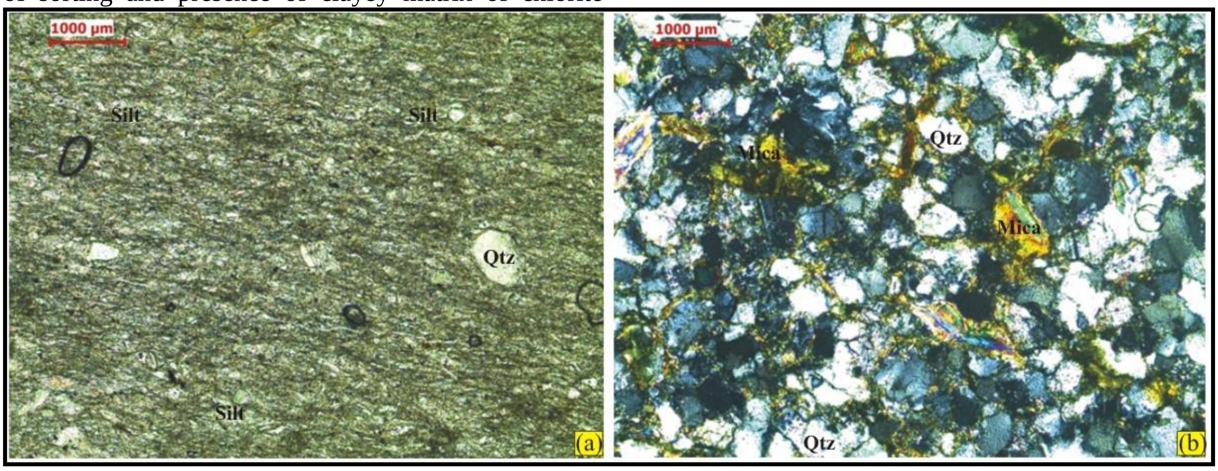

Fig: 10. Photomicrographs showing (a) Siltstone with scattered quartz grains (b) Sandstone with subround to round quartz grains and elongated micas

Kawari section is dominantly composed of sandstone (Fig 10b) with sub round to round quartz grains and elongated micas, loosely packed fine grains of feldspar and muscovite floating in matrix supported material (>15%), with interbedded mud laminations. Bent mica flakes indicate mechanical compaction. The quartz grains are corroded which enhances the porosity of the rock (Lin et al., 2019). The indurated nonfissile siltstone has moderate to poor orientation of clay minerals and a predominance of silt over clay-sized material. The original lamination appears to have been destroyed with apparent difference in orientation of detrital quartz grains. Quartz with abundant fluid inclusions or vacuoles is usually derived from a source of low-temperature origin, like hydrothermal vein (Adams and Mackenzie, 1998).

3. TREHGAM FORMATION-KRALPORA SECTION

Mixed Carbonate –clastic Facies

Trehgam Formation has one of its best outcrops at Kralpora which represents a lithosection dominated by limestone with interbedded sandstone or siltstone. Limestones dominate bedding at Kralpora section from micritic bottom layer with interbedded siltstone or fine sandstone towards top of the section. This is followed by meter-thick fine sandstone with calcite cement. Towards upper part, the section is again dominated by carbonates with prominent recrystallized limestone showing well developed crystals of calcite (neomorphism) along with pseudo pellets. Trehgam Formation is characterised by pelsparite (Fig 11a) with uniformly distributed sparry calcite, corroded pellets with patches of algae also discernible in the micro sections. Calcitization of micrite is prevalent uniformly throughout the section.

From the lateral and vertical facies variations it can be deduced that the lithosection at Kralpora demonstrates the formation of carbonate part within warmer, sub-tropical conditions. Moreover the silty or sandy beds can be inferred as a result of fall in sea level giving rise to shallow and higher energy siliciclastic sediments. The deposition of sandstone and shale beds indicates shift from deep-water and low energy to shallow-water high energy environment and vice-versa that has given rise to alternate areno-argillaceous beds with carbonate-dominated deposition within Kralpora section of Trehgam Formation.

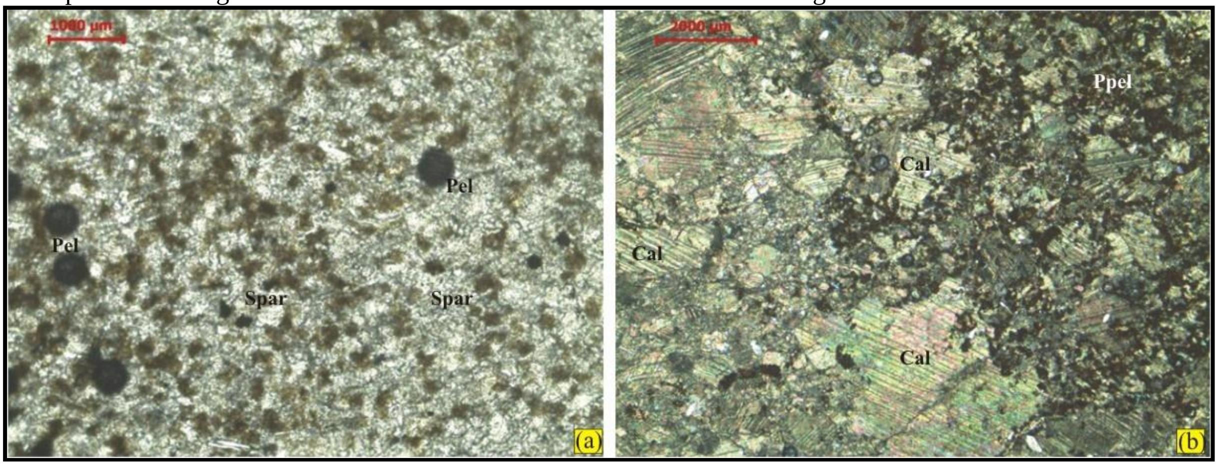

Fig: 11. Photomicrographs showing (a) Pelsparite with uniformly distributed sparry calcite and corroded pellets. Patches of algae are also discernible in the thin sections. (b) Recrystallized limestone showing well developed crystals of calcite (neomorphism) along with pseudo pellets (Ppel). Calcitization of micrite is prevalent uniformly throughout the thin sections.

The patches of algae discernible in pelsparite, and recrystallized limestone (Fig 11b) show well developed crystals of calcite (neomorphism) along with pseudo pellets. Calcitization of micrite is prevalent uniformly. The neomorphic features apart from pseudopellets (Fig 11b) are similar to recrystallized limestone (Fig 8b) of Zachaldar section. In Kralpora section intergrannular spaces are characterised with carbonate cement as evident from high interference colours under crossed nicols. The limestone (Fig 11a) is composed of pelsparite with uniformly distributed sparry calcite and corroded pellets. Recrystallization and neomorphism are processes involved in transformation of minerals in situ into their polymorphs (Dickson, 2003). However, the gap exists with respect to the term recrystallization as it is restricted to strain induced transformation (Bathurst, 1958) but it has been used for any change in form without a change in mineral species. The carbonate cement in fine sandstone is typical indication of regressive environment that led to the deposition of sandy layer with available in situ carbonate that was incorporated as cement. However, regression has remained short-lived as the bed is followed by alternate limestone and shale beds towards the top of the section. The only sandstone sample (KRL2) from this formation got plotted in subarkose field in QFL diagram (Fig 12).

RESULTS AND DISCUSSION

The Lolab Formation has shown alternating phases of regression and transgression environments. The deposition of lower part of Lolab Formation has taken place in high energy environment with indications of mixing as reflected by bimodal sandstone (Fig 5a). It is followed by rise in sea level (transgression) as is indicated by low energy silty and shale-dominated lithologies. Towards middle part of lithosection the regression has given way to deposition of sandstone characterised by diagenetic quartz veins followed again by transgression and resultant fining of sediments upward. The environment of deposition for lower part of Lolab Formation has largely been deep water that provides low-energy environment favourable for argillaceous deposition. Shales form under environmental conditions in which fine sediments are abundant and energy is sufficiently low to allow settling of suspended fine particles. Such favourable conditions for shale deposition are particularly available below the wave base (Boggs, 1995). In sandstones of upper part of Lolab Formation, the strain is reflected by quartz with undulose extinction. Chemical compaction has resulted in the formation of concavo-convex and sutured grain contacts, both caused by pressure solution. The sandstones at Geerhatti display point to sutured grain contacts developed as a result of progressive burial. The grain-to-grain contacts are suggesting that the grains were mechanically compacted.

Table 2: Modal composition of sandstones from early Palaeozoic succession in Kupwara District of North-western Kashmir in the study area.

Formation	Sample No.	Quartz %	Feldspar %	Lithic fragments / others %
TREHGAM FORMATION	KRL2	70	20	10
NUTNUS FORMATION	GG1	80	15	5
	ZB1C	75	15	10
	ZBT3	70	20	10
LOLAB FORMATION	GH1	75	20	5
	GH2	80	15	5
	GH3	75	10	15
	GH4	65	10	25
	SRK1	60	10	30
	TM7	65	10	25

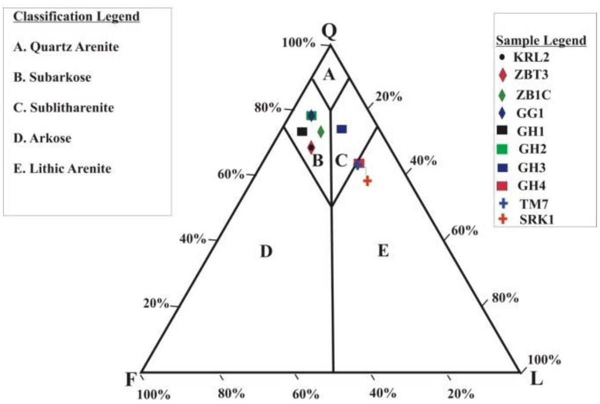

Fig-12: Classification of sandstones from early Palaeozoic succession of north-western Kashmir in the study area.

In Lolab Formation, the difference in response to diagenetic compaction between lower and upper parts is recognised by development of subtle foliated fabric in incompetent argillaceous beds of lower part and sutured contact development with fracturing in competent quartz- rich upper part. Moreover, the overlying sediment load warrants a greater diagenetic stress for bottom beds. The coarsening of sediments towards middle of the section is evidence of seaward shift of shoreline followed by transgression as indicated by fining upwards. However, upper part of Lolab Formation in the study area has got low-matrix coarse sandstone at Geerhatti indicating higher energy conditions in comparison to lower part with indications of estuarine sedimentation. Quartz overgrowths in upper part (Geerhatti section) of Lolab Formation reduce porosity of these sedimentary rocks. Sands respond differently to processes involved for porosity reduction with changes in basin tectonics. The sorting depends on the range of the sediment sizes, deposition rate, the strength and variation in energy of the agent of deposition (Amaral and Pryor, 1977). The poorly sorted silty-sandstone towards top of the section indicates low textural maturity. The fractured grains of K-feldspar with high relief appear to be deformed post deposition otherwise being fractured and cleavable would have preferably disintegrated during the course of transit due to attrition. The petrographic signatures show a gradual shift from a bimodal sedimentation in estuaries at bottom of the section where both silt-size and coarse-size sand have mixed to deep water sedimentation followed by very coarse grained sandstones indicating shallowing of the basin towards top of the section. Moreover, such a sharp shift in grain size from deep water fine shaly sediments to coarse sandstone can be attributed to fast basin-uplift during the process of sedimentation. The difference in silty-shale to shale-dominated bottom part and coarse sandstone-dominated upper part showing bimodality brings forth two different depositional settings with respect to depth and energy conditions of the basin.

The lower part of Nutnus Formation (overlying Lolab Formation) at Zachaldar has carbonate beds within siliciclastics indicating a shift in sea level from shallow shelf to deep shelf or slope as well as temperature change necessary for carbonate deposition.

Depositional margins have a low relief from platform to slope and basins; by-pass margins have a characteristic steeper relief shifting the deposition of platform-sourced sediment on lower slopes and adjacent basinal plains. This means that during the deposition of the lower part of Nutnus Formation, the basinal setup was possibly between deep basinal part and shelf favourable for carbonate precipitation within the warm photic zone. The upper part of Nutnus Formation is dominated by siliciclastic sedimentation with silts and sands reflecting change in sea level giving way to shelf deposition. The Kawari section in continuity of Wadpora section seems to represent a deep slope to continental rise environments. The effect of water-rock interaction has been time dependent as well as variable with alkalinity or acidity of water. In terms of hydrophysical effects, the dissolution of rocks results in reduction of the physical and mechanical properties by reducing the interconnection between the mineral particles and the effectiveness of lithostatic pressure. These effects deteriorate the physical and mechanical properties of rocks by altering the mineral components and microstructure of rocks, such as the particle size, represented by micritic texture towards the top with onset of calcitization (Sparry calcite). The formation of sparry calcite from micrite involves a set of intermediate processes including genesis of dense liquid phases inside the aqueous solution in organized (meta)stable clusters that serve as precursors to the formation of amorphous calcium carbonate (ACC) micro crystals (Cartwright et al., 2012). This ACC can either be hydrated or anhydrous (Ihli et al., 2014). Its aging gives rise to formation of calcium carbonate polymorphs like vaterite, aragonite, calcite depending on the physicochemical conditions (Gebauer et al., 2008; Rodriguez-Blanco et al., 2011; Sun et al., 2015), e.g. temperature, depth or hydrostatic pressure, chemical composition of the solution, including pH, salinity, Mg content, etc. (Tai and Chen, 1998; Wolthers et al., 2012; Blue et al., 2017). Dehydration of ACC in turn provides another driving force (i.e. an energetic contribution) to give orientation to the crystallization process towards a particular polymorph (Ihli et al., 2014). The stable crystalline phase may also nucleate directly from the solution, without the genesis of cluster precursors (Nielsen et al., 2014). In view of the classic nucleation theory, surface tension plays an important role in the evolution of a nucleus. However, published data on surface energies of calcium carbonate polymorphs are scattered and inconsistent (Aquilano et al., 1997; Sun et al., 2015). The dominance of carbonates in the section indicates a warm sub-tropical climate as most modern carbonate deposition demonstrates a positive correlation between such deposition and the equatorial belt as well as areas of warm ocean currents (Wilson, 1975).

Chilingar et al., (1967) has graphically presented that neritic carbonates exist mainly to north and south of the equator within latitudes of 30º. However, biogenic elements are rarely seen in Trehgam pore geometry, and crack morphology. The physical and chemical water–rock reactions result in the generation of secondary porosity of the rock followed by slowing down of the process of porosity enhancement. This finally moves to a state of equilibrium after many associated processes of hydrolysis, corrosion, oxidation, and reduction along with ionic exchange giving interim stability to the rock (Qiao et al., 2017). It has been established that round and well round grains which are unfractured are least affected by surface corrosion, whereas round grains which are fractured are more prone to embayments and surface corrosion. The constituent grains are cemented by iron oxide (isotropic in X-polars) and partly by chlorite having first order yellow. Chlorite being readily recognized by its birefringence and morphology, commonly grows in sedimentary regime and has a tendency to form within the entire range of temperatures and pressures from moderate diagenetic burial through green-schist grade of metamorphism. The Trehgam Formation has significant representation of carbonates at Kralpora section. The carbonate beds occur around middle of the section and are Formation which indicates absence of sustenance-temperature and/or nutrients for biogenic agents. This warrants a possibility of deep environment necessary for micritic precipitation rather than a biogenic contribution or lime mud formation by the erosion and abrasion of micritized grains (Reid et al., 1992). Micritic limestones form by $CaCO_3$ 'rain' triggered by inorganic precipitation in the water column (Kazmierczak et al., 1996).

The line between metamorphism-induced recrystallization and diagenesis in carbonates of both basal part of Nutnus Formation and carbonates of Kralpora section is drawn by the degree of transformation of micrite into calcite. The degree of calcite crystallization has been higher in Zachaldar section representing lower part of Nutnus Formation in comparison to that of Kralpora section of Trehgam Formation. Bathurst (1966) employed the term "micritization" to describe alteration or grain-diminution (Wolf, 1965) of original skeletal grains to a cryptocrystalline nature by repeated algal micro-borings and subsequent filling of these borings by micritic precipitate. Micrite is formed by several processes including destructive micritization by the micro boring organisms, positive development of micrite, related to epilithic organisms, and inequitable dissolution and recrystallization (Flügel, 2004). The carbonate-dominated section of Trehgam Formation without any traces of biogenic imprints and micritic nature at Kralpora indicates shifts in temperature of the basin as well as the depth of sedimentation in an environment adverse to biota but favourable for micrite precipitation. This is referred to as inequitable dissolution and recrystallization (Flügel, 2004), the recrystallization has not been able to keep pace with the precipitate deposition to poly-phase transformation of micrite or ACC to calcite owing to unfavourable conditions.

CONCLUSION

The facies and petrographic evidences of the early Palaeozoic successions from Lolab Formation through Nutnus Formation to Trehgam Formation suggest varying depositional environments. Provenance of these rocks has been of mixed nature with monocrystalline quartz dominant in sandstones indicating greater contribution from igneous sources.

The diagenetic responses have varied between argillaceous lower part of Lolab Formation and its arenaceous upper part in the study area. These responses to mechanical compaction and cementation are in harmony with difference in their composition as well as their depth of burial and/or position in stratigraphic column. The transgression-regression cycles have continued through Nutnus Formation well up to Trehgam Formation. The Nutnus Formation shows warm and deep environment represented by biogenic traces-rich carbonates in its basal part followed by shallower argillaceous to arenaceous sediments towards its upper part. The change from carbonate to siliciclastic deposition is due to temperature changes as well as depth of the basin that might have shifted carbonate deposition further north of study area in the Tethyan realm making way for non-carbonate deposition. Diagenetic evidences are suggestive of higher burial-residence time for carbonates of Nutnus Formation (lower part with higher degree of calcite recrystallization) than those of the Trehgam Formation. This is in harmony with the stratigraphic position of these formations as geothermal gradient warrants higher diagenetic temperatures for deeper formations in comparison to their shallower counterparts. With fine argillaceous deep-water sediments in lower part of Lolab Formation, coarsening in its middle part followed again by alternate fining and coarsening towards top, along with carbonate alternations with siliciclastic sedimentation in Nutnus and Trehgam formations, it is concluded that there are five transgressive-regressive cycles that have shaped the formations of early Palaeozoic of the north-western Kashmir in the study area.

Acknowledgements

The first author acknowledges the University Grants Commission, New Delhi for providing fellowship under Faculty Improvement Programme and the Department of Higher Education, Union Territory of Jammu and Kashmir for necessary permissions to carry out the research work. The authors are thankful to Prof. G. M. Bhat, University of Jammu for his valuable suggestions during this study. The discussions with Mr. Abdul Qayoom Pall (GSI) have made significant improvements in the draft of this paper. The quality of paper improved due to suggestions by two anonymous reviewers. The facilities developed by the Department of Geology, University of Jammu, under DST–FIST and UGC–SAP schemes were used during this work.

References

Adams, A., & MacKenzie, I. (1998). Carbonate Sediments and Rocks under the Microscope: a colour atlas. CRC Press.

Amaral, E. J., & Pryor, W. A. (1977). Depositional environment of the St. Peter sandstone deduced by textural analysis. *Journal of Sedimentary Research*, *47*(1), 32-52.

Aquilano, D., Rubbo, M., Catti, M. and Pavese, A. (1997) Theoretical equilibrium and growth morphology of CaCO3 polymorphs I. Aragonite. *J. Cryst. Growth,* 182, 168–184.

Baiyegunhi, C., Liu, K., & Gwavava, O. (2017). Diagenesis and reservoir properties of the permian Ecca Group sandstones and mudrocks in the Eastern Cape Province, South Africa. *Minerals*, *7*(6), 88.

Basu, A., Young, S.W., Suttner, L.J., James, W.C., Mack, G.H., (1975). Re-evaluation of the use of undulatory extinction and polycrystallinity in detrital quartz for provenance interpretation. *Journal of Sedimentary Petrology*, 45, 873-882.

Bathurst, R. G. (1961). Diagenetic fabrics in some British Dinantian limestones. *Geological Journal*, *2*(1), 11-36.

Bathurst, R. G. C. (1966). Boring algae, micrite envelopes and lithification of molluscan biosparites. *Geological Journal*, *5*(1), 15-32.

Bhargava, O. N. (2011). Early Palaeozoic palaeogeography, basin configuration, palaeoclimate and tectonics in the Indian Plate. *Facets of Phanerozoic. Mem. Geol. Soc. India*, 78, 69-99.

Blöchl, B., Kirchner, D., & Stadlbauer, E. (1998). Die hygrische Dehnung von Baumberger Kalksanstein–tonmineralogische und gesteinsphysikalische Aspekte. *Arbeitshefte zur Denkmalpflege in Niedersachsen*, *15*, 46-53.

Blue C. R., Giuffre A., Mergelsberg S., Han N., De Yoreo J. J. and Dove P. M. (2017). Chemical and physical controls on the transformation of amorphous calcium carbonate into crystalline CaCO3 polymorphs. *Geochimica et Cosmochimica Acta*, 196, 179–196.

Boggs, S. (1995). Principles of Sedimentology and Stratigraphy (Vol. 774). New Jersey: Prentice Hall.

Cartwright, J. H., Checa, A. G., Gale, J. D., Gebauer, D., & Sainz‐Díaz, C. I. (2012). Calcium carbonate polyamorphism and its role in biomineralization: how many amorphous calcium carbonates are there?. *Angewandte Chemie International Edition*, *51*(48), 11960-11970.

Chilingar, G. V., Bissell, H. J., & Wolf, K. H. (1967). Diagenesis of carbonate rocks. In *Developments in sedimentology* (Vol. 8, pp. 179-322). Elsevier.

Chima, P., Baiyegunhi, C., Liu, K., & Gwavava, O. (2018). Diagenesis and rock properties of sandstones from the Stormberg Group, Karoo Supergroup in the Eastern Cape Province of South Africa. *Open Geosciences*, 10(1), 740-771.

Crook, K. A. (1974). Lithogenesis and geotectonics: the significance of compositional variation in flysch arenites (graywackes).

Dabbagh, M. E., Rogers, J. W. (1983). Depositional environments and tectonic significance of the Wajid Sandstone of southern Saudi Arabia. *Journal of African Earth Sciences*, 1, 47-57.

Dickinson, W. R. (1970). Interpreting detrital modes of graywacke and arkose. *Journal of Sedimentary Research*, *40*(2), 695-707.

Dickinson, W. R. and Suczek, C. A. (1979). Plate tectonics and sandstone compositions; *Am. Assoc. Pet. Geol. Bull.* **63** 2164–2182.

Dickson, J. A. D. (2003). Neomorphism and Recrystallization. *Encyclopedia of Sediments and Sedimentary Rocks (ed. Middleton GV).* Kluwer Academic Publishers, Boston, 460-462.

Draganits, E., Grasemann, B., & Braddy, S. J. (1998). Discovery of abundant arthropod trackways in the ?Lower Devonian Muth Quartzite (Spiti, India): implications for the depositional environment. *Journal of Asian Earth Sciences*, *16*(2-3), 109-118.

Eriksson, K. A., Taylor, S. R., & Korsch, R. J. (1992). Geochemistry of 1.8-1.67 Ga mudstones and siltstones from the Mount Isa Inlier, Queensland Australia: Provenance and tectonic implications. *Geochimica et Cosmochimica Acta*, *56*(3), 899-909.

Flugel, E., & Flügel, E. (2004). Microfacies of Carbonate Rocks: Analysis, Interpretation and Application. Springer Science & Business Media.

Folk, R. L. (1959). Practical petrographic classification of limestones. *AAPG bulletin*, *43*(1), 1-38.

Folk, R. L. (1965). Some aspects of recrystallization in ancient limestones.

Folk, R. L., (1968). Bimodal supermature sandstones of the Desert floor, pp. 9-32, Int. Geo/.Congo Report, 23rd. Session, Czechoslavakia, Proc. Sec. 8.

Gebauer, D., Völkel, A., & Cölfen, H. (2008). Stable prenucleation calcium carbonate clusters. *Science*, *322*(5909), 1819-1822.

Ghosh, S. K., & Sengupta, S. (1999). Boudinage and composite boudinage in superposed deformations and syntectonic migmatization. *Journal of Structural Geology*, *21*(1), 97-110.

Goel, R. K., Kato, M., Jain, A. K., & Srivastava, S. S. (1987). Fauna from the" Muth Quartzite", Garhwal Himalaya, India. *北海道大学理学部紀要*, *22*(2), 247-257.

Ihli J., Wong W. C., Noel E. H., Kim Y.-Y., Kulak A. N., Christenson H. K., Duer M. J. and Meldrum F. C. (2014). Dehydration and crystallization of amorphous calcium carbonate in solution and in air. *Nat. Commun*. 5.

Kazmierczak, J., Coleman, M. L., Gruszczynski, M., & Kempe, S. (1996). Cyanobacterial key to the genesis of micritic and peloidal limestones in ancient seas. *Acta Palaeontologica Polonica*, *41*(4), 319-338.

Lander, R. H., & Walderhaug, O. (1999). Predicting porosity through simulating sandstone compaction and quartz cementation. *AAPG bulletin*, *83*(3), 433-449.

Lin, Y., Zhou, K., Gao, R., Li, J., & Zhang, J. (2019). Influence of chemical corrosion on pore structure and mechanical properties of sandstone. *Geofluids*, *2019*.

McLennan, S. M., Taylor, S. R., McCulloch, M. T., & Maynard, J. B. (1990). Geochemical and Nd Sr isotopic composition of deep-sea turbidites: crustal evolution and plate tectonic associations. *Geochimica et Cosmochimica Acta*, *54*(7), 2015-2050.

Nielsen, M. H., Aloni, S. and De Yoreo, J. J. (2014). In situ TEM imaging of CaCO3 nucleation reveals coexistence of direct and indirect pathways. *Science* 345, 1158–1162.

Pandita, S. K. & Bhat, G. M. (1995). Petrographic and facies evaluation of Middle Siwalik Subgroup Jammu, Himalaya. *Journal of Geological Society of India*, 46: 369–374.

Pandita, S. K., Bhat, S. K., Kotwal, S. S., Singh, Y. And Thakur, K. K. (2014). Provenance and tectonic settings of the Lower Siwalik Subgroup, Jammu, Northwest Himalaya. *The Palaeobotanist*, 63, 17-23.

Parcha, S. K. (2021). Stratigraphy and the Fossil record of the Palaeozoic and Mesozoic Tethyan sequences of North-western Himalaya. *Himalayan Geology*, *42*(1), 1-68.

Paterson, M. S., & Weiss, L. E. (1968). Folding and boudinage of quartz-rich layers in experimentally deformed phyllite. *Geological Society of America Bulletin*, *79*(7), 795-812.

Prothero, D. R., & Schwab, F. (1996). An Introduction to Sedimentary Rocks and Stratigraphy. *Sedimentary Geology, New York, WH Freeman and Company*, 575.

Qiao, L., Wang, Z., & Huang, A. (2017). Alteration of mesoscopic properties and mechanical behavior of sandstone due to hydro-physical and hydro-chemical effects. *Rock Mechanics and Rock Engineering*, *50*(2), 255-267.

Raina, B. K. & Razdan, M. L., (1975). Geology of parts of Machhal, Lolab and Kandi-Shiu areas of Kupwara, Hundwara and Sopore tehsils, Baramulla Distt, J & K State *(Unpub. GSI Report)*

Reed, F.R.C., (1912). Ordovician and Silurian fossils of central Himalayas. *Palaeont. Indica, Geol. Surv. India.* Ser. 15,7 (2): 1-168.

Reed, J. J. (1962). The importance of lithology in determining response to metamorphism and tectonic forces. *New Zealand Journal of Geology and Geophysics*, *5*(1), 86-91.

Reid, R. P., Macintyre, I. G., & Post, J. E. (1992). Micritized skeletal grains in northern Belize Lagoon; a major source of Mg-calcite mud. *Journal of Sedimentary Research*, *62*(1), 145-156.

Rodriguez-Blanco, J. D., Shaw, S., & Benning, L. G. (2011). The kinetics and mechanisms of amorphous calcium carbonate (ACC) crystallization to calcite, via vaterite. *Nanoscale*, *3*(1), 265-271.

Roser, B. P., & Korsch, R. J. (1986). Determination of tectonic setting of sandstone mudstone suites using SiO2 content and K2O/Na2O ratio. Journal of Geology, 94, 635–650.

Roser, B. P., & Korsch, R. J. (1988). Provenance signatures of sandstone mudstone suite determined using discrimination function analysis of major element data. Chemical Geology, 67, 119–139.

Schwab, F. L.,(1975). Framework mineralogy and chemical composition of continental margin-type sandstone: Geology, v. 3, p. 487-490.

Shah, S. K., (1968). A lithostratigraphic classification of Lower Palaeozoic slate group of Pohru Valley of North Western Kashmir. *University Review*, *2*, 10-17.

Shah, S.K., (1972). Palaeo-ecological studies of the Cambrian--Ordovician formation of north-western Kashmir. University Review, Jammu, 4: 1--7.

Shah, S. K. (1982). Cambrian stratigraphy of Kashmir and its boundary problems. *Precambrian Research*, *17*(2), 87-98.

Shah, S. K., & Sudan, C. S., (1983). Trace fossils from the Cambrian of Kashmir and their stratigraphic significance.

Shah, S. K., & Sudan, C. S. (1987). Damesellidae from the Cambrian of Kashmir. *Journal of the Geological Society of India*, *29*(5), 503-509.

Shah, S. K. (1991). Stratigraphic setting of the Phanerozoic rocks along the northern boundary of the Indian plate. *Physics and Chemistry of the Earth*, *18*, 317-328.

Sun, W., Jayaraman, S., Chen, W., Persson, K. A., & Ceder, G. (2015). Nucleation of metastable aragonite CaCO3 in seawater. *Proceedings of the National Academy of Sciences*, *112*(11), 3199-3204.

Tai, C. Y., and Chen, F. B. (1998). Polymorphism of CaCO3, precipitated in a constant-composition environment. AIChE J. 44, 1790–1798.

Talent, J. A., Goel, R. K., Jain A. K. and Pickett J. W. (1988) Silurian and Devonian of India, Nepal and Bhutan: Biostratigraphic and Palaeobiogeographic Anomalies. *Cour. Forsch.-Inst. Senckenberg* **106**, 1-57.

Wadia, D. N. (1934). The Cambrian-Trias sequence of north-western Kashmir (parts of Muzaffarabad and Baramula districts). *Records of the Geological Survey of India*, *68*(2), 121-176.

Webster, G. D., Rexroad, C. B., & Talent, J. A. (1993). An evaluation of the VJ Gupta conodont papers. *Journal of Paleontology*, *67*(3), 486-493.

Weltje, G. J., & Eynatten, H. V. (2004). Quantitative provenance analysis of sediments: Review and outlook. Sedimentary Geology, 171, 1–11.

Wilson, J. L. (1975). Principles of carbonate sedimentation. In *Carbonate Facies in Geologic History* (pp. 1-19). Springer, New York, NY.

Wolf, K. H. (1965). 'Grain-diminution'of algal colonies to micrite. *Journal of Sedimentary Research*, *35*(2), 420-427.

Wolthers, M., Nehrke, G., Gustafsson, J. P. and Van Cappellen P. (2012). Calcite growth kinetics: modeling the effect of solution stoichiometry. Geochimica et Cosmochimica Acta 77, 121–134.

Worden, R. H., Griffiths, J., Wooldridge, L. J., Utley, J. E. P., Lawan, A. Y., Muhammed, D. D., ... & Armitage, P. J. (2020). Chlorite in sandstones. *Earth-Science Reviews*, *204*, 103105.

Received: 9th May, 2021
Revised Accepted: 27th July, 2021

JOURNAL INDIAN ASSOCIATION OF SEDIMENTOLOGISTS ISSN NO 2582 – 2020
Vol. 38, Issue 2, 2021, pp. 115-121
DOI: https://doi.org/10.51710/jias.v38i2.202

Sulphur study of the Palaeogene coals from Jaintia Hills, Meghalaya, NE India: Implications for palaeoenvironment, utilisation prospects, and environmental impacts

Manabendra Nath
Department of Geology
Gurucharan College, Silchar-788004
Email: dr.manabendra.nath@gmail.com

Abstract

Coal samples of Eocene age (Shella Formation) from four different mines (Bapung, Jaintia, Sutunga, and Lakadong) of the Jaintia Hills of Meghalaya, Northeast India, were collected and investigated to observe the sulphur content and to understand the palaeoenvironment, utilisation prospects, and environmental impact. The study reveals that these coal samples contain sulphur in higher concentration (4.46% to 7.26%) both organic and inorganic forms. There are 3 coal seams exposed in the area. The organic sulphur is higher (2.53%-5.49%) than the inorganic forms (1.26%-1.77%). The upper seam is found to contain higher concentration of sulphur than the lower seam. Intra seam pyritic sulphur also shows an upward increasing trend. The high sulphur content in the coal seams suggests the marine influence in the peat-forming swamps. These coals are classified as High Sulphur coal (>1%) which is the main obstacle in the utilization although high volatile matter and hydrogen content strongly suggest that these coals are good for liquefaction. Moreover, during coal combustion emissions of sulphur dioxide produce acid rain, affecting the environment of the mine areas.

Keywords: Sulphur, palaeoenvironment, utilisation, marine, environment, Meghalaya.

INTRODUCTION

The occurrence of sulphur (S) in the Palaeogene coals of India attracted the attention of early workers (LaTouche 1882; Ghosh 1964; Ahmed 1971).The North Eastern coal fields are mainly scattered in Arunachal Pradesh, Assam, Nagaland, and Meghalaya in nearly 70 individual coal deposits (Mishra and Ghosh 1996). The Palaeogene coal deposits are of good quality, having characteristically low ash content and high caking properties. But the only drawback of these coals is the high amount of sulphur (10% or more), mainly in the organic form. (Ahmed and Bora, 1981)

In the northeast region of India, coal contains both organic and inorganic forms of sulphur. Pyritic and sulphate sulphur together commonly referred to as inorganic sulphur. The NE coalfields have been studied for their physicochemical and petrographic characteristics (Ahmed and Bora, 1981; Chandra *et al.*, 1983; Mishra, 1992; Ahmed and Rahim, 1996; Mishra and Ghosh, 1996; Singh and Singh, 2000, 2001, 2003; Singh *et al.*, 2012b). The Geological Survey of India (GSI) studied the regional tectono-stratigraphy of various coalfields of NE India (Karunakaran, 1974; Satsangi and Parlda, 1980; Raja Rao, 1981; Nayak, 2013).

Important contributions have been made by several authors on the stratigraphy, structures, and tectonics of NE India (Mallet, 1876; Biswas, 1962; Bhandari *et al.*, 1973; Dasgupta and Biswas, 2000; Acharyya, 2007). The provenance of the Barail Formation in Assam has been studied by Srivastava and Pandey (2011).

The present study has been carried out on the coalfields of the Jaintia Hills district of Meghalaya. The coal seams occur in the Lakadang sandstone member of Shella Formation of Jaintia Group of Eocene age. The coal deposits of the Jaintia Hills of Meghalaya have been studied by different workers for desulphurization, the environmental impact of mining, assessment of coal quality, etc. (Ahmed and Bora, 1981; Chandra *et al.*, 1983; Sarma, 2005; Nayak, 2013; Sahoo *et al.*, 2014). The objective of this paper is to decipher the palaeoenvironmental conditions of the coal seams, also to observe the utilisation prospects and environmental impacts based on chemical and petrographic studies. The present study will provide a framework that could help future gasification and liquefaction studies.

Geological Setting

The Geological and location map of Maghalaya is given as figure 1. Meghalaya, India, contains coal deposits within Palaeogene strata. Reserves calculated for Northeast India account for 593.81 MT (Indian Bureau of Mines, 2019), out of which Meghalaya alone have 89.04 MT of coal. Seven coal mines occur in the Jaintia Hills. Bapung, Jarain, and Sutunga coal mines are important amongst them (Fig. 2). Together, they are grouped as the “Bapung coalfield” (Singh and Singh, 2000).

A well-developed sequence of the lower Palaeogene sediments is exposed at Jaintia Hills and constitutes the type area of the Jaintia Group where coal seams are associated with the Lakadong sandstone member of the Sylhet Formation (Raja and Rao, 1981) Sutunga and Jarain villages in the valleys. A low regional dip of 3° towards the south is observed in these

Table 1. Geological succession of Jaintia hills coalfield of Meghalaya (modified after Raja Rao, 1981; GSI, 2009)

Age	Group	Formation	Member	Lithology
Palaeocene-Eocene	Jaintia Group	Kopili Formation (50 m)	----------	Shale, Sandstone, marl, and coal
		Shella Formation (600 m) (earlier Sylhet Formation)	Prang Limestone	Fossiliferous argillaceous limestone
			Nurpuh sandstone	Sandstone with subordinate calcareous bands
			Umlatdoh limestone	Foraminiferal limestone containing a few sandstone bands
			Lakadong sandstone	Coal bearing sandstone
			Lakadong limestone	Fossiliferous limestone
			Theria sandstone	Medium to coarse-grained ferruginous sandstone containing thin coal seams, calcareous shales and at places clay bands
		Langpar Formation (100 m)	----------	Calcareous shale, sandstone, limestone
Archaean	Meghalaya Gneissic Complex			Gneisses, Schists and Granites

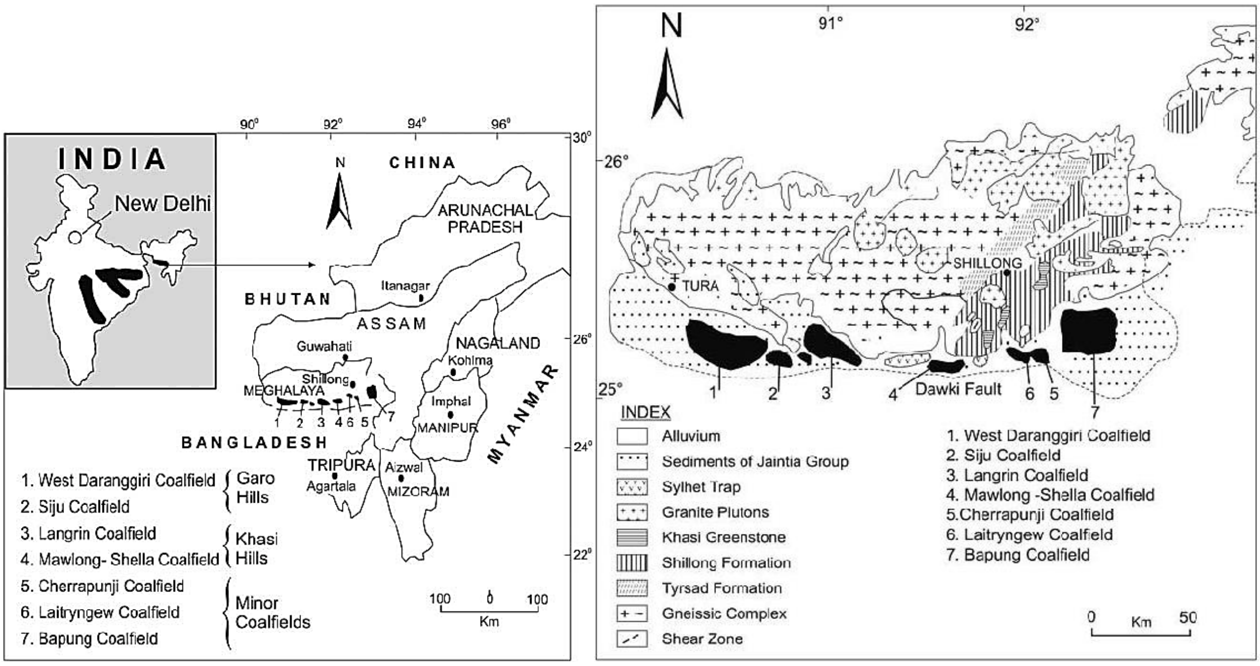

Figure 1. Location and geological map of Meghalaya, North-eastern India (after Singh *et al.*, 2015)

A generalised stratigraphic sequence is shown in table 1.The Meghalaya Palaeogene coal deposits are presumed to have been formed over platform areas under stable shelf conditions (Raja Rao, 1981; Singh and Singh, 2000). In the study area (Fig. 2) eight coal seams have been recognised at Bapung (3), Jarain (2), Sutunga (2), and Lakadong (1). In the Bapung coalfield, only the lower seams are persistent, which vary in thickness from 0.3 to 1.5 m. In some places in the Bapung area, the upper and middle seams become very thin, ranging in thickness from 0.1 m to 0.5 m. All three coal seams are associated with the Lakadong sandstone which strikes in an ESE-WNW direction with south-westerly dips varying from 3° to 6°. Two coal seams are well exposed in Sutunga and Jarain area. The lower seam occurs in the basal part of the Lakadong sandstone over the Lakadong Limestone. These seams are well exposed towards the east and north of the

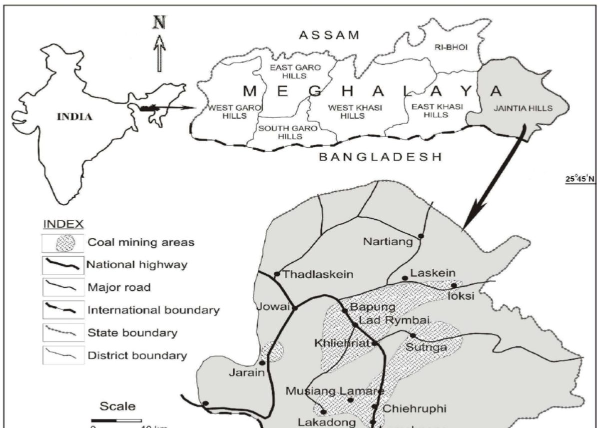

Figure 2. Outline map showing the coal mining areas in Jaintia Hill of Meghalaya in northeast India and the sample locations (Nayak, 2013).

seams. The thickness of the seam varies from 0.3 m to 1 m and 0.1 m -1.7 m in these coalfields respectively. There occurs a 0.3 m to 2.1 m thick coal seam at Lakadong.

following the guidelines of the Bureau of Indian Standards (BIS): 1350 (BIS 2003) and American

Table 2 Results of proximate analysis in weight percent of the coalfields of Jaintia hills

Site/Source	Sample No/Seam	air-dried basis			
		Moisture (%)	Ash (%)	Volatile Matter (%)	Fixed Carbon (%)
Bapung Coalfield	I	2.81	2.20	42.15	52.84
	II	1.81	1.30	40.25	56.64
	III	1.72	1.22	41.20	55.86
Jarain Coalfield	I	1.90	1.11	43.21	53.78
	II	1.50	1.91	44.02	52.57
Sutunga Coalfield	I	2.11	1.10	41.25	55.54
	II	1.62	1.02	40.62	56.74
Lakadong	I	2.20	1.82	42.25	53.73

Table 3: Sulphur content of coal samples (in wt. %) from Jaintia Hills.

Site/Source	Sample No/ Seam	Total S	Pyrite S	Sulphate S	Organic S
Bapung Coalfield	I	7.26	0.97	0.80	5.49
	II	5.25	0.82	0.72	3.71
	III	4.02	0.72	0.62	2.68
Jarain Coalfield	I	5.65	0.86	0.64	4.15
	II	4.12	0.83	0.59	2.70
Sutunga Coalfield	I	4.46	0.69	0.58	3.19
	II	3.79	0.65	0.61	2.53
Lakadong	I	4.78	0.61	0.57	3.60

Material and Methods

Coal samples were collected following pillar sampling method from the exposed outcrops of the coalfields of Jaintia Hills located in deep mines. The samples were crushed to <72 mesh and <18 mesh sizes for chemical and petrographic tests, respectively. Proximate and sulphur analyses were performed by Society for Testing and Materials, ASTM D5373-08 (2008), respectively. A Leica DM 2700 P advanced petrological microscope aided with MSP 200 coal photometer and fluorescence attachment was used for petrography following standard practices and norms of the International Committee for Coal and Organic Petrology as described in Singh and Jha (2018b).

Table 4: Petrographic composition of Jaintia Coals (in volume %).

Site/Source	Sample No/ Seam	Vitrinite	Liptinite	Inertinite	Mineral Matter
Bapung Coalfield	I	81.76	3.11	11.17	3.96
	II	80.05	3.66	13.95	2.34
	III	78.05	4.84	15.25	1.86
Jarain Coalfield	I	79.24	0.68	18.02	2.06
	II	77.92	1.72	18.74	1.62
Sutunga Coalfield	I	78.54	2.39	16.79	2.28
	II	76.25	3.09	18.92	1.74
Lakadong	I	79.32	1.28	17.02	2.38

Results and Discussion

Megascopic characterization

The coals of the area are black and generally are hard and compact but soft and friable varieties are also observed in the field. The coals break with a cubical fracture but the hard one breaks with sub-conchoidal to conchoidal fracture. Most of the coals when exposed to the sun easily disintegrate into small chips. Sometimes very thin pyrite bands are observed. They show dull to glassy lustre. On weathering the coal breaks parallel to the bedding plane. These coals are seen as a homogenous mass of vitrain. Megascopically, the coal indicates a high sulphur content, which occurs as minute yellow particles or granules.

Sulphur content of the coals

The results of the proximate analysis of the Jaintia Hills coals are presented in table 2. From table 3, it is observed that very high sulphur concentration is present in these coals. The total sulphur content of the coals varies from 3.82% to 7.26%, which is much higher than the recommended permissible limit of sulphur (as per the classification scheme of Chou (2012)) with <1%, 1-3%, and >3% are categorized as low, medium, and high sulphur coal, respectively.

The inorganic constitutes pyritic sulphur varies from 0.61% to 0.97% and sulphate sulphur from 0.58% to 0.80%. The organic sulphur, which dominates the inorganic forms, varies from 2.53% to 5.49%. From table 3, it is seen that total sulphur content (of each of the four coalfields) increases from the bottom to the top of a seam (e.g., Bapung 4.02% to 7.26%).

This intra-seam vertical variation of sulphur has been attributed to the fact that pH values decrease with depth (i.e. alkalinity increases upward from bottom to the surface) as a result sulphur content increases upward in the sequence since the alkaline condition is conducive to the deposition of sulphur (Chandra *et al.*, 1983) and also that there was more marine influence at the top of the peat. Some binary plots have been made to explore the possible relationships among the maceral groups and total sulphur (Fig. 3).

Relation of group maceral with total sulphur

The petrographic composition of the Jaintia coals is presented in table 4. A linear relationship is observed when plots are made of vitrinite vs. total sulphur. In the case of the inertinite vs total sulphur plot, an inverse relationship is observed, since leptinites in these coals are very few. From these relationships, it emerges that the precursors of vitrinite and liptinite macerals have evolved under a high water table, high pH, and low Eh conditions. Such conditions allow the reduction of sulphate to sulphide and provide an ideal situation for the formation of pyrite and organic sulphur in good concentration.

Palaeoenvironment

As per the observation of Teichmüller (1962), the coals with marine influence are generally rich in sulphur, hydrogen, and nitrogen contents and are characterized by a higher volatile matter content than other coals of the same rank. In the Jaintia coal mines, similar conditions seem to be applicable, which have relatively high S and volatile matter contents.

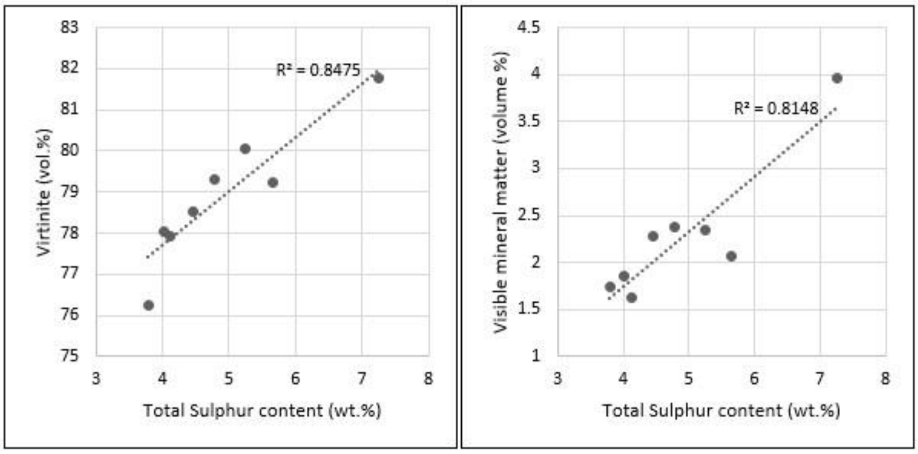

Figure 3. Correlation of microscopic constituents (vol. %) with total sulphur content (wt. %)

Organic sulphur might originate from the complexing of sulphur from sulphate ions and hydrogen sulphide by humic acids during the process of coalification (Casagrande*et al.,* 1979). Irrespective of the form, such a high concentration of sulphur in coal indicates a marine origin because freshwater contains only 0 to 10 ppm sulphur and henceforth, even if there is a prolonged circulation of fresh water through the peat, it cannot account for much sulphur in the coal. Chou (1990) indicates that most of the sulphur in coals with more than one percent sulphur comes from sea water. Price and Shieh (1979) have shown that in high sulphur coals (>0.8% S), about 63% of the sulphur is derived from seawater by sulphate reduction and the rest is derived from original vegetation. Therefore, in the Jaintia Hills, the high sulphur content in the coal seams perhaps can be explained by the repeated influx of seawater (Nayak, 2013) with an intermittent hiatus during which the water table was not enough to sink the swamp vegetation. The findings of Singh and Singh (2000) also corroborate this point of view. The model proposed by Singh and Singh (1996) shows that the coals of the study area formed under alternating oxic and anoxic moor conditions (Fig. 4). Since the Jaintia Hills coal seams occur in the Lakadong sandstone member that is sandwiched between two limestone members: the underlying Lakadong limestone and overlying Umlatdoh limestone, Raja Rao (1981) also suggested that these formations have formed due to intermittent marine transgression and regression during the Eocene period.

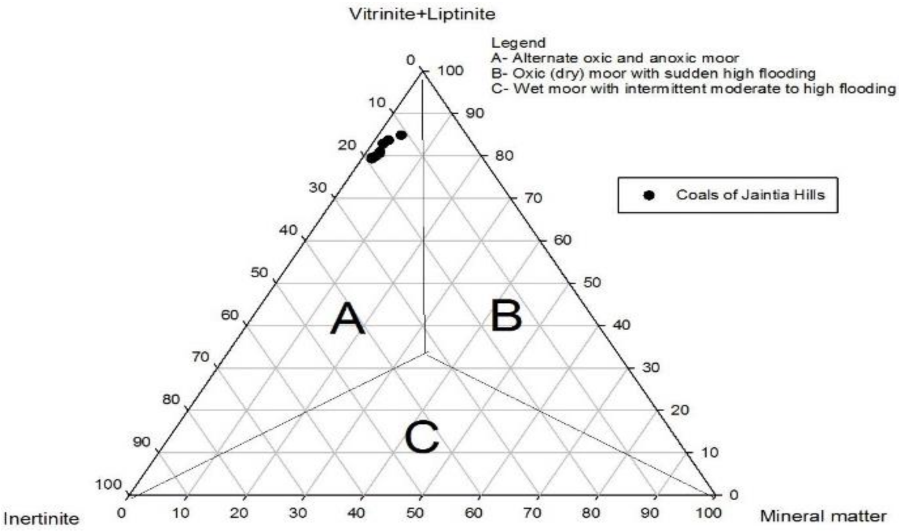

Figure 4. Depositional conditions of Jaintia Hills coals based on maceral and mineral matter content (after Singh and Singh 1996).

Table 5 Result of ultimate analysis of the coal samples of Jaintia Hills.

		Dry, mineral matter free (dmmf) basis				
Site/Source	Sample No/ Seam	Carbon (%)	Hydrogen (%)	Nitrogen (%)	Sulphur (%)	Oxygen (%)
Bapung Coalfield	I	74.28	6.62	2.56	7.26	9.28
	II	75.36	5.13	2.71	5.25	11.55
	III	75.02	6.23	2.80	4.02	11.93
Jarain Coalfield	I	74.58	6.42	1.68	5.65	11.67
	II	73.34	5.92	2.11	4.12	14.51
Sutunga Coalfield	I	72.89	5.03	1.75	4.46	15.87
	II	75.67	5.52	1.32	3.79	13.70
Lakadong	I	72.02	5.86	2.10	4.78	15.24

Utilisation and Prospects

The majority of the coals of Jaintia Hills of Meghalaya are supplied to Assam and Bangladesh for use in brick and other industries. The presence of high volatile matter and significant concentration of hydrogen (Table 5) strongly suggest that these coals may be good for liquefaction and gasification (Singh and Jha, 2018a). In addition, these coals can produce coke or, at least, can be used in a blend for coking purposes. The high sulphur content is the main obstacle in the utilization of these coals; it is strongly felt that the possible method for desulphurization should be evolved through research and development activities. Recently, desulphurization of coal with bacterial biomass (Singh *et al.,* 2012a, 2013, 2018; Singh, 2018) has come up with a new insight into such problems. If this problem is solved, then these remotely located coal deposits may turn out to be an asset for the people of Meghalaya.

Environmental impacts

As coal contains a high amount of sulphur (dominant organic sulphur) the problems of pollution both in air and water is evident. During the burning of coals in the open air, SO_2 gas emits which further reacting with air produces SO_3. The produced SO_3 get dissolved in water and produces H_2SO_4,which causes acid aerosols and acid rain in the area. Besides, a high amount of sulphur present in pyrite also causes acid mine drainage (Graham and Sarofim 1998).

Conclusions

The high organic sulphur content of the Palaeogene Jaintia Hills coals indicates their marine origin and the formation associated with coals have witnessed both marine transgression and regression phases. Besides, as the coal deposits are rich in vitrinite and low in ash, good coke can be produced and can be used as a blend for coking purposes. High sulphur is the only limiting factor and needs to be eliminated before any use. Moreover, sulphur dioxide emitted during coal combustion is a principal source of acid rain which affects the environment badly in the study areas.

Acknowledgement

The author is thankful to the Central Drug Research Institute (CDRI), Lucknow (Head of the Department) for elemental analysis and to the Birbal Sahni Institute of Palaeosciences (BSIP), Lucknow for petrographic analysis. The authors are grateful to the anonymous reviewers, whose constructive comments have significantly improved the quality of the present paper.

References

Acharyya, S.K. (2007). Evolution of the Himalayan Paleogene foreland basin, influence of its litho-packet on the formation of thrust-related domes and windows in the Eastern Himalayas–A review. Journal of Asian Earth Sciences, 31: 1–17.

Ahmed, M. (1971). Petro-chemical study of coal, Laitryngew coalfield, K. & J Hills, Assam. J. Geol. Soc. Assam, 1: 17–20.

Ahmed, M. and J.P. Bora (1981). Geochemistry of tertiary coal, Bapung coalfield, Jaintia Hills, Meghalaya. J Assam SciSoc, 24: 9–10.

Ahmed, M. and A. Rahim (1996). Abundance of sulfur in Eocene coal beds from Bapung, Northeast India. International Journal of Coal Geology, 30: 315–318.

ASTM D5373-08. (2008). Standard Test Methods for Instrumental Determination of Carbon, Hydrogen, and Nitrogen in Laboratory Samples of Coal, l, ASTM International, West Conshohocken, PA.

Bhandari, L.L., Fuloria, R.C. and V.V. Sastri (1973). Stratigraphy of Assam Valley, India. AAPG Bulletin, 57: 642–654.

BIS. (2003). Methods of Test for Coal and Coke (2nd Revision of IS: 1350). Part I, Proximate Analysis, Bureau of Indian Standards, New Delhi.

Biswas, B. (1962). Structure of the Mahadek, Lonpar, Cherra, and Tura Formations, Assam, Bulletin of the Geological. Mining and Metallurgical Society of India, 25: 1-48

Casagrande, D.J., Siefert, K., Berschinsk, C. and N. Sutton (1979). Sulfur in peat forming system of the Okefenokee swamp and Florida Everglades : origin of sulfur in coal. Geochim. Cosmochim. Acta, 41: 161–167.

Chandra, D., Mazumdar, K. and S. Basumallick (1983). Distribution of sulphur in the tertiary coals of Meghalaya, India. International Journal of Coal Geology, 3: 63–75.

Chou, C.L. (2012). Sulfur in coals: A review of geochemistry and origins. International Journal of Coal Geology, 100: 1–13.

Dasgupta, A.B. and A.K. Biswas (2000). Geology of Assam: Geological Society of India. Bangalore, 169p.

Ghosh, T.K. (1964). On Tertiary coal from Daranggiri, Assam, Quart. QJ Geol. Soc. India, 36: 91–94.

Graham, K.A. and A.F. Sarofim (1998). Inorganic Aerosols and Their Role in Catalyzing Sulfuric Acid Production in Furnaces. Journal of the Air & Waste Management Association, 48: 106–112.

Indian Bureau of Mines. (2019). Indian Minerals Yearbook 2019 (Part-III: Mineral Reviews), 58th ed.

Karunakaran, C. (1974). Geology and mineral resources of the states of India. Part IV-Arunachal Pradesh, Assam, Manipur, Meghalaya, Mizoram, Nagaland and Tripura. Geological Survey of India, Miscellaneous Publication, 30: 1–124.

LaTouche, T.H.D. (1882). The Daranggiri Coal-field, Garo Hills, Assam. Rec. Geol. Surv. India, 15: 175–178.

Mallet, F.R. (1876). On the coal fields of the Naga Hills, bordering the Lakhimpur and Sibsagar Districts. Geological Survey of India, Memoir, 12: 269–363.

Mishra, B.K. (1992). Tertiary coals of Makum Coalfield, Assam, India: Petrography, genesis and sedimentation. Palaeobotanist, 39: 309–326.

Mishra, H.K. and R.K. Ghosh (1996). Geology, petrology and utilisation potential of some Tertiary coals of the northeastern region of India. International Journal of Coal Geology, 30: 65–100.

Nayak, B. (2013). Mineral matter and the nature of pyrite in some high-sulfur tertiary coals of Meghalaya, northeast India. Journal of the Geological Society of India, 81: 203–214.

Price, F.T. and Y.N. Shieh (1979). Fractionation of sulfur isotopes during laboratory synthesis of pyrite at low temperatures. Chemical Geology, 27: 245–253.

Raja Rao, C.S. (1981). Coalfields of India, Coalfields of North Eastern India. Bulletin of the Geological Survey of India, Series A, No. 45, I, 75.

Sahoo, P.K., Tripathy, S., Panigrahi, M.K. and S.M. Equeenuddin (2014). Geochemical characterization of coal and waste rocks from a high sulfur bearing coalfield, India: Implication for acid and metal generation. Journal of Geochemical Exploration, 145: 135–147.

Sarma, K. (2005). Impact of Coal Mining on Vegetation: A Case Study in Jaintia Hills District of Meghalaya, India. 1–85. International institute for geo-information science and earth observation enschede (The Nederlands) and Indian institute of remote sensing, nation- al remote sensing agency (NRSA), Department of space, Dehradun, India.

Satsangi, P.P. and K. Parlda (1980). A new fossil crab from Garo Hills, Meghalaya. Journal of Geological Society of India (Online archive from Vol 1 to Vol 78), 21: 302–305.

Singh, A.K. (2018). Classification and Potential Utilization of Eocene Coals of Meghalaya, North East India. Journal of the Geological Society of India, 91: 181–187.

Singh, A.K. and M.K. Jha (2018a). Hydrocarbon potential of Permian coals of South Karanpura Coalfield, Jharkhand, India. Energy Sources, Part A: Recovery, Utilization and Environmental Effects, 40: 163–171.

Singh, A.K. and M.K. Jha (2018b). Petrochemical evaluation and classification of coal deposits of BarkaSayal area, South Karanpura Coalfield and suggestion for its proper utilisation. International Journal of Oil, Gas and Coal Technology, 18: 39–54.

Singh, A.K., Singh, M.P. and P.K. Singh (2015). Microstructural relation of macerals with mineral matter in Eocene coal. Energy Sources, Part A: Recovery, Utilization and Environmental Effects, 37: 1089–1097.

Singh, A.K., Kumar, A., Singh, P.K., Singh, A.L. and A. Kumar (2018). Bacterial desulphurization of low-rank coal: A case study of Eocene Lignite of Western Rajasthan, India. Energy Sources, Part A: Recovery, Utilization and Environmental Effects, 40: 1199–1208.

Singh, A.L., Singh, P.K., Kumar, A. and M.P. Singh (2012a). Desulfurization of Selected Hard and Brown Coal Samples from India and Indonesia with *Ralstoniasp*and *Pseudoxanthomonas sp.* Energy Exploration & Exploitation, 30: 985–998.

Singh, M.P. and A.K. Singh (2000). Petrographic characteristics and depositional conditions of Eocene coals of platform basins, Meghalaya, India. International Journal of Coal Geology, 42: 315–356.

Singh, M.P. and A.K. Singh (2001). Source rock characteristics and maturation of Palaeogene coals, Northeast India. Journal of the Geological Society of India, 57: 353–368.

Singh, M.P. and A.K. Singh (2003). Hydrocarbon emigration through microfracturing in vitrinite: An example from the Oligocene coals of Borjan coalfield, Nagaland. Journal of the Geological Society of India, 61: 170–176.

Singh, M.P. and P.K. Singh (1996). Petrographic characterization and evolution of the Permian coal deposits of the Rajmahal basin, Bihar, India. International Journal of Coal Geology, 29: 93–118.

Singh, P.K., Singh, M.P., Singh, A.K. and A.S. Naik (2012b). Petrographic and Geochemical Characterization of Coals from Tiru Valley, Nagaland, NE India. Energy Exploration & Exploitation, 30: 171–191.

Singh, P.K., Singh, A.L., Kumar, A. and M.P. Singh (2013). Control of different pyrite forms on desulfurization of coal with bacteria. Fuel, 106: 876–879.

Srivastava, S.K. and N. Pandey (2011). Search for provenance of Oligocene Barail sandstones in and around Jotsoma, Kohima, Nagaland. Journal of the Geological Society of India, 77: 433-442.

Teichmüller, M (1962) Die Genese der Kohle. CR 4th IntCongr Carbon Strat Geol, Heerlen 1958, 4: 699-722.

Received: 8th September, 2021
Revised Accepted: 27th December, 2021

OBITUARY

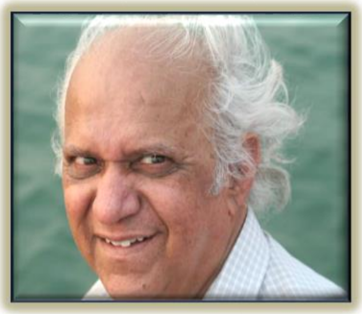

Professor I B Singh
(1943-2021)

Professor Indra Bir Singh, a celebrated sedimentologist who inspired many generations of geology students of India, breathed his last on 11th February 2021. Professor Singh was born on 8th July 1943 in Lucknow. He received early education from the Lucknow Christian College and later joined the University of Lucknow in 1956 and completed B.Sc. (Hons.) in 1961 and M.Sc. in geology in 1962. He joined Oil and Natural Gas Corporation for a brief period. He registered for his Ph. D. at the Technical University, Stuttgart, Germany on "Sedimentology of the Keuper Lias boundary layers, Württemberg" and received Doctor rerum naturalium (Latin for 'doctor of natural sciences'). He joined as Research Associate at Senckenberg Institute, Wilhelmshaven, Germany and subsequently worked as Post-doctoral fellow at the Oslo University, Norway during 1967-68. He again joined Senckenberg Institute in 1969 and worked on modern shallow marine sediments till 1972 when he returned to India and joined the Department of Geology, University of Lucknow.

Prof. Singh was a versatile teacher and researcher who immensely contributed to the stratigraphy of the Lesser Himalaya, depositional history of Vindhyans of Central India, Bagh-Lameta beds, Jurassic succession of western India, Siwaliks, Karewas of Kashmir and Deltas of East Coast. His main contribution is on the resolution of age controversy of the Krol - Tal sequence of the Lesser Himalaya which was earlier considered a Mesozoic succession. He presented his paper reporting Trilobite from the Krol - Tal sequence during the 4th convention of the Indian Association of sedimentologists at Aligarh Muslim University in February 1984. I am witness to the criticism he received during his presentation alleging false reporting of the fossil trilobite from the sequence. But his observations and arguments challenging the Mesozoic age to Krol-Tal sequence was later demonstrated by him and his students proving its Precambrian-Cambrian age. Professor Singh and his students also made a discovery by identifying the contribution of interfluves (doab) processes in fluvial domain of the Ganga Plain. His has also made discovered food grain domestication in India suggesting agricultural evolution and domestication of rice cropping in India during Holocene.

His famous book "Depositional Sedimentary Environments" co-authored with Prof. H. E. Reineck, was published in 1973 which has been also translated in Russian and Chinese languages and is still being used as a reference book. He was keen to revise the book but unfortunately that couldn't materialize because of his pressing academic and research engagements; he once told me. He has also published another important book "Delta Sedimentation: East Coast of India' co-authored with A.S.R. Swamy" in 2006.

Prof. Singh has supervised 16 doctoral students and published about 200 research articles which have been widely quoted internally. Prof. Singh was elected Fellow of Indian National Science Academy in 1995. He is the recipient of the National Mineral Award, Government of India and National Award for excellence in Earth System Science in 2014 and L. Rama Rao Birth Centenary Award of the Geological Society of India (1996). In 2020, during the centennial foundation day of the University of Lucknow, he was recognised as an illustrious faculty member of the university. He was the Fellow of Alexander von Humboldt Foundation, Germany during 1988 – 1989. He served as a visiting professor at European and American universities including Uppsala, Sweden; Erlangen-Nuremberg (1998-99), Halle/Saale, and Louisiana State University, Baton Rouge (1984-86).

In Professor Singh geological fraternity in general and sedimentology have lost an excellent teacher, impeccable mentor, a theoretician having practical approach in understanding the nature and natural processes. Professor Singh is survived by his wife, two sons, numerous students and friends.

G. M. Bhat
University of Jammu
bhatgm@jugaa.com

OBITUARY

Professor A. H. M. Ahmad
(1961-2021)

Professor A.H.M. Ahmad, affectionately known as 'Hasnat Sir' by his students, was born in Azamgarh (Uttar Pradesh) on January 22, 1961. He spent his early days in Azamgarh and then movedto Bhivandi (Maharashtra), where he completed his early education. He received his graduation, post-graduation, M.Phil., and Ph.D. from Department of Geology, Aligarh Muslim University in 1980, 1982, 1984 and 1989 respectively. In 1993, he was appointed as a Lecturer in the same department, then promoted to Associate Professor in 2001, Professor in 2014, and Chairperson in 2019, a position he held until his death.

Professor Ahmad authored 116 research articles and book chapters in prestigious national and international journals over his 37-year research career, supervised 14 doctorates and 02 M.Phil. theses, completed 7 projects, and attended several workshops and national/international conferences. He specialised in sedimentology and served as treasurer of the Indian Association of Sedimentologists, as well as a member of the IGCP-506 and the Palaeontological Society of India. Professor Ahmad, in addition to being a bright academician, was also a remarkable administrator who served as Warden of various halls of residence of Aligarh Muslim University and as Deputy Proctor of the University.

Prof. Ahmad is well known sedimentologist in the country as well as an outstanding teacher of sedimentary and petroleum geology. Precambrian and Mesozoic sedimentary facies and basin analyses, recent sedimentary environments, provenance, tectonic settings, and diagenetic evolution were among his research interests. He employed microfacies analysis, geochemical approach, and isotopic examination of sedimentary rock to better understand the geodynamics of the Kachchh and Jaisalmer basins. His series of studies on Jurassic rocks from Kachchh and Jaisalmer anticipated their evolution, depositional environments, paragenetic sequence, and porosity evolution in relation to reservoir quality. However, he was also captivated by Precambrian geology, particularly the North Delhi Fold Belt and the Vindhyan Supergroup of rocks, which have a lot to say about Proterozoic cratonic evolution.

Regardless of the fact that he had been suffering from acute renal failure for about 5 years and had to undergo excruciating dialysis three times a week, he continued to do his job, whether it was supervising scholars or teaching undergraduate and graduate students. Even after overcoming all of this difficulty in his last few years, he maintained a strong commitment to academic excellence; he is without a doubt the bravest man we have ever met. After a protracted battle with renal failure, he got a bacterial infection in his lungs, which led to his death after a one-and-a-half month vigil at Fortis Escort Hospital in Delhi on August 14, 2021 at around 10 a.m.

Although he was not physically present between us, he had made an indelible impact on our lives through the way he treated with us and, most significantly, the humble and kind manner in which he spoke to us. When you talked to him, he was a friend; when you asked him a question, he was a teacher; and when you sought his advice, he was a wise man. Prof. Ahmad was an excellent supervisor, a dependable researcher, and a gifted educator. To his associates, he was modest, humble, friendly, cherished, respected, responsible, and an influencer. This will be our greatest tribute to him: we will preserve his vision and goal in front of us, and we will pray to the Almighty for eternal peace and patience for his bereaved family. He left behind his wife, son, and daughter along with a legacy of students that he encouraged to carry the spark of sedimentology forward! The tragic death of *Hasnat Sahab* (as he was profoundly known) has left a huge vacuum in India's Sedimentological society in general and our department in particular.

Faiz Ahmad, Shaikh Asjad
M. Adnan Quasim
Department of Geology,
Aligarh Muslim University
Aligarh 202002, India

ACHKNOWLEDGEMENTS

The Editorial Board of the Journal of Indian Association of Sedimentologists (JIAS) place on record appreciation for their cooperation in the process of handling the articles published in Volume 38(2) and review process.

Professor Ghulam Jeelani

Dr. Izrar

Professor Irfan Mondal

Professor R. Nagendra

Professor S. K. Pandita

Dr. Waquar Ahmed

Dr. Nurul Absar

Professor G. N. Nayak

Dr. V. S. Hegde

Dr. Ahsan ul Haq

Professor subir Sarkar

Dr. Anudab Manda;

Dr. Sunipa Mandal

Professor Mahender Kotha

Dr. Mateen Hafiz

Professor V. A. Joshi

Professor G. M. Bhat

Dr. Bashir Ahmad